860

January 14, 1992

A SEARCH FOR NEUTRINO OSCILLATIONS

USING THE FERMILAB DEBUNCHER

M.J. Murtagh
Brookhaven National Laboratory, Upton, NY 11973

J. Boyer, Y. Ho, W. Lee*, E. Mannel, and J. Mechalakos
Columbia University, 538 West 120th St., New York, NY 10027

A. Bross, M. Gormley, C. Kim, S. O'Day, and Y. Park
Fermilab Accelerator Laboratory, P.O. Box 500, Batavia, IL 60510

K.S. Kang and D.W. Kim
Kangnung National University, Kangnung, Korea

J.S. Kang
Korea University, Seoul, Korea

J. Kim
Seoul National University, Seoul, Korea

* Spokesman

A SEARCH FOR NEUTRINO OSCILLATIONS USING THE FERMILAB DEBUNCHER

Section I INTRODUCTION

This is a proposal for an appearance search for $\nu_e \rightarrow \nu_\tau$ oscillations using a neutrino beam from the Fermilab Debuncher Ring. While the primary focus of the experiment is on the $\nu_e \rightarrow \nu_\tau$ oscillation, the experiment is also sensitive to a wide range of parameters for $\nu_e \rightarrow \nu_\mu$ oscillations and to a lesser extent $\nu_\mu \rightarrow \nu_\tau$. The addition of a second identical detector at some later time at 5–10km from the Debuncher would greatly expand the present search and would be particularly interesting for the $\nu_\mu \rightarrow \nu_\tau$ search. The increased flux available when the new Main Ring Injector is operational would also be a great advantage for this long baseline phase of the experiment.

The Fermilab Debuncher naturally produces a time separated neutrino beam with a uniform energy distribution in the range 3–9GeV, so most of the beam is above threshold for producing τ leptons. During conventional collider operation negative pions, muons and electrons are captured along with the $\bar{p}$'s in the Debuncher ring. In a few turns the negative pions decay to give negative muons and muon antineutrinos. The muons, some of which are trapped in the ring, decay over many turns producing muon neutrinos and electron antineutrinos. Since antineutrinos produce positive leptons when they interact the only beam sources which can produce positive muons are the early muon antineutrinos from the pion decays or electron antineutrinos from the muon decays which have oscillated to muon antineutrinos or to tau antineutrinos which subsequently decayed to positive muons. In principal then the observation of positive muons in the final state is a clear signal for the presence of tau leptons which can only come from oscillations. The absence of a real beam background of positive muons should make this a relatively straightforward measurement. The only significant background is from real or fake positive muons in conventional neutrino interactions. This is addressed in detail below but it does not significantly limit the search.

In principal then the normal collider debuncher operation produces time separated neutrino beams of early muon antineutrinos from negative pion decay and later muon neutrinos and electron antineutrinos from captured muon decays. Unfortunately this flux is not adequate for the oscillation searches being proposed. However if one severs the connection to collider running and uses the Debuncher to collect positive pions then a significant event rate increase is achievable. Part of this increase comes from a change

in the machine operation and the remainder comes from the difference of neutrino and antineutrino cross sections and various improvements in the accelerator and Debuncher operations. The flux from the regular collider operation is adequate for testing and tuning up the detector. However for the actual data taking dedicated debuncher operation to collect positive pions is required. This operation is compatible with fixed target operations.

The detector for the experiment would be located in line with one of the straight sections of the Debuncher ring. For acceptance reasons it is advantageous to locate it as close to the ring as possible but there must be adequate shielding to reduce the stray beam flux from the Debuncher. The detector is relatively simple since its primary requirement is to identify and measure the signs of muons above 1 GeV. As with most neutrino detectors it consists of a primary module which is then repeated to give enough mass to get an acceptable event rate for the process of interest. The primary module here consists of a toroid to provide field, a scintillator plane to provide event timing and tracking chambers to measure the muon tracks. The present estimate is that such a detector and a suitable hall will take ~ 2 years to build and should cost $\leq$ \$7M.

The primary physics being addressed by this proposal, namely the existence of a massive, 17 keV, neutrino is very topical and if this experiment can proceed without delay it is very likely that it can have a significant impact on this question. However, independent of the fate of the 17 keV neutrino this experiment will significantly improve the mixing angle limits of previous oscillation searches using electron neutrino beams or electron final state signatures.

The mixing angle limit for $\nu_\mu \rightarrow \nu_e$ will improve by an order of magnitude while the mixing angle limit for $\nu_e \rightarrow \nu_\tau$ will improve from 8×10^{-2} to 3×10^{-3}. The long baseline phase of the experiment will improve the mass difference limit at maximal mixing for $\nu_\mu \rightarrow \nu_\tau$ from 0.25 ev^2 to 0.05 eV^2.

Section II PHYSICS MOTIVATION

The conjecture that neutrinos might oscillate has been the subject of much theoretical speculation and experimental effort (Ref. II.1). While there have occasionally been experimental indications of positive results none of these have been confirmed by other experiments and indeed most have gradually subsided in the light of different or improved experiments. Accelerator based oscillation searches have primarily focused on $\nu_\mu \rightarrow \nu_e$ oscillations (Fig. II.1a). Accelerator neutrino beams are predominantly muon neutrino beams with $\sim 1\%$ contamination of electron neutrinos. Since the ratio of ν_e to ν_μ in the beam is essentially determined by the ratio of pions to kaons in the beam from the production target, one is looking for an increase in rate of electrons in a relatively well understood situation. While these experiments have produced the majority of oscillation results they are limited by the beam contamination of ν_e, electron identification problems in counter experiments and the lack of a sign measurement on the shower. Accelerator based searches for ν_μ oscillations to final states other than ν_e have for the most part been disappearance experiments (Fig. II.1b,c). The most notable exception is the Fermilab emulsion experiment 531. Disappearance experiments are inherently limited in their mixing angle limits as they involve the subtraction of large numbers. They are also devoid of any clear signature and rely totally on calculations of the neutrino flux as a function of distance from the source. Experiment 531 was an appearance experiment which looked in emulsion for short lived particles which could be consistent with τ's. This experiment has a relative large mass limit as it was a high energy experiment. There are essentially no accelerator limits for ν_e beams as there are no high flux electron neutrino beams. The limits (Fig. II.1c) from reactor experiments have good mass range but they have very restricted mixing angle limits as they are disappearance experiments.

The most intriguing hint of neutrino oscillations is in the realm of solar neutrinos. The disagreement between the solar model calculations and the measurement of solar neutrino fluxes can be interpreted in a very elegant way using the MSW (Ref. II.2) matter oscillation conjecture. This provides neutrino oscillation solutions with a mass difference in the 10^{-6}eV^2 to 10^{-4}eV^2 range. If one assumes that the mixing is greatest between the nearest mass states then this would be interpreted as mixing between ν_e and ν_μ. If one also assumes that there is a reasonable neutrino mass hierarchy such as naturally occurs in many Grand Unified Theories then one might expect to observe $\nu_\mu \rightarrow \nu_\tau$ oscillations in the energy regime of available accelerators (Ref. II.3). For example if the neutrino masses

scale as the square of the corresponding quark or lepton masses then the tau neutrino mass could be 10^4 times the muon neutrino mass or in the range $10^{-2}eV^2$ to $1eV^2$.

A few years ago Simpson (Ref. II.4) reported evidence for the existence of a 17keV neutrino in an experiment to measure the beta spectrum of Tritium. The mixing of this electron neutrino was $\sim 1\%$. Recently Simpson repeated this measurement for ^{35}S with similar conclusions. In addition a number of other measurements of beta spectra for different materials have also produced positive results with the same value for the neutrino mass. The situation is not clear since several spectrometer experiments have failed to observe this reported effect. If this effect is real it would likely involve a $\nu_e \rightarrow \nu_\tau$ oscillation since $\nu_e \rightarrow \nu_\mu$ oscillations with these parameters have been ruled out by existing accelerator searches.

The indications from all the present evidence and conjecture is that the most fruitful areas for neutrino oscillation searches at accelerators are in the channels $\nu_\mu \rightarrow \nu_\tau$ and, in light of the 17keV neutrino results, particularly in the $\nu_e \rightarrow \nu_\tau$ channel. To date these have been the least explored channels.

The proposed experiment is for a clean ν_e beam with no ν_μ contamination. Since most of the beam energy spectrum is above the threshold for tau production it is ideal for $\nu_e \rightarrow \nu_\tau$ searches. The detector is close to the target so the E/L for the experiment is ~ 100. This will restrict the mass difference squared limit to 5–10 eV^2. While this is more than adequate for the range suggested by the Simpson result it is not in the range of $\nu_\mu \rightarrow \nu_\tau$ suggested by the solar neutrino conjectures. However the results in this channel will be a significant improvement in mixing angle over the present disappearance results and lower in mass than the E531 emulsion results(Fig. II.1b). An extension of the present experiment which involves the addition of a second detector at a large distance from the Debuncher could lower the Δm^2 limit for $\nu_\mu \rightarrow \nu_\tau$ oscillations to the region suggested by the solar neutrino experiments.

Section III THE NEUTRINO BEAM

The Fermilab Debuncher ring is a strong focusing synchrotron with a circumference of 500 meters, situated between Giese and Indian Roads (Fig. III.1). During normal collider running it accepts negative secondaries which originate at the antiproton production target and are transported through the AP-2 beam line. Secondaries whose phase space coordinates lie within the momentum acceptance [$8.9GeV/c \pm 2\%$] and transverse admittance [$A(x) = A(y) = 25\pi\text{mm} \times mrad$] of the Debuncher ring are injected and captured in the Debuncher. The particle composition of the first-turn beam in the Debuncher is dominated by pions, but contains electrons, muons, and antiprotons as well.

For the last several months, parasitic to the running of E-760, measurements of the fluxes of pions, electrons, muons and antiprotons which are injected into and circulate in the Debuncher have been made. The Appendix contains a detailed summary of the novel experimental technique used, together with the measured results for the circulating muon flux in the Debuncher.

As described in the Appendix, the measurements are quoted in terms of the ratio of the muon flux to the antiproton flux. The measured result is $\mu^-/\bar{p} = 1.0 \pm 0.2$; the muon and antiproton fluxes which circulate in the Debuncher are nearly identical.

From the measured $\mu^-/\bar{p}$ ratio one can calculate the number of muons per day that are available in the Debuncher when it is used parasitically as a source of electron neutrinos. In this calculation the following known and mostly in progress upgrades are included;

1. After completion of the Linac upgrade (but prior to the existence of the Main Injector) the proton flux on the antiproton target will be 3×10^{12} protons per pulse.
2. The cycle time of the Main Ring will be reduced from 2.6 secs to 2.1 seconds.
3. By 1994 the $\bar{p}/p$ ratio in the Debuncher will increase, due to improvements in the Debuncher aperture and the lithium lens, from its current value of 2.0×10^{-5} to 3.0×10^{-5}.
4. In addition the overall operating efficiency of the Main Ring, the target station and Debuncher is assumed to be 80%. This type of efficiency is required for reasonable collider operation.

With these assumptions, the number of muons per day available in the Debuncher during parasitic operation, after the Linac upgrade, will be;

$$\frac{\mu^-}{\text{day}} = \frac{60 \times 60 \times 24}{2.1} \times (3 \times 10^{12}) \times (3 \times 10^{-5} \times 0.8) = 3 \times 10^{12}$$

This muon flux which is available parasitically during collider running is a significant source of neutrinos but, as noted earlier, it is not adequate for the experiment in question. However, if one does not insist on running parasitic to the collider, the muon flux can be increased by at least an order of magnitude. The flux of muons circulating in the Debuncher would be optimized in this mode of operation as follows:

1. Change the polarity of the AP-2 line and the Debuncher.

   The inclusive yield of π^+ is approximately equal to that of π^- for 120 GeV protons on a heavy target (Ref. III.1). Such a modification would only require a polarity reversal of the magnets in the AP-2 line and the Debuncher. Polarity reversals of this type are quite straight-forward and typically require 2–3 hours to complete.

   This switch also implies that the experiment is a search for neutrino and not antineutrino oscillations which yields almost a factor of 2 increase in event rate because of the difference in cross sections for neutrinos and antineutrinos.

2. Operate the AP-2 line and the Debuncher at higher momenta.

   The Appendix summarizes both the calculations of the flux of circulating muons as well as the flux measurements that have been made with both the AP-2 beam line and the Debuncher ring operating at a central momentum of 9 GeV/c. The simulation model is being used to explore the improvement in flux that can be achieved by running the AP-2 beam line at a slightly higher momentum than the Debuncher. Preliminary results from the simulations indicate that running the transport line at 2% higher momentum increases the flux of circulating muons by a factor of two.

   This result should be verified at the earliest possible opportunity by remeasuring the muon flux with the central momentum of the transport line set 2% higher. In calculating the neutrino event rates this expected increase in the muon flux is used, but the rates should be regarded as preliminary until this improvement is experimentally verified.

   The maximum energy at which the Debuncher can be run is determined primarily by the field quality of the dipoles in the ring. At the Debuncher's design momentum of 9 GeV/c the field quality is extremely uniform: $\Delta B/B < 2 \times 10^{-4}$ within $\pm$2.0in.. At higher excitation currents the flatness of the field deteriorates. For example, magnetic measurements of the Debuncher dipoles at 10 GeV/c indicate that the

non-uniformity of the field is roughly 2.5 times larger (i.e., $\Delta B/B < 5 \times 10^{-4}$ within $\pm$2.0in.). Consequently the dynamic aperture at 10 GeV/c is likely to be somewhat smaller than at the design momentum. However, in using the Debuncher as a muon storage ring, one is concerned only with the dynamic aperture for the first 300 turns of circulating beam (after which time 90% of the muons have decayed). Computer simulations will be required to establish the maximum energy at which the Debuncher can be run as a storage ring. The energy can probably be raised by at least 10% above the design value.

For the event rate calculations discussed below it is assumed that the Debuncher is operating at 10GeV/c. In this case not only does one gain the factor of two improvement in the muon flux as noted above from the simulation calculations but there is also an increase in the number of π^+ at 10GeV/c relative to the number at 9GeV/c. This increase is calculated to be an additional factor of 1.4. (Ref. III.2)

3. Operate the Main Ring in "Multi-batch" mode.

   For antiproton production the Main Ring is currently operated in "single-batch" mode - in which one batch of 82 bunches is injected at 8 GeV into the Main Ring every 2.1 seconds, accelerated to flat top, extracted and targeted. With 2×10^{12} protons per batch and a 2.1 second cycle time the (time) average intensity is 0.95×10^{12} protons per second.

   In a "multi-batch" mode of operation, N batches are injected at 8GeV, accelerated to flat top simultaneously, and extracted one at a time to the production target, with as short an interval between extraction cycles as possible. With 10 batches, extracted at a 15 Hz. rate, the Main Ring cycle time would be:

$$T = 2.1 + (10-1)\cdot(1/15) + (10-1)\cdot(1/15) = 3.3\text{seconds}$$

   and the (time) average intensity would be:

$$I = (10 \times 2 \times 10^{12})/(3.3) = 6.1 \times 10^{12}\text{protons/sec.}$$

   This multi-batch operation yields an average intensity which is 6.4 times greater than single batch.

   Two hardware improvements are necessary to implement multi-batch operation with the parameters sketched above: (1) a Main Ring extraction kicker with a rise and fall

time of 0.5 microseconds; and (2) a rapid-cycling (15 Hz) lithium lens downstream of the production target. There appears to be sufficient space in the E-17 medium straight section of the Main Ring to accommodate a kicker with these characteristics, i.e., no significant changes to the Main Ring lattice are required. To build a reliable, rapid-cycling lithium lens would require significant lead-time and a substantial development effort. However, much of the groundwork for such an effort has been carried out by the Novosibirsk group (Ref. III.3) who have tested prototype liquid lithium lenses with significantly larger diameters than would be required.

The overall enhancement which results from these modifications is $2 \times 1.4 \times 6.4 = 18$. Consequently the number of muons per day in the Debuncher for this optimized mode of running is 5.4×10^{13}.

In summary the Debuncher in its normal operating mode for collider running does not have adequate flux for the experiment being proposed. However by switching from negative to positive pion capture and by altering the operation of the machine a significant increase in the muon flux in the Debuncher ring can be achieved. The decay of this stored muon beam produces a clean beam of electron neutrinos which is time separated from the beam background of muon neutrinos and so is ideal for searches for rare neutrino processes which produce negative muons in the final state. In addition, since the flux of pions/muons is well measured in the Debuncher it should be possible to absolutely normalize the neutrino flux by a straightforward decay calculation.

Section IV EVENT RATES

In estimating neutrino fluxes and interaction rates, it is assumed that the Debuncher is used to store positive muons, in a non-parasitic, multi-batch mode of operation, with an integrated muon flux of $5.4 \times 10^{13}\mu^+$/day. Only 13% of the muons decay in the straight section of the Debuncher pointing at the detector. In addition the first few turns (~ 10) are dominated by ν_μ from pion decay and the present electronic design is only active for 400 μsecs. This amounts to cutting 25% of the captured muon flux. Consequently the useful muon flux is $0.13 \times 0.75 \times 5.4 \times 10^{13}\mu^+$/day or $5.3 \times 10^{12}\mu^+$/day.

The muon neutrino energy distribution from the decay of the primary 9GeV/c pions in the Debuncher is shown in Fig. IV.1a while the muon antineutrino and electron neutrino energy distributions from the captured 9GeV/c secondary muon decays are shown in Fig. IV.1b and Fig. IV.1c respectively. All these calculations are for the neutrinos which are emitted at less than 10mr from the initial meson or muon direction. This corresponds to the neutrinos with the potential to interact in a 1m radius fiducial volume detector.

The number of pions and muons as a function of turn number is shown in Fig. IV.2. As noted earlier, after a few (~ 10) turns the neutrino flux from pion decays is negligible. The muon flux continues to be significant for at least two hundred turns.

In the decay $\mu \rightarrow e^+ + \nu_e + \bar{\nu}_\mu$, the energy and angular distribution of ν_e and $\bar{\nu}_\mu$ are

$$\frac{d^2 N_{\bar{\nu}_\mu}}{dx\ d(\cos(\theta))} = x^2(3-2x)\left[1 - \left(\frac{1-2x}{3-2x}\right)\cos(\theta)\right]$$

and

$$\frac{d^2 N_{\nu_e}}{dx\ d(\cos(\theta))} = x^2(1-x)[1-\cos(\theta)]$$

where $x = E_\nu/(m_\mu/2)$ and θ is the angle between the muon neutrino and the polarization vector in the muon rest system (Ref. IV.1).

Initially, the μ^+ polarization is left handed. Assuming that there is no dynamic depolarization mechanism, the number of high energy ($E_\nu > 6$GeV) ν_e and $\bar{\nu}_\mu$ entering the detector are time separated, as can be seen in Fig. IV.3 which shows the number of ν_e and $\bar{\nu}_\mu$ as a function of turn number.

The electron neutrino spectra for Debuncher settings to capture 9GeV/c, 10GeV/c and 11GeV/c particles are shown in Fig. IV.4a,b,c. Clearly with increasing energy of the ring the fraction of the neutrinos above the tau threshold increases as does the overall event rate as the mean energy is higher. The quasi elastic cross sections for ν_e, $\bar{\nu}_e$, ν_τ, and

$\bar{\nu}_\tau$ are shown in Fig. IV.5 while the inelastic cross sections are shown in Fig. IV.6. It is clear from these distributions that, for the Debuncher energy regime, the tau cross section is predominantly quasi elastic and single pion while the conventional neutrino interactions are dominantly deep inelastic.

The integral of the flux × cross section for the relevant neutrino species and partial cross sections is shown in Table IV.1. The effects of Fermi motion are included in the calculation. This has little effect on the basic neutrino rates but it does increase the tau neutrino rates by $\sim$ 10%. It is clear from these numbers that a 10% increase in the Debuncher energy produces a significant increase in the tau event rate. It is not yet clear how much the energy of the Debuncher can be increased with the present magnets but some increase is expected.

In calculating the event rate it is assumed that all neutrinos produced within 10mrad of the nominal muon beam direction pass through the fiducial volume of the detector. As will be clear when the detector is discussed later this is a very reasonable approximation. The detector will start 15m from the end of the Debuncher straight section. It consists of 600 modules, each containing 5cms Fe absorber and space for timing and position measuring detectors for a total dimension in the beam direction of $\sim$ 60m. Therefore a 1m radius fiducial volume will contain a 10mr beam divergence.

The following rate calculation is for a 10GeV/c Debuncher setting. The expected improvement in rate from running the Debuncher at a higher field can be determined from Table IV.1. As discussed above the number of useful muons per day is 5.3×10^{12}. Assuming that the detector has the 600 modules of Fe defined above and the 10mrad beam is contained in the fiducial volume the electron neutrino event rate per day is given by

$$\#\nu_e \text{ interactions/day} = \#\mu \times F_{\nu_e} \times Mz = 1670.$$

$\#\mu = 5.3 \times 10^{12}, F_{\nu_e} = 224.9 \times 10^{-40}\text{cm}^2/\mu$ is defined in Table IV.1 and $M_Z = 6 \times 10^{23} \times 7.87 \times 5 \times 600\text{cm}^2$ is the longitudinal fiducial tonnage.

If one assumes 200 day run then the total number of ν_e interactions is

$$\#\nu_e \text{ interactions} = 330 \times 10^3.$$

A similar calculation for the number of $\bar{\nu}_\mu$ interactions yields

$$\#\bar{\nu}_\mu \text{ interactions} = 200K.$$

TABLE IV.1

$F_{\nu_\mu} \equiv \int \mathrm{FLUX}(E)\sigma(E)dE \quad 10^{-40}\mathrm{cm}^2/\mathrm{muon}$ for ν_μ

	$E = 9$GeV	$E = 10$GeV	$E = 11$GeV
QE	17.2	19.5	21.8
CCSP	15.9	18.1	20.2
CCDIS	76.4	94.3	113.8
TOTAL	109.5	131.9	155.8

$F_{\nu_e} \equiv \int \mathrm{FLUX}(E)\sigma(E)dE \quad 10^{-40}\mathrm{cm}^2/\mathrm{muon}$ for ν_e

	$E = 9$GeV	$E = 10$GeV	$E = 11$GeV
QE	22.9	25.6	28.1
CCSP	21.1	23.7	26.0
CCDIS	145.2	175.6	206.0
TOTAL	189.2	224.9	260.1

$F_{\nu_\tau} \equiv \int \mathrm{FLUX}(E)\sigma(E)dE \quad 10^{-40}\mathrm{cm}^2/\mathrm{muon}$ for ν_τ

	$E = 9$GeV	$E = 10$GeV	$E = 11$GeV
QE	6.5	8.3	10.0
CCSP	2.8	3.9	5.0
CCDIS	4.5	7.2	10.6
TOTAL	13.8	19.4	25.6

$F_{\bar{\nu}_\mu} \equiv \int \mathrm{FLUX}(E)\sigma(E)dE \quad 10^{-40}\mathrm{cm}^2/\mathrm{muon}$ for $\bar{\nu}_\mu$

	$E = 9$GeV	$E = 10$GeV	$E = 11$GeV
QE	16.8	19.2	21.3
CCSP	16.0	18.2	20.2
CCDIS	75.6	91.7	107.8
TOTAL	108.4	129.1	149.3

For the purpose of calculating the signal from oscillations into τ neutrinos the oscillation parameters are taken to be those of Simpson viz. mass difference of 17 keV and a mixing angle $\sin^2(\alpha) = 0.8\%$ or $\sin^2(2\alpha) = 3.2\%$. For such a high mass difference $\sin^2(1.27 \times \Delta m^2 \times L/E) \sim 0.5$ and

$$\#\nu_\tau \text{ interactions} = 0.5 \times 0.032 \times \#\nu_e \text{ interactions} \times \left(\frac{F_{\nu_\tau}}{F_{\nu_e}}\right)$$
$$= 455.$$

Only 17% of the produced tau will decay into negative muons and in addition, as is discussed below, only 80% of the muons will be in the acceptance of the detector. Consequently the number of observed negative muons from tau neutrinos produced by the oscillation of electron neutrinos is $455 \times 0.17 \times 0.8$ or

No. Observed negative muons = 63.

In other words if one assumes a total of 200 days running there would be a total signal of 62 events or 40 quasi elastic or single pion events if there is a 17keV neutrino which oscillates from ν_e with a few percent mixing ($\sin^2(2\alpha) \sim 3\%$).

The actual oscillation limits which this experiment can set if there is no such heavy neutrino are presented later after the potential backgrounds are discussed.

Section V BACKGROUNDS

The primary signature for a charged current neutrino interaction is a fast, relatively forward going lepton. This feature is retained even if one considers the secondary muons from tau decay. The acceptance for such muons in the present experiment if one requires the muon to be greater than 1GeV/c and to have an angle to the beam direction with $\cos\theta < 0.8$ is $\sim 80\%$. Since the ν_τ cross section at Debuncher energies is primarily quasi elastic, genuine τ interactions will be characterized not just by a forward going energetic muon but also by a relatively low multiplicity event. A typical quasi elastic τ event is shown in Fig. V.1. The cleanliness of the event and the lack of additional connected tracks is apparent.

The primary background sources for this experiment are charm production which produces genuine muons but in high multiplicity events and pions in conventional deep inelastic interactions which produce fake muons either because they decay or they accidentally pass the muon selection criteria. A typical background charm event is shown in Fig. V.2. In the present very preliminary analysis one requires τ candidates to be very clean events. If it is assumed that this is equivalent to selecting only quasi elastic on single pion final states then (Table IV.1) 70% of the signal events are retained. As the Debuncher energy increases this reduces the acceptance and since the overall event rate is quite low one will in practice try to relax these cuts to increase the event sample. However for the present proposal tight cuts are applied as many details of the event topology in this detector are not yet understood.

The present background estimates are based on Monte Carlo calculations. The event generator, ETEST(Ref. V.1) was developed for the E776 neutrino experiment at Brookhaven National Laboratory and has been extensively tested in that experiment. The Charm and deep inelastic scattering production is from the CCFR Fermilab neutrino collaboration (Ref. V.2). The results from these calculations are thought to be adequate for the present study. Work is also in progress to determine the expected background from the actual data taken by the E776 collaboration in the wide band neutrino beam at BNL. While this beam peaks at 1.3GeV/c there is a long tail and approximately 7% of the flux at the E776 location is above 4GeV.

The primary source of fake muons from pion production will be $\bar{\nu}_\mu$ interactions

$\bar{\nu}_\mu$ charged current (CC)

single pion (SP)	$\bar{\nu}_\mu N \rightarrow \mu^+ \pi^- N'$
deep inelastic (DEEP)	$\bar{\nu}_\mu N \rightarrow \mu^+ \pi^- X$

neutral current (NC)

single pion (SP)	$\bar{\nu}_\mu N \rightarrow \bar{\nu}_\mu \pi^- N'$
deep inelastic (DEEP)	$\bar{\nu}_\mu N \rightarrow \bar{\nu}_\mu \pi^- N'$

and the equivalent reactions for ν_e ($\mu^+ \rightarrow e^+$ in the above). It should be noted that for a pion to fake a 1GeV/c muon it has to either decay without a visible kink or traverse 6 λ of Fe without an apparent interaction. In Table V.1 the results of the Monte Carlo calculation for a sample of $\bar{\nu}_\mu$ interactions is summarized. The generated events are divided between charged and neutral currents and the contribution from single pion and deep inelastic contributions are separated. At these energies there are few energetic pions in the events and the requirement that the energetic pion be in the beam direction and that the μ^+ from the charged current process is not observable significantly reduces the potential background. The final cut is a crude cleanliness cut and requires that there be less than 0.5GeV of additional visible energy in the event. As expected this cut has little effect on the single pion events but significantly reduces the deep inelastic contribution. A practical definition of cleanliness for this detector is under study but it is clear that this will be an effective cut is removing false tau candidates from the final sample. It is clear from Table V.1 that none of the charged current events and less than 10^{-3} of the neutral current events produce a pion candidate event which will pass the simple geometric cuts for muon candidates. Since the neutrino cross section is twice the antineutrino cross section, the ν_e neutral current sample will produce approximately twice as many background candidates as the $\bar{\nu}_\mu$ neutral current sample. Unlike the $\bar{\nu}_\mu$ charged current sample the ν_e charged current sample will contribute to the background because the leading lepton, in this case an electron, will probably not be easy to identify because of the thickness of the absorber plates. Assuming some of the electrons are visible the background contribution will be roughly the same as the ν_e neutral current contribution just from the ratio of charged to neutral cross sections. The total background sample will therefore be 5×10^{-3} of the $\bar{\nu}_\mu$ neutral current sample. This corresponds to 1,000 events for the 200 day run being considered. The probability that a pion will traverse 6λ without interaction is such that

less than 3 of these tracks should survive as a true muon candidate. It is likely that a few percent ($\lesssim$ 1%) will decay. This would yield at most 10 background candidates. However few of the decay muons will have sufficient energy to pass the 1GeV/c muon range requirement. Consequently one would expect at most a few background events in the sample.

Further analysis of the potential pion background is in progress. This involves generation of additional Monte Carlo events in all channels and the inclusion of pion decay studies in the detector simulation.

The charm background can only arise in $\bar{\nu}_\mu$ interactions since the ν_e interactions at these energies will produce a single positive charm particle which decays to a μ^+ and not a μ^-. Also the neutrino energy is relatively low so the $\bar{\nu}_\mu$ neutral current production of charm pairs will be suppressed. Consequently the only relevant charm production is the production of D mesons in $\bar{\nu}_\mu$ charged current interactions. The calculated number of such events in the sample is 240. Since the branching ration to muons is approximately 10% this will yield 24 negative muons in the sample. However, if one requires the muon to have momentum greater than 1GeV/c, to be within 37° of the beamline and that there be no additional tracks in the event, then the number of surviving events in the sample will be negligible.

TABLE V.I

PION BACKGROUND CALCULATION FOR $\bar{\nu}_\mu$ INTERACTIONS

	CC		NC		
	SP	DEEP	SP	DEEP	TOTAL
N_{gen}	1,957	6,465	697	2,681	11,800
$E_\pi \geq 1.\text{GeV}$ $\theta_\pi \leq 37°$	37	629	8	202	876
$(E_{\mu+} < .5\text{GeV})$	0	36	4.3	159	199
$K_X < .5\text{GeV}$	0	0	3.6	7.2	11

In summary there is no evidence that there will be a significant background for the proposed τ signature of an energetic muon ($P_\mu > 1\text{GeV/c}$) in the forward direction $\cos\theta_e >$ .8 in a very clean event ($K_{\text{tot}} < 0.5$ GeV).

Section VI OSCILLATION LIMITS

The probability that a neutrino of type ν_a and energy E_ν(GeV) oscillates to a neutrino of type ν_b at a distance L (Km) from the neutrino source is given by

$$P(\nu_a \rightarrow \nu_b) = \sin^2 2\alpha \ \sin^2\left(1.27\Delta m^2 \frac{L}{E}\right)$$

where Δm^2 (eV^2) is the difference in mass of the neutrino mass eigenstates. In the limit of small Δm^2 this simplifies to

$$\Delta m^2 \sin 2\alpha \leq 0.8 \frac{E}{L}\sqrt{P}$$

while for very large Δm^2 it reduces to

$$\sin^2 2\alpha \leq 2P.$$

As is clear from the above formula, the small Δm^2 limit is controlled by the E/L for the experiment while the mixing angle limit is really determined by the statistical and systematic errors on the measurement. For the present proposal $E/L \sim 7/0.07 = 100$ so the emphasis in these measurements will be on the mixing angle limit. On the other hand if, for the second phase of the experiment, the detector is moved to 10Km and one considers the ν_μ spectrum with mean energy $\sim$ 3GeV, then the E/L is reduced to 0.3 and one can now attain a very good Δm^2 limit at maximal mixing.

The number of neutrinos of type ν_b ($\#\nu_b$) produced by the oscillations of neutrinos of

the type ν_a is given by

$$\begin{aligned}\#\nu_b &= P(\nu_a \rightarrow \nu_b) \times \#\nu_a \\ &= P \times \#\nu_a\end{aligned}$$

Therefore the number of ν_b interactions ($\#\nu_b^{\text{int}}$) is given by

$$\begin{aligned}\#\nu_b^{\text{int}} &= \#\nu_b \times \sigma_{\nu_b} \times M_Z \\ &= P \times \#\nu_a \times \sigma_{\nu_b} \times M_Z \\ &= P \times \#\mu \times \text{Flux}(\nu_a) \times \sigma_{\nu_b} \times M_Z\end{aligned}$$

and

$$\begin{aligned}\#\nu_a^{\text{int}} &= \#\nu_a \times \sigma_{\nu_a} \times M_Z \\ &= \#\mu \times \text{Flux}(\nu_a) \times \sigma\nu_a \times M_Z\end{aligned}$$

or

$$\begin{aligned}\frac{\#\nu_b^{\text{int}}}{\#\nu_a^{\text{int}}} &= P\,\frac{\text{Flux}(\nu_a) \times \sigma_{\nu_b}}{\text{Flux}(\nu_a) \times \sigma_{\nu_a}} \\ &= P\,\frac{F_{\nu_b}}{F_{\nu_a}}.\end{aligned}$$

Therefore

$$P(\nu_a \rightarrow \nu_b) \equiv \frac{\#\nu_b^{\text{int}}}{\#\nu_a^{\text{int}}} \times \frac{F_{\nu_a}}{F_{\nu_b}}$$

where ν_i^{int} is the number of interactions of neutrino type i and F_{ν_i} is the integral of Flux $\times$ cross section for neutrino type i as listed in Table IV.1.

For the calculations below it is assumed that at most 4 background events are observed and this is consistent with the expected number so $\#\nu_b$ from oscillations is $4 - 4 = 0$ or 3.7 to 90% confidence.

The total number of interactions expected for each of the primary neutrino species in the beam for a 200 day run is given in Table VI.1 for possible Debuncher energy settings of 9Gev, 10Gev and 11Gev. The ν_e and $\bar{\nu}_\mu$ rates are obtained as discussed in Section IV. The ν_μ rate is considerably higher because the ν_μ arise from the direct decay of the primary pion beam and the π/μ ratio at the entrance to the Debuncher is 50/1.

The following calculations are for the 10Gev/c Debuncher setting and the limits are calculated using only the quasi elastic and single pion events as that is probably the analysis mode and running conditions which will be used in the experiment.

The number of accepted ν_e quasi elastic and single pion interactions is $0.8 \times 75 \times 10^3$ or 60×10^3. Since the ν_μ and ν_e cross sections are the same it follows that for $\nu_e \rightarrow \nu_\mu$

TABLE VI.1

Number of Events in the Detector

Debuncher Energy	9 GeV	10 GeV	11 GeV
ν_e (all)	220×10^3	336×10^3	466×10^3
ν_e (QE, SP only)	50×10^3	75×10^3	93×10^3
$\bar{\nu}_\mu$ (all)	126×10^3	196×10^3	266×10^3
$\bar{\nu}_\mu$ (QE, SP, DEEP)	38×10^3	57×10^3	75×10^3
ν_μ (π decay) (all)	6.3×10^6	9.8×10^6	14×10^6
ν_μ (QE, SP)	1.9×10^6	2.8×10^6	3.8×10^6

oscillations

$$P = 3.7/(60 \times 10^3) = 6 \times 10^{-5}.$$

Consequently the oscillation limits are;

$$\begin{aligned} \text{Large}\Delta m^2 \qquad & \sin^2(2\alpha) \leq 1.2 \times 10^{-4} \\ \text{Small}\Delta m^2 \qquad & \Delta m^2 \sin 2\alpha \leq 5.6\text{eV}^2 \end{aligned}$$

For the limit on $\nu_e \rightarrow \nu_\tau$ oscillations

$$P = 3.2/(60 \times 10^3) \times (F_{\nu_e}/F_{\nu_\tau}) = 2 \times 10^{-4}$$

where F_{ν_e} and F_{ν_τ} are given in Table IV.1. In this case the number of ν_τ candidates is given by $3.2/(0.17 \times 0.8)$ where 0.17 is the $\tau \rightarrow \mu$ branching ratio and 0.8 is the muon acceptance. The corresponding oscillation limits are therefore;

$$\begin{aligned} \text{Large}\Delta m^2 \qquad & \sin^2(2\alpha) \leq 3.2 \times 10^{-3} \\ \text{Small}\Delta m^2 \qquad & \Delta m^2 \sin 2\alpha \leq 3\text{eV}^2 \end{aligned}$$

The actual limit curves for both these results are shown in Fig. VI.1.

For completeness it is possible to calculate the expected long baseline oscillation limit for $\nu_\mu \rightarrow \nu_\tau$ if the same mass detector is placed at 10Km. The flux in the detector is reduced by $(L_1/L_2)^2$ or $(0.1/10)^2 = 10^{-4}$ while the ν_μ flux is approximately 50 times the

ν_e flux being used above (Table IV.1). This implies that the actual event rate in the 10Km detector is 5×10^{-3} of the ν_e flux or 375 events. In this case

$$P = 2.3/(0.17 \times 0.8) \times 1/375 = 4.5 \times 10^{-2}$$

and the corresponding limits are

$$\begin{array}{lrcl} \text{Large}\Delta m^2 & \sin^2(2\alpha) & \leq & 0.1 \\ \text{Small}\Delta m^2 & \Delta m^2 \sin 2\alpha & \leq & 0.8 \times 3/10 \times 2.1 \times 10^{-1} \\ & & = & 0.05 \end{array}$$

Section VII DETECTOR DESIGN

In order to achieve the experimental goals the detector system must have the following attributes:

- Angular acceptance out to 10 mrad for neutrinos generated at the center of the Debuncher straight section.
- Sufficient mass to be able to detect the number of events needed to satisfy the physics objectives.
- Momentum and charge determination for muons above 1.0 GeV/c.

A preliminary design of a detector to accomplish these goals has been made. The detector is a conventional iron toroid design using Iarocci tubes to measure the position of charge tracks, and scintillator to determine the particle direction from time-of-flight measurements. The detector is modular in design. Each toroid module contains 40 planes of iron absorber, 40 planes of Iarocci tubes, and 4 planes of scintillator. A four turn coil is used to provide the toroidal field. A schematic drawing of a single toroid module is shown in Fig. (VII.1). The total detector consists of 15 modules which are hexagonally shaped with a 1.25 m radius. The overall length of the detector is 183 feet.

Toroid Modules:

Each module consists of 40 planes of hexagonal shaped iron absorber 2 in. thick. Following each plane of iron is a plane of Iarocci tubes used for measuring the track position. In addition following every tenth plane of Iarocci tubes is a plane of 1 in. thick scintillator for time-of-flight measurements. The gap spacing between the planes of iron absorber is 2.5 in. for gaps containing both Iarocci tubes and scintillator and 1.25 in. for gaps containing only Iarocci tubes. The total length for a complete module excluding supporting frame is 135 in. with an estimated mass of 82.0 tons. The total mass of the completed detector is estimated to be 1.23×10^3 tons.

A four inch diameter opening passes through the center of the module to accommodate the water cooled copper conductor for the toroid coil. The coil is four turns looping around each side of the module to provide a toroidal field in the iron. A current of 2750 amps is used to saturate the field in the iron toroids at 18 Kgauss. The total power consumption for the full detector is estimated to be 300 Kw.

Scintillator:

In order to determine the flight direction for charged particles each module contains 4 planes of scintillator. The scintillator planes are hexagon shaped to match the iron absorber and 1 in. thick, with the same transverse measurements of the iron absorber plates. A schematic drawing of a scintillator plane is shown in Fig. (VII.2). The scintillation light is collected by two $1.0 \times 1/2$ in.^{2} waveshifter bars imbedded in the scintillator. The waveshifter is read out by a photomultiplier tube located on the top end the waveshifter for a total of 2 pmt's per plane of scintillator.

Iarocci Tubes:

Tracking information is provided by the Iarocci tubes. Iarocci tubes have been successfully used in a number of experiments. They have been proven to rugged devices that can be mass produced at a relatively low cost (Ref. VII.1).

The Iarocci planes will be constructed from 8-tube modules 250 cm long. The structure of an 8-tube module is shown schematically in Fig. (VII.3). The module is constructed from an open PVC profile with eight 0.9×0.9 cm^2 cells separated by 0.1 cm thick walls. The profile is coated on the interior with a high resistivity graphite paint to form the cathode surface. A 100 μm diameter Cu/Be wire is strung down the center of each cell, supported approximately every 50 cm by PVC spacers. The profile is inserted into a PVC sleeve and sealed at each end by an endcap to form the gas volume. The endcap assembly provides connections for HV and gas. The overall width of the module is approximately 8.4 cm. The Iarocci planes consist of 30 modules containing 240 wires.

The Iarocci modules are inserted into a large 2.5×2.5 m^2 outer sleeve to form a completed Iarocci plane. This double sleeve arrangement allows for easy replacement of the 8 tube modules should that become necessary. To accommodate the copper coil for the toroid, the central 8-tube module will consist of two 120.0 cm long modules. These two modules will be separated by 8.6 cm in the center to form the opening for the copper coils.

The outer sleeve is constructed of 1/6 in. thick glass-steel laminate with copper cladding on each side. The laminate will be routed on one side to form 0.9 cm wide copper strip to provide the readout for the Iarocci tubes. The strip will run vertically on one side and horizontally on the other side to form simultaneous x-y readout.

Iarocci tubes are conventionally operated using a gas mixture of 25% Argon and 75% of isobutane. This gas mixture however has the disadvantage of being extremely flammable. The SLD collaboration has investigated nonflammable gas mixtures for use in the SLD Warm Iron Calorimeter (Ref. VII.2). These studies indicate that a mixture of

2.5% Argon, 9.5% isobutane, and 88% CO_2 posses the same operating characteristics as the Argon-isobutane mixture, but is considered nonflammable by the U.S. Bureau of Mines. This gas mixture will be used and the Iarocci tubes operated at a voltage of approximately 4.9Kv. The resulting signals should be sufficiently large to avoid signal-to-noise problems and allow the use of low-cost front end electronics.

Assembly:

The toroid modules will be constructed as single units by stacking planes of iron, Iarocci tubes, and scintillator on a support structure. Once all the planes have been installed, the copper coils of the toroid will be installed and finally gas, cooling water, and electrical connections will be made to form a completed module. It is assumed that the experimental hall is of sufficient size to allow the construction *in situ*.

Trigger and Data Acquisition Electronics:

Three types of triggers are required for the experiment:

1. A "machine trigger" which defines a 400 μsec interval, during which the time of each Iarocci chamber hit is written into digital memory with a 100 nsec resolution, and the photomultiplier times are recorded with a 3 nsec resolution.
2. A "background trigger" which produces the same recording process as the "machine trigger", but is generated when the machine is "off".
3. A "cosmic ray calibration trigger" which selects cosmic ray muons that penetrate a significant number of detector planes. A coincidence of 2 or more widely spaced scintillator planes trigger the detector readout. In this mode the memory time base is shortened to about 1 μsec so that hits older then 1 μsec are overwritten providing a memory record of the last 1μsec.

Iarocci Tube Readout:

Signals from the readout strips are discriminated by "time over threshold" comparators with the outputs stretched to at least 150 nsec and sampled every 100 nsec. Each output is written into 1 bit of a 4K byte memory where the address is driven by a 12 bit counter that is incremented every 100 nsec during the trigger interval. The memories are readout at the end of the trigger interval with times assigned according to the addresses of the hits.

The readout is organized into cards that mount on the chambers and contain the comparators, memory, and control for 96 channels. Readout strips are connected to the card with short mass terminated flat cable. A clock and test pulse is sent to each card via an "equal time fanout system".

The storage for signals is provided by 4K byte memory chips. Each memory is readout via a local bus in 0.5 msec. This bus is daisy chained from card to card for x-planes and separately for y-planes. Each bus is cabled to a crate mounted "encoder card" where the data is zero suppressed. The "encoder card" sends an 8 bit memory select address with 4096 "read increments", resulting in a readout time of less then 50 μsec.

The "encoder card" assigns a time equal to the address of each leading edge hit and a signal address. The data is stored internally so that the encoders can operate simultaneously. The data is then sent to a crate link card connected to the crate back plane. The crates are distributed along the detector and linked with "twist and flat" cable. The system is completely data driven, where the data stream to the data acquisition computer is written to memory via a data channel with a flag bit in the data to distinguish data types, and an interrupt to signal the completion. A separate control link provides commands and diagnostic data to the crates.

Photomultiplier Readout:

The photomultiplier signals are discriminated and sorted into 100 nsec time bins using the same clock as the Iarocci readout system. A linear interpolation time with a 3 nsec resolution is produced by integrating a constant current over the interval from the discriminator leading edge to the following clock edge and digitizing the output with a 7 bit FADC. The direct photomultiplier signal can also be stretched and sampled with a second 10 MHz FADC and written into a second 4K byte memory. Flag bits are written into those words containing discriminated data.

As with the Iarocci system readout, the 4K byte memories are addressed by 12 bit counters incremented every 100 nsec during the trigger interval. During readout, an absolute time is assigned to flagged words from the memory address along with the interpolation time and pulse height.

The readout is organized into cards for 8 photomultiplier outputs containing the discrimination, pulse sorting, time interpolation, pulse height, memory storage, and readout functions. A clock and test pulse input are included on each card. The cards mount in crates and use the same crate link and data driven structure as the Iarocci readout system.

TABLE VII.1

DETECTOR SUMMARY

Dimensions	$8.4 \times 8.4 \times 183.0 ft^3$
Tonnage	1.2K tones
Number of Iarocci Tubes per plane	240
Number of electronics Channels per plane	480
Number of planes of Iarocci tubes	600
Total number of Iarocci Tubes	144,000
Total number of electronics channels	288,000
Number of planes of scintillator	60
Number of photomultiplier tubes	120

System Control:

Trigger type information is distributed via the control links. Trigger timing is implicit in the fast clocks which are sent as bursts during the trigger interval with the required number of cycles. The clock is generated centrally and fanned out with equal times to all front end data acquisition elements. Memory address counters are reset from the leading clock.

Data is written directly to computer memory via the data channel input. Higher level triggers are carried out in software. The data is ordered by readout according to event number, data type, increasing signal number and time. Interrupts are used to indicate the completion of data streams, starting addresses, and word counts. A multiple event buffer space is setup in computer memory so that the event processing time can be averaged over many events for efficient utilization of the processing bandwidth. The computer regulates the data acquisition by inhibiting triggers whenever the processing gets to far behind. Error flags and diagnostic data inserted into the data stream, together with the test pulse system, provide for system maintenance.

Detector Summary

The physical characteristics of the detector summarized in Table VII.1. Event rates are based on one year of running time.

Rough Cost Estimate

A rough cost estimate for the construction of the proposed detector and electronics has been made and is summarized in Table VII.2

TABLE VII.1

COST SUMMARY

		Module	15 Modules
Toroid:	Steel	$70,000.	
	Coils	7,000.	
	Support Structure	25,000.	
	Total Toroid	102,000.	$1,530,000.
Iarocci Tubes		54,000.	810,000.
Scintillator		8,000.	120,00.
Electronics:	Iarocci Tubes	123,000.	
	PMT bases	1,000.	
	Total Electronics	124,000.	1,860,000.
Sub Total		$288,000.	$4,320,000.
40% Contingency		115,000.	1,728,000.
Total		$403,000.	$6,045,000.

Section VIII DETECTOR LOCATION

There are three viable locations for situating the detector that would be used in this experiment. The beginning of the detector should be located 15 meters downstream from the end of one of the three straight sections of the Debuncher. While any of these three locations would be suitable for the physics program of this experiment, there are different practical and topological complications associated with each of the three potential locations. The least expensive and least perturbing location for an experimental pit to house the detector would require a detailed analysis by the Fermilab Construction Engineering Section. Consequently, in this section the size of the experimental pit is selected to illustrate the approximate construction costs.

The proposed experimental pit would bear a strong resemblance to an accelerator beam enclosure, such as the Antiproton Rings Enclosure which houses the Debuncher and Accumulate rings. In addition, the construction techniques used to build the experimental pit would probably rely upon existing methods for constructing beam enclosures.

The experimental pit that is needed to house the detector would be approximately 200 feet long and 20 feet wide. In making a rough estimate of the major civil construction costs, one assumes that a concrete floor 3 feet thick, concrete walls 1.5 feet thick, and a concrete ceiling 2 feet thick would be adequate. For a pit of this size the volume of dirt that would have to be excavated is $(200' \times 20' \times 23') = 3430$ cubic yards. Assuming a figure of \$7/(cubic yard) for excavation of dirt yields a cost of \$24K. The concrete walls, floor and roof of the pit would require 35,000 cubic feet of concrete. Using a cost estimate of \$280/(cubic yard) for the concrete yields a cost of \$336K.

The thrust of these crude cost estimates is to point out that the civil construction costs of the experimental pit are reasonable. A more accurate estimate of the cost of constructing the experimental pit would require a professional analysis by the Fermilab Construction Engineering Section.

Appendix A

We have measured the flux of circulating muons in the Debuncher by employing a slight modification of a technique used by G. Dugan in 1987 to measure the number of pions and electrons which get injected into the Debuncher. This technique relies upon the use of a non-destructive, ref pickup to measure the bunch structure of the beam on a turn-by-turn basis.

The beam arrives in the Debuncher, at the location of the pickup, in 84 narrow bunches ($\sigma_t \approx 1$ nsec) with a spacing of about 18 nsec. The fast particles (pions, muons and electrons) are separated from the slow particles (antiprotons) by about 8 nsec and hence fast and slow particles can be identified by looking at the time structure of the output from the ref pickup. As the beam circulates in the Debuncher, the pions decay in a few turns ($\gamma c\tau_\pi \approx 1$ turn), while the electrons spiral into the low energy edge of the machine, due to the emission of synchrotron radiation, and are lost after 14 turns. After more than 14 turns the only particles left are muons and antiprotons.

The results of turn-by-turn measurements made in 1987 are summarized in Fig. A1. In these data there was no indication of a signal representing circulating muons - which are expected to be the only fast particles remaining beyond turn number 14. The absence of a "bunched" muon signal for turn 15, however, is not necessarily an indication that there are no muons in the debuncher. This can be understood by calculating the muon debunching time:

$$T_D = \frac{(\Delta T)_{ref}}{\frac{\eta \delta P}{P}}$$

For muons, $\eta = .017$ and $T_D = 27.6\mu$sec (17 turns), i.e., the muons are completely debunched after 17 turns and, consequently, induce no signal on the ref pickup. We have checked the rate at which muons debunch by performing a simulation which uses the longitudinal difference equations to study the bunch shape as a function of turn number in the Debuncher. The results, shown in Fig. A2 for a bunch injected ($N = 1$) with $\Delta t = \pm 0.5$ nsec and $\delta P/P = \pm 2.0\%$, illustrate the rate at which the injected muons debunch and indicate complete debunching in 15–17 turns. The ref pickup technique is thus not sensitive to circulating muons in turns beyond turn 14.

An examination of Fig. A1 suggests that it is straight-forward to measure the bunched muon signal by killing the electrons in the beam prior to injection into the Debuncher and then measuring the number of fast particles on turns 5–11 using the ref pickup.

The most appealing method for killing the electrons is to insert a lead radiator at the end of the AP-2 transport line. Between the last two quadrupoles in this line (IQ32 and IQ33), the betatron amplitudes are reasonably small (4–8m.) and the emittance blowup of the muon bunches due to multiple scattering should be small.

We have studied the effectiveness of radiator thicknesses of 0.25, 0.50, and 1.0 radiation lengths on removing electrons from the beam at the end of the AP-2 transport line. The program EGS was used to determine the energy of the leading (maximum energy) electron exiting the radiator for electrons of energy 9.0 GeV incident on the radiator. (The simulation was also checked analytically using a formula from Tsai [Ref. A.1].) The results are shown in Figure A3. If we impose an 8.7 GeV cut on the electron energy for it to be captured in the Debuncher, then for radiator thicknesses of 0.25, 0.50, and 1.0 radiation length, 40%, 11%, and 0.15% respectively of the incident electrons will survive the cut. We have chosen to use a radiator thickness of 1 radiation length in order to guarantee that electrons do not contribute to our muon signal.

Our measurements were performed, parasitic to the running of E-760, during the last several months. A one radiation length lead absorber was inserted into the AP-2 transport line completely eliminating electrons from the beam. We used a Tektronix DSA 602 digital sampling analyzer to measure the time structure of the signal from the pickup. The DSA 602 has an analog bandwidth of 1 GHz, samples at 2 Giga-samples/second, and has a memory depth of 32,000 samples. We could, therefore, capture data for nine turns during a measurement. The data were taken in the following manner. Each measurement was an average over 64 pulses (each pulse containing 84 bunches). We first captured data for turns 1 through 9 and then set the DSA trigger delay to capture turns 9 through 17. The two data sets were normalized such that the $\bar{p}$ flux for turn 9 was equal. Fig. A4 shows the raw data for approximately 10 bunches for turns 3,4, and 5. In turns 3 and 5, we see the 8 nsec separation between the $\beta = 1$ particles and the $\bar{p}$'s. On the even turns, the $\bar{p}$ bunches are approximately in time with the $\beta = 1$ particles and thus the ref bunch structure shows only one peak. Therefore, in order to determine the individual particles fluxes, only data from the odd turns was usable. For each of the odd turns between turns 3 and 11, we averaged 60 of the 84 bunches to produce a "bunch averaged" time structure for each of the turns. The data for turns 5,7,9, and 11 are shown in Fig. A5. These data were fit to two Gaussians plus a constant (the fit curves are also shown in Fig. A5). From the fit parameters (amplitude and σ) we could then determine, for each turn, the area under the two Gaussians. These numbers are directly proportional to the flux of $\beta = 1$ particles and

$\bar{p}$'s. In order to determine the flux of muons, we then only had to make a correction for the number of pions remaining at each turn. In order to do this, we used the measured $\beta = 1$ particle flux from turn 1, assumed that this entire flux was due to pions, calculated the number of pions remaining after each turn, and then subtracted that number from the measured $\beta = 1$ flux for that turn to determine the number of muons. Our results are shown in Table A1 for turns 3–11.

Table A.1

Particle Flux Measurements

Turn	Flux($\beta = 1$)	Flux($\bar{p}$)	$\frac{(\beta=1)}{\bar{p}}$	$\frac{\mu}{\bar{p}}$
1	33572	—	—	—
3	6251	2126	2.94	0.80
5	2232	1287	1.73	1.12
7	1597	1171	1.36	1.27
9	1306	1132	1.15	1.14
11	934	1122	0.83	0.83

We have also modeled the AP-2 line and the Debuncher ring in a DECAY_TURTLE simulation in order to compare our muon flux measurements with expectations. The simulation uses measured magnetic field strengths and gradients for the beam line and ring magnets, and measured apertures for all elements. Particles are ray-traced from the target station, through the AP-2 beam line, through the Debuncher injection channel and through the first three revolutions in the Debuncher. We compare the results of the simulation to the muon flux measurements by calculating the ratio of the expected number of muons after three turns in the ring to the number of pions at the end of the beam line. An ion chamber measurement of the pion flux at the end of the beam line allows us to normalize the calculation.

This model calculation of the circulating muon flux accounts for the contribution from pion decay in both the beam line as well as the ring, and consequently should be directly comparable to the muon flux measurement. The calculated flux agrees with the experimental data to within 10% and reinforces our belief that we have a reasonably good representation of the aperture limitations in both the transport line and the Debuncher ring.

REFERENCES

Ref II.1: BNL Neutrino Workshop, M. Murtagh Ed., 1987.

$\nu_e \rightarrow \nu_\mu$

BNL 776: Borodovsky, Ph. D. disertation, Columbia University (1991), Physical Review Letter to be published.

BNL 734 : L. Ahrens et al., Phys. Rev. D31, 2732 (1985).

CHARM: R. Eichler, Nucl. Phys. B (Proc. Suppl.) 3, 389 (1988).

BEBC PS: C. Angelini et al., Phys. Lett. 179B, 307(1986).

LAMPF: T. Dombeck et al., Phys. Lett. 194B, 591 (1987).

GOSGEN: G. Zacek et al., Phys. Rev. D34, 2621 (1986).

$\nu_e \rightarrow \nu_\tau$

BEBC SPS: O. Erriquez et al., Phys. Lett. 102B, 73 (1981).

FNAL 531: N. Ushida et al., Phys. Rev. Lett. 57, 2897 (1986).

FNAL B.C. (Bubble Chamber): N.J. Baker et al., Phys. Rev. Lett. 47, 1576 (1981).

LAMPF : P. Nemethy et al., Phys. Rev. D23, 262 (1981).

$\nu_\mu \rightarrow \nu_\tau$

CCFR: I. E. Stockdale et al., Phys. Rev. Lett. 52, 1384 (1984).

CDHS: F. Dydak et al., Phys. Lett. 134B, 281 (1984).

CHARM: F. Bergsma et al., Phys. Lett. 142, 103 (1984).

Ref II.3: S.P. Mikheyev and A.Yu. Smirnov, Nuovo Cimento 9C, 17 (1986);

L. Wolfenstein, Phys. Rev. D17, 2369 (1978).

Ref II.3: W.J. Marciano, "Neutrino Physics – A Theoretical Perspective" BNL Neutrino Workshop, M. Murtagh Ed., 1987.

Ref II.4: J.J. Simpson, PRL 54, 1891 (1985).

Ref III.1 Bromberget al., Nuclear Physics B107, 82 (1976).

Ref III.2 P.A. Aarnio et al., " A Long Writeup of the FLUKA86 Program", CERN Divisional Report TIS-RP/168 (1986).

Ref III.3 B.F. Bayanov, T.A. Vseolozhskaya, Yu.N. Petrov, and G.I. Silvestrov

"The Investigation and Design Development of Lithium Lenses With Large Operating Lithium Volume."
(Novosibirsk, IYF), Proceedings, High Energy Accelerators, 587-590 (1988).

Ref IV.1 E.D. Cummins and P.H. Bucksbaum, "Weak Interactions of Leptons and Quarks", Cambridge Univeristy Press.

Ref V.1: N. Kondakis, Ph.D. Thesis, Columbia University (1989).

Ref V.2: P.G. Reuteus, Ph.D. Thesis, University of Chicago (1986).

Ref VII.1: W. Busza, "Experiance with Iarocci Tubes Produced on a Large Scale", Published in SLAC Colliding Beam, 210 (1987).

Ref VII.2 A.C. Benvenuti et al., Nucl. Instr. and Meth. A284, 339 (1989).

Ref A.1 Y. Tsai, Rev. of Mod .Phys. Vol. 46, No. 4, 815 (1974).

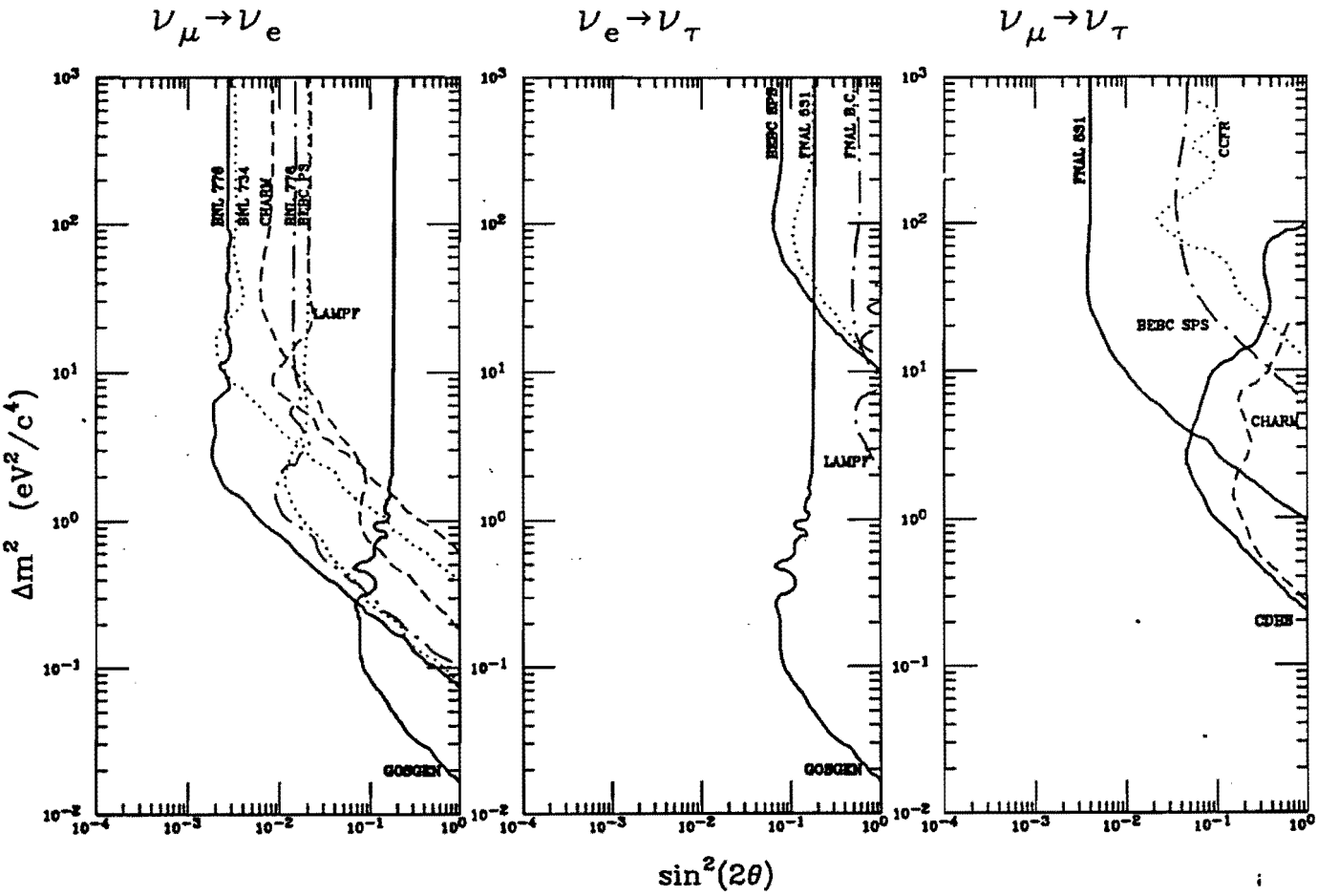

Fig. II.1: Current neutrino oscillation limits for a) $\nu_e \rightarrow \nu_\mu$, b) $\nu_e \rightarrow \nu_\tau$, and c) $\nu_\mu \rightarrow \nu_\tau$.

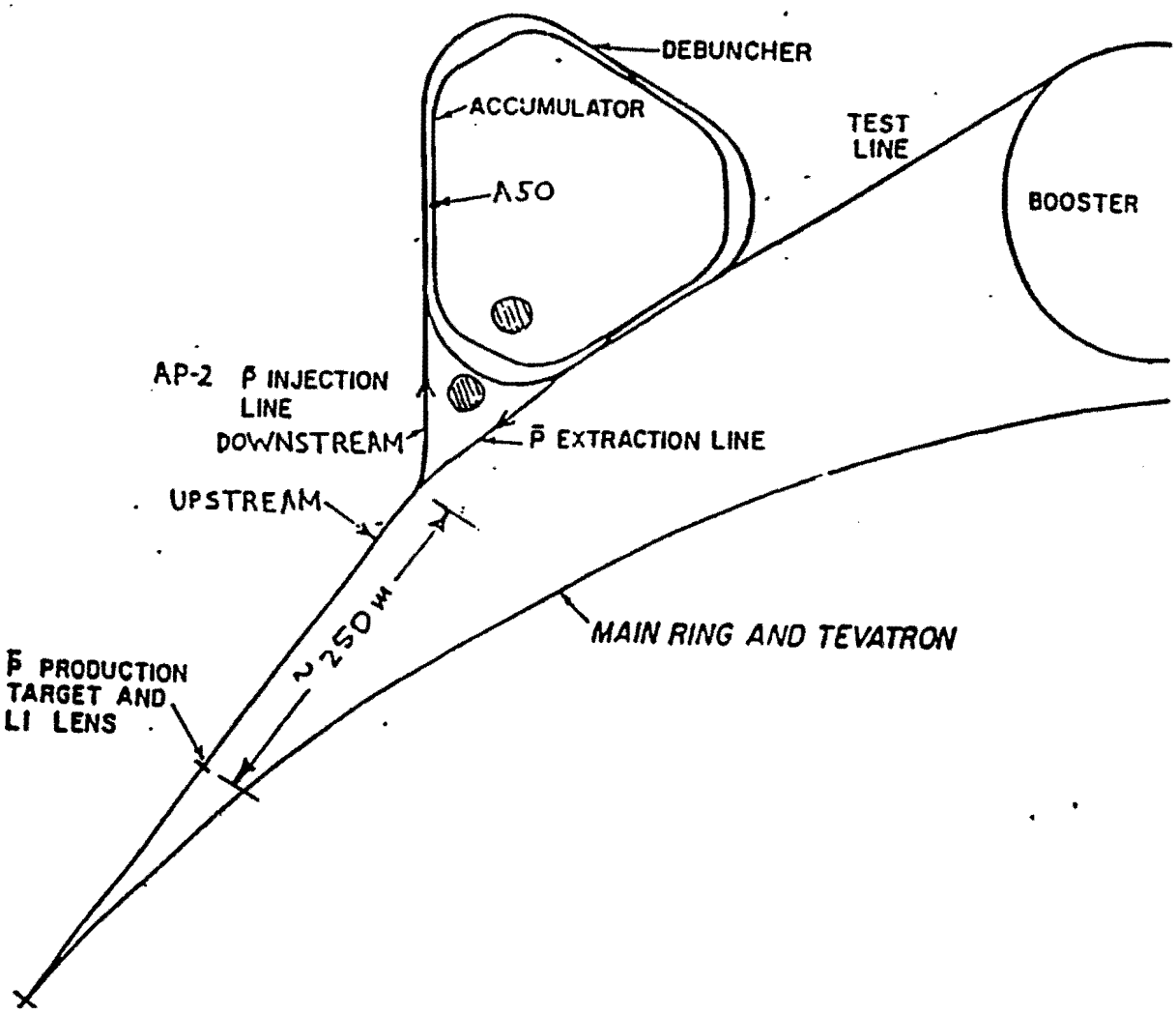

Fig. III.1: Fermilab Debuncher storage ring.

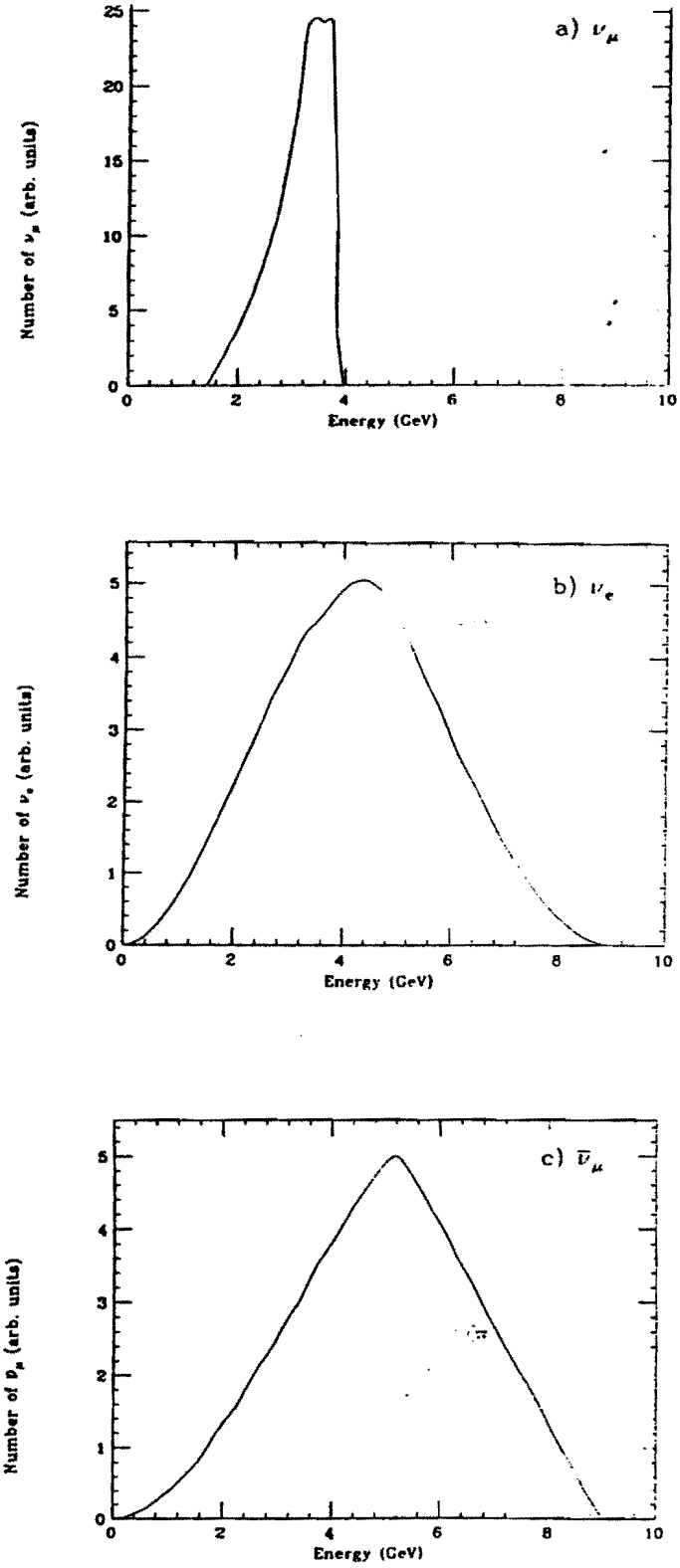

Fig. IV.1: ν_e energy spectra from the Debuncher with a 10 mrad cut. The Debuncher energy is 9 GeV.

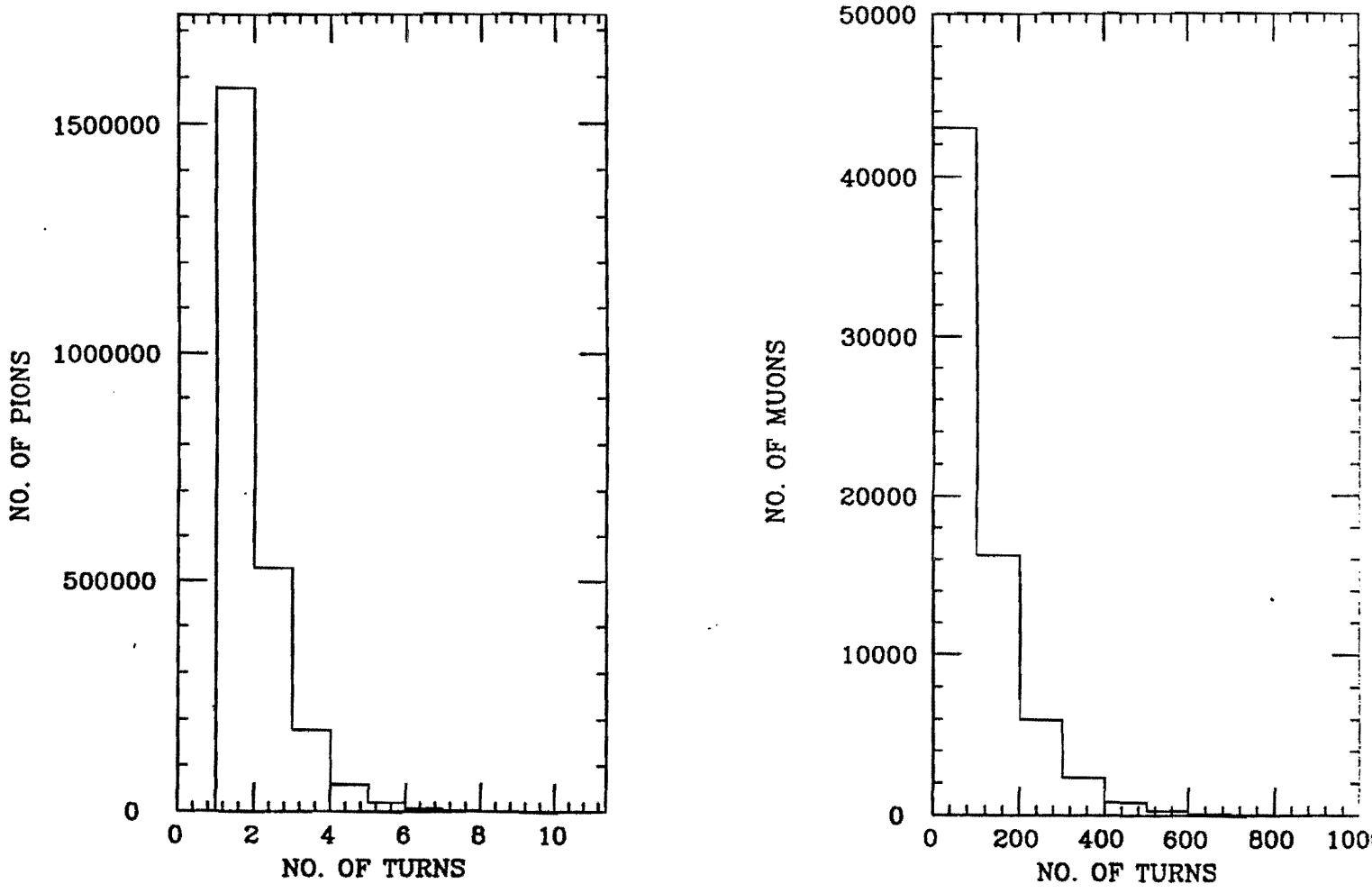

Fig. IV.2: The number of pions and muons in the Debuncher as a function of number of revolutions.

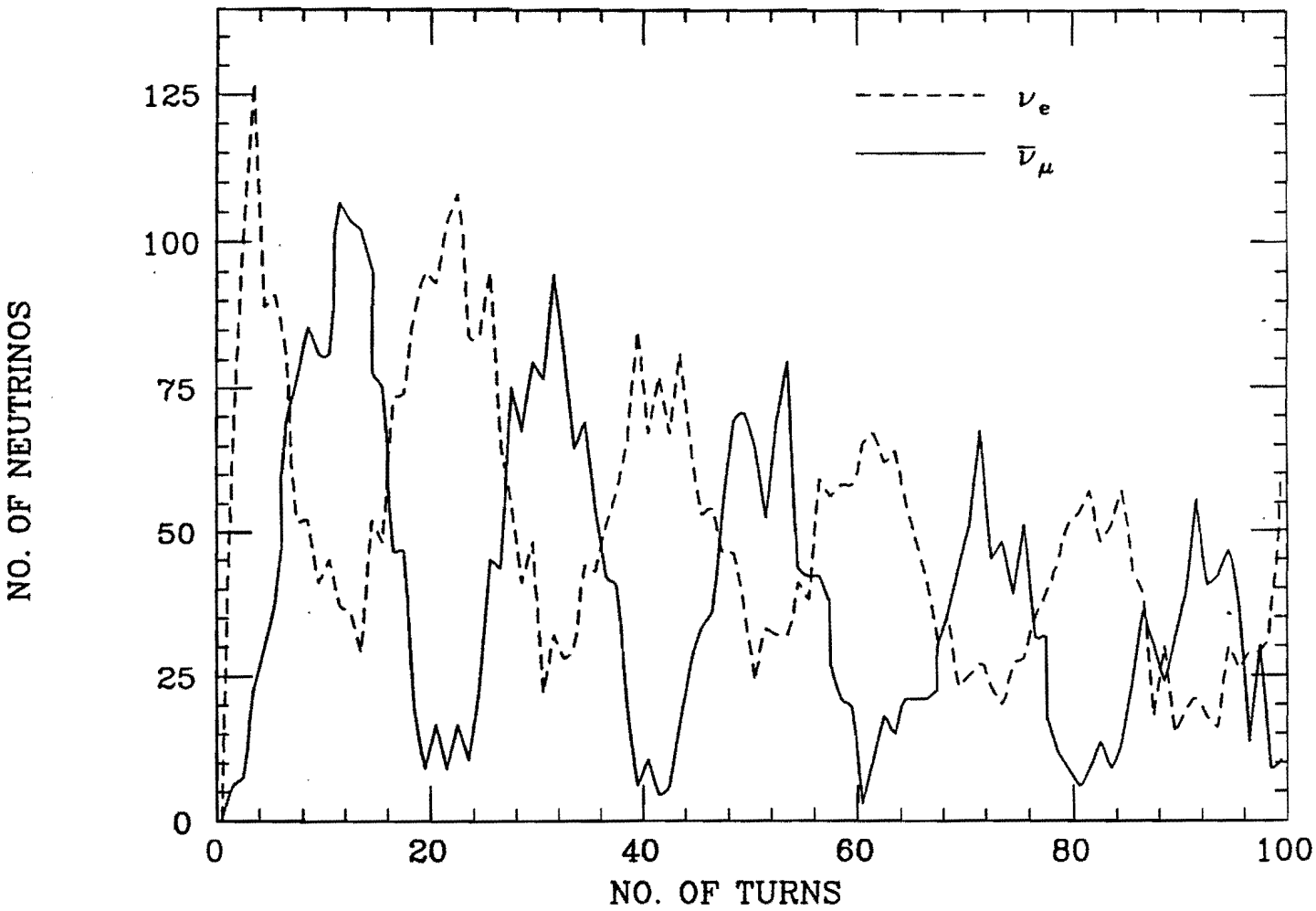

Fig. IV.3: The number of high energy ν_e and $\bar{\nu}_\mu$ accepted by the detector as a function of number of turns. A 10 mrad, 6 GeV energy cut is applied.

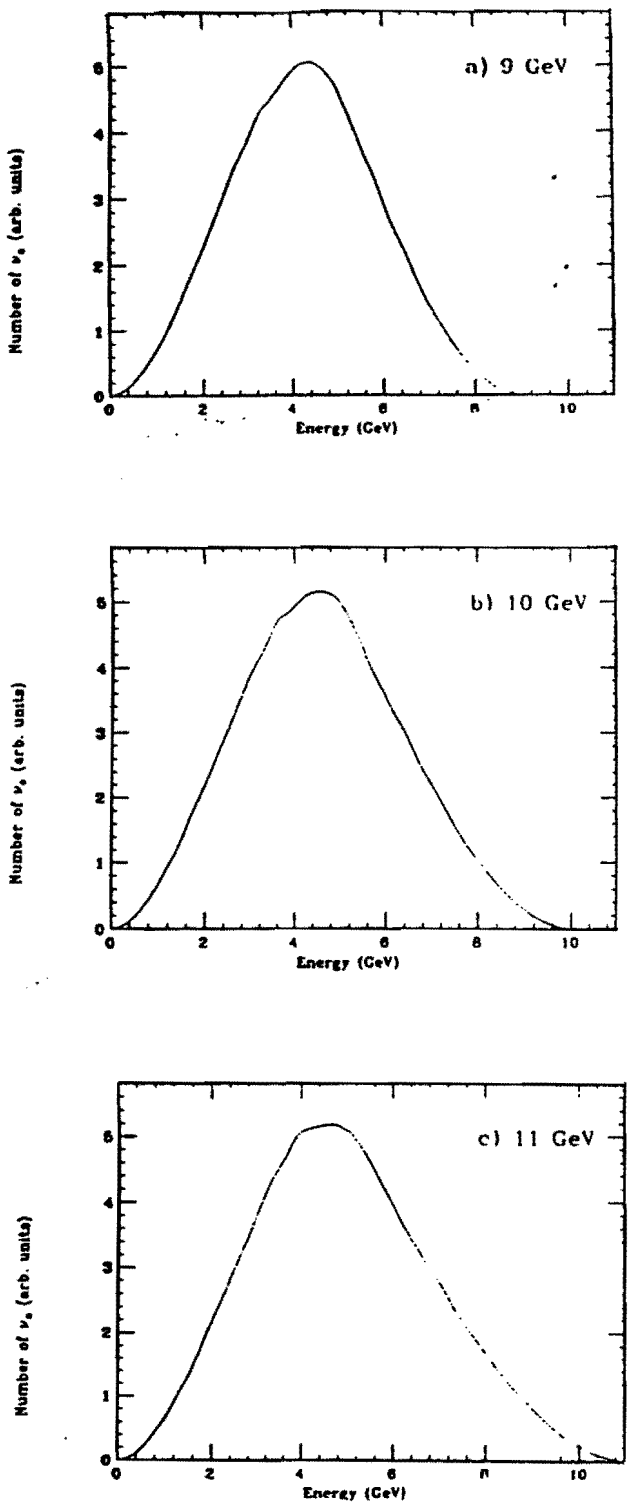

Fig. IV.4: ν_e energy spectra for Debuncher energies of a) 9 GeV, b) 10 GeV, and c) 11 GeV with a 10 mrad cut.

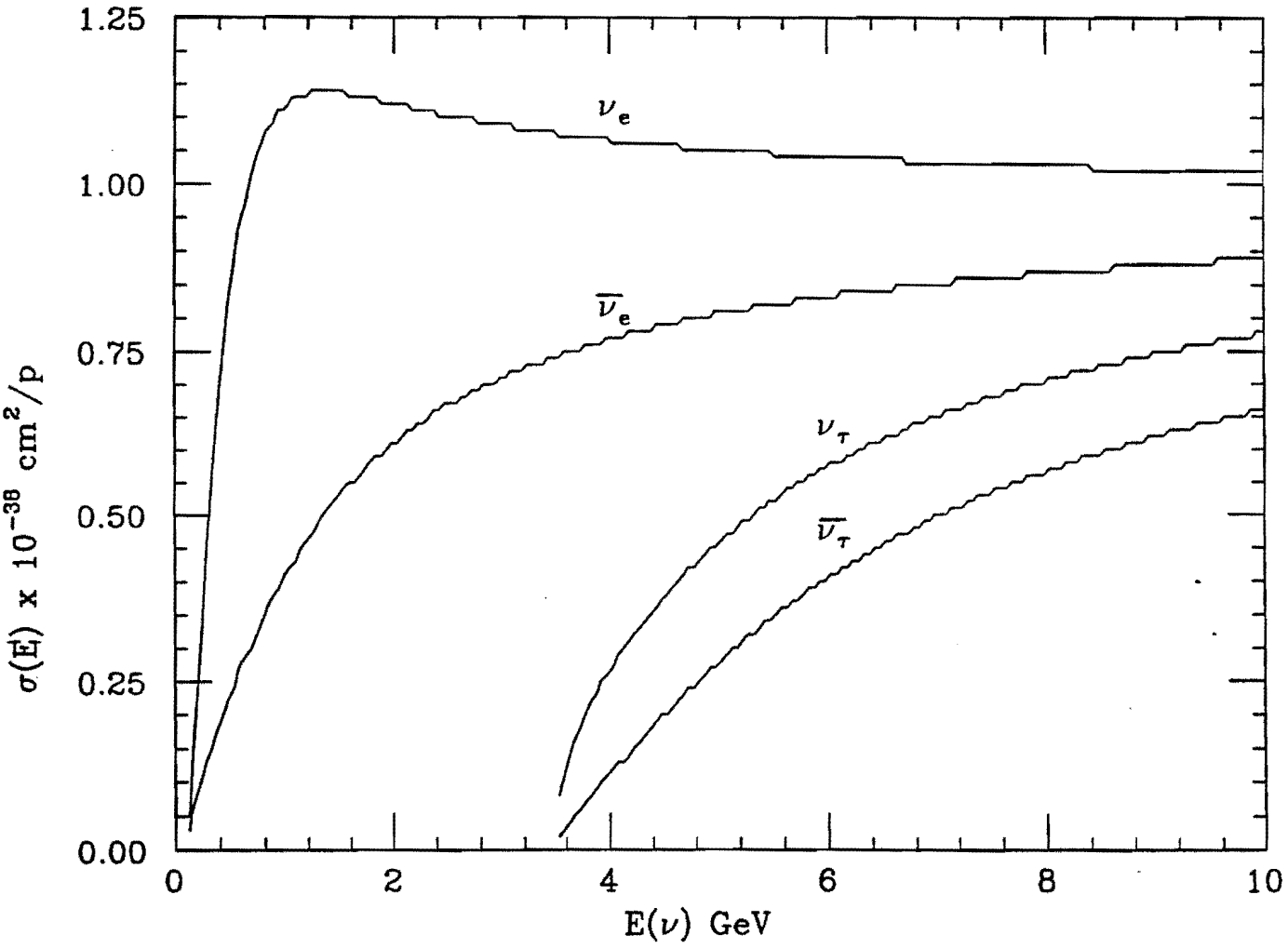

Fig. IV.5: Quasi elastic cross section for ν_e, $\bar{\nu}_e$, ν_μ, and $\bar{\nu}_\mu$.

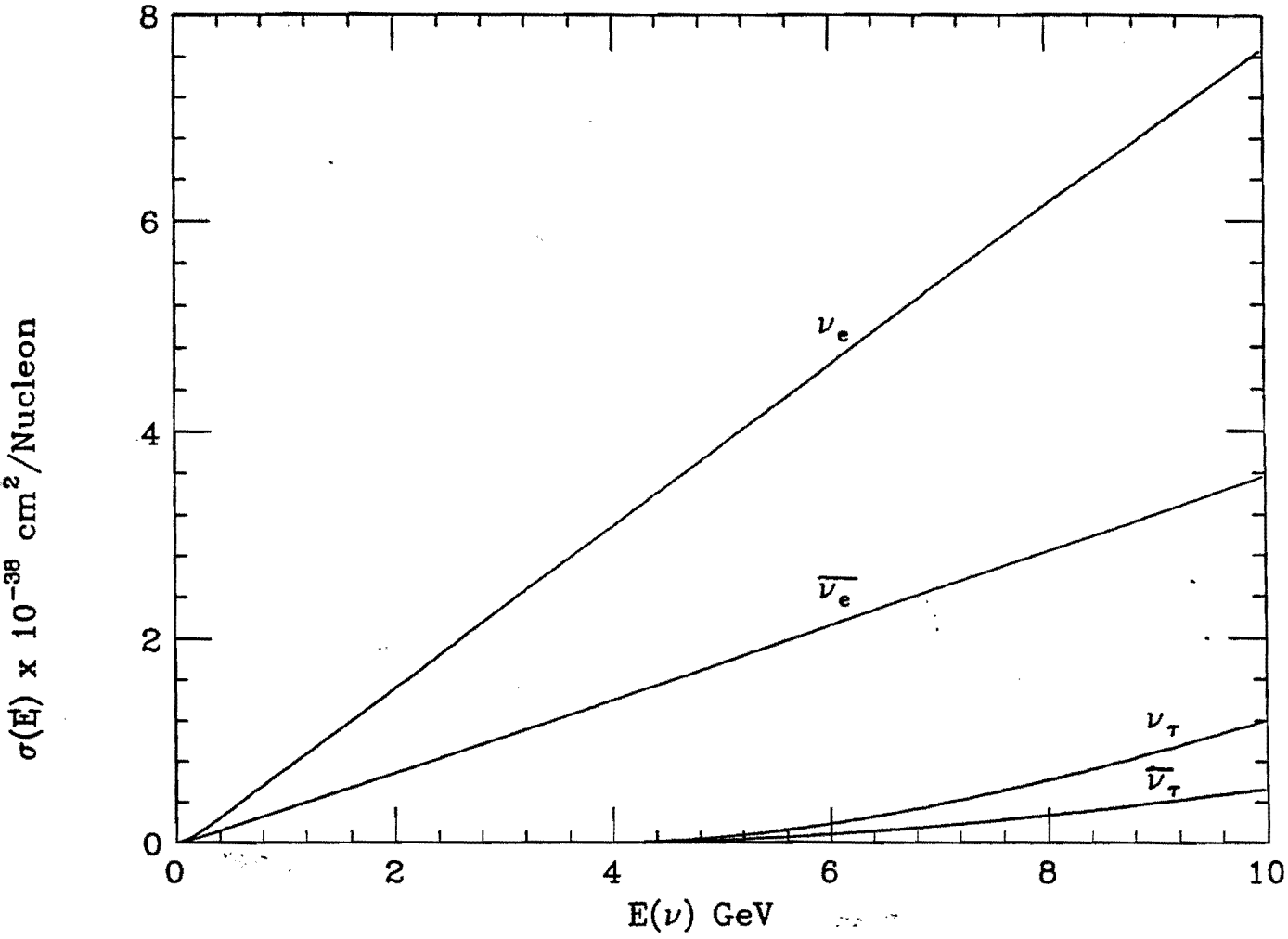

Fig. IV.6: Inelastic cross section for ν_e, $\bar{\nu}_e$, ν_μ, and $\bar{\nu}_\mu$.

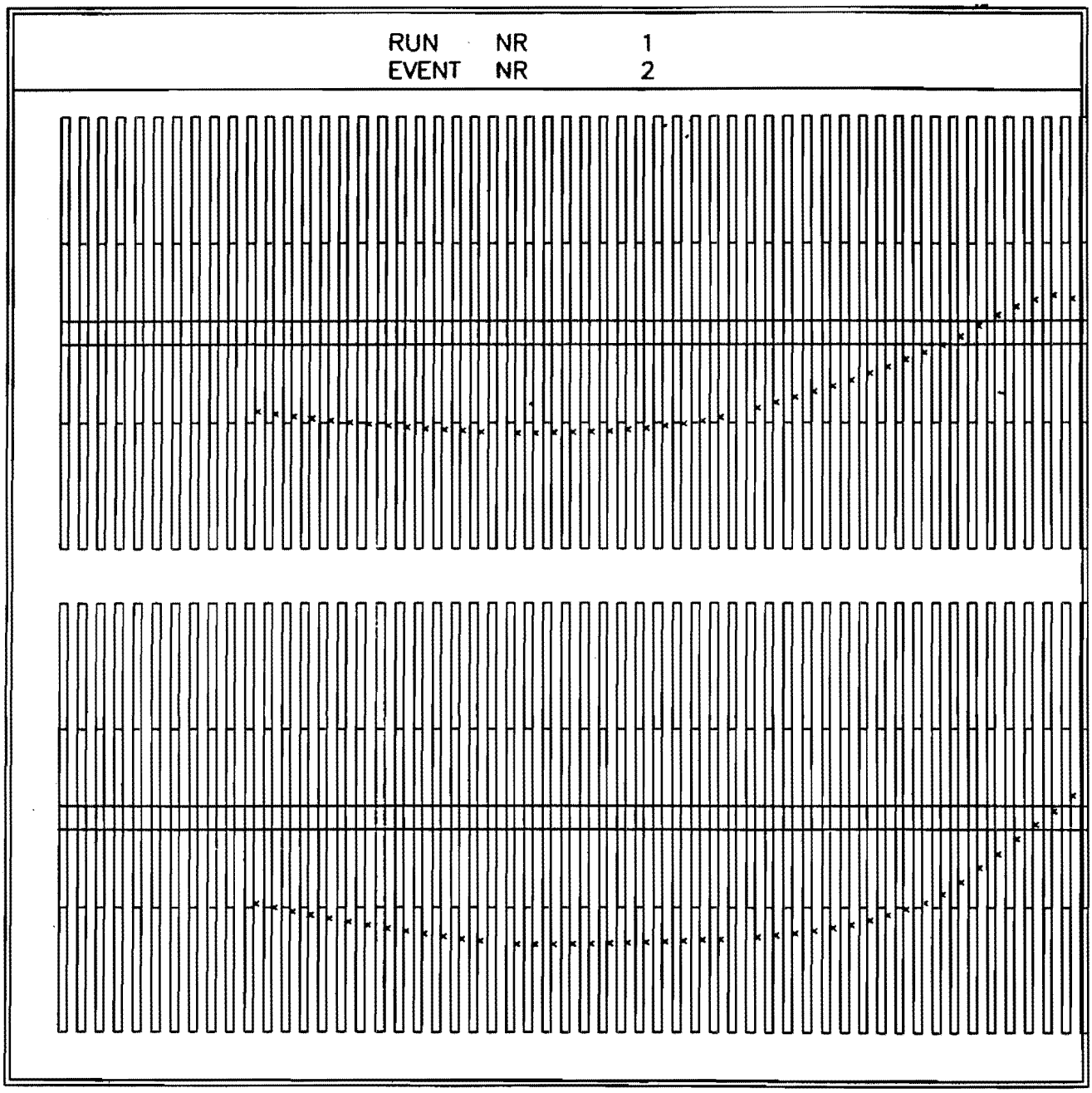

Fig. V.1: A typical quasi elastic τ event using a GEANT simulation of the proposed detector.

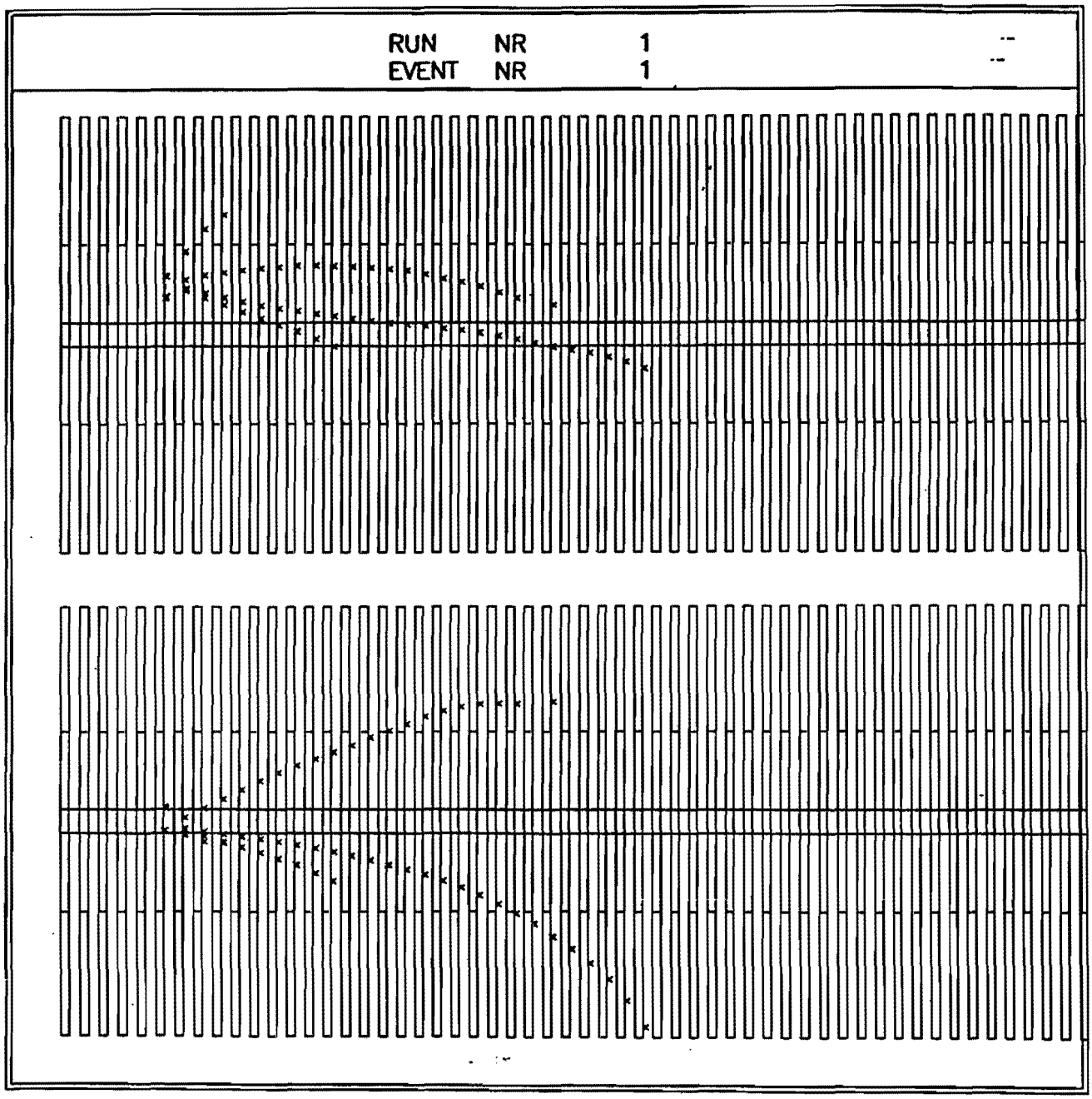

Fig. V.2: A typical charm event using a GEANT simulation of the proposed detector.

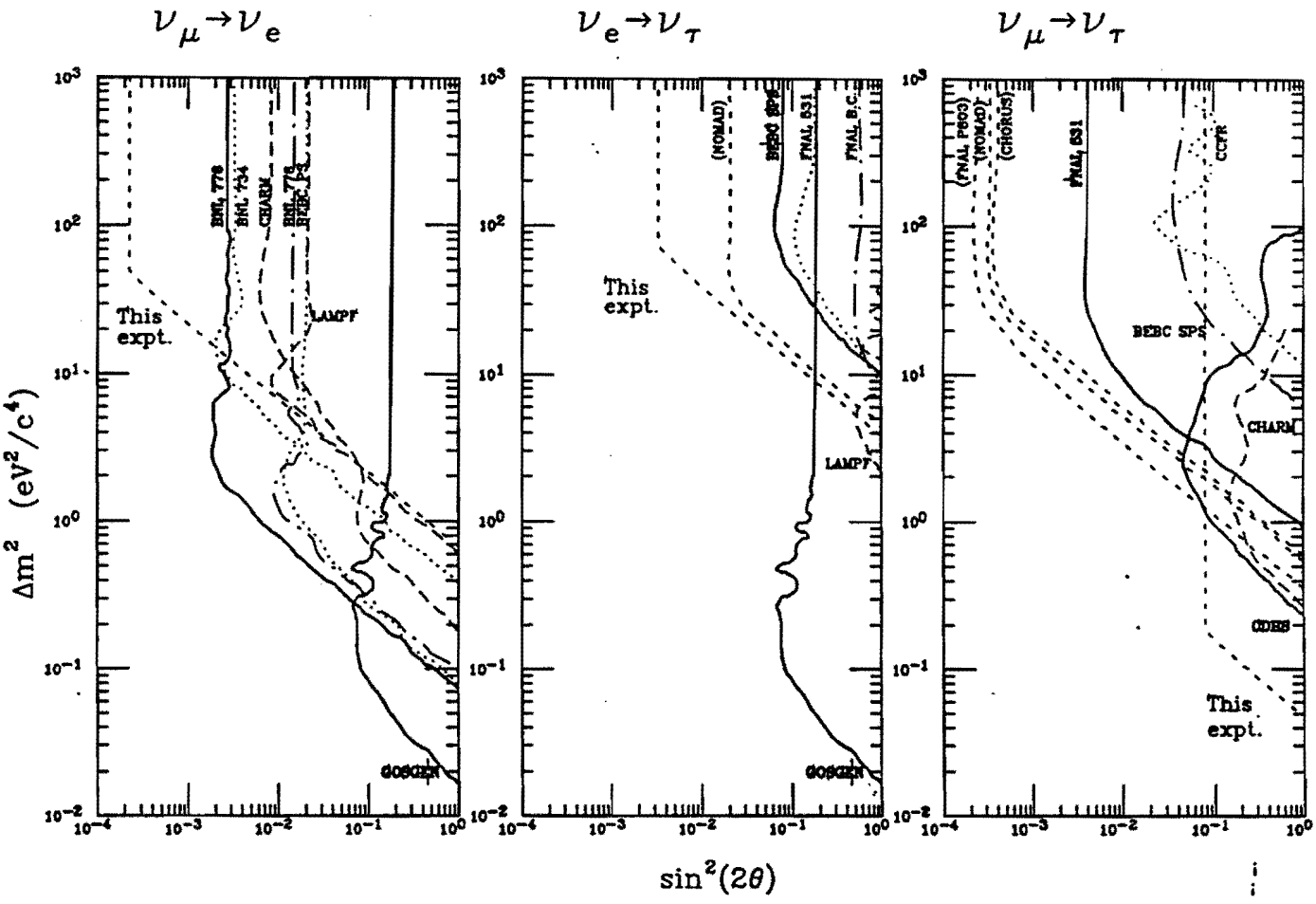

Fig. VI.1: Current neutrino oscillation limits for a) $\nu_e \rightarrow \nu_\mu$, b) $\nu_e \rightarrow \nu_\tau$, and c) $\nu_\mu \rightarrow \nu_\tau$. Proposed experimental limits included.

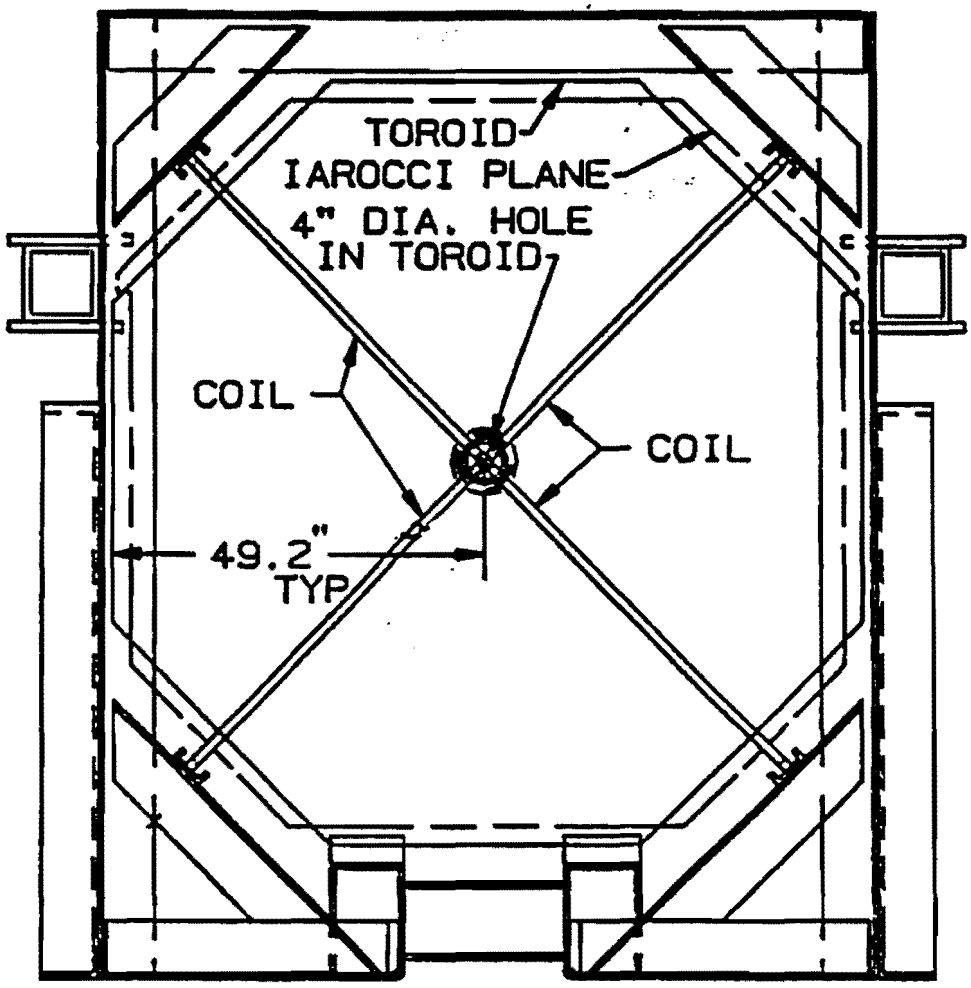

Fig. VII.1a: Schematic drawing of the proposed detector (front view).

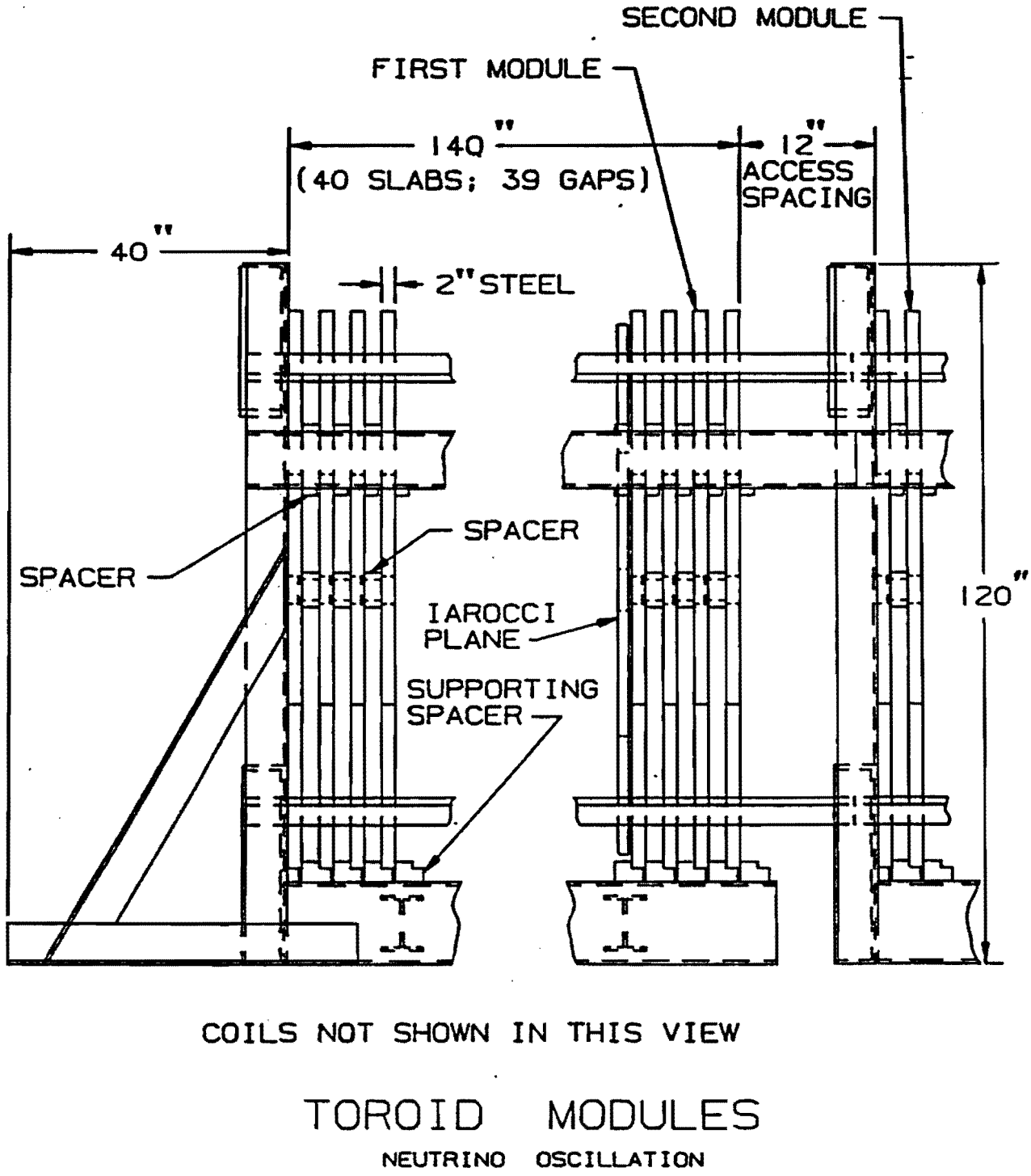

Fig. VII.1b: Schematic drawing of the proposed detector (side view).

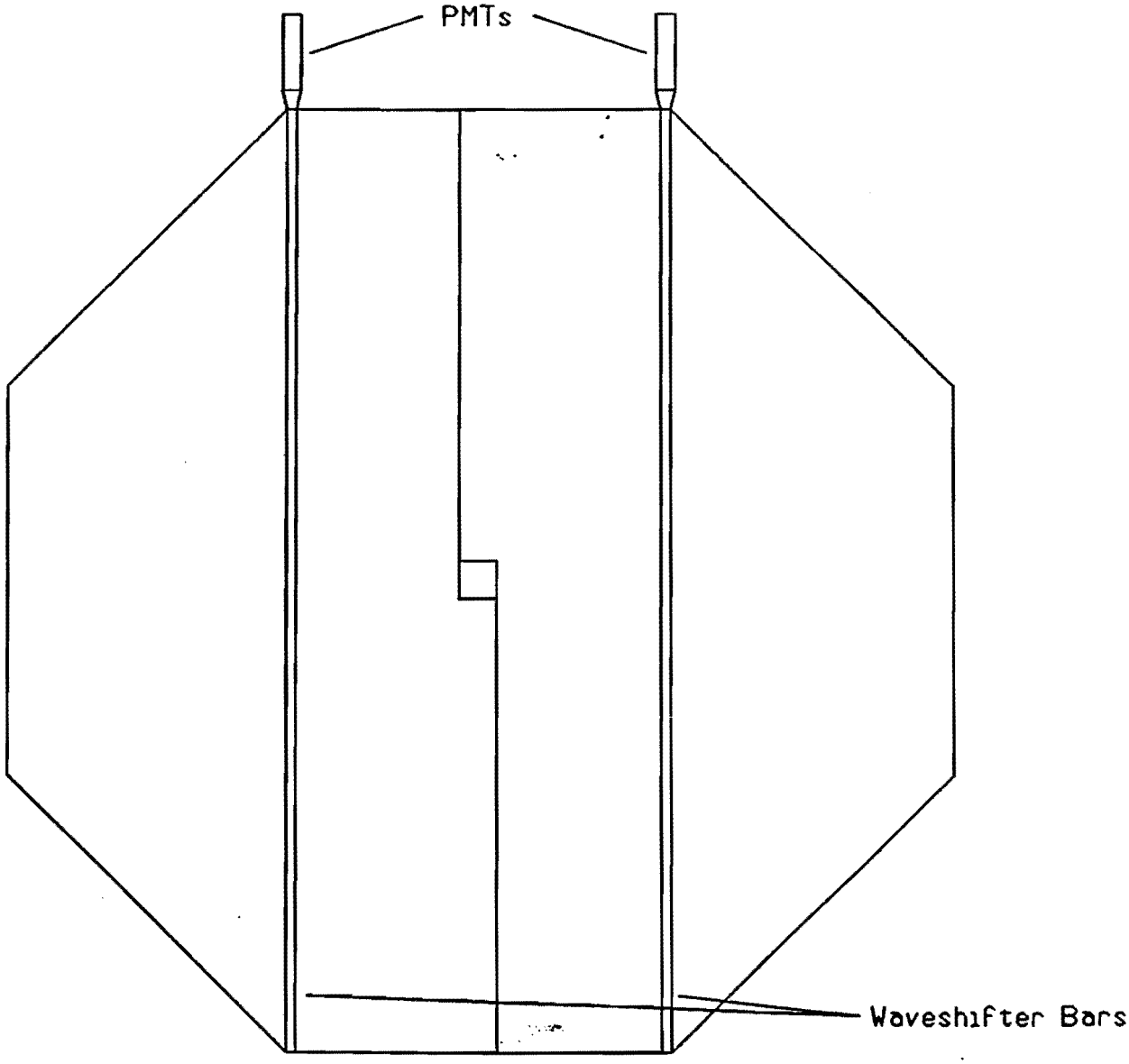

Fig. VII.2: Schematic drawing of a scintillator plane.

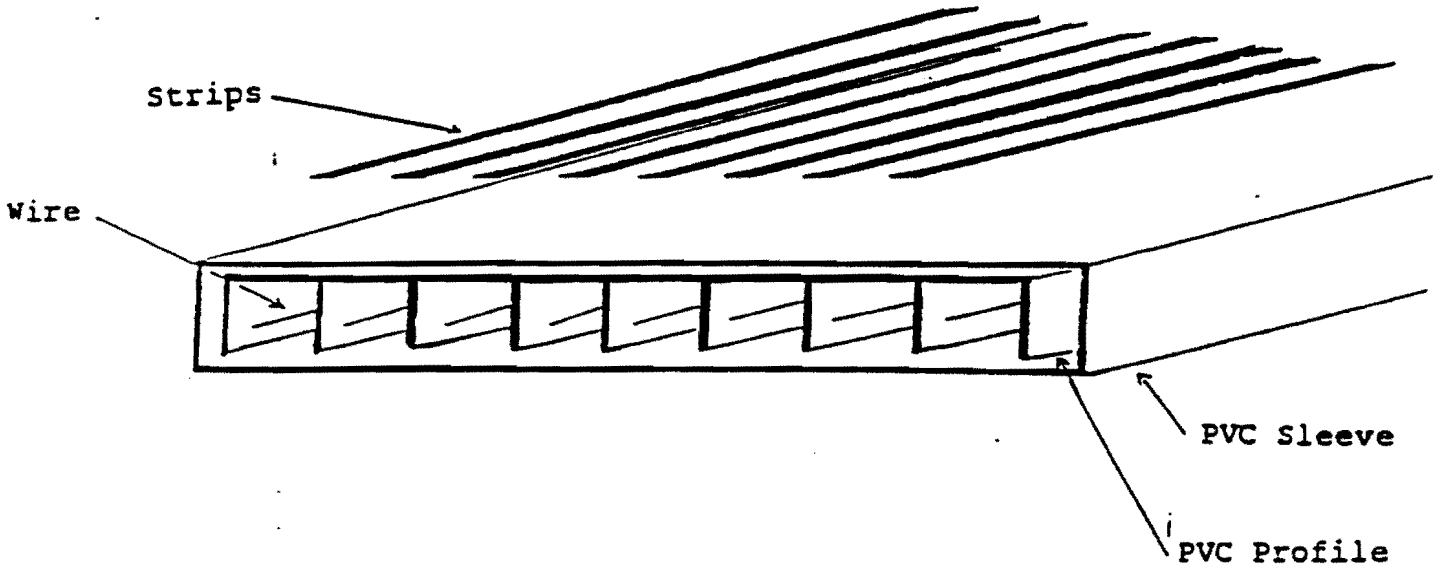

Fig. VII.3: Schematic drawing of an Iarocci tube module.

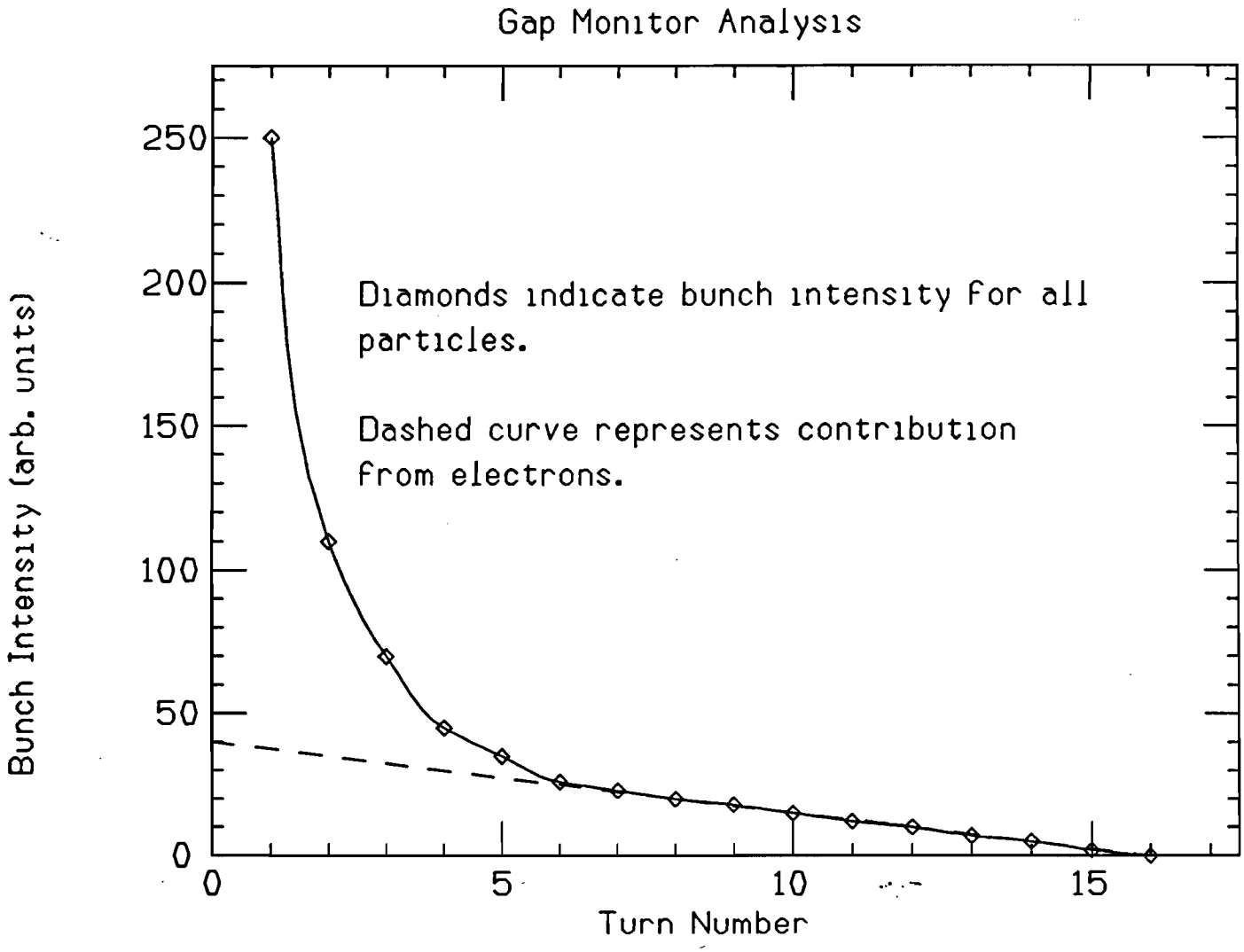

Fig. A1: 1987 μ flux measurement results.

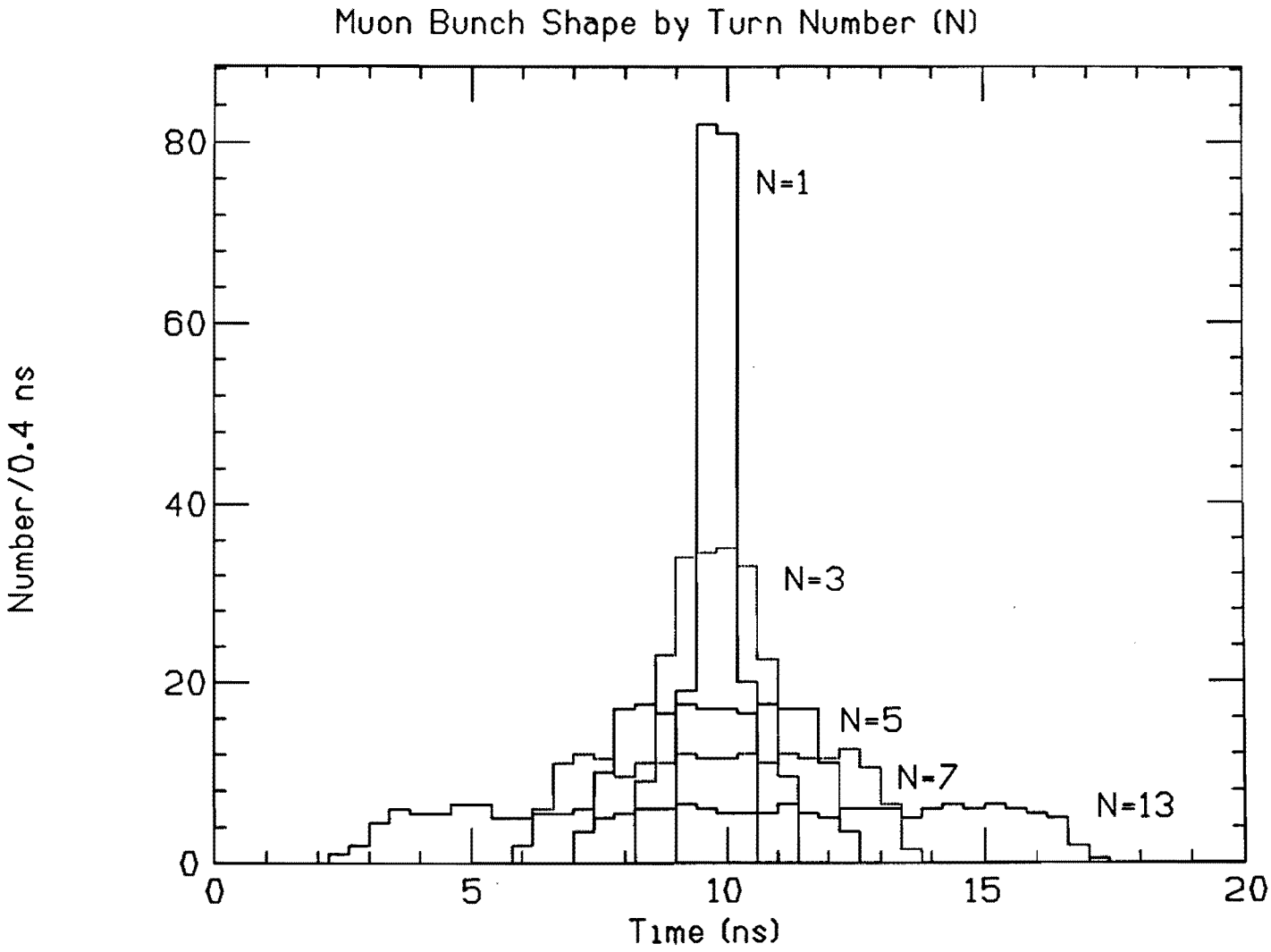

Fig. A2: μ bunch shape as a function of turn number.

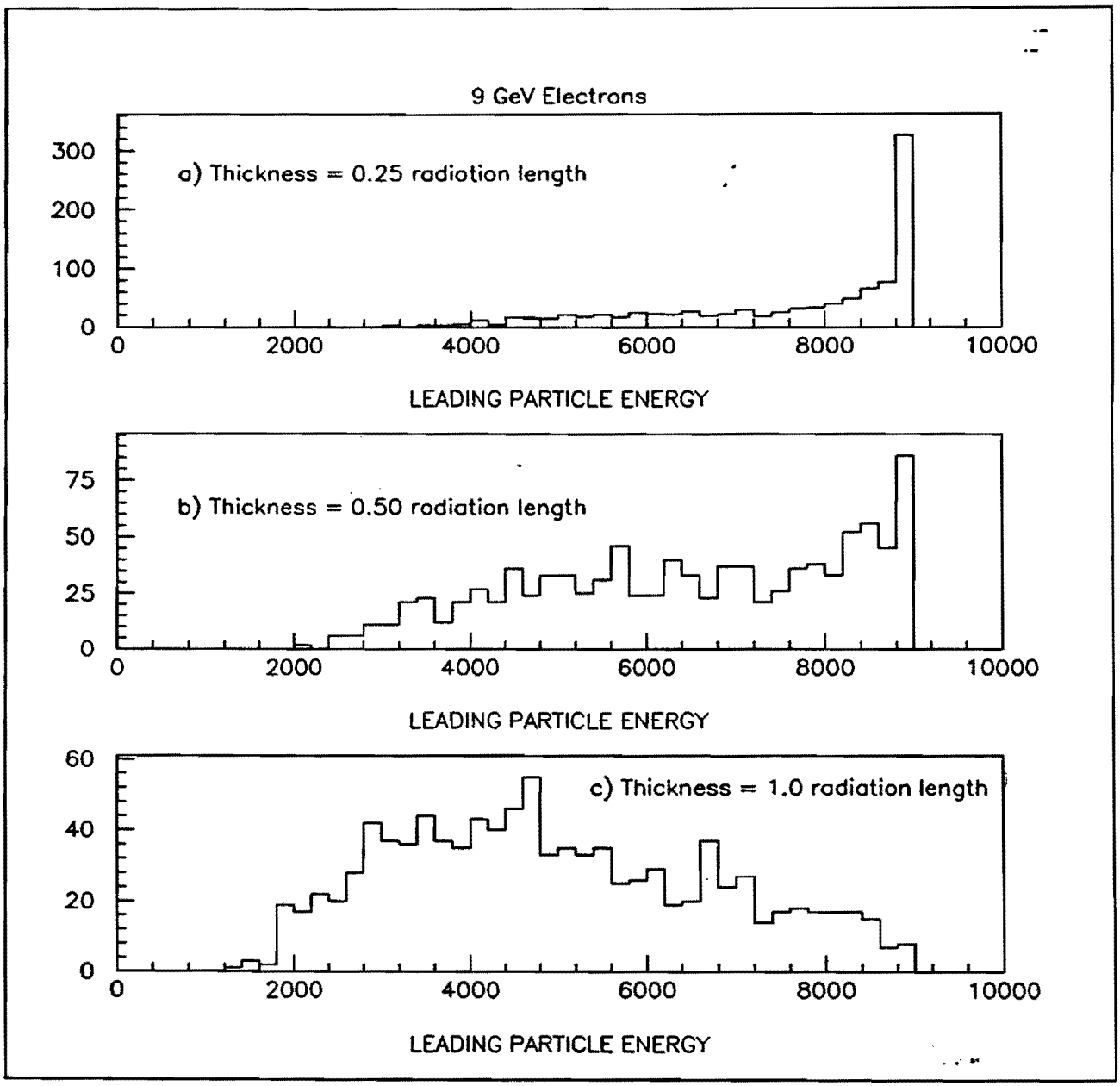

Fig. A3: Leading e^- energy for a) 0.25 rad length lead, b) 0.50 rad. length lead, and c) 1.00 rad length lead.

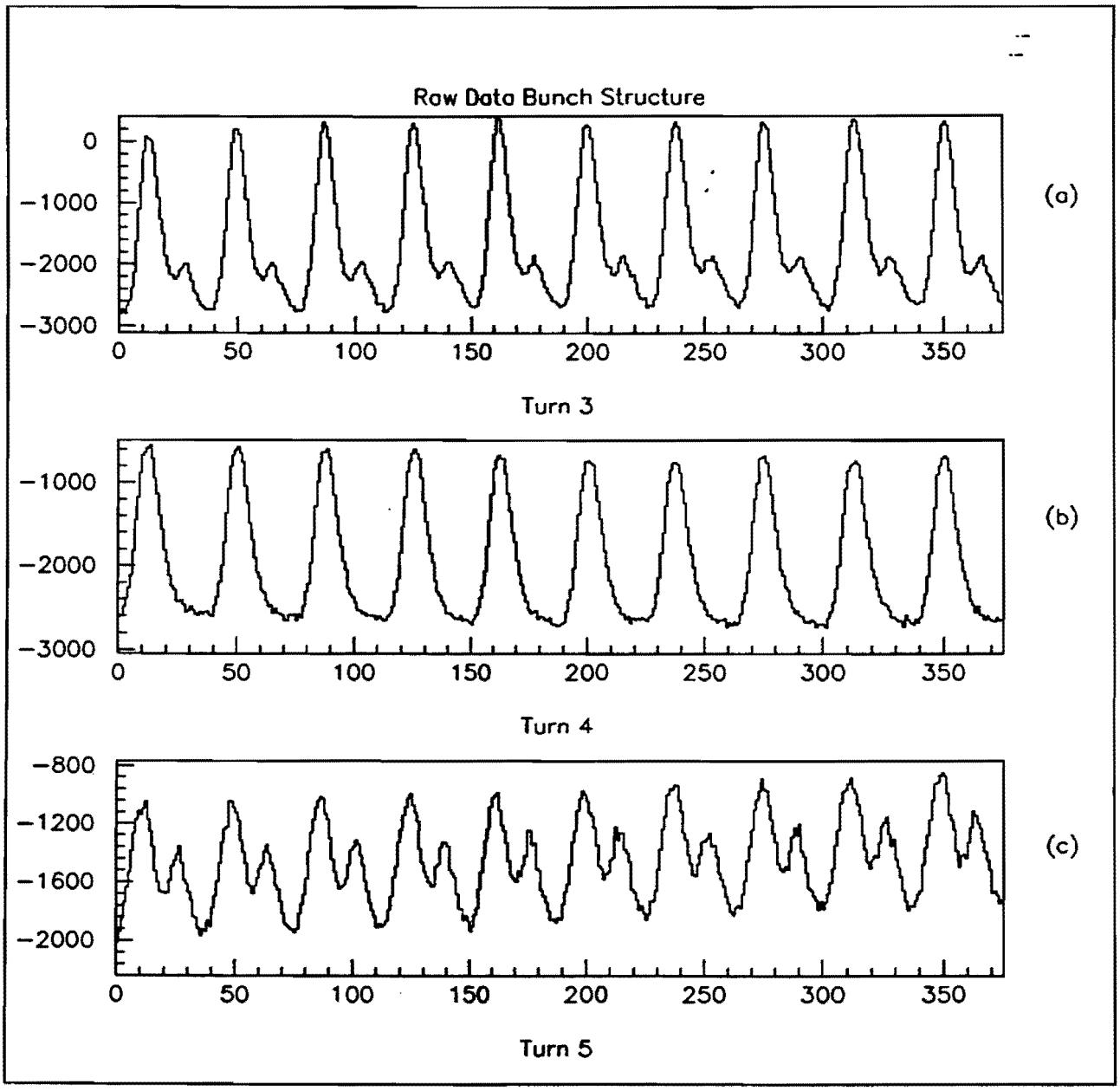

Fig. A4: Debuncher bunch structure for a) turn 3, b) turn 4, and c) turn 5.

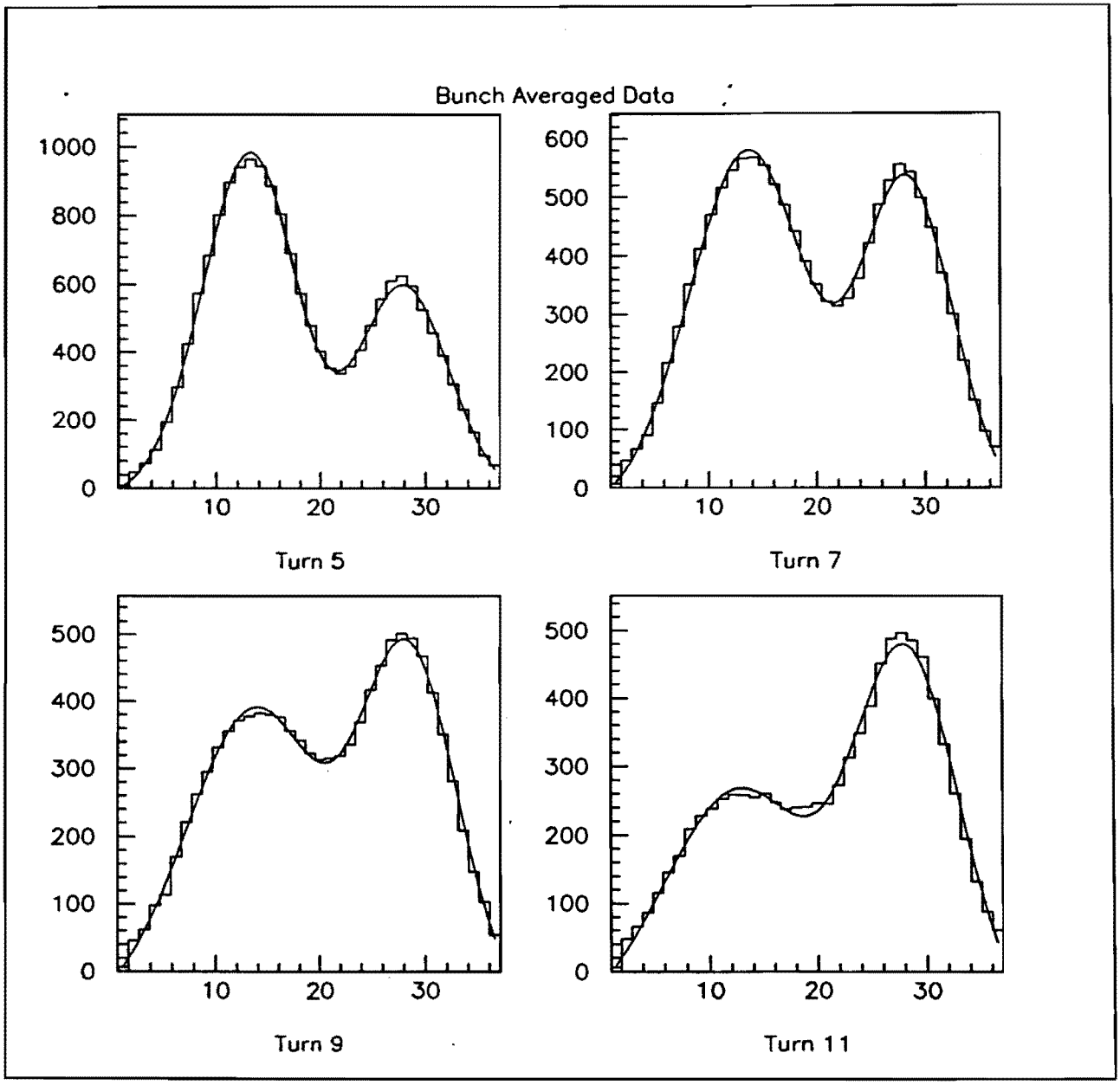

Fig. A5: Time averaged bunch structure for turns 5, 7, 9, and 11. The fit results of double Gaussian plus constant function is superimposed on the data.

"corrected"

2/92

P-860

A SEARCH FOR NEUTRINO OSCILLATIONS

USING THE FERMILAB DEBUNCHER

M.J. Murtagh
Brookhaven National Laboratory, Upton, NY 11973

J. Boyer, Y. Ho, W. Lee*, E. Mannel, and J. Mechalakos
Columbia University, 538 West 120th St., New York, NY 10027

A. Bross, M. Gormley, C. Kim, S. O'Day, and H. Park
Fermilab Accelerator Laboratory, P.O. Box 500, Batavia, IL 60510

K.S. Kang and D.W. Kim
Kangnung National University, Kangnung, Korea

J.S. Kang
Korea University, Seoul, Korea

J. Kim
Seoul National University, Seoul, Korea

* Spokesman

P-860

A SEARCH FOR NEUTRINO OSCILLATIONS USING THE FERMILAB DEBUNCHER

Section I INTRODUCTION

This proposal describes a unique program that utilizes a rather unconventional neutrino beam from the Fermilab Debuncher ring in order to study neutrino oscillations. While the primary focus of the experiment is on $\nu_e \rightarrow \nu_\tau$ oscillation, the experiment is also sensitive to a wide range of parameters for $\nu_e \rightarrow \nu_\mu$ oscillations and, to a lesser extent, $\nu_\mu \rightarrow \nu_\tau$. Although the initial phase of the program would focus on a short baseline experiment, the addition of a second detector at some later time at 5–10 km from the Debuncher would greatly expand the initial search and would be particularly interesting for a $\nu_\mu \rightarrow \nu_\tau$ oscillation study. The increased flux available when the new Main Ring Injector is operational would also be a great advantage for this long baseline phase of the experiment.

During conventional collider operation, negative pions, muons, and electrons are captured along with the $\bar{p}$'s in the Debuncher ring. Within the first few turns, the majority of negative pions decay to give negative muons and muon antineutrinos. The muons which are trapped in the ring, decay over many turns producing muon neutrinos and electron antineutrinos. The Debuncher, therefore, naturally produces a time-separated electron antineutrino beam. Its energy distribution is in the range 3–9 GeV, so most of the beam is above the threshold for producing τ leptons. Since antineutrinos produce positive leptons when they interact, there are only two beam sources which can produce positive muons. The first comes from "early" muon antineutrinos from the pion decays. The second is from the "late" electron antineutrinos which have oscillated to muon antineutrinos or to tau antineutrinos. In principle, then, the observation of positive muons in the detector during the latter part of the Debuncher beam cycle (after the first 10 turns, or 10 pion lifetimes) is a clear signal for the presence of neutrino oscillations. The absence of a real beam background of positive muons should make this a relatively straightforward measurement. The only significant background is from real or fake positive muons from conventional neutrino interactions. This is addressed in detail below, but it does not significantly limit the search.

In principle, then, the normal collider Debuncher operation produces time-separated neutrino beams of early muon antineutrinos from negative pion decay and late muon neutrinos and electron antineutrinos from captured muon decays. Unfortunately, this flux

is not adequate for the oscillation searches being proposed. However, if one severs the connection to collider running and uses the Debuncher to collect positive pions, then a significant event rate increase is achievable. Part of this increase comes from a change in the machine operation, and the remainder comes from the difference between neutrino and antineutrino cross sections plus various improvements in the accelerator and Debuncher operations. Although the flux from the regular collider operation is adequate for testing and tuning up the detector, actual data taking would require dedicated debuncher operation to collect positive pions. This operation is, however, compatible with fixed target running.

The detector for the experiment would be located in line with one of the straight sections of the Debuncher ring. For acceptance reasons, it is advantageous to locate it as close to the ring as possible, while still allowing for adequate shielding to reduce the stray beam flux from the Debuncher. The detector is relatively simple, since its primary requirement is to identify and measure the signs of muons above 1 GeV. As with most neutrino detectors, it consists of a primary module which is then repeated to give enough mass to get an acceptable event rate for the process of interest. The primary module consists of a toroid to provide a magnetic field, scintillator planes to provide event timing, and tracking chambers to measure the muon tracks. The present estimate is that such a detector and a suitable hall will take ~ 2 years to build and should cost $\leqq$ \$7M.

The primary physics being addressed by this proposal, namely the existence of a massive, 17 keV, neutrino, is very topical. If this experiment can proceed without delay, it is very likely that it can have a significant impact on this question. Irrespective of the fate of the 17 keV neutrino, this experiment will significantly improve the mixing angle limits of previous oscillation searches using electron neutrino beams or electron final state signatures.

The mixing angle limit for $\nu_\mu \rightarrow \nu_e$ will improve by an order of magnitude, while the mixing angle limit for $\nu_e \rightarrow \nu_\tau$ will improve from 8×10^{-2} to 3×10^{-3}. The long baseline phase of the experiment will improve the mass difference limit at maximal mixing for $\nu_\mu \rightarrow \nu_\tau$ from 0.25 eV^2 to 0.05 eV^2.

Section II PHYSICS MOTIVATION

The conjecture that neutrinos might oscillate has been the subject of much theoretical speculation and experimental effort (Ref. II.1). While there have occasionally been experimental indications of positive results, none of these have been confirmed by other experiments. Indeed, the strength of most of these results has gradually diminished in light of different or improved experiments.

Accelerator based oscillation searches have primarily focused on $\nu_\mu \rightarrow \nu_e$ oscillations (Fig. II.1a). Accelerator neutrino beams are predominantly muon neutrino beams with $\sim 1\%$ contamination from electron neutrinos. Since the ratio of ν_e to ν_μ in the beam is essentially determined by the ratio of pions to kaons in the beam from the production target, one is looking for an increase in the rate of electrons in a relatively well understood situation. While these experiments have produced the majority of oscillation results, they are limited by the beam contamination from ν_e, electron identification problems in counter experiments, and the lack of a sign measurement on the shower.

With the most notable exception being the Fermilab emulsion experiment E531, accelerator based searches for ν_μ oscillations to final states other than ν_e have, for the most part, been disappearance experiments (Fig. II.1b,c). Disappearance experiments are inherently limited in their mixing angle limits as they involve the subtraction of large numbers. They are also devoid of any clear signature and rely totally on calculations of the neutrino flux as a function of distance from the source. In contrast to this situation, experiment E531 was an appearance experiment which looked in an emulsion target for short lived particles which could be consistent with τ's. This experiment had a relatively large mass limit, as it was a high energy experiment. There are essentially no accelerator limits for ν_e beams, since there are no high flux electron neutrino beams. The limits (Fig. II.1c) from reactor experiments have good mass range but, since they are disappearance experiments, again obtain very restricted mixing angle limits.

The most intriguing hint of neutrino oscillations is in the realm of solar neutrinos. The disagreement between the solar model calculations and the measurement of solar neutrino fluxes can be interpreted in a very elegant way using the MSW (Ref. II.2) matter oscillation conjecture. This provides neutrino oscillation solutions with a mass difference in the 10^{-6} eV^2 to 10^{-4} eV^2 range. If one assumes that the mixing is greatest between the nearest mass states, then this would be interpreted as mixing between ν_e and ν_μ. If one also assumes that there is a reasonable neutrino mass hierarchy such as naturally occurs

in many Grand Unified Theories, then one might expect to observe $\nu_\mu \rightarrow \nu_\tau$ oscillations in the energy regime of available accelerators (Ref. II.3). For example, if the neutrino masses scale as the square of the corresponding quark or lepton masses, then the tau neutrino mass could be 10^4 times the muon neutrino mass or in the range 10^{-2} eV^2 to 1 eV^2.

A few years ago, Simpson (Ref. II.4) reported evidence for the existence of a 17 keV neutrino in an experiment to measure the beta spectrum of Tritium. The mixing of this electron neutrino was $\sim$ 1%. Recently, Simpson repeated this measurement for ^{35}S with similar conclusions. In addition, a number of other measurements of beta spectra for different materials have also produced positive results with the same value for the neutrino mass. The situation is not clear, however, since several spectrometer experiments have failed to observe this reported effect. If this effect is real, it would likely involve a $\nu_e \rightarrow \nu_\tau$ oscillation since $\nu_e \rightarrow \nu_\mu$ oscillations with these parameters have been ruled out by existing accelerator searches.

The indications from all the present evidence and conjecture are that the most fruitful areas for neutrino oscillation searches at accelerators are in the channels $\nu_\mu \rightarrow \nu_\tau$ and, in light of the 17 keV neutrino results, particularly in the $\nu_e \rightarrow \nu_\tau$ channel. To date these have been the least explored channels.

The proposed experiment is for a clean ν_e beam with no ν_μ contamination. Since most of the beam energy spectrum is above the threshold for tau production, it is ideal for $\nu_e \rightarrow \nu_\tau$ searches. The detector is close to the target, so the E/L for the experiment is $\sim$ 100. This will restrict the mass difference squared limit to 5–10 eV^2. While this is more than adequate for the range suggested by the Simpson result, it is not in the range of $\nu_\mu \rightarrow \nu_\tau$ suggested by the solar neutrino conjectures. Nonetheless, the results in this channel for this experiment will be a significant improvement in mixing angle over the present disappearance results and lower in mass than the E531 emulsion results (Fig. II.1b). An extension of the initial experiment which would involve the addition of a second detector at a large distance from the Debuncher could lower the Δm^2 limit for $\nu_\mu \rightarrow \nu_\tau$ oscillations to the region suggested by the solar neutrino experiments.

Section III THE NEUTRINO BEAM

The Fermilab Debuncher ring is a strong focusing synchrotron with a circumference of 500 meters, situated between Giese and Indian Roads (Fig. III.1). During normal collider running, it accepts negative secondaries which originate at the antiproton production target and are transported through the AP-2 beam line. Secondaries whose phase space coordinates lie within the momentum acceptance [8.9 GeV/c $\pm 2\%$] and transverse admittance $[A(x) = A(y) = 25\pi\text{mm} \times mrad]$ of the Debuncher ring are injected and captured in the Debuncher. The particle composition of the first-turn beam in the Debuncher is dominated by pions, but contains electrons, muons, and antiprotons as well.

For the last several months, parasitic to the running of E-760, measurements of the fluxes of pions, electrons, muons, and antiprotons which are injected into and circulate in the Debuncher have been made. The Appendix contains a detailed summary of the novel experimental technique used, together with the measured results for the circulating muon flux in the Debuncher.

As described in the Appendix, the measurements are quoted in terms of the ratio of the muon flux to the antiproton flux. The measured result is $\mu^-/\bar{p} = 1.0 \pm 0.2$; the muon and antiproton fluxes which circulate in the Debuncher are nearly identical.

From the measured $\mu^-/\bar{p}$ ratio one can calculate the number of muons per day that are available in the Debuncher when it is used parasitically as a source of electron antineutrinos. In this calculation, the following known and mostly-in-progress upgrades are included:

1. After completion of the Linac upgrade (but prior to the existence of the Main Injector) the proton flux on the antiproton target will be 3×10^{12} protons per pulse.
2. The cycle time of the Main Ring will be reduced from 2.6 to 2.1 seconds.
3. By 1994 the $\bar{p}/p$ ratio in the Debuncher will increase, due to improvements in the Debuncher aperture and the lithium lens, from its current value of 2.0×10^{-5} to 3.0×10^{-5}.

In addition, the overall operating efficiency of the Main Ring, the target station and Debuncher is assumed to be 80%. This type of efficiency is required for reasonable collider operation.

With these assumptions, the number of muons per day available in the Debuncher during parasitic operation, after the Linac upgrade, will be;

$$\frac{\mu^-}{\text{day}} = \frac{60 \times 60 \times 24}{2.1} \times (3 \times 10^{12}) \times (3 \times 10^{-5} \times 0.8) = 3 \times 10^{12}$$

This muon flux, which is available parasitically during collider running, is a significant source of neutrinos but, as noted earlier, is not adequate for the experiment in question. However, if one does not insist on running parasitic to the collider, the muon flux can be increased by at least an order of magnitude. The flux of muons circulating in the Debuncher would be optimized in this mode of operation as follows:

1. Change the polarity of the AP-2 line and the Debuncher.

   The inclusive yield of π^+ is approximately equal to that of π^- for 120 GeV protons on a heavy target (Ref. III.1). Such a modification would only require a polarity reversal of the magnets in the AP-2 line and the Debuncher. Polarity reversals of this type are quite straight-forward and typically require 2–3 hours to complete.

   This switch also implies that the experiment is a search for neutrino and not antineutrino oscillations. This yields almost a factor of 2 increase in event rate due to the difference in cross sections for neutrinos and antineutrinos.

2. Operate the AP-2 line and the Debuncher at higher momenta.

   The Appendix summarizes the calculations of the flux of circulating muons as well as the flux measurements that have been made with both the AP-2 beam line and the Debuncher ring operating at a central momentum of 9 GeV/c. The simulation model is being used to explore the improvement in flux that can be achieved by running the AP-2 beam line at a slightly higher momentum than the Debuncher. Preliminary results from the simulations indicate that running the transport line at 2% higher momentum increases the flux of circulating muons by a factor of two.

   This result should be verified at the earliest possible opportunity by remeasuring the muon flux with the central momentum of the transport line set 2% higher. In calculating the neutrino event rates, this expected increase in the muon flux is used, but the rates should be regarded as preliminary until this improvement is experimentally verified.

   The maximum energy at which the Debuncher can be run is determined primarily by the field quality of the dipoles in the ring. At the Debuncher's design momentum of 9 GeV/c the field quality is extremely uniform: $\Delta B/B < 2 \times 10^{-4}$ within ± 2.0 in. At higher excitation currents, the flatness of the field deteriorates. For example, magnetic measurements of the Debuncher dipoles at 10 GeV/c indicate that the non-uniformity of the field is roughly 2.5 times larger (i.e., $\Delta B/B < 5 \times 10^{-4}$

within ±2.0 in.). Consequently, the dynamic aperture at 10 GeV/c is likely to be somewhat smaller than at the design momentum. However, in using the Debuncher as a muon storage ring, one is concerned only with the dynamic aperture for the first 300 turns of circulating beam (after which time 90% of the muons have decayed). Computer simulations will be required to establish the maximum energy at which the Debuncher can be run as a storage ring. The energy can probably be raised by at least 10% above the design value.

For the event rate calculations discussed below, it is assumed that the Debuncher is operating at 10 GeV/c. In this case not only does one gain the factor of two improvement in the muon flux noted above from the simulation calculations, but there is also an increase in the number of π^+ at 10 GeV/c relative to the number at 9 GeV/c. This increase is calculated to be an additional factor of 1.4. (Ref. III.2)

3. Operate the Main Ring in "Multi-batch" mode.

   For antiproton production, the Main Ring is currently operated in "single-batch" mode in which one batch of 82 bunches is injected at 8 GeV into the Main Ring every 2.1 seconds, accelerated to flat top, extracted and targeted. With 2×10^{12} protons per batch and a 2.1 second cycle time the (time) average intensity is 0.95×10^{12} protons per second.

   In a "multi-batch" mode of operation, N batches are injected at 8 GeV, accelerated to flat top simultaneously, and extracted one at a time to the production target, with as short an interval between extraction cycles as possible. With 10 batches, extracted at a 15 Hz. rate, the Main Ring cycle time would be:

$$T = 2.1 + (10 - 1) \cdot (1/15) + (10 - 1) \cdot (1/15) = 3.3 \text{ seconds}$$

   and the (time) average intensity would be:

$$I = (10 \times 2 \times 10^{12})/(3.3) = 6.1 \times 10^{12} \text{ protons/sec.}$$

   This multi-batch operation yields an average intensity which is 6.4 times greater than single batch.

   Two hardware improvements are necessary to implement multi-batch operation with the parameters sketched above: (1) a Main Ring extraction kicker with a rise and fall time of 0.5 microseconds; and (2) a rapid-cycling (15 Hz) lithium lens downstream

of the production target. There appears to be sufficient space in the E-17 medium straight section of the Main Ring to accommodate a kicker with these characteristics; i.e., no significant changes to the Main Ring lattice are required. Building a reliable, rapid-cycling lithium lens would require significant lead-time and a substantial development effort. However, much of the groundwork for such an effort has been carried out by the Novosibirsk group (Ref. III.3), who have tested prototype liquid lithium lenses with significantly larger diameters than would be required.

The overall enhancement which results from these modifications is $2 \times 1.4 \times 6.4 = 18$. Consequently, the number of muons per day in the Debuncher for this optimized mode of running is 5.4×10^{13}.

In summary, the Debuncher, in its normal operating mode for collider running, does not have adequate flux for the experiment being proposed. However, by switching from negative to positive pion capture and by altering the operation of the machine, a significant increase in the muon flux in the Debuncher ring can be achieved. The decay of this stored muon beam produces a clean beam of electron neutrinos which is time separated from the beam background of muon neutrinos and is, therefore, ideal for searches for rare neutrino processes which produce negative muons in the final state. In addition, since the flux of pions/muons is well measured in the Debuncher, it should be possible to absolutely normalize the neutrino flux by a straightforward decay calculation.

Section IV EVENT RATES

In estimating neutrino fluxes and interaction rates, it is assumed that the Debuncher is used to store positive muons, in a non-parasitic, multi-batch mode of operation, with an integrated muon flux of $5.4 \times 10^{13}\mu^+$/day. Only 13% of the muons decay in the straight section of the Debuncher pointing at the detector. In addition, the first few turns (~ 10) are dominated by ν_μ from pion decay, and the present electronic design is only active for 400 μsecs. This amounts to cutting 25% of the captured muon flux. Consequently, the useful muon flux is $0.13 \times 0.75 \times 5.4 \times 10^{13}\mu^+$/day or $5.3 \times 10^{12}\mu^+$/day.

The muon neutrino energy distribution from the decay of the primary 9 GeV/c pions in the Debuncher is shown in Fig. IV.1a; while the muon antineutrino and electron neutrino energy distributions from the captured 9 GeV/c secondary muon decays are shown in Fig. IV.1b and Fig. IV.1c respectively. All these calculations are for the neutrinos which are emitted at less than 10 mrad from the initial meson or muon direction. This corresponds to neutrinos with the potential to interact in a 1m radius fiducial volume detector.

The number of pions and muons as a function of turn number is shown in Fig. IV.2. As noted earlier, after a few (~ 10) turns, the neutrino flux from pion decays is negligible. The muon flux continues to be significant for at least two hundred turns.

In the decay $\mu \rightarrow e^+ + \nu_e + \bar{\nu}_\mu$, the energy and angular distribution of ν_e and $\bar{\nu}_\mu$ are

$$\frac{d^2 N_{\bar{\nu}_\mu}}{dx\ d(\cos(\theta))} = x^2(3-2x)\left[1 - \left(\frac{1-2x}{3-2x}\right)\cos(\theta)\right]$$

and

$$\frac{d^2 N_{\nu_e}}{dx\ d(\cos(\theta))} = x^2(1-x)[1-\cos(\theta)]$$

where $x = E_\nu/(m_\mu/2)$ and θ is the angle between the muon neutrino and the polarization vector in the muon rest system (Ref. IV.1).

Initially the μ^+ polarization is left handed. Assuming that there is no dynamic depolarization mechanism, the number of high energy ($E_\nu > 6$ GeV) ν_e and $\bar{\nu}_\mu$ entering the detector are time separated. This can be seen in Fig. IV.3 which shows the number of ν_e and $\bar{\nu}_\mu$ into the detector as a function of turn number.

The electron neutrino spectra for Debuncher settings to capture 9 GeV/c, 10 GeV/c, and, 11 GeV/c particles are shown in Fig. IV.4a,b,c. Clearly, with increasing energy of the ring, the fraction of the neutrinos above the tau threshold increases, as does the overall event rate, since the mean energy is higher. The quasi elastic cross sections for ν_e, $\bar{\nu}_e$, ν_τ,

and $\bar{\nu}_\tau$ are shown in Fig. IV.5 while the inelastic cross sections are shown in Fig. IV.6. It is clear from these distributions that, for the Debuncher energy regime, the tau cross section is predominantly quasi elastic and single pion while the conventional neutrino interactions are dominantly deep inelastic.

The integrals of the flux $\times$ cross section for the relevant neutrino species and partial cross sections are shown in Table IV.1. The effects of Fermi motion are included in the calculation. This has little effect on the basic neutrino rates, but does increase the tau neutrino rates by $\sim$ 10%. It is clear from these numbers that a 10% increase in the Debuncher energy produces a significant increase in the tau event rate. It is not yet clear how much the energy of the Debuncher can be increased with the present magnets but some increase is expected.

In calculating the event rate, it is assumed that all neutrinos produced within 10 mrad of the nominal muon beam direction pass through the fiducial volume of the detector. As will be clear when the detector is discussed later, this is a very reasonable approximation. The detector will start 15 m from the end of the Debuncher straight section. Consisting of 600 modules, each module containing a 5 cm Fe absorber plate and space for timing and position measuring detectors for a total dimension in the beam direction of $\sim$ 60 m, with a radius of 1.25 m. Therefore, a 1 m radius fiducial volume will contain a 10 mrad beam divergence.

The following rate calculation is for a 10 GeV/c Debuncher setting. The expected improvement in rate from running the Debuncher at a higher field can be determined from Table IV.1. As discussed above, the number of useful muons per day is 5.3×10^{12}. Assuming that the detector has the 600 modules of Fe defined above and the 10mrad beam is contained in the fiducial volume the, electron neutrino event rate per day is given by

$$\mathrm{N}_{\nu_e} \text{ interactions/day} = N_\mu \times F_{\nu_e} \times Mz = 1689$$

where $\mathrm{N}_\mu = 5.3 \times 10^{12}, F_{\nu_e} = 224.9 \times 10^{-40}\mathrm{cm}^2/\mu$ is defined in Table IV.1 and $Mz = 6 \times 10^{23} \times 7.87 \times 5 \times 600\mathrm{cm}^2$ is the longitudinal fiducial tonnage. If one assumes 200 day run, then the total number of ν_e interactions is

$$\mathrm{N}_{\nu_e} \text{ interactions} = 337 \times 10^3.$$

A similar calculation for the number of $\bar{\nu}_\mu$ interactions yields

$$\mathrm{N}_{\bar{\nu}_\mu} \text{ interactions} = 193 \times 10^3.$$

TABLE IV.1

$F_{\nu_\mu} \equiv \int \mathrm{FLUX}(E)\sigma(E)dE \quad 10^{-40}\mathrm{cm}^2/\mathrm{pion}$ for ν_μ

	$E = 9$ GeV	$E = 10$ GeV	$E = 11$ GeV
QE	17.2	19.5	21.8
CCSP	15.9	18.1	20.2
CCDIS	76.4	94.3	113.8
TOTAL	109.5	131.9	155.8

$F_{\nu_e} \equiv \int \mathrm{FLUX}(E)\sigma(E)dE \quad 10^{-40}\mathrm{cm}^2/\mathrm{muon}$ for ν_e

	$E = 9$ GeV	$E = 10$ GeV	$E = 11$ GeV
QE	22.9	25.6	28.1
CCSP	21.1	23.7	26.0
CCDIS	145.2	175.6	206.0
TOTAL	189.2	224.9	260.1

$F_{\nu_\tau} \equiv \int \mathrm{FLUX}(E)\sigma(E)dE \quad 10^{-40}\mathrm{cm}^2/\mathrm{muon}$ for ν_τ

	$E = 9$ GeV	$E = 10$ GeV	$E = 11$ GeV
QE	6.5	8.3	10.0
CCSP	2.8	3.9	5.0
CCDIS	4.5	7.2	10.6
TOTAL	13.8	19.4	25.6

$F_{\bar{\nu}_\mu} \equiv \int \mathrm{FLUX}(E)\sigma(E)dE \quad 10^{-40}\mathrm{cm}^2/\mathrm{muon}$ for $\bar{\nu}_\mu$

	$E = 9$ GeV	$E = 10$ GeV	$E = 11$ GeV
QE	16.8	19.2	21.3
CCSP	16.0	18.2	20.2
CCDIS	75.6	91.7	107.8
TOTAL	108.4	129.1	149.3

The total number of interactions expected for each of the primary neutrino species in the beam for a 200 day run is given in Table IV.2 for possible Debuncher energy settings of 9 Gev, 10 Gev, and 11 Gev. The ν_μ rate is considerably higher because the ν_μ's arise from the direct decay of the primary pion beam, and the π/μ ratio at the entrance to the Debuncher is 50/1.

TABLE IV.2

Number of Events in the Detector

Debuncher Energy	9 GeV	10 GeV	11 GeV
ν_e (all)	220×10^3	337×10^3	466×10^3
ν_e (QE, SP only)	50×10^3	75×10^3	93×10^3
$\bar{\nu}_\mu$ (all)	126×10^3	193×10^3	266×10^3
$\bar{\nu}_\mu$ (QE, SP, DEEP)	38×10^3	57×10^3	75×10^3
ν_μ (π decay) (all)	6.3×10^6	9.8×10^6	14×10^6
ν_μ (QE, SP)	1.9×10^6	2.8×10^6	3.8×10^6

For the purpose of calculating the signal for oscillations into τ neutrinos, the oscillation parameters are taken to be those of Simpson, viz., mass difference of 17 keV and a mixing angle of $\sin^2(\alpha) = 0.8\%$ or $\sin^2(2\alpha) = 3.2\%$. For such a high mass difference, $\sin^2(1.27 \times \Delta m^2 \times L/E) \sim 0.5$, the number of ν_τ interactions for a 200 day running period is

$$\mathrm{N}_{\nu_\tau} \text{ interactions} = 0.5 \times 0.032 \times N_{\nu_e} \text{ interactions} \times \left(\frac{F_{\nu_\tau}}{F_{\nu_e}}\right)$$

$$= 465.$$

The branching ratio for $\tau^- \rightarrow \mu^- \bar{\nu}_\mu \nu_\tau$ is 17% and the acceptance for muons from tau decays is 80%. Consequently the number of μ^- from the decays of τ^- produced by $\nu_e \rightarrow \nu_\tau$ oscillations is

$$\text{No. Observed negative muons} = 465 \times 0.17 \times 0.80$$

$$= 63.$$

In other words, if one assumes a total of 200 days running, there would be a total signal of 63 events (40 quasi elastic and single pion events) if there is a 17 keV neutrino which oscillates from ν_e with a few percent mixing ($\sin^2(2\alpha) \sim 3\%$).

The actual oscillation limits which this experiment can set if there is no such heavy neutrino are presented later after the potential backgrounds are discussed.

Section V BACKGROUNDS

The primary signature for a charged current neutrino interaction is a fast, relatively forward going, lepton. This feature is retained even if one considers the secondary muons from tau decay. The acceptance for such muons in the present experiment, if one requires the muon to be greater than 1 GeV/c and to have an angle to the beam direction with $\cos\theta < 0.8$, is $\sim 80\%$. Since the ν_τ cross section at Debuncher energies is primarily quasi elastic, genuine τ interactions will be characterized not just by a forward going energetic muon but also by a relatively low multiplicity event. A typical quasi elastic τ event is shown in Fig. V.1. The figure shows a 5 GeV tau neutrino interacting to produce a 4.5 GeV tau decaying to a 4 GeV muon. Only hits from the charged tracks in the event are shown. The cleanliness of the event, characterized by the lack of additional connected tracks, is apparent.

The primary background sources for this experiment are charm production, which produces genuine muons in high multiplicity events, and pions in conventional deep inelastic interactions. These latter interactions produce fake muons, either because they decay, or because they accidentally pass the muon selection criteria. A typical background charm event is shown in Fig. V.2. In the present, very preliminary, analysis one requires τ candidates to be very clean events consisting of a single forward going track with no additional hits associated with the vertex. If it is assumed that this is equivalent to selecting only quasi elastic and single pion final states, then 70% (Table IV.1) of the signal events are retained. As the Debuncher energy increases, this acceptance is reduced. Since the overall event rate is quite low, one will in practice, try to relax these cuts to increase the event sample. However, for the present proposal, tight cuts are applied since many details of the event topology in this detector are not yet fully understood.

Present background estimates are based on Monte Carlo calculations using the event generator ETEST (Ref. V.1) developed for the E776 neutrino experiment at Brookhaven National Laboratory and extensively tested in that experiment. The Charm and deep inelastic scattering production calculations are from the CCFR Fermilab neutrino collaboration (Ref. V.2). The results from these calculations are thought to be adequate for the present background study. Work is also in progress to determine the expected background from the actual data taken by the E776 collaboration in the wide band neutrino beam at BNL. While this beam momentum peaks at 1.3 GeV/c, there is a long tail, and approximately 7% of the flux at the E776 location is above 4 GeV.

The primary source of fake muons from pion production will be in $\bar{\nu}_\mu$ interactions;

$\bar{\nu}_\mu$ charged current (CC)

single pion (SP)	$\bar{\nu}_\mu N \rightarrow \mu^+ \pi^- N'$
deep inelastic (DEEP)	$\bar{\nu}_\mu N \rightarrow \mu^+ \pi^- X$

$\bar{\nu}_\mu$ neutral current (NC)

single pion (SP)	$\bar{\nu}_\mu N \rightarrow \bar{\nu}_\mu \pi^- N'$
deep inelastic (DEEP)	$\bar{\nu}_\mu N \rightarrow \bar{\nu}_\mu \pi^- N'$

and the equivalent reactions for ν_e ($\mu^+ \rightarrow e^-$ in the above). For a pion to fake a 1 GeV/c muon, it has to either decay without a visible kink or traverse 6 interaction lengths Fe without an apparent interaction. In Table V.1 the results of the Monte Carlo calculation for a sample of $\bar{\nu}_\mu$ interactions are summarized. The generated events are divided between charged and neutral currents and the contribution from single pion and deep inelastic contributions are separated. At these energies, there are few energetic pions in the events. The potential background is further reduced by requiring that the energetic pion be in the beam direction and the μ^+ from the charged current process is not observed. The final cut to reduce the background is a crude cleanliness cut requiring that there be less than 0.5 GeV of additional visible energy in the event. As expected, this cut has little effect on the single pion events but significantly reduces the deep inelastic contribution. A practical definition of cleanliness for this detector is under study, but it is clear that this will be an effective cut in removing false tau candidates from the final sample.

As can be seen in Table V.1, none of the charged current events and fewer than 10^{-3} of the neutral current events produce a pion candidate event which will pass the simple geometric cuts for muon candidates. Since the neutrino cross section is twice the antineutrino cross section, the ν_e neutral current sample will produce approximately twice as many background candidates as the $\bar{\nu}_\mu$ neutral current sample. Unlike the $\bar{\nu}_\mu$ charged current sample, the ν_e charged current sample will contribute to the background since the leading lepton, in this case an electron, will probably not be easy to identify due to the thickness of the absorber plates. Assuming some of the electrons are visible, this background contribution will be roughly the same as the ν_e neutral current contribution, just from the ratio of charged to neutral cross sections. The total background sample is estimated to be 5×10^{-3} of the $\bar{\nu}_\mu$ neutral current sample. This corresponds to 1,000 events for the 200 day run being considered. The probability that a pion will traverse

6 interaction lengths of Fe without interacting is such that fewer than 3 of these tracks should survive as true muon candidates. It is likely that a few percent ($\leq 1\%$) of the pions will decay, yielding at most 10 background candidates. However, because few of the decay muons will have sufficient energy to pass the 1 GeV/c muon range requirement, one would expect at most a few background events in the final sample.

Further analysis of the potential pion background is in progress. This involves generation of additional Monte Carlo events in all channels and the inclusion of pion decay studies in the detector simulation.

The charm background can only arise in $\bar{\nu}_\mu$ interactions, since the ν_e interactions at these energies will produce a single positive charm particle which decays to a μ^+ and not a μ^-. Also, the antineutrino energy is relatively low, so the $\bar{\nu}_\mu$ neutral current production of charm pairs will be suppressed. Consequently, the only relevant charm production is the production of D mesons in $\bar{\nu}_\mu$ charged current interactions. The calculated number of such events in the sample is 240. Since the branching ration to muons is approximately 10% this will yield 24 negative muons in the sample. However, if one requires the muon to have momentum greater than 1 GeV/c, be within 37° of the beamline, and there are no additional tracks in the event, then the number of surviving events in the sample will be negligible.

TABLE V.I

PION BACKGROUND CALCULATION FOR $\bar{\nu}_\mu$ INTERACTIONS

	CC		NC		
	SP	DEEP	SP	DEEP	TOTAL
N_{gen}	1,957	6,465	697	2,681	11,800
$E_\pi \geq 1.\text{GeV}$ $\theta_\pi \leq 37°$	37	629	8	202	876
$(E_{\mu+} < .5\text{GeV})$	0	36	4.3	159	199
$K_\Sigma < .5\text{GeV}$	0	0	3.6	7.2	11

In summary, there is no evidence that there will be a significant background for the proposed τ signature of an energetic muon ($P_\mu > 1$ GeV/c) in the forward direction ($\cos\theta_e > .8$) in a very clean event ($K_{\text{tot}} < 0.5$ GeV).

Section VI OSCILLATION LIMITS

The probability that a neutrino of type ν_a and energy E_ν (GeV) oscillates to a neutrino of type ν_b at a distance L (Km) from the neutrino source is given by

$$P \equiv P(\nu_a \rightarrow \nu_b) = \sin^2 2\alpha \ \sin^2\left(1.27\Delta m^2 \frac{L}{E}\right),$$

where Δm^2 (eV^2) is the difference in mass of the neutrino mass eigenstates. This probability is compared to the experimental error in order to determine the region in the Δm^2-$\sin^2 2\alpha$ space to which the detector is sensitive. The region in Δm^2-$\sin^2 2\alpha$ space excluded experimentally is given by

$$P \leq \sin^2 2\alpha \ \sin^2\left(1.27\Delta m^2 \frac{L}{E}\right).$$

In the limit of small Δm^2 the excluded region simplifies to

$$\Delta m^2 \sin 2\alpha \geq 0.8 \frac{E}{L}\sqrt{P},$$

while for very large Δm^2 it reduces to

$$\sin^2 2\alpha \geq 2P.$$

As is clear from the above formula, the small Δm^2 limit is controlled by the E/L for the experiment, while the mixing angle limit is determined by the statistical and systematic errors on the measurement. For the present proposal, $E/L \sim 100$, so the emphasis in these measurements will be on the mixing angle limit. On the other hand if, for the second phase of the experiment, the detector is moved to 10 Km and one considers the ν_μ spectrum with mean energy $\sim$ 3.5 GeV, then the E/L is reduced to 0.3, and one can now attain a very good Δm^2 limit at maximal mixing.

The number of ν_a interactions in the detector, $N^{\rm int}_{\nu_a}$, is given by:

$$N^{\rm int}_{\nu_a} = M_Z \int \phi_{\nu_a} \, \sigma_{\nu_a} \, dE.$$

The flux of neutrinos of type ν_b, ϕ_{ν_b}, produced by the oscillations of neutrinos of the type ν_a to type ν_b is given by

$$\phi_{\nu_b} = P \times \phi_{\nu_a}.$$

therefore the number of ν_b interactions in the detector is

$$N_{\nu_b}^{\rm int} = M_Z \int \phi_{\nu_b}\, \sigma_{\nu_b}\, dE$$
$$= M_Z \int P\, \phi_{\nu_a}\, \sigma_{\nu_b}\, dE.$$

Assuming that the probability of oscillation does not change rapidly as a function of E over the range considered, then

$$\frac{N_{\nu_b}^{\rm int}}{N_{\nu_a}^{\rm int}} = P \times \frac{\int \phi_{\nu_a}\, \sigma_{\nu_b}\, dE}{\int \phi_{\nu_a}\, \sigma_{\nu_a}\, dE}$$
$$= P \times \frac{F_{\nu_b}}{F_{\nu_a}}.$$

Therefore

$$P(\nu_a \rightarrow \nu_b) \equiv \frac{N_{\nu_b}^{\rm int}}{N_{\nu_a}^{\rm int}} \times \frac{F_{\nu_a}}{F_{\nu_b}}$$

where $N_{\nu_i}^{\rm int}$ is the number of interactions of neutrino type i and F_{ν_i} is the integral of Flux $\times$ cross section for neutrino type i as listed in Table IV.1.

If no events above background are observed, then upper limits for Δm^2 and $\sin^2 2\alpha$ can be calculated for $\nu_e \rightarrow \nu_\mu$ and $\nu_e \rightarrow \nu_\tau$ oscillations. For the upper limit calculations presented here, it is assumed that the Debuncher is operating at 10 GeV and only quasi elastic and single pion events are considered. The event rates for the three neutrino species were discussed in Section IV and summarized in Table IV.2.

The limits for $\nu_e \rightarrow \nu_\mu$ oscillations can then be determined as follows:

$$P(\nu_e \rightarrow \nu_\mu) = \frac{N_{\nu_\mu}^{\rm int}}{N_{\nu_e}^{\rm int}} \times \frac{F_{\nu_e}}{F_{\nu_\mu}},$$

where $N_{\nu_i}^{\rm int}$ is the number of quasi elastic and single pion interactions for neutrino species ν_i and F_{ν_i} is the corresponding cross section. For ν_e and ν_μ interactions the cross sections are the same. So the probability of $\nu_e \rightarrow \nu_\mu$ oscillations is

$$P(\nu_e \rightarrow \nu_\mu) = \frac{N_{\nu_\mu}^{\rm obs} - N_{\nu_\mu}^{\rm back}}{\text{Acceptance} \times N_{\nu_e}^{\rm int}}.$$

If the number of observed events is the same as the expected background events then an upper limit on the oscillation probability can be determined based on the experimental

errors. The upper limit for the proposed experiment is

$$\begin{aligned} P(\nu_e \to \nu_\mu) &\leq \frac{1.3 \times \delta}{N_{\nu_e}^{\rm int}} \\ &\leq \frac{1.3 \times 2.8}{60 \times 10^3} \\ &\leq 6.0 \times 10^{-5} \end{aligned}$$

where δ is the experimental error and 1.3 corresponds to 90% of the area under one side of the Gaussian. For large Δm^2 the upper limit is

$$\begin{aligned} \sin^2 2\alpha &\leq 2 \times 6 \times 10^{-5} \\ &\leq 1.2 \times 10^{-4}, \end{aligned}$$

while for small Δm^2 and maximal mixing the upper limit is

$$\begin{aligned} \Delta m^2 &\leq .8 \times \frac{E}{L}\sqrt{6 \times 10^{-5}} \\ &\leq 0.3\ eV^2, \end{aligned}$$

where E is 5 GeV and L is 0.1 Km.

A similar calculation leads to the upper limits for $\nu_e \to \nu_\tau$ oscillations;

$$\begin{aligned} P &\leq \frac{1.3 \times \delta}{\text{Acceptance} \times BR(\tau \to \mu\nu\nu) \times N_{\nu_e}^{\rm int}} \times \frac{F_{\nu_e}}{F_{\nu_\tau}} \\ &\leq \frac{1.3 \times 2.8}{0.8 \times 0.17 \times 75. \times 10^3} \times \frac{25.6 + 23.6}{8.3 + 3.9} \\ &\leq 1.4 \times 10^{-3}. \end{aligned}$$

The limit for large Δm^2 is

$$\sin^2 2\alpha \leq 2.8 \times 10^{-3}$$

and for small Δm^2 and maximal mixing is

$$\Delta m^2 \leq 1.5\ eV^2.$$

In the future, the experiment can be easily expanded to include a long baseline detector which would explore a new low Δm^2 region in the $\nu_\mu \to \nu_\tau$ channel. If a second detector of the same mass is located at 10 Km, then the flux will be reduced by $(L_1/L_2)^2$ or $(0.1/10)^2 = 10^{-4}$. The event rate for all ν_μ interactions in the second detector will be

$$\begin{aligned} N_{\nu_\mu}^{\rm int} &= 2 \times 10^7 \times 10^{-4} \\ &= 2000, \end{aligned}$$

where we have assumed a factor of 2 increase in the flux due to the MRI. In addition no attempt has been made to optimize the parameters. If the number of events observed in the second detector is the same as the expected number based on the rate in the first detector and the experimental error is dominated by the event rate in the second detector, then the upper limit of the mixing probability is

$$\begin{aligned} P &\leq \frac{1.3 \times \delta}{\text{Acceptance} \times N_{\nu_\mu}} \\ &\leq \frac{1.3\sqrt{2000}}{0.8 \times 2000} \\ &\leq 3.6 \times 10^{-2}. \end{aligned}$$

The limit for small Δm^2 at maximal mixing is then

$$\begin{aligned} \Delta m^2 &\leq 0.8 \times \frac{E}{L}\sqrt{P} \\ &\leq 0.8 \times \frac{3.5}{10.}\sqrt{3.6 \times 10^{-2}} \\ &\leq 0.05 \text{ eV}^2. \end{aligned}$$

Section VII DETECTOR DESIGN

In order to achieve the experimental goals the detector system must have the following attributes:

- Angular acceptance out to 10 mrad for neutrinos generated at the center of the Debuncher straight section.
- Sufficient mass to be able to detect the number of events needed to satisfy the physics objectives.
- Momentum and charge determination for muon energies above 1.0 GeV.

A preliminary design of a detector to accomplish these goals has been made. The detector is a conventional modular iron toroid design using Iarocci tubes to measure the position of charge tracks and scintillator to determine the particle direction from time-of-flight measurements. Each toroid module contains 40 planes of iron absorber, 40 planes of Iarocci tubes, and 4 planes of scintillator. A four turn coil is used to provide the toroidal field. A schematic drawing of a single toroid module is shown in Fig. (VII.1). The total detector consists of 15 modules which are hexagonally shaped with a 1.25 m radius and an overall length of 183 feet.

Toroid Modules:

Each module consists of 40 planes of hexagonal shaped, 2 in. thick iron absorber. Following each plane of iron is a plane of Iarocci tubes used for measuring the track position. In addition, following every tenth plane of Iarocci tubes is a plane of 1 in. thick scintillator for time-of-flight measurements. The gap spacing between the planes of iron absorber is 2.5 in. for gaps containing both Iarocci tubes and scintillator and 1.25 in. for gaps containing only Iarocci tubes. The total length for a complete module excluding supporting frame is 135 in. with an estimated mass of 82.0 tons. The total mass of the completed detector is estimated to be 1.23×10^3 tons.

A four inch diameter opening passes through the center of the module to accommodate the water cooled copper conductor for the toroid coil. The coil is four turns looping around each side of the module to provide a toroidal field in the iron. A current of 2750 amps is used to saturate the field in the iron toroids at 18 Kgauss. The total power consumption for the full detector is estimated to be 300 Kw.

Scintillator:

In order to determine the flight direction for charged particles, each module contains 4 planes of scintillator. The scintillator planes are hexagon shaped to match the iron absorber and 1 in. thick with the same transverse measurements as the iron absorber plates. A schematic drawing of a scintillator plane is shown in Fig. VII.2. The scintillation light is collected by two $1.0 \times 1/2$ in.^{2} waveshifter bars imbedded in the scintillator. The waveshifter is read out by a photomultiplier tube located on the top end of each bar.

Iarocci Tubes:

Tracking information is provided by the Iarocci tubes. Iarocci tubes have been successfully used in a number of experiments and have been proven to be rugged devices that can be mass produced at a relatively low cost (Ref. VII.1).

The Iarocci planes will be constructed from 8-tube modules 250 cm long. The structure of an 8-tube module is shown schematically in Fig. VII.3. The module is constructed from an open PVC profile with eight 0.9×0.9 cm^2 cells separated by 0.1 cm thick walls. The profile is coated on the interior with a high resistivity graphite paint to form the cathode surface. A 100 μ m diameter Cu/Be wire is strung down the center of each cell, supported approximately every 50 cm by PVC spacers. The profile is inserted into a PVC sleeve and sealed at each end by an endcap to form the gas volume. The endcap assembly provides connections for high voltage and gas. The overall width of the module is approximately 8.4 cm. The Iarocci planes consist of 30 modules containing 240 wires.

The Iarocci modules are inserted into a 2.5×2.5 m^2 outer sleeve to form a complete Iarocci plane. This double sleeve arrangement allows for easy replacement of the 8 tube modules, should that become necessary. To accommodate the copper coil for the toroid, the central 8-tube module will consist of two 120.0 cm long modules. These two modules will be separated by 8.6 cm in the center to form the opening for the copper coils.

The outer sleeve is constructed of 1/6 in. thick glass-steel laminate with copper cladding on each side. The laminate will be routed on one side to form a 0.9 cm wide copper strip to provide the readout for the Iarocci tubes. The strip will run vertically on one side and horizontally on the other side to form simultaneous x-y readout.

Iarocci tubes are conventionally operated using a gas mixture of 25% Argon and 75% isobutane. This gas mixture however has the disadvantage of being extremely flammable. The SLD collaboration has investigated nonflammable gas mixtures for use in the SLD Warm Iron Calorimeter (Ref. VII.2). These studies indicate that a mixture of 2.5% Argon,

9.5% isobutane, and 88% CO_2 possesses the same operating characteristics as the Argon-isobutane mixture, but is considered nonflammable by the U.S. Bureau of Mines. This nonflammable gas mixture will be used and the Iarocci tubes operated at a voltage of approximately 4.9Kv. The resulting signals should be large enough to avoid signal-to-noise problems and will allow the use of low-cost front end electronics.

Assembly:

The toroid modules will be constructed as single units by stacking planes of iron, Iarocci tubes, and scintillator on a support structure. Once all the planes have been installed, the copper coils of the toroid will be installed and, finally, gas, cooling water, and electrical connections will be made to form a completed module. It is assumed that the experimental hall is of sufficient size to allow the construction *in situ*.

Trigger and Data Acquisition Electronics:

Three types of triggers are required for the experiment:

1. A "machine trigger" which defines a 400 μsec interval, during which the time of each Iarocci chamber hit is written into digital memory with a 100 nsec resolution, and the photomultiplier times are recorded with a 3 nsec resolution.
2. A "background trigger" which produces the same recording process as the "machine trigger" but is generated when the machine is "off".
3. A "cosmic ray calibration trigger" which selects cosmic ray muons that penetrate a significant number of detector planes. A coincidence of 2 or more widely spaced scintillator planes triggers the detector readout. In this mode the memory time base is shortened to about 1 μsec so that hits older then 1 μsec are overwritten providing a memory record of the last 1μsec.

Iarocci Tube Readout:

Signals from the readout strips are discriminated by "time over threshold" comparators, with the outputs stretched to at least 150 nsec and sampled every 100 nsec. Each output is written into 1 bit of a 4K byte memory where the address is driven by a 12 bit counter that is incremented every 100 nsec during the trigger interval. The memories are read out at the end of the trigger interval, with times assigned according to the addresses of the hits.

The readout is organized into cards that mount on the chambers and contain the comparators, memory, and control for 96 channels. Readout strips are connected to the card with short mass terminated flat cable. A clock and test pulse are sent to each card via an "equal time fanout system".

The storage for signals is provided by 4K byte memory chips. Each memory is read out via a local bus in 0.5 msec. This bus is separately daisy-chained from card to card for x-planes and for y-planes. Each bus is cabled to a crate-mounted "encoder card" where the data are zero suppressed. The "encoder card" sends an 8 bit memory select address with 4096 "read increments," resulting in a readout time of less then 50 μsec.

The "encoder card" assigns a time equal to the address of each leading edge hit and a signal address. The data are stored internally so that the encoders can operate simultaneously. The data are then sent to a crate link card connected to the crate back plane. The crates are distributed along the detector and linked with "twist and flat" cable. The system is completely data driven; the data stream to the data acquisition computer is written to memory via a data channel. The stream contains a flag bit to distinguish among data types and an interrupt to signal the completion. A separate control link provides commands and diagnostic data to the crates.

Photomultiplier Readout:

The photomultiplier signals are discriminated and sorted into 100 nsec time bins using the same clock as the Iarocci readout system. A linear interpolation time with a 3 nsec resolution is produced by integrating a constant current over the interval from the discriminator leading edge to the following clock edge and digitizing the output with a 7 bit FADC. The direct photomultiplier signal can also be stretched and sampled with a second 10 MHz FADC and written into a second 4K byte memory. Flag bits are written into those words containing discriminated data.

As with the Iarocci system readout, the 4K byte memories are addressed by 12 bit counters incremented every 100 nsec during the trigger interval. During readout, an absolute time is assigned to flagged words from the memory address along with the interpolation time and pulse height.

The readout is organized into cards for 8 photomultiplier outputs containing the discrimination, pulse sorting, time interpolation, pulse height, memory storage, and readout functions. A clock and test pulse input are included on each card. The cards mount in crates and use the same crate link and data driven structure as the Iarocci readout system.

System Control:

Trigger type information is distributed via the control links. Trigger timing is implicit in the fast clocks which are sent as bursts during the trigger interval with the required number of cycles. The clock is generated centrally and then is fanned out with equal times to all front end data acquisition elements. Memory address counters are reset from the leading clock.

Data are written directly to computer memory via the data channel input. Higher level triggers are carried out in software. The data are ordered by readout according to event number, data type, increasing signal number, and time. Interrupts are used to indicate the completion of data streams, starting addresses, and word counts. A multiple event buffer space is set up in computer memory so that the event processing time can be averaged over many events for efficient utilization of the processing bandwidth. The computer regulates the data acquisition by inhibiting triggers whenever the processing gets too far behind. Error flags and diagnostic data inserted into the data stream, together with the test pulse system, provide for system maintenance.

Detector Summary

The physical characteristics of the detector are summarized in Table VII.1.

TABLE VII.1

DETECTOR SUMMARY

Dimensions	$8.4 \times 8.4 \times 183.0 ft^3$
Tonnage	1.2K tones
Number of Iarocci Tubes per plane	240
Number of electronics Channels per plane	480
Number of planes of Iarocci tubes	600
Total number of Iarocci Tubes	144,000
Total number of electronics channels	288,000
Number of planes of scintillator	60
Number of photomultiplier tubes	120

Rough Cost Estimate

A rough cost estimate for the construction of the proposed detector and electronics has been made and is summarized in Table VII.2

TABLE VII.1

COST SUMMARY

		Module	15 Modules
Toroid:	Steel	$70,000.	
	Coils	7,000.	
	Support Structure	25,000.	
	Total Toroid	102,000.	$1,530,000.
Iarocci Tubes		54,000.	810,000.
Scintillator		8,000.	120,00.
Electronics:	Iarocci Tubes	123,000.	
	PMT bases	1,000.	
	Total Electronics	124,000.	1,860,000.
Sub Total		$288,000.	$4,320,000.
40% Contingency		115,000.	1,728,000.
Total		$403,000.	$6,045,000.

Section VIII DETECTOR LOCATION

There are three viable locations for situating the detector that would be used in this experiment. The beginning of the detector should be located 15 meters downstream from the end of one of the three straight sections of the Debuncher. While any of these three locations would be suitable for the physics program of this experiment, there are practical and topological complications associated with each of them. Arriving at the least expensive and least perturbing location for an experimental pit to house the detector would require a detailed analysis by the Fermilab Construction Engineering Section. Consequently, in this section the size of the experimental pit is selected to illustrate the approximate construction costs.

The proposed experimental pit would bear a strong resemblance to an accelerator beam enclosure, such as the Antiproton Rings Enclosure which houses the Debuncher and Accumulate rings. In addition, the construction techniques used to build the experimental pit would probably rely upon existing methods for constructing beam enclosures.

The experimental pit that is needed to house the detector would be approximately 200 feet long and 20 feet wide. In making a rough estimate of the major civil construction costs, one assumes that a concrete floor 3 feet thick, concrete walls 1.5 feet thick, and a concrete ceiling 2 feet thick would be adequate. For a pit of this size the volume of dirt that would have to be excavated is $(200' \times 20' \times 23') = 3430$ cubic yards. Assuming a figure of \$7/(cubic yard) for excavation of dirt yields a cost of \$24K. The concrete walls, floor, and roof of the pit would require 35,000 cubic feet of concrete. Using a cost estimate of \$280/(cubic yard) for the concrete yields a cost of \$336K.

The thrust of these crude cost estimates is to point out that the civil construction costs of the experimental pit are reasonable. A more accurate estimate of the cost of constructing the experimental pit would require a professional analysis by the Fermilab Construction Engineering Section.

Appendix A

We have measured the flux of circulating muons in the Debuncher by employing a slight modification of a technique used by G. Dugan in 1987 to measure the number of pions and electrons which get injected into the Debuncher. This technique relies upon the use of a non-destructive, ref pickup to measure the bunch structure of the beam on a turn-by-turn basis.

The beam arrives in the Debuncher, at the location of the pickup, in 84 narrow bunches ($\sigma_t \approx 1$ nsec) with a spacing of about 18 nsec. The fast particles (pions, muons and electrons) are separated from the slow particles (antiprotons) by about 8 nsec. Hence, fast and slow particles can be identified by looking at the time structure of the output from the ref pickup. As the beam circulates in the Debuncher, the pions decay in a few turns ($\gamma c\tau_\pi \approx 1$ turn), while the electrons spiral into the low energy edge of the machine, due to the emission of synchrotron radiation, and are lost after 14 turns. After more than 14 turns the only particles left are muons and antiprotons.

The results of turn-by-turn measurements made in 1987 are summarized in Fig. A1. In these data there was no indication of a signal representing circulating muons - which are expected to be the only fast particles remaining beyond turn number 14. The absence of a "bunched" muon signal for turn 15, however, is not necessarily an indication that there are no muons in the debuncher. This can be understood by calculating the muon debunching time:

$$T_D = \frac{(\Delta T)_{ref}}{\frac{\eta \delta P}{P}}$$

For muons, $\eta = .017$ and $T_D = 27.6\mu$sec (17 turns), i.e., the muons are completely debunched after 17 turns and, consequently, induce no signal on the ref pickup. We have checked the rate at which muons debunch by performing a simulation which uses the longitudinal difference equations to study the bunch shape as a function of turn number in the Debuncher. The results, shown in Fig. A2 for a bunch injected ($N = 1$) with $\Delta t = \pm 0.5$ nsec and $\delta P/P = \pm 2.0\%$, illustrate the rate at which the injected muons debunch and indicate complete debunching in 15–17 turns. The ref pickup technique is thus not sensitive to circulating muons in turns beyond turn 14.

An examination of Fig. A1 suggests that it is straightforward to measure the bunched muon signal by killing the electrons in the beam prior to injection into the Debuncher and then measuring the number of fast particles on turns 5–11 using the ref pickup.

The most appealing method for killing the electrons is to insert a lead radiator at the end of the AP-2 transport line. Between the last two quadrupoles in this line (IQ32 and IQ33), the betatron amplitudes are reasonably small (4–8m.) and the emittance blowup of the muon bunches due to multiple scattering should be small.

We have studied the effectiveness of radiator thicknesses of 0.25, 0.50, and 1.0 radiation lengths on removing electrons from the beam at the end of the AP-2 transport line. The program EGS was used to determine the energy of the leading (maximum energy) electron exiting the radiator for electrons of energy 9.0 GeV incident on the radiator. (The simulation was also checked analytically using a formula from Tsai [Ref. A.1].) The results are shown in Figure A3. If we impose an 8.7 GeV cut on the electron energy for it to be captured in the Debuncher, then for radiator thicknesses of 0.25, 0.50, and 1.0 radiation length, 40%, 11%, and 0.15%, respectively, of the incident electrons will survive the cut. We have chosen to use a radiator thickness of 1 radiation length in order to guarantee that electrons do not contribute to our muon signal.

Our measurements were performed, parasitic to the running of E-760, during the last several months. A one radiation length lead absorber was inserted into the AP-2 transport line, completely eliminating electrons from the beam. We used a Tektronix DSA 602 digital sampling analyzer to measure the time structure of the signal from the pickup. The DSA 602 has an analog bandwidth of 1 GHz, samples at 2 Giga-samples/second, and has a memory depth of 32,000 samples. We could, therefore, capture data for nine turns during a measurement. The data were taken in the following manner. Each measurement was an average over 64 pulses (each pulse containing 84 bunches). We first captured data for turns 1 through 9 and then set the DSA trigger delay to capture turns 9 through 17. The two data sets were normalized such that the $\bar{p}$ flux for turn 9 was equal. Fig. A4 shows the raw data for approximately 10 bunches for turns 3,4, and 5. In turns 3 and 5, we see the 8 nsec separation between the $\beta = 1$ particles and the $\bar{p}$'s. On the even turns, the $\bar{p}$ bunches are approximately in time with the $\beta = 1$ particles and thus the ref bunch structure shows only one peak. Therefore, in order to determine the individual particles fluxes, only data from the odd turns were usable. For each of the odd turns between turns 3 and 11, we averaged 60 of the 84 bunches to produce a "bunch averaged" time structure for each of the turns. The data for turns 5,7,9, and 11 are shown in Fig. A5. These data were fit to two Gaussians plus a constant. (The fit curves are also shown in Fig. A5.) From the fit parameters (amplitude and σ) we could then determine, for each turn, the area under the two Gaussians. These numbers are directly proportional to the flux of $\beta = 1$ particles and

$\bar{p}$'s. In order to determine the flux of muons, we then only had to make a correction for the number of pions remaining at each turn. In order to do this, we used the measured $\beta = 1$ particle flux from turn 1, assumed that this entire flux was due to pions, calculated the number of pions remaining after each turn, and then subtracted that number from the measured $\beta = 1$ flux for that turn to determine the number of muons. Our results are shown in Table A.1 for turns 3–11.

Table A.1

Particle Flux Measurements

Turn	Flux($\beta = 1$)	Flux($\bar{p}$)	$\frac{(\beta=1)}{\bar{p}}$	$\frac{\mu}{\bar{p}}$
1	33572	—	—	—
3	6251	2126	2.94	0.80
5	2232	1287	1.73	1.12
7	1597	1171	1.36	1.27
9	1306	1132	1.15	1.14
11	934	1122	0.83	0.83

We have also modeled the AP-2 line and the Debuncher ring in a DECAY_TURTLE simulation in order to compare our muon flux measurements with expectations. The simulation uses measured magnetic field strengths and gradients for the beam line and ring magnets and measured apertures for all elements. Particles are ray-traced from the target station, through the AP-2 beam line, through the Debuncher injection channel and through the first three revolutions in the Debuncher. We compare the results of the simulation to the muon flux measurements by calculating the ratio of the expected number of muons after three turns in the ring to the number of pions at the end of the beam line. An ion chamber measurement of the pion flux at the end of the beam line allows us to normalize the calculation.

This model calculation of the circulating muon flux accounts for the contribution from pion decay in the beam line as well as the ring. Consequently, it should be directly comparable to the muon flux measurement. The calculated flux agrees with the experimental data to within 10% and reinforces our belief that we have a reasonably good representation of the aperture limitations in both the transport line and the Debuncher ring.

REFERENCES

Ref II.1: BNL Neutrino Workshop, M. Murtagh Ed., 1987.

References for limits in Fig. II.1:

$\nu_e \rightarrow \nu_\mu$

BNL 776: L. Borodovsky et al., Phys. Rev. Lett. 68, 274(1992).
BNL 734 : L. Ahrens et al., Phys. Rev. D31, 2732 (1985).
CHARM: R. Eichler, Nucl. Phys. B (Proc. Suppl.) 3, 389 (1988).
BEBC PS: C. Angelini et al., Phys. Lett. 179B, 307(1986).
LAMPF: T. Dombeck et al., Phys. Lett. 194B, 591 (1987).
GOSGEN: G. Zacek et al., Phys. Rev. D34, 2621 (1986).

$\nu_e \rightarrow \nu_\tau$

BEBC SPS: O. Erriquez et al., Phys. Lett. 102B, 73 (1981).
FNAL 531: N. Ushida et al., Phys. Rev. Lett. 57, 2897 (1986).
FNAL B.C. (Bubble Chamber): N.J. Baker et al., Phys. Rev. Lett. 47, 1576 (1981).
LAMPF : P. Nemethy et al., Phys. Rev. D23, 262 (1981).

$\nu_\mu \rightarrow \nu_\tau$

CCFR: I. E. Stockdale et al., Phys. Rev. Lett. 52, 1384 (1984).
CDHS: F. Dydak et al., Phys. Lett. 134B, 281 (1984).
CHARM: F. Bergsma et al., Phys. Lett. 142, 103 (1984).

Ref II.2: S.P. Mikheyev and A.Yu. Smirnov, Nuovo Cimento 9*C*,17 (1986);
L. Wolfenstein, Phys. Rev. *D*17, 2369 (1978).

Ref II.3: W.J. Marciano, "Neutrino Physics – A Theoretical Perspective"
BNL Neutrino Workshop, M. Murtagh Ed., 1987.

Ref II.4: J.J. Simpson, PRL 54, 1891 (1985).

Ref III.1 Bromberget al., Nuclear Physics *B*107, 82 (1976).

Ref III.2 P.A. Aarnio et al., " A Long Writeup of the FLUKA86 Program",
CERN Divisional Report TIS-RP/168 (1986).

Ref III.3 B.F. Bayanov, T.A. Vseolozhskaya, Yu.N. Petrov, and G.I. Silvestrov
"The Investigation and Design Development of Lithium Lenses With

Large Operating Lithium Volume."
(Novosibirsk, IYF), Proceedings, High Energy Accelerators,
587-590 (1988).

Ref IV.1 E.D. Cummins and P.H. Bucksbaum, "Weak Interactions of Leptons and Quarks", Cambridge University Press.

Ref V.1: N. Kondakis, Ph.D. Thesis, Columbia University (1989).

Ref V.2: P.G. Reuteus, Ph.D. Thesis, University of Chicago (1986).

Ref VII.1: W. Busza, "Experience with Iarocci Tubes Produced on a Large Scale", Published in SLAC Colliding Beam, 210 (1987).

Ref VII.2 A.C. Benvenuti et al., Nucl. Instr. and Meth. A284, 339 (1989).

Ref A.1 Y. Tsai, Rev. of Mod .Phys. Vol. 46, No. 4, 815 (1974).

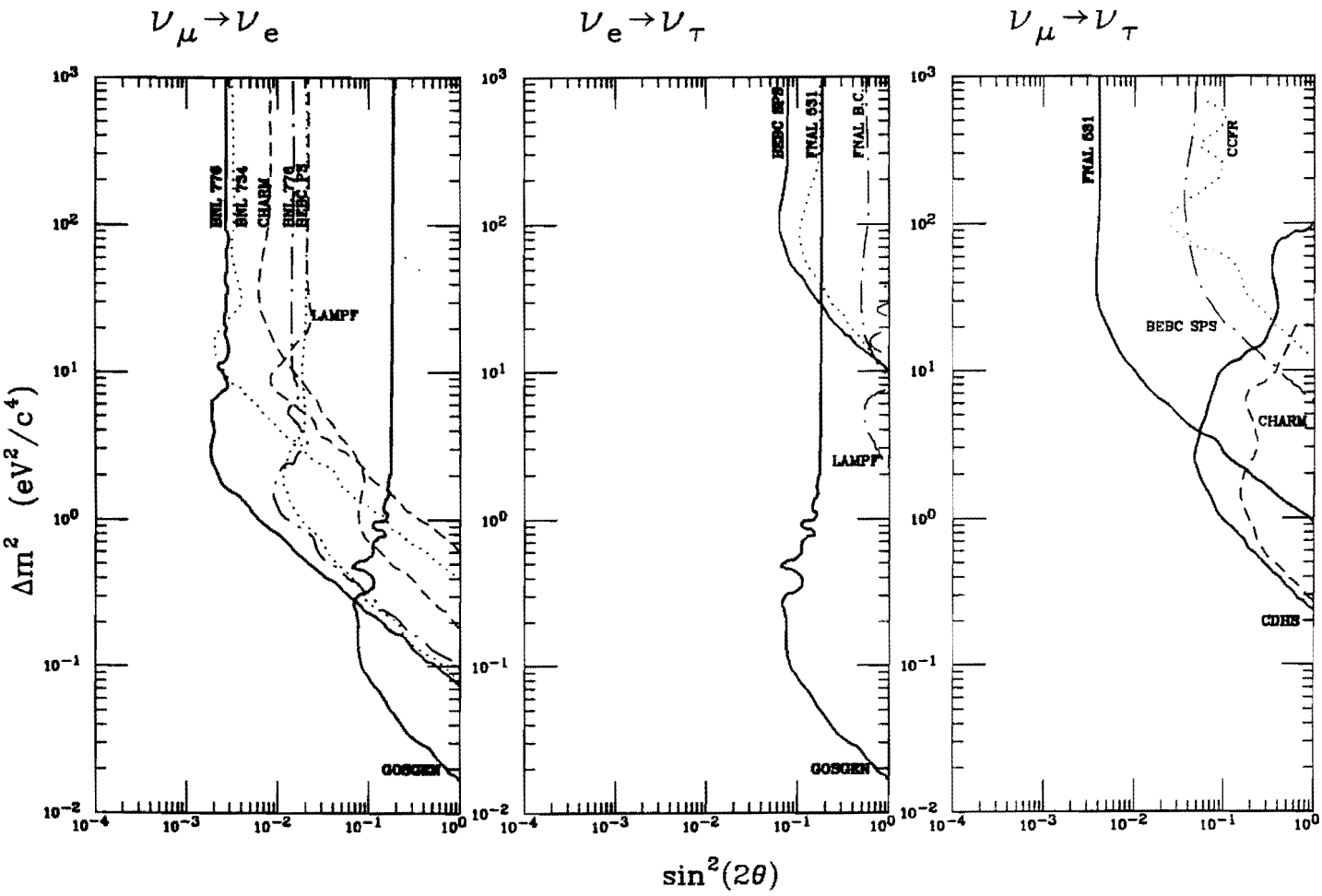

Fig. II.1: Current neutrino oscillation limits for a) $nu_e \rightarrow \nu_\mu$, b) $\nu_e \rightarrow \nu_\tau$, and c) $\nu_\mu \rightarrow \nu_\tau$.

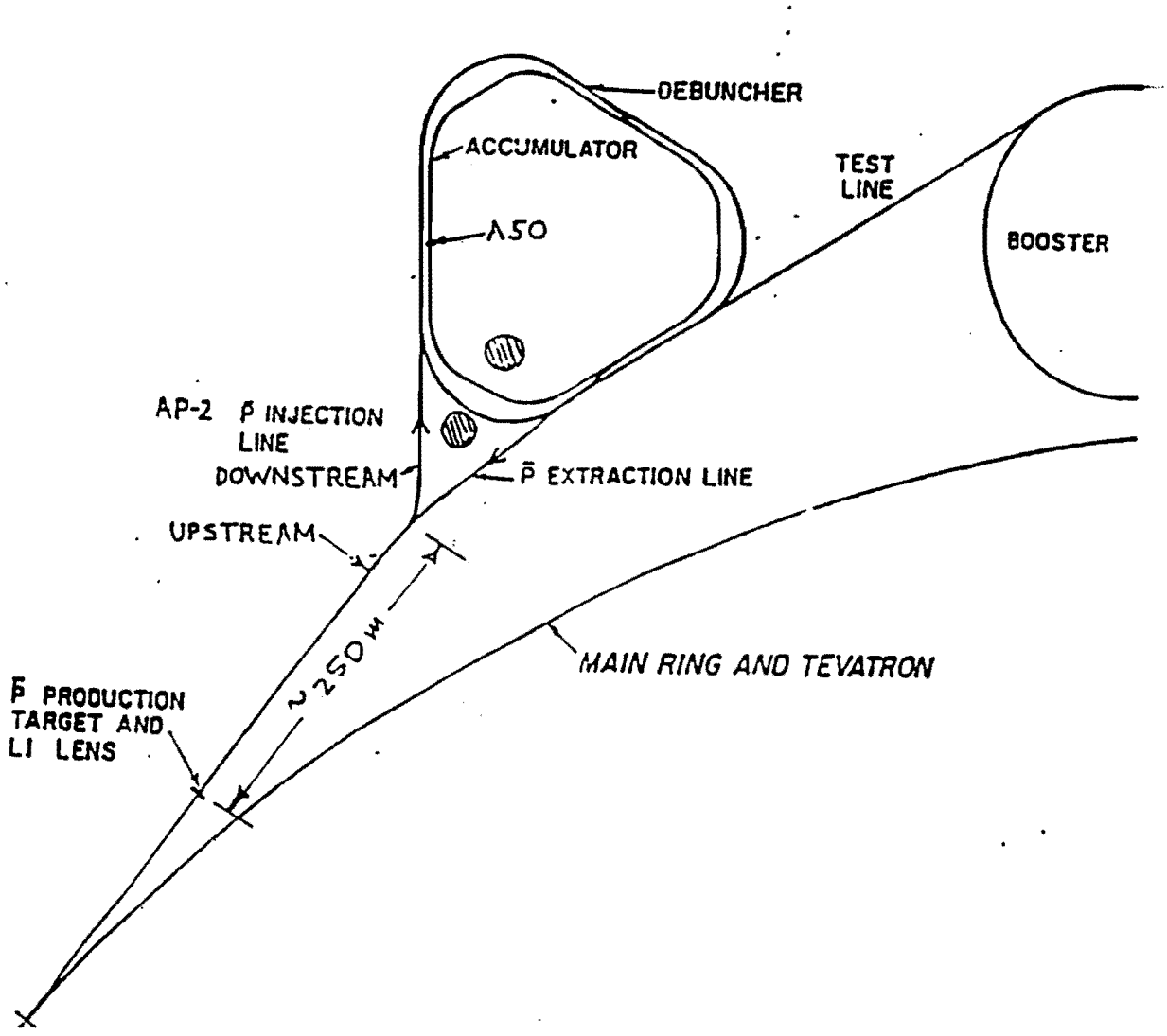

Fig. III.1: Fermilab Debuncher storage ring.

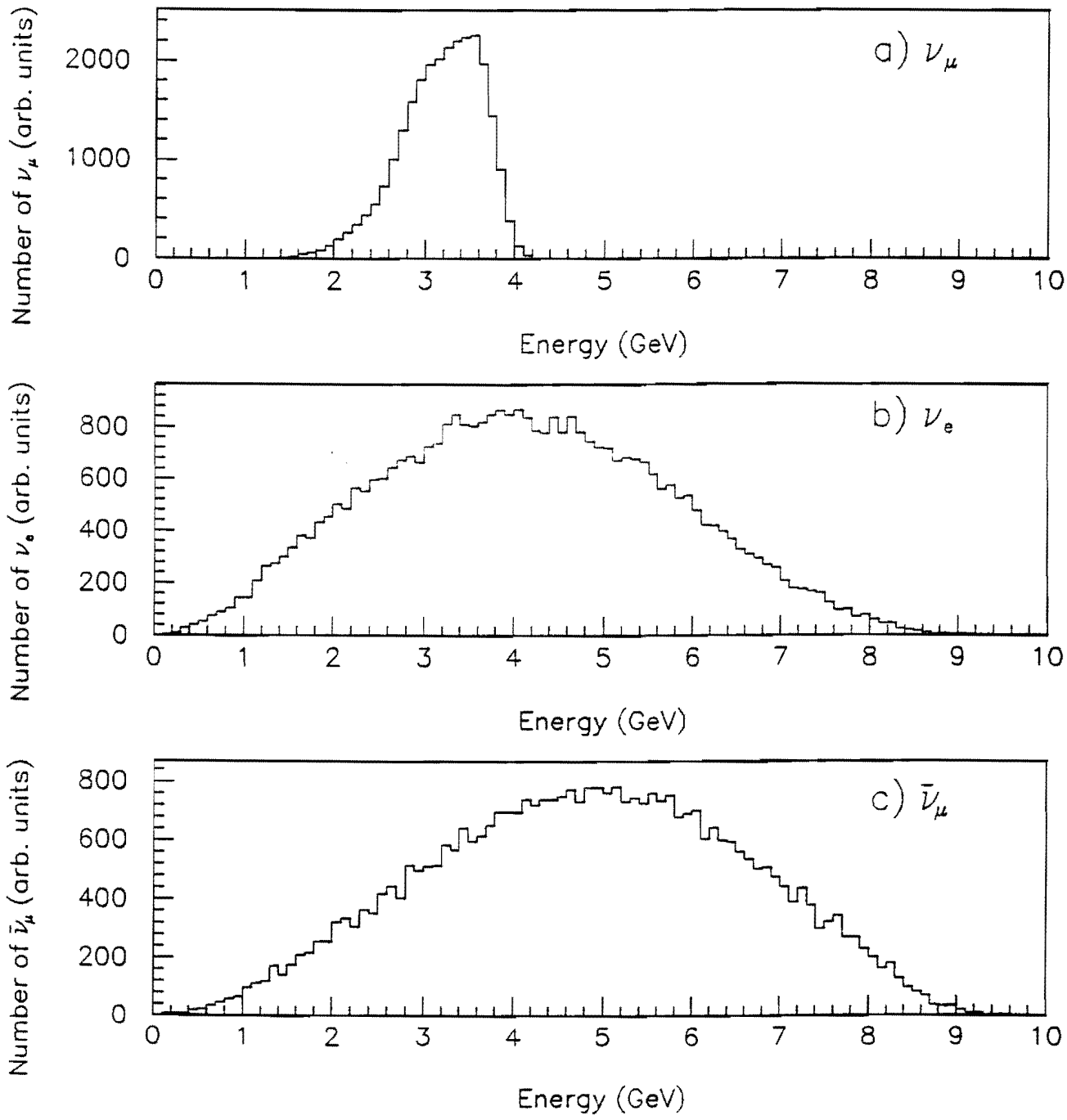

Fig. IV.1: ν_e energy spectra from the Debuncher with a 10 mrad cut. The Debuncher energy is 9 GeV.

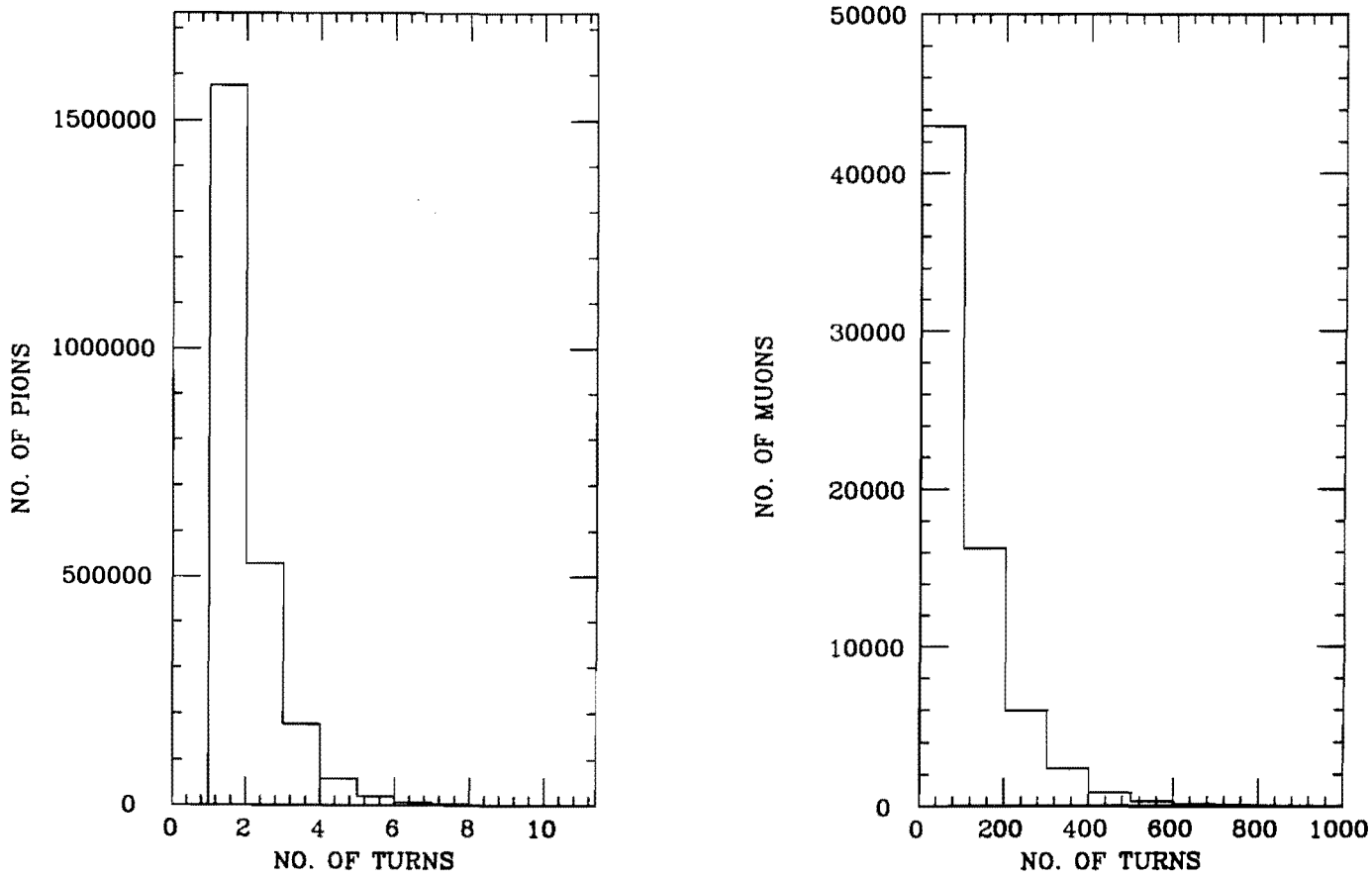

Fig. IV.2: The number of pions and muons in the debuncher as a function of number of revolutions.

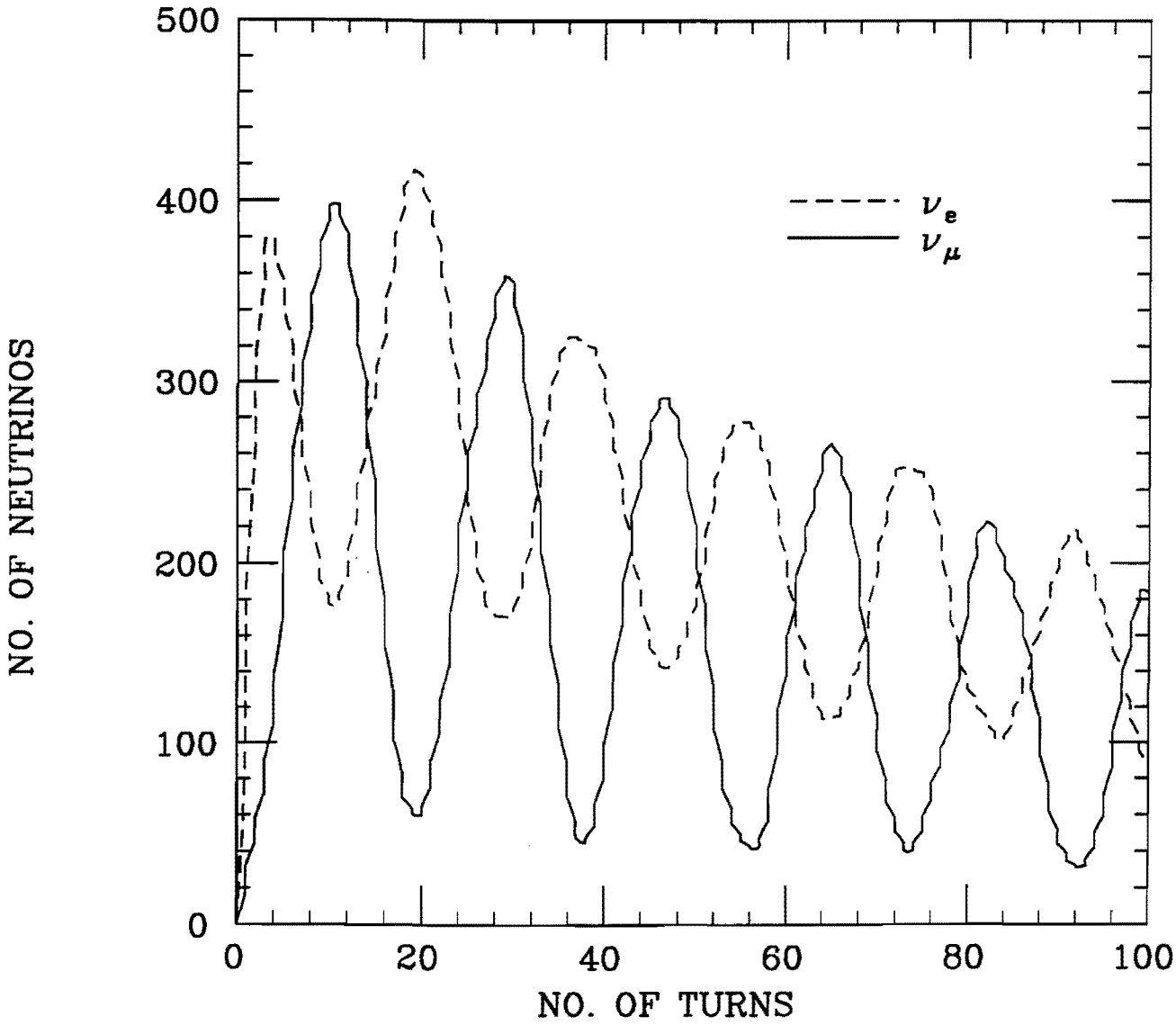

Fig. IV.3: The number of high energy ν_e and $\bar{\nu}_\mu$ accepted by the detector as a function of number of turns. A 10 mrad, 6 GeV energy cut is applied.

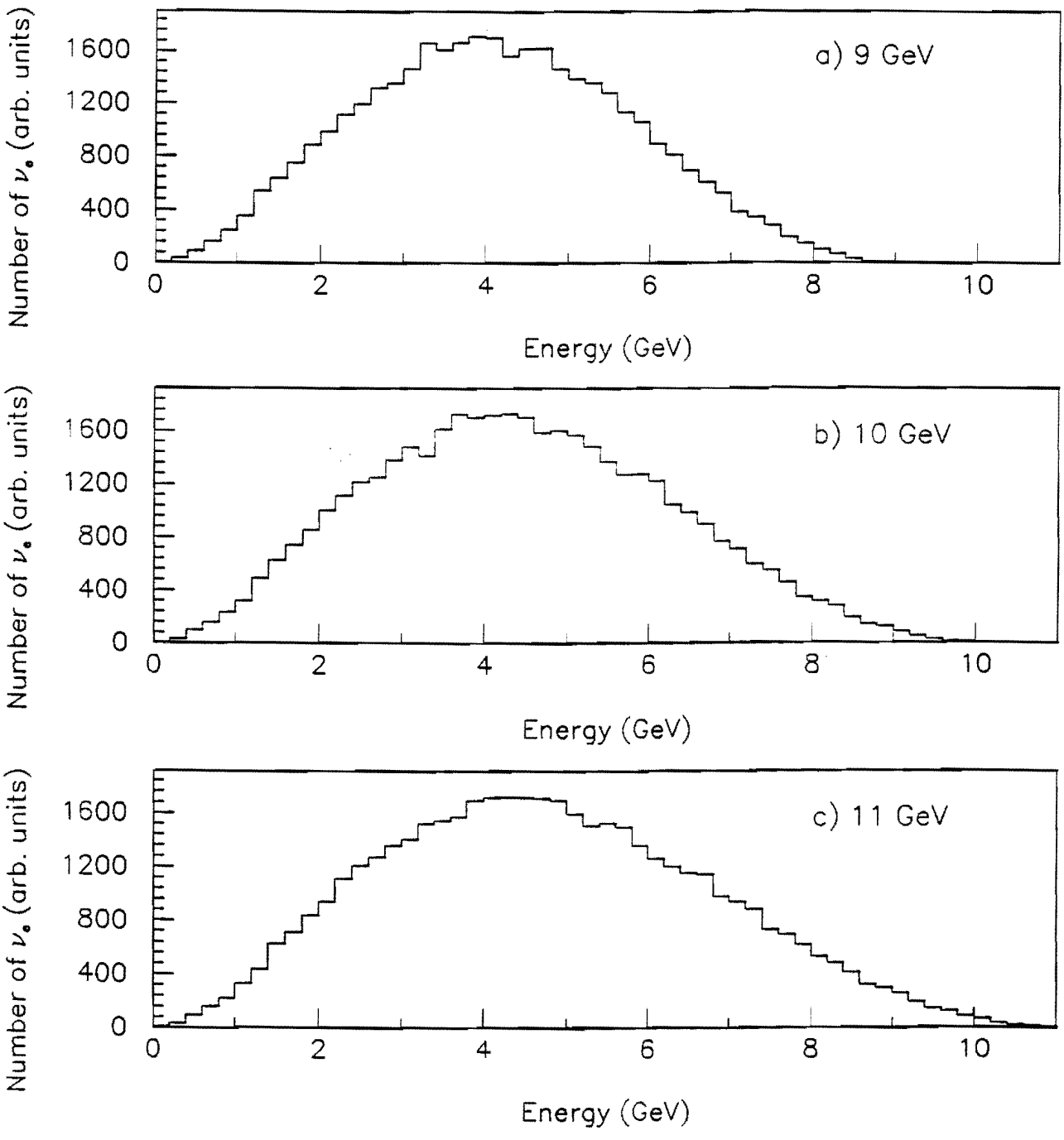

Fig. IV.4: ν_e energy spectra for debuncher energies of a) 9 GeV, b) 10 GeV, and c) 11 GeV with a 10 mrad cut.

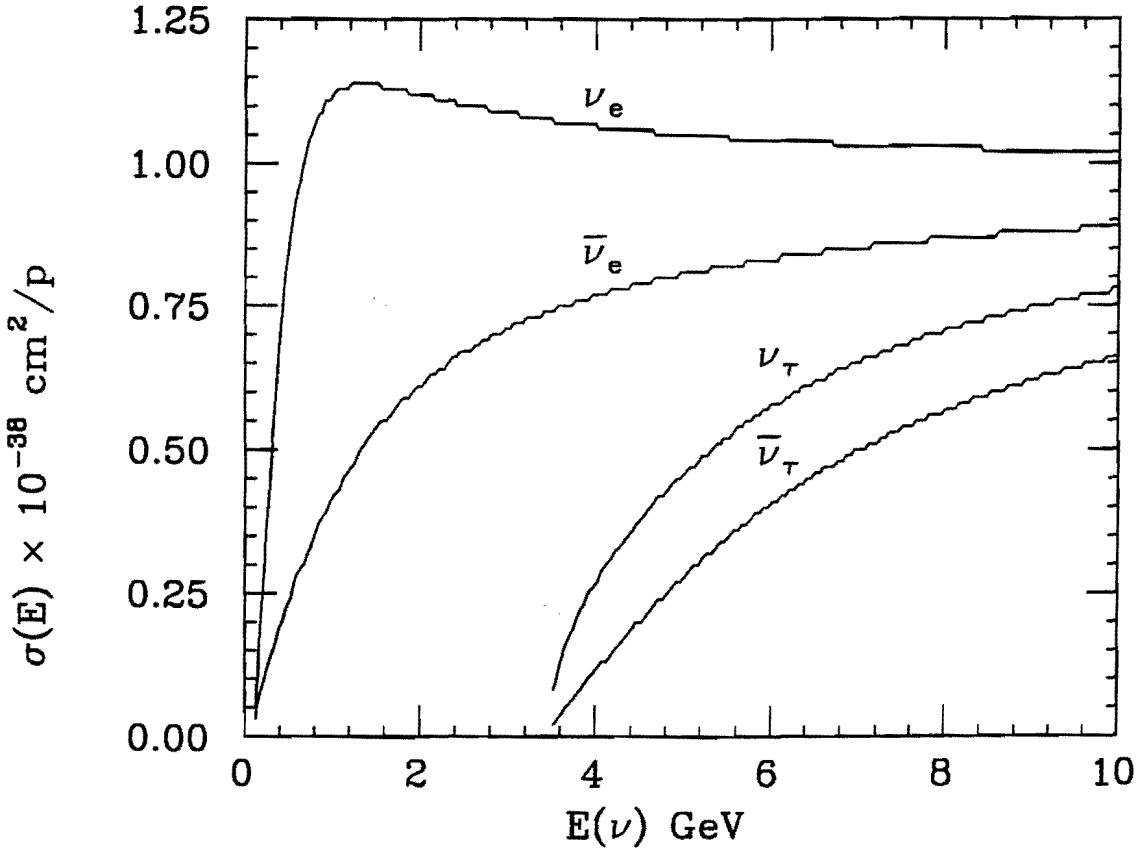

Fig. IV.5: Quasi elastic cross section for ν_e, $\bar{\nu}_e$, ν_μ, and $\bar{\nu}_\mu$.

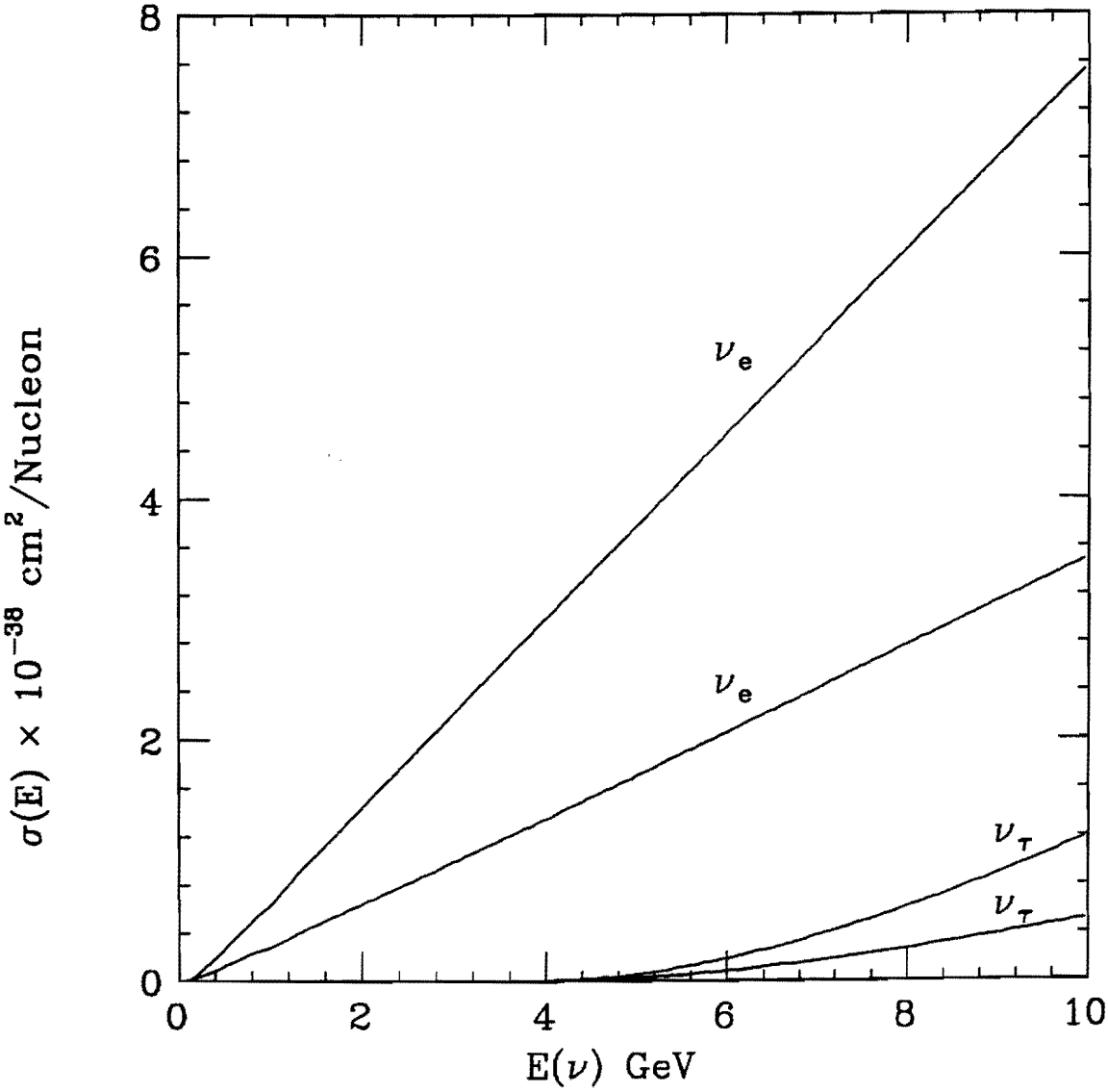

Fig. IV.6: Inelastic cross section for ν_e, $\bar{\nu}_e$, ν_μ, and $\bar{\nu}_\mu$.

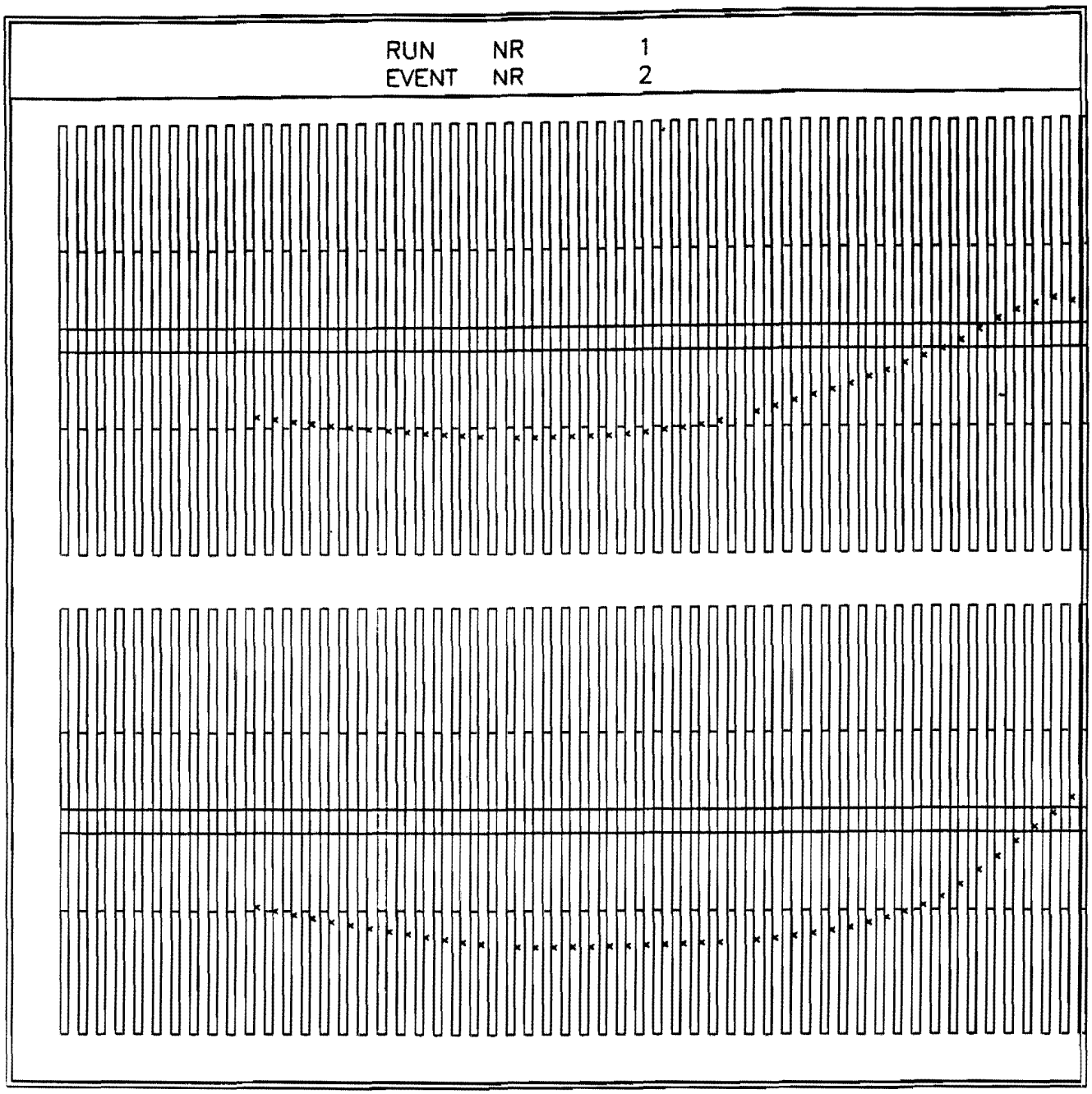

Fig. V.1: A typical quasi elastic τ event using a GEANT simulation of the proposed detector. The figure depicts a 5 GeV ν_τ interacting to produce a 5 GeV τ^+ decaying to a 4.5 GeV μ^+.

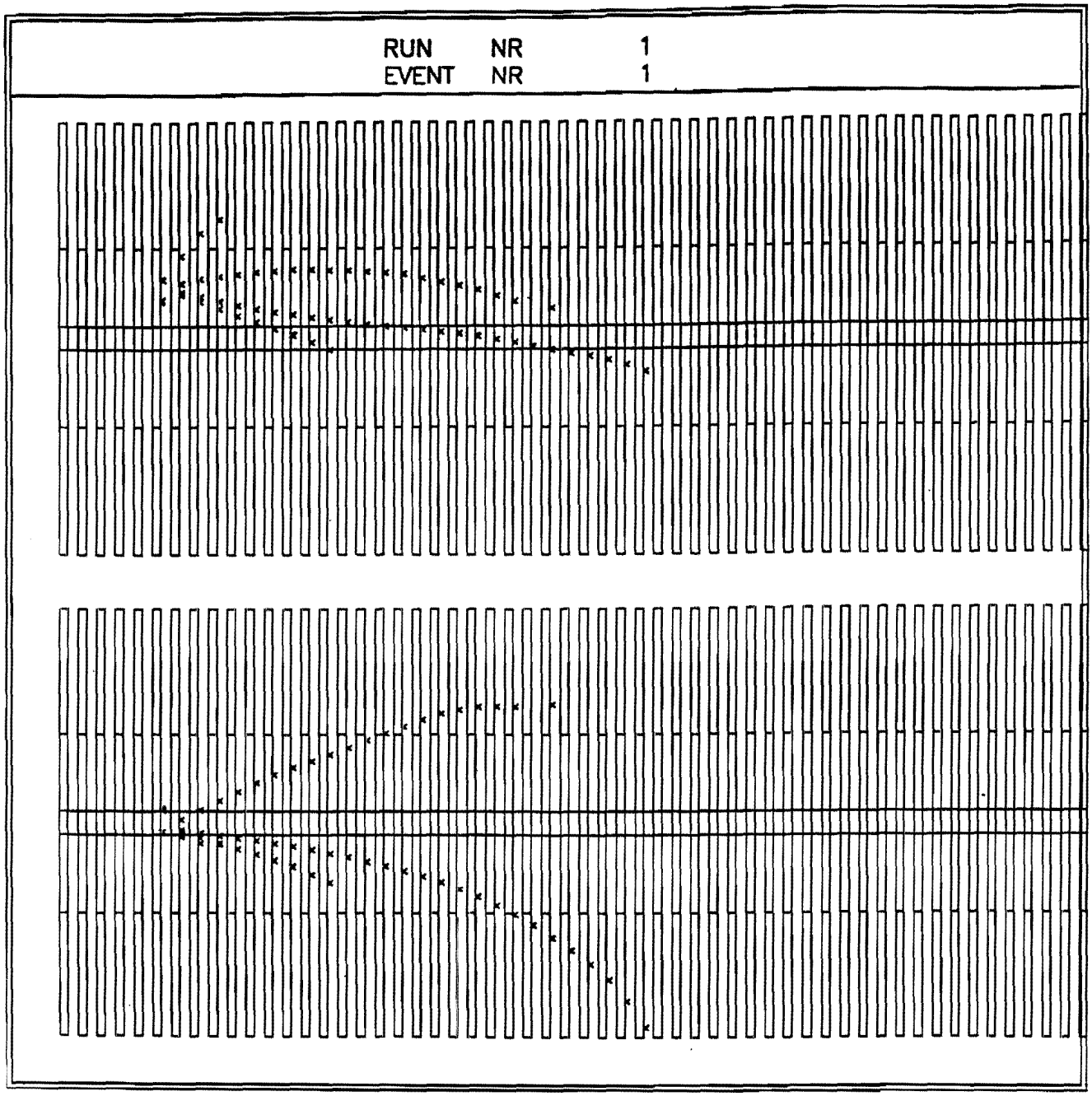

Fig. V.2: A typical charm event using a GEANT simulation of the proposed detector. The event depicts a 7 GeV $\bar{\nu}_\mu$ producing a 1.5 GeV μ^+ and 2.9 GeV D^-, which decays to a 1.5 GeV μ^-, 0.6 GeV ν and 0.6 GeV K^{*0}.

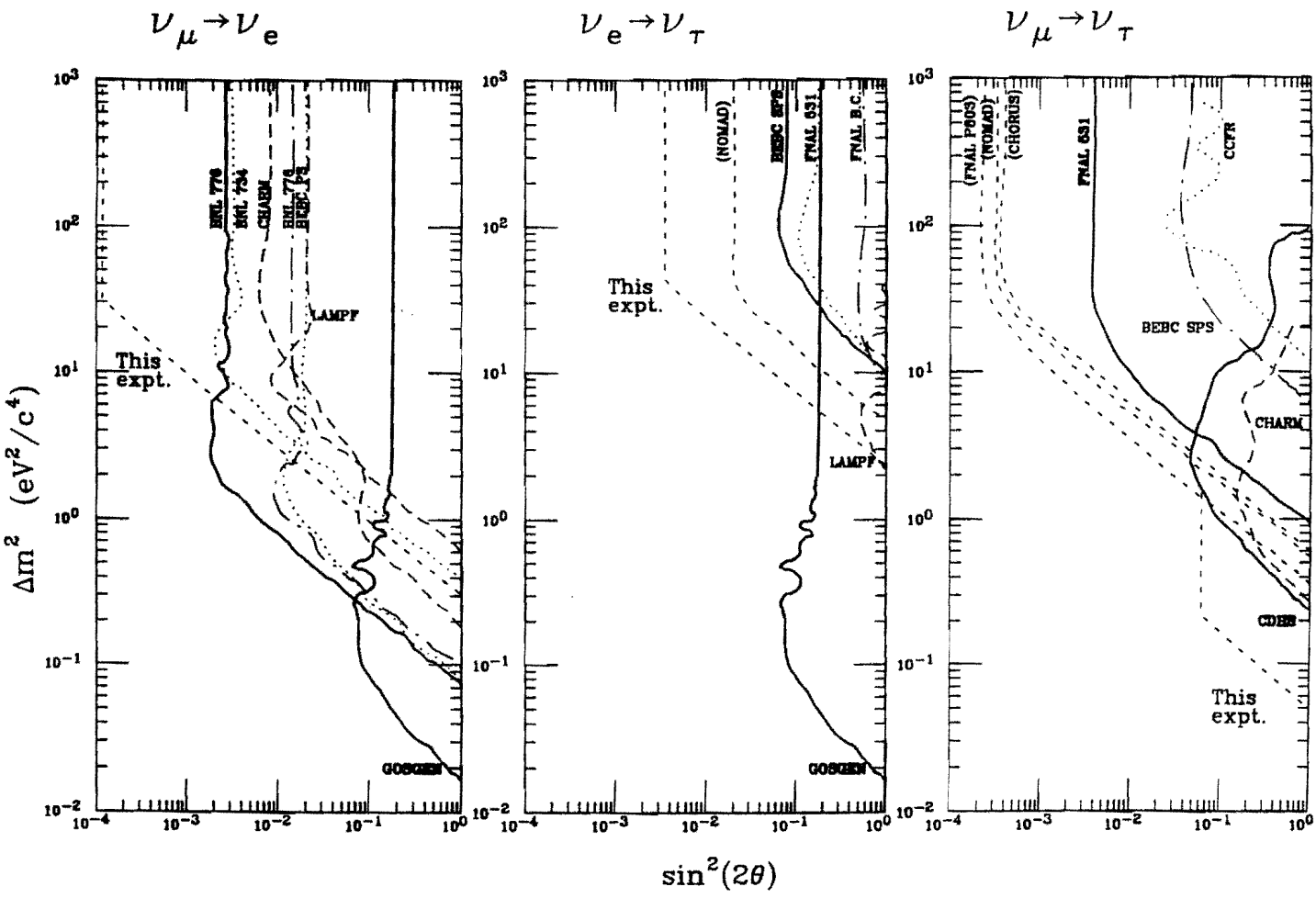

Fig. VI.1: Current neutrino oscillation limits for a) $\nu_e \rightarrow \nu_\mu$, b) $\nu_e \rightarrow \nu_\tau$, and c) $\nu_\mu \rightarrow \nu_\tau$. Proposed experimental limits included.

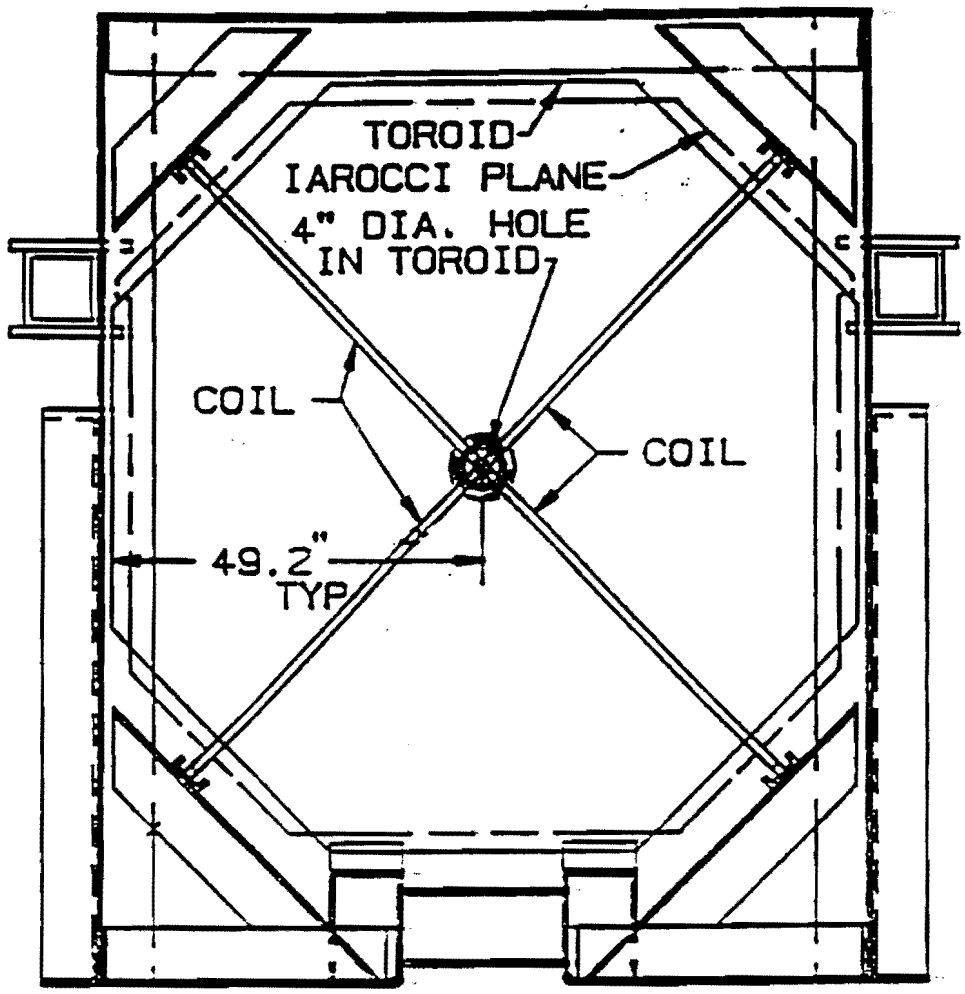

Fig. VII.1a: Schematic drawing of the proposed detector (front view).

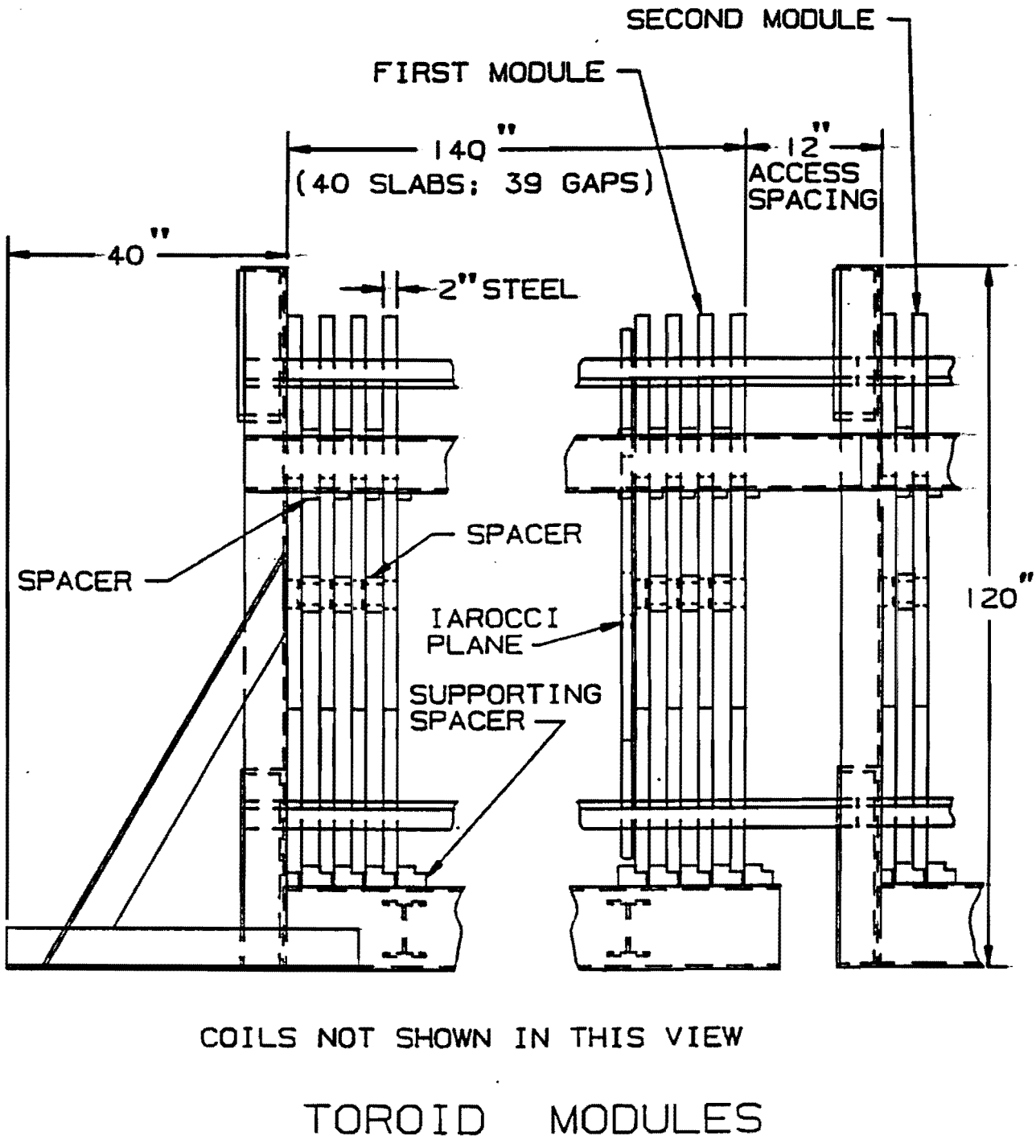

Fig. VII.1b: Schematic drawing of the proposed detector (side view).

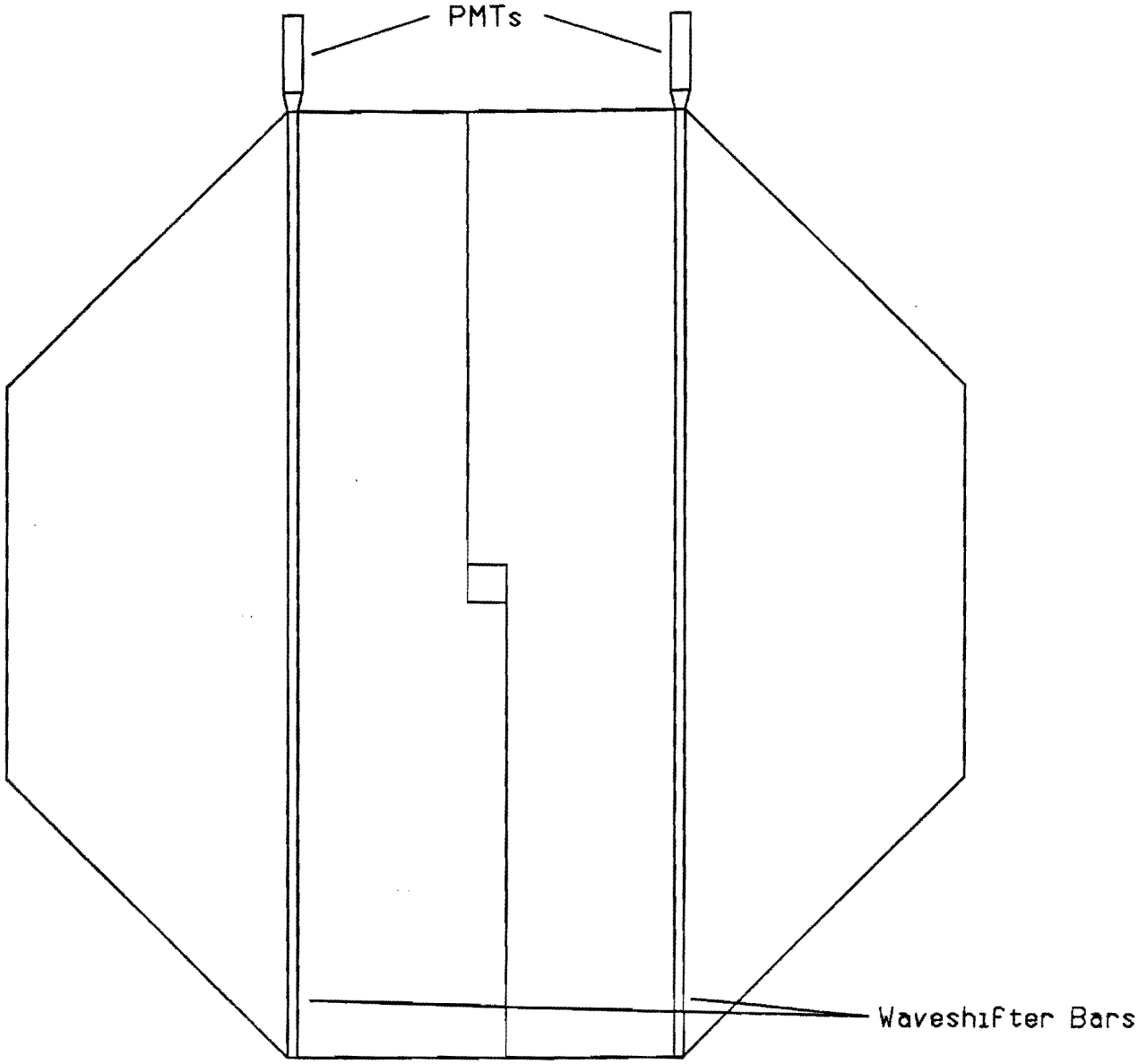

Fig. VII.2: Schematic drawing of a scintillator plane.

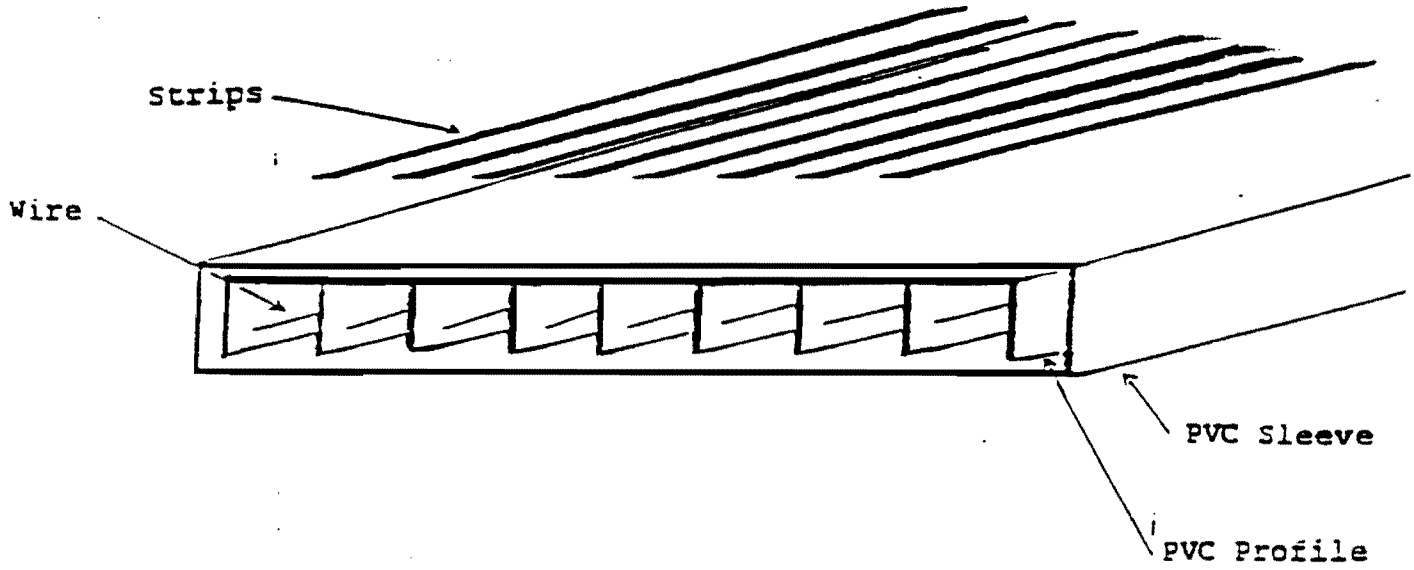

Fig. VII.3: Schematic drawing of an Iarocci tube module.

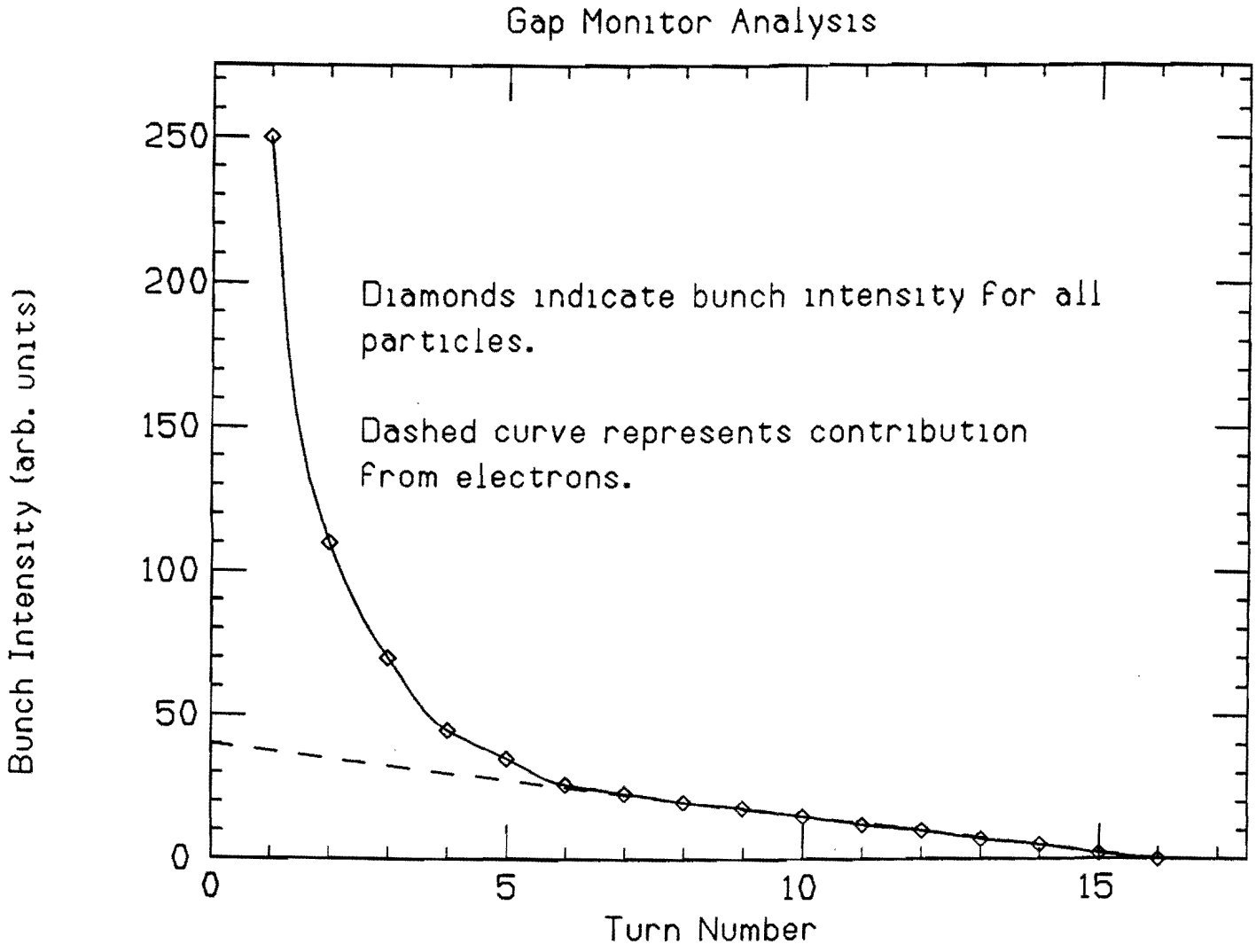

Fig. A1: 1987 μ flux measurement results

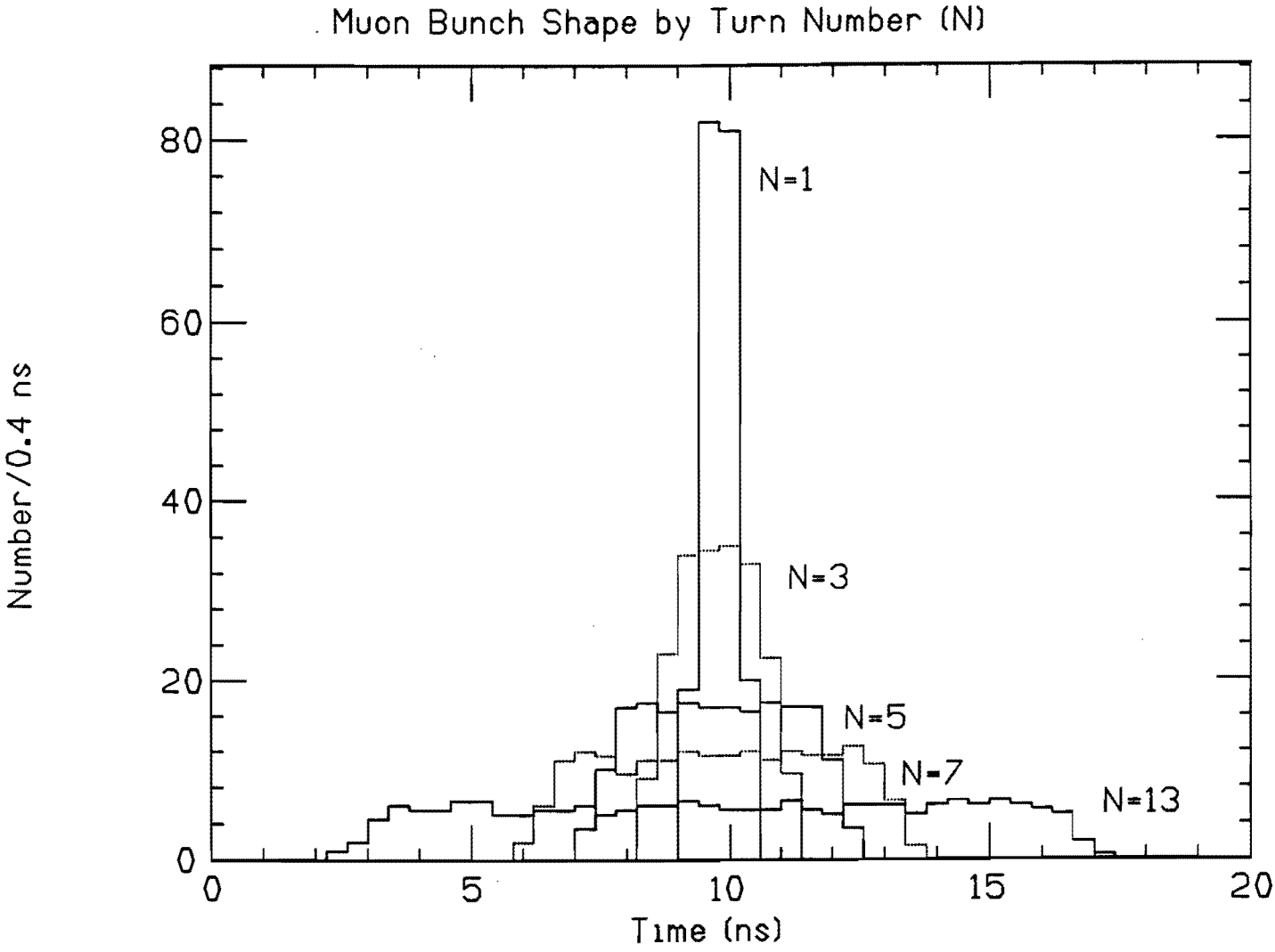

Fig. A2: μ bunch shape as a function of turn number.

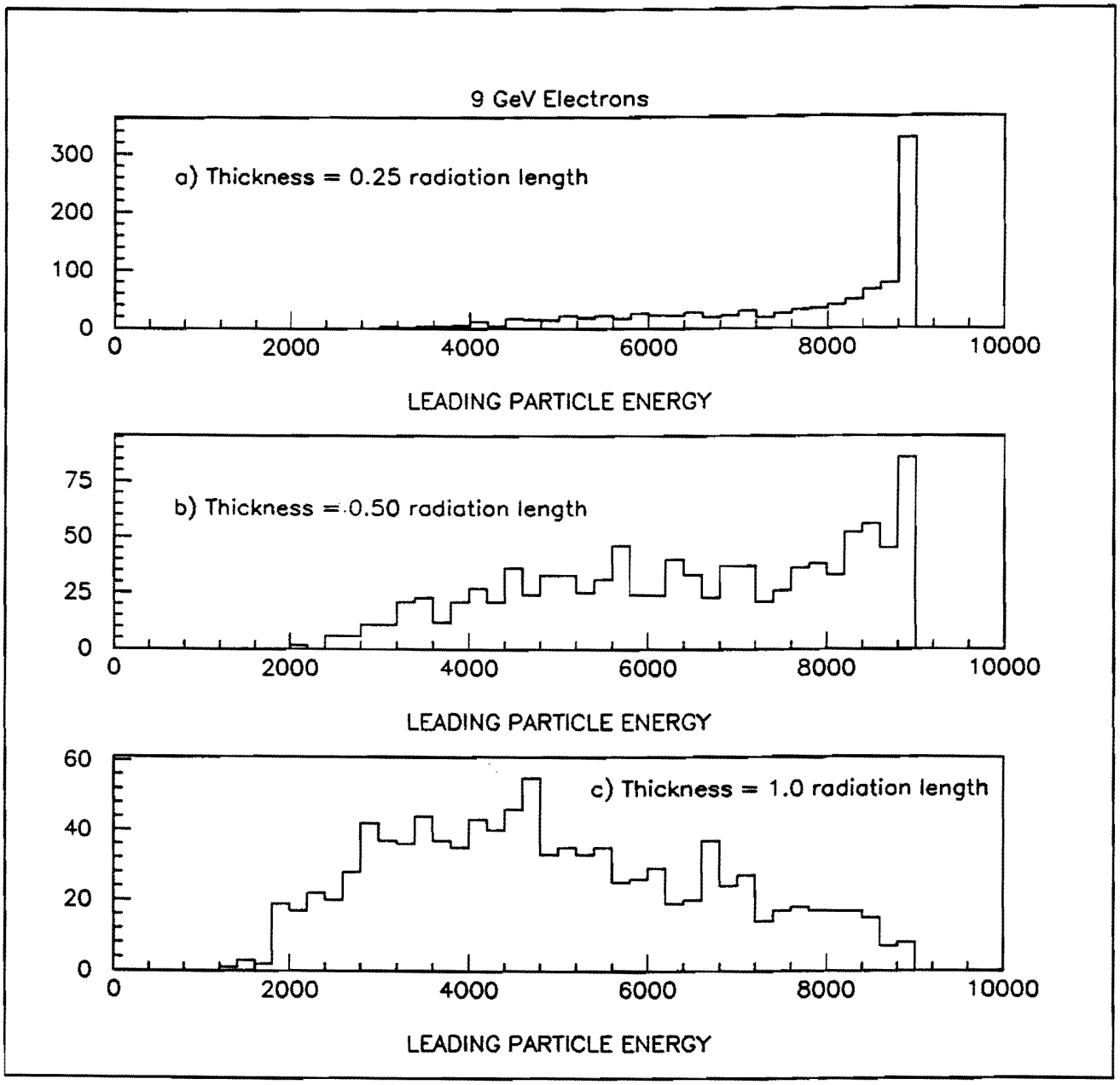

Fig. A3: Leading e^- energy for a) 0.25 rad length lead, b) 0.50 rad. length lead, and c) 1.00 rad length lead.

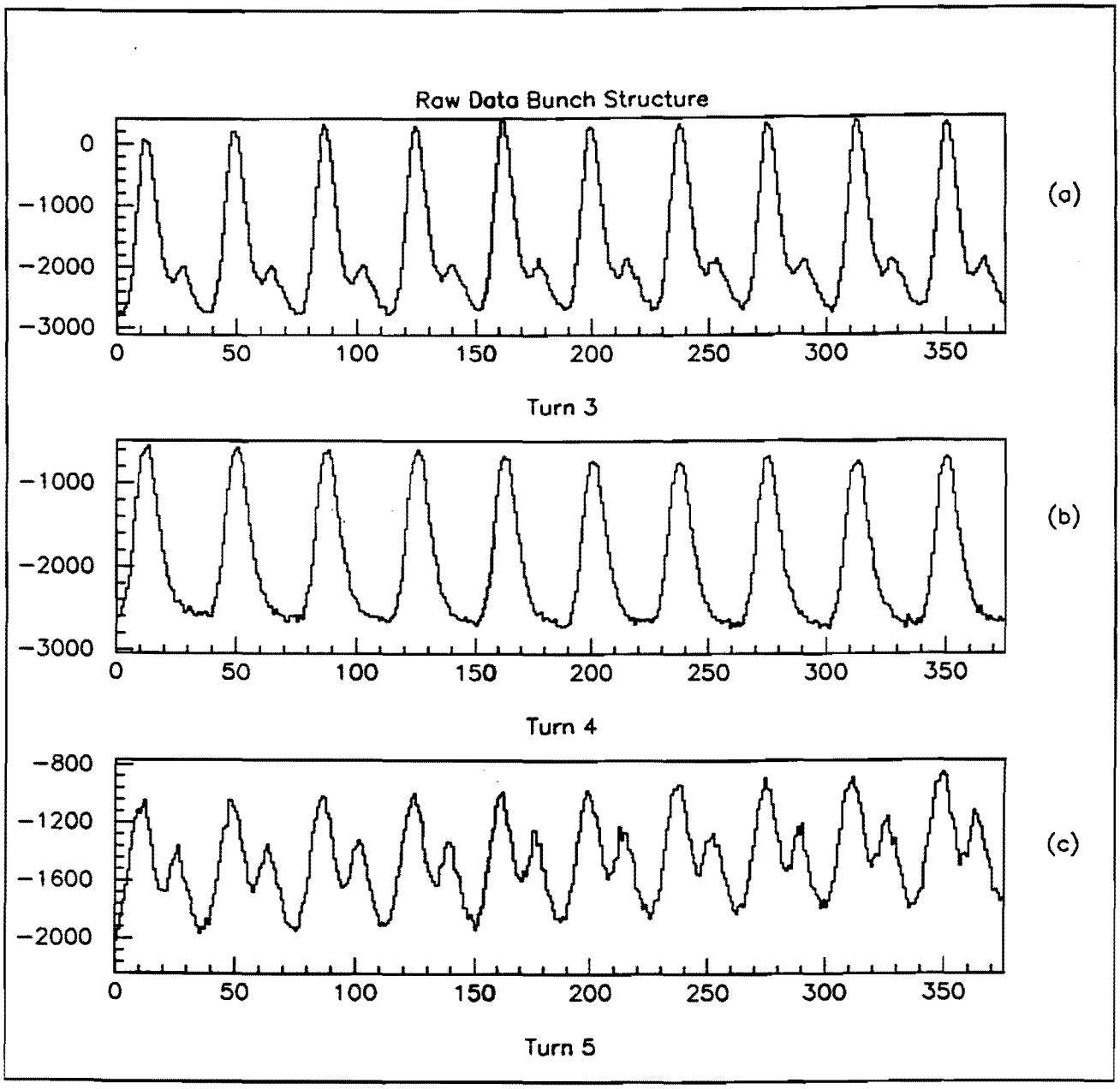

Fig. A4: Debuncher bunch structure for a) turn 3, b) turn 4, and c) turn 5.

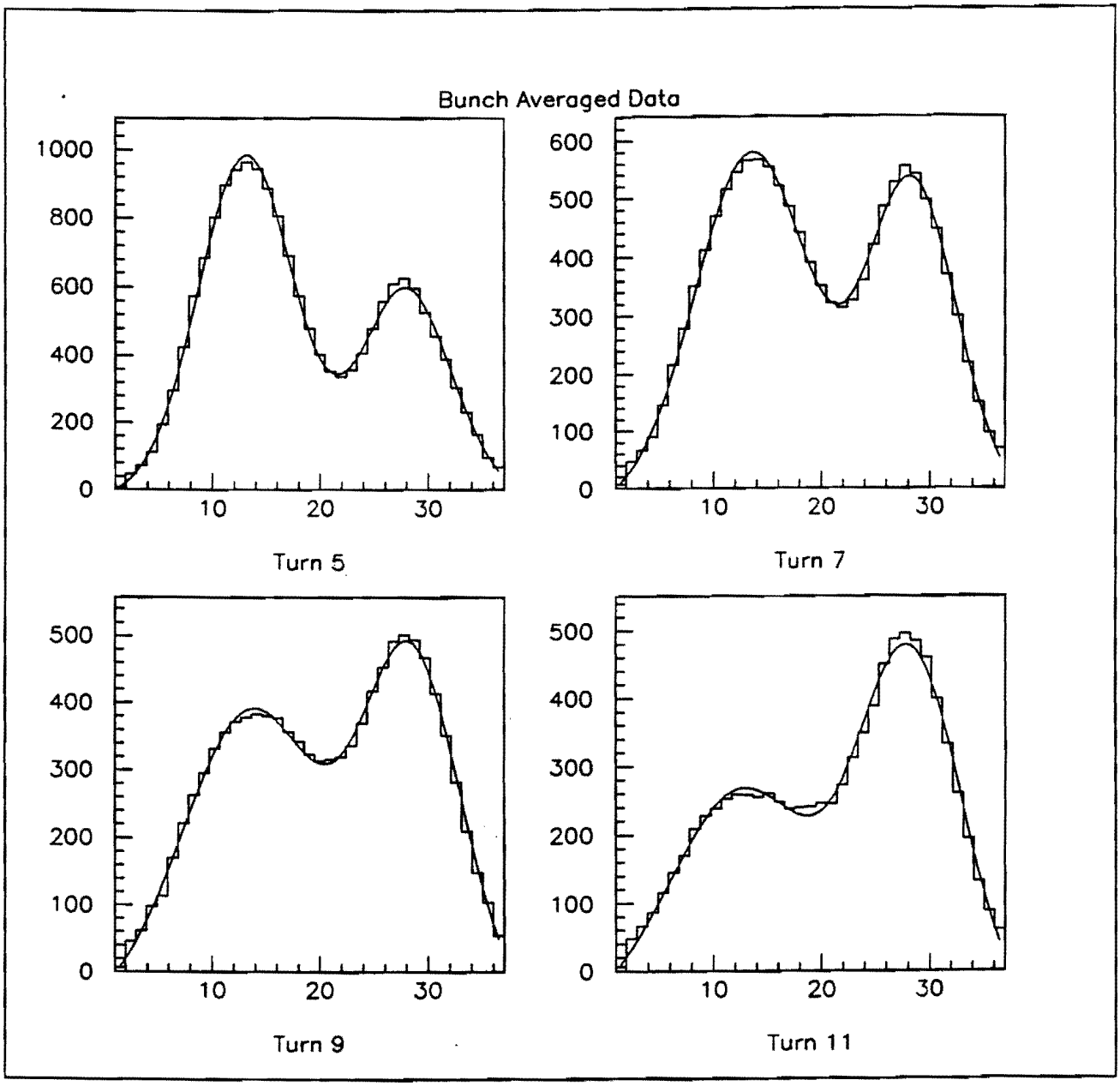

Fig. A5: Time averaged bunch structure for turns 5, 7, 9, and 11. The fit results of double Gaussian plus constant function is superimposed on the data.

ADDENDUM TO FERMILAB PROPOSAL 860

June 1, 1992

I. INTRODUCTION

P860 is a proposal to carry out a series of neutrino oscillation searches using the Fermilab Debuncher Ring as a muon storage ring. Initially, pions and muons from the antiproton production target are collected in the Debuncher. The pions decay in a few turns to give additional muons and neutrinos, while the muons decay over a few hundred turns to give electron neutrinos and muon antineutrinos. There are many advantages in this choice of beam. First, the Debuncher exists and in almost all running conditions, especially after the new Main Injector is operational, can supply an adequate neutrino flux for the experiment. The neutrinos are time separated by species so the basic search for $\nu_e \rightarrow \nu_\tau$ oscillations is a search for the wrong sign lepton as a function of the spill time, a relatively simple signature. Also the energy spectrum of the neutrinos from muon decays is such that one can do an appearance search for tau neutrinos.

The primary goal of P860 is a sensitive appearance search for $\nu_e \rightarrow \nu_\tau$ oscillations. Since the detector will be placed as near to the Debuncher as possible, the sensitivity is primarily in the mixing angle. This is the only dedicated ν_e oscillation search currently being proposed and is orthogonal to earlier reactor disappearance searches which are extremely limited in mixing angle but have a reasonable sensitivity in mass difference. Other proposed oscillation searches are primarily ν_μ oscillation searches, but they have some sensitivity to ν_e oscillations as there is typically a small ($\sim 1\%$) ν_e component in the neutrino beam. Since the ν_e component in this case is a small contamination in the ν_μ beam, it is less likely that these experiments can positively identify a ν_e oscillation signal if it is present. The experiment is also sensitive to $\nu_e \rightarrow \nu_\mu$ oscillations. The expected sensitivity in this case is significantly better than currently published limits.

The second phase of the experiment is a search for ν_μ oscillations via ν_μ disappearance. This phase would be a 2 detector experiment with a second detector located a few kilometers from the Debuncher providing good Δm^2 sensitivity. This would be orthogonal to the $\nu_\mu \rightarrow \nu_\tau$ appearance experiments presently under construction at CERN and the proposed emulsion experiment P803 at Fermilab. These are all sensitive to small mixing

angles but are not sensitive to small Δm^2. There are indications that it may be important to look in this region. As noted in the P860 proposal, the inference from the solar neutrino data is to search for ν_μ oscillations at small Δm^2 (Fig. I.1). In addition, the recent results from Kamiokande and IMB of a depletion of atmospheric muon neutrinos relative to electron neutrinos can be interpreted as as an oscillation effect at small Δm^2 with reasonably large mixing (Fig. I.1). For this experiment the far detector would be aligned, not with a leg of the Debuncher, but with the AP-2 transfer line, as the pion flux is significantly higher in this case. The expected Δm^2 sensitivity in P860 is not dissimilar from what one could get at Brookhaven and it is probably competitive with some of the long baseline experiments which have been suggested for Fermilab using the Main Injector.

In the original proposal, it was argued that to obtain an adequate neutrino flux it was necessary to accumulate positives in the Debuncher and to run the Main Ring in a multi-batch mode. This was under the assumption that the experiment would run before the Main Injector was operational. Since the proposal was submitted, a number of different running conditions have been considered which will provide an adequate flux for the experiment. In all of these cases, we would be running together with other users. The various running options are detailed below.

1. Before the Main Injector.

As noted in the original P860 proposal, the flux available running in a single batch mode is not adequate for this experiment. However, the flux is suitable for the test we have planned for 1994. To do physics we need to run the Main Ring in a multi-batch mode. Our preference would be to run positives, as there is an additional factor of 2 improvement in interaction rate. However, we can run in Collider mode with negative flux. This is a change from the proposal where we specifically requested running with positives. With adequate funding we believe that we could be ready for this run by 1996. This mode of operation requires the construction of a fast extraction kicker for the Main Ring and the development of a new lithium lens for the antiproton target station. It is likely that the fast kicker could be the same as the one presently under development for the Main Injector and the new lithium lens is needed for any multi-batch mode of running. We believe that in one 200 day run in this configuration we can complete the $\nu_e \rightarrow \nu_\tau$ phase of the experiment.

2. After the Main Injector

In this case, we can run in either single or multi-batch mode. Again, multi-batch mode is preferred and in the optimum situation this would improve our rate by a factor of 3 over

single-batch operation. The rates for multi-batch running for collider operation in this case are about 50% higher than those obtained in the multi-batch mode before the Main Injector. If we run positives with the fixed target program and receive half the batches, then the rates are comparable to those in the Collider mode. If we were able to complete the $\nu_e \rightarrow \nu_\tau$ phase of the experiment before the Main Injector is available, then the focus of the Main Injector phase of the experiment would be on the ν_μ disappearance search.

The primary constraint on the experiment, from our perspective, is the funding to build the detector. We expect to be able to build a prototype module by 1994 with minimal Fermilab help and, if funding becomes available, to build the complete detector by 1996. If the Main Injector will be on-line by 1996 then we see no advantage in asking for the multi-batch mode of running with the present Main Ring. However, if the Main Injector will be delayed until 1998 or later, we would hope that the multi-batch mode for the Main Ring is seriously considered.

In order to preserve our momentum, to build the collaboration and, most importantly, to understand the feasibility of our proposal, we believe it is very important that we mount a test with a prototype detector module at the Debuncher by 1994. We believe that we can make this prototype with minimal Fermilab funding and that the flux from the Debuncher, running parasitically to the Collider operation, will be adequate for this test. The Fermilab members of the collaboration would like to assume responsibility for the scintillator in the prototype detector. This will require some modest R&D support and funds to buy the required scintillator and its attendant readout. In addition, it will be necessary for Fermilab to provide a suitable detector building at the Debuncher for this test and perhaps to provide some support for the installation and operation of the equipment. Our belief is that the development and construction of the new lithium lens is a critical path and long lead time item and we would hope that work on this project would begin very soon.

II. EVENT RATES AND LIMITS

The rates in the P860 proposal are based on the Main Ring and Debuncher parameters listed in Table II.1. The Main Ring numbers are those expected after the Linac Upgrade is completed, while the $\mu^-/\bar{p}$ ratio was measured recently in the Debuncher (Appendix A in P860).

TABLE II.1: Debuncher Parameters

Proton/Pulse:	3×10^{12}
$\bar{p}/p$:	3×10^{-5}
Cycle time:	2.1 Sec
$\mu^-/\bar{p}$:	1.0
π^-/μ^-:	50.
Running Eff:	0.80

The calculated numbers of pions and muons per day in the Debuncher are

$$\begin{aligned}\text{Pions/day} &= (3 \times 10^{12}) \times (3.0 \times 10^{-5}) \times (3600 \times 24/2.1) \times 50 \times .80 \\ &= 1.5 \times 10^{14}\end{aligned}$$

and,

$$\begin{aligned}\text{Muons/day} &= (3 \times 10^{12}) \times (3.0 \times 10^{-5}) \times (3600 \times 24/2.1) \times .80 \\ &= 3.0 \times 10^{12}.\end{aligned}$$

While this flux is inadequate for a serious oscillation experiment, it is sufficient for test purposes.

The proposal advocates running the Main Ring in a multi-batch mode which appears quite feasible from a machine operation viewpoint and requires few new components to be built. The multi-batch mode of operation will increase the flux by a factor of 6.4.

This flux is actually down by a factor of $2 \times 1.4 = 2.8$ from the proposal. It is now thought that projected improvement factors arising from operating the Debuncher at 10 GeV ($\times 1.4$) and operating the transfer line at a 2% higher momentum ($\times 2.0$) can not be realized. In addition, the proposal requested a change in the polarity of the Debuncher so that one would do the experiment with neutrinos and not antineutrinos. This would give an additional factor of two improvement in the interaction rate due to differences in the cross sections for neutrinos and antineutrinos.

There are several proposed operational modes for the Main Injector. It appears that all of these can yield an adequate flux for this experiment. For single-batch-antiproton-production the number of protons/pulse will increase to 5.0×10^{12} with a cycle time of 1.5 seconds. This provides an improvement of 2.3 with respect to the present parasitic Main Ring running. The Main Injector can also be operated in a multi-batch mode. In this case four batches of protons are injected into the Main Injector and accelerated to 120 GeV. The first batch of protons in used to produce $\overline{p}$'s for accumulation. After the $\overline{p}$'s have been

transferred to the accumulator, the remaining 3 batches are extracted and targeted on the $\overline{p}$ production target. The resulting negative beam from each batch is dumped from the Debuncher after approximately 500 turns. The repetition rate for this mode of operation will increase to 1.9 seconds, yielding an improvement of $4 \times 1.5/1.9 = 3.2$ over the normal Main Injector $\overline{p}$ production operation.

For calculating the event rates in the detector, four modes of operation are considered. The first two use the Main Ring in multi-batch mode with both a positive and negative polarity setting for the Debuncher. The remaining two are for Main Injector running in both single-batch and multi-batch modes of operation with a negative polarity setting for the Debuncher.

The important quantity for calculating the event rates is the integral of the neutrino flux times the cross section, F_ν, for the neutrino species in question. The flux $\times$ cross sections for the neutrinos in question and for positive and negative running conditions are given in Table II.2. In this table, the values for quasi-elastics (QE), charged current single pion production (CCSP), and charged current deep inelastic scattering (CCDIS) are listed separately. It is important to note here that the ν_τ events are predominantly quasi-elastic or single pion events while the backgrounds will be predominantly deep inelastic events. The calculations assume the Debuncher is operating at 9 GeV and there is a 10 mrad cut on the neutrino angle with respect to the beam direction.

The number of events for each species of neutrino running for the four operating modes described above are summarized in Tables II.3 and II.4. For the Main Ring mode of operation, the running period is for 200 days, while the Main Injector modes are for 400 days of running. In these calculations the longitudinal fiducial tonnage ($\rho \times N_0 \times dZ$) of the detector is taken to be

$$7.87 \times 600 \times 6.02 \times 10^{23} \times 5.04 = 1.4 \times 10^{28} \mathrm{cm}^{-2}.$$

A livetime factor of 0.9 (in P860 0.75 was used) is assumed, and only 13% of the muons decay in the Debuncher straight section pointing at the detector.

The expected oscillation limits for the various running scenarios described above can be calculated from the event rates given in Tables II.3 and II.4 and the flux factors in Table II.2 using the formalism developed in the original P860 proposal (Section VI. Oscillation Limits). The background numbers used in these calculations are scaled from those in the P860 proposal to the appropriate number of events for the various calculations. The limits for the $\nu_e \rightarrow \nu_\tau$ appearance search are shown in Fig. II.1 .

Clearly, running positives with the Main Injector in a multi-batch mode is the preferred mode but all of these limits are quite respectable. The mixing angle limit for $\nu_e \rightarrow \nu_\mu$ is significantly better than present results. The $\nu_e \rightarrow \nu_\tau$ limit is significantly better in mixing angle than both existing data and the proposed CERN experiment (NOMAD) and appears to be comparable to the proposed Fermilab emulsion experiment (P803). It should be noted again that in P803 the ν_e beam is a small contamination in the ν_μ beam and so clearly establishing a ν_e oscillation signal might be quite difficult for P803.

Following the completion of the $\nu_e \rightarrow \nu_\tau$ oscillation search, the emphasis of the experiment would be on a long baseline, 2 detector ν_μ disappearance search. For this phase there are two possible options for the second detector. The first is to construct a second identical detector, leaving the first detector near the debuncher to monitor the ν_μ flux and continue with the $\nu_e \rightarrow \nu_\tau$ search should the physics justify it. The second option would involve moving a portion, $\sim$ 90%, of the near detector to the far detector location. The remaining 10% of the detector would remain located near the Debuncher straight section to monitor the ν_μ flux. For both options, the far detector would be located in line with the the AP-2 transfer line to the Debuncher. The neutrino flux arising from pion decays in the AP-2 transfer line has the advantage of higher flux, $\sim$ 20, than the neutrino flux in the Debuncher. For the purposes of calculating the event rates, locations for the long baseline detector of 3 km and 10 km from the end of the AP-2 transfer line are considered. In addition, two energy settings, 3 GeV and 9 GeV, for the AP-2 transfer line and Debuncher will be used. Clearly, the 9 GeV operation is compatible with Collider running but the 3 GeV setting is not.

Understanding and accounting for the difference in the neutrino energy and flux at the two detectors is crucial for the ν_μ disappearance search. Given an angle θ between the pion and neutrino in the lab frame, $\gamma^2\theta^2 << 1$ for the far detector. For the near detector, events with $\gamma^2\theta^2 << 1$ are also chosen. In this case, determination of both the neutrino flux and energy in the near and far detectors is straightforward. Note that the average angular divergence of the pion beam in both the AP-2 transfer line and the Debuncher is $\sim$ 1 mrad.

Charged current ν_μ events will be identified as all events with a clearly identified muon. Since the detectors will have good energy resolution, the sensitivity of this phase of the experiment will be dominated by the statistics in the far detector. In order to minimize the systematics, the two detectors should be identical.

TABLE II.2: F_ν for 9 GeV positive and negative Debuncher settings.

$F_{\nu_\mu} \equiv \int \mathrm{FLUX}(E)\sigma(E)dE \quad 10^{-40}\mathrm{cm}^2/\mathrm{pion}$ for ν_μ

Beam Polarity	Positive	Negative
QE	17.2	11.3
CCSP	15.9	10.8
CCDIS	76.4	34.3
TOTAL	109.5	56.5

$F_{\nu_e} \equiv \int \mathrm{FLUX}(E)\sigma(E)dE \quad 10^{-40}\mathrm{cm}^2/\mathrm{muon}$ for ν_e

Beam Polarity	Positive	Negative
QE	22.9	16.2
CCSP	21.1	15.4
CCDIS	145.2	66.2
TOTAL	189.2	97.8

$F_{\nu_\tau} \equiv \int \mathrm{FLUX}(E)\sigma(E)dE \quad 10^{-40}\mathrm{cm}^2/\mathrm{muon}$ for ν_τ

Beam Polarity	Positive	Negative
QE	6.5	4.2
CCSP	2.8	1.8
CCDIS	4.5	2.0
TOTAL	13.8	8.0

$F_{\bar{\nu}_\mu} \equiv \int \mathrm{FLUX}(E)\sigma(E)dE \quad 10^{-40}\mathrm{cm}^2/\mathrm{muon}$ for $\bar{\nu}_\mu$

Beam Polarity	Positive	Negative
QE	16.8	22.7
CCSP	16.0	21.0
CCDIS	75.6	166.2
TOTAL	108.4	210.0

TABLE II.3: Number of events in detector; Main Ring, Multi-Batch Operation

ν_μ interactions (π decay).

Beam Polarity	Positive	Negative
QE	550K	350K
CCSP	500K	340K
CCDIS	2400K	1100K
TOTAL	3400K	1800K

ν_e interactions (μ decay).

Beam Polarity	Positive	Negative
QE	14K	10K
CCSP	13K	10K
CCDIS	92K	42K
TOTAL	120K	62K

$\overline{\nu}_\mu$ interactions (μ decay).

Beam Polarity	Positive	Negative
QE	11K	14K
CCSP	10K	13K
CCDIS	47K	100K
TOTAL	69K	130K

TABLE II.4: Number of events in detector; Main Injector Operation

ν_μ interactions (π decay).

	Single-Batch	Multi-Batch
QE	260K	810K
CCSP	240K	770K
CCDIS	780K	2500K
TOTAL	1300K	4000K

ν_e interactions (μ decay).

	Single-Batch	Multi-Batch
QE	7K	23K
CCSP	7K	22K
CCDIS	30K	95K
TOTAL	44K	140K

$\overline{\nu}_\mu$ interactions (μ decay).

	Single-Batch	Multi-Batch
QE	10K	33K
CCSP	10K	30K
CCDIS	75K	240K
TOTAL	95K	300K

The neutrino flux from pion decays in the AP-2 transfer line is calculated to be 20 times larger than the neutrino flux from pion decays in the Debuncher. This increase arises from the fact that the pion decay distance in AP-2 is 150 m while only 13% of the pion decays beyond 280 m provide the Debuncher flux, and the momentum bite of the AP-2 transfer line is $\pm 8\%$ compared to $\pm 2\%$ for the Debuncher. In order to calculate the number of pions at 3 GeV compared to 9 GeV, the Monte Carlo EVENTQ developed for BNL E776 using the secondary particle production model NUCRIN for projectile momentum was used. The number of pions at 3 GeV relative to 9 GeV was determined to be 0.7 and 0.9 for positive and negative beams respectively. The numbers of charged current ν_μ events expected to be observed in the far detector for a 200 day run operating the Main Injector in a multi-batch mode with negative beam are summarized in Table II.5.

TABLE II.5: Number of events in long baseline detector.

	3 GeV	9 GeV
3 km. positive	10K	125K
3 km. negative	5K	65K
10 km. positive	0.9K	11K
10 km. negative	0.4K	6K

The ν_μ disappearance limits for both 9 GeV and 3 GeV running are also shown in Fig. II.1 as $\nu_\mu \rightarrow \nu_\tau$ limits. The effects of a systematic error have been include in the calculation. In this case, the improvement over earlier results is orthogonal to the expected improvements from both the CERN experiments and Fermilab P803. This search will cover much of the allowed region indicated by the atmospheric neutrino experiments.

III. TEST DETECTOR

Work has begun on the design of a prototype toroid module for the P860 detector. The construction of the prototype will provide an opportunity to refine the design of the final toroid module, and to develop the construction techniques needed to build the complete detector. Using the prototype detector in the neutrino beam from the Debuncher will provide an understanding of the detector response to charged particles and allow a measurement of the event rates and neutrino energy spectrum, which can be directly

compared to the event rates and spectrum calculated from muon decay. In addition to the test studies, the prototype module will be used as the first module of the complete detector.

The prototype can be ready to run at Fermilab in 1994 and will run parasitic at that time. This running should have no impact on the Collider operation and minimal impact on E760 which may run in the Accumulator at that time. Clearly, P860 will have no impact on E760 if data taking is restricted only to the periods when $\bar{p}$'s are being stacked for E760. The issues are with regard to deceleration and data taking for E760 and here one must consider background from continuous debuncher running and potential radiation damage to their calorimeter. The most likely time for a noticeable background increase to occur would be during debuncher beam injection. Beam injected from the AP-2 line is primarily electrons and pions. During the first 4 turns in the debuncher, most of the pions decay away while during the first 13 turns, the electrons are lost due to synchrotron radiation. If E760 were to "gate-off" their experiment during this time they would have only only 20 μsec of deadtime. Experience to date suggests that extra radiation damage would be minimal since E760's calorimeter is in place at all times and stacking has gone on 2 days each week for the past few runs. Some time should be allocated to the testing of the running modes relevant to 1996 running during the first 10 percent of the 1994 run. If there is no conflict with E760 data taking during this initial period, then P860 would be able run continuously.

The current design of the prototype module calls for 40 planes of 2 in. thick octagonally shaped iron absorber with a radius of 30 in. Following each plane of iron is a plane of Iarocci tubes used for measuring the track position. After every fifth plane of Iarocci tubes is a plane of 0.5 in. thick scintillator for time-of-flight measurements and triggering. The gap spacing between each plane of iron absorber is 2.5 in. for gaps containing both Iarocci tubes and scintillator, and 1.25 in. for gaps containing only Iarocci tubes. The total length of the detector excluding the outer support structure is 150 in. with an estimated mass of 39 tons.

A four turn copper coil looping once around each side of the detector will provide the toroidal field used to measure the muon momenta. The coil is constructed from a 1×1 in.^{2} square copper tubing with a 3/8 in. diameter central opening for water cooling. The coil will pass through a 4.5 in. diameter opening in the center of the module. A current of 5000 amps will saturate the field in the iron toroid at approximately 18 Kg. The total power consumption for the module is estimated to be 30 Kw.

The tracking information for charged particles will be provided by 39 planes of Iarocci

tubes, one located after each plane of iron. The planes will consist of 20 conventionally designed eight cell Iarocci modules ranging in length from 26 in. to 60 in. Each plane of Iarocci tubes contains 160 wires, for a total of 6,240 wires in the complete module.

Readout of the Iarocci tubes will be done by capacitive coupling to 0.9 cm wide conducting strips located on either side of the PVC sleeve. The strips will run vertically on one side and horizontally on the other side to form simultaneous x-y readout of the streamer position. Neighboring pairs of strips are coupled to reduce the total number of channels. There are a 80 channels per plane per view, giving a total of 6,240 channels for the complete module. The Iarocci tubes will be read out using the Flash ADC system from BNL E776. This readout system will allow the response of the Iarocci tube system to be studied in detail.

The Iarocci tubes will use the nonflammable gas mixture developed by the SLD collaboration for use in the SLD Warm Iron Calorimeter. This gas is 2.5% Argon, 9.5% Isobutane, and 88% CO_2, and possesses the same characteristics as the "standard" Argon-Isobutane mixture traditionally used in Iarocci tubes.

Each scintillator plane will consist of a 0.5 in. thick octagonal sheet of scintillator readout with wavelength shifting fiber (WLS). Recent cost reductions in scintillator plate and rapid developments in scintillating fiber technology make this design relatively straightforward. The WLS fiber readout approach yields a detector with very uniform response over its entire surface, a very high efficiency for single mip's (99%), and eliminates the need for complicated light guides and/or waveshifter bars. The fibers will be read out at each end so that the detector's time response, $T_{left} + T_{right}$, is independent of hit position within the counter. This information can be then be used in the trigger to distinguish between cosmic ray muons and muons from neutrino interactions. The PMT's will be read out into the E776 TDC system.

Two types of triggers will be used for the test run in 1994. The "machine" trigger which will require that there be a hit in at least three neighboring scintillator planes during the first 500 microseconds after beam is injected into the Debuncher. The second trigger is the "cosmic ray" calibration trigger. This trigger will be used during the interspill period and require that there be hits in several consecutive scintillator planes.

Currently, 36 planes of 2 in. thick 60×60 in.^{2} iron from the Caltech-Fermilab neutrino experiment E21 are in storage at FNAL. In addition, the readout electronics, flash ADC and TDC modules, Nevis transport system, and the gas distribution system from E776 will be used for the prototype modules. The Iarocci tubes for the prototype will be constructed

by Nevis. The Fermilab members of the collaboration are interested in developing and constructing the scintillator planes for the prototype.

For meaningful tests to be performed in the Debuncher neutrino beam, a detector hall and counting house will need to be constructed. The most likely site for the detector hall is immediately downstream of the AP-50 enclosure. The detector hall will need to be of sufficient size both to house the detector module and to provide assembly space. In addition, the hall should have cooling water for the magnet coils, and sufficient power to power the magnet and read out electronics. The total power requirement for the prototype module is approximately 150 Kw. Initial construction of the prototype module will take place at Nevis. After assembly and testing using cosmic rays, the module will be disassembled and transferred to Fermilab for reassembly in the detector hall.

The prototype module will be ready for data taking by 1994, and the event rates for the different neutrino species under the expected operating mode at that time is summarized in the table below. The rates were calculated assuming that the tests would be made in a totally parasitic mode using a 9 GeV negative beam. The rates were calculated assuming that the interaction occurred within the first 30 planes of the module to provide a sufficient measurement of the muon momentum. The beam parameters for the event rate calculations are as given in Table II.1. The event rate per day in the prototype module for each neutrino species is given in Table III.1. A run of 100 days will yield over 7,000 anti-muon neutrino and 600 muon neutrino events to study the detector response and the ability to distinguish positive and negative muons.

TABLE III.1: Event rate for prototype detector.

Neutrino Species	Events/Day
$\bar{\nu}_\mu$ (π decay)	77.
$\bar{\nu}_e$ (μ decay)	3.
ν_μ (π decay)	6.

Design work for the prototype module has begun at Nevis. Construction of the module will begin with approval for test running in 1994, with the summer of 1993 as the target date for completing the construction. The completed module will then be fully tested at Nevis using cosmic rays, before it is moved to Fermilab in late 1993 or early 1994.

A preliminary cost estimation for the construction of the prototype module has been made and is summarized in Table III.2. The source of existing components is also indicated where appropriate.

TABLE III.2: Prototype cost summary.

Iron plates	From E21 at Fermilab
Coil	5K
Support Structure	15K
Iarocci Tubes	20K
Scintillator	15K (Fermilab)
PMTs/Bases	from E776
ADC/TDC system	from E776
Miscellaneous	20K
Total	75K

In summary, a prototype module for the proposed P-860 detector can be constructed for approximately \$75K. It will take approximately 1.5 years to construct and install in a detector hall located downstream of the AP-50 enclosure. A 1 year run in parasitic mode will provide sufficient events for a detailed study of the detector response to muons and pions and for a measurement of the efficiency of the detector for determining the charge of muons.

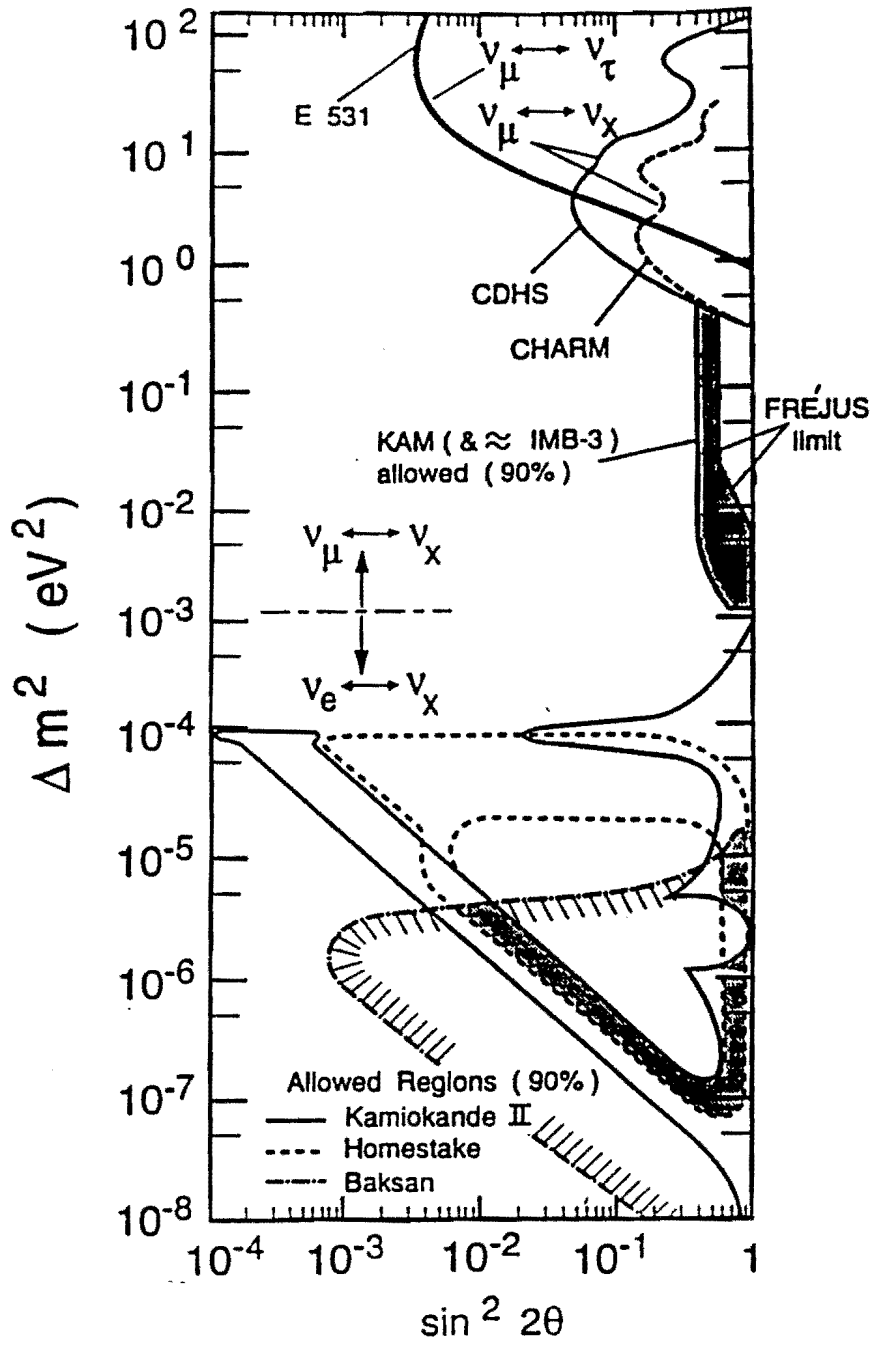

Fig. I.1 Summary of all available data for the neutrino oscillation channels $\nu_\mu \to \nu_x$ and $\nu_e \to \nu_x$ bearing on the $\Delta m^2 - \sin^2 2\theta$ region shown. The shaded areas are allowed for neutrino oscillations. "Survey of Atmospheric Neutrino Data and Implications for Neutrino Mass and Mixing", E.W. Beier et al., Submitted to Phys. Lett. B.

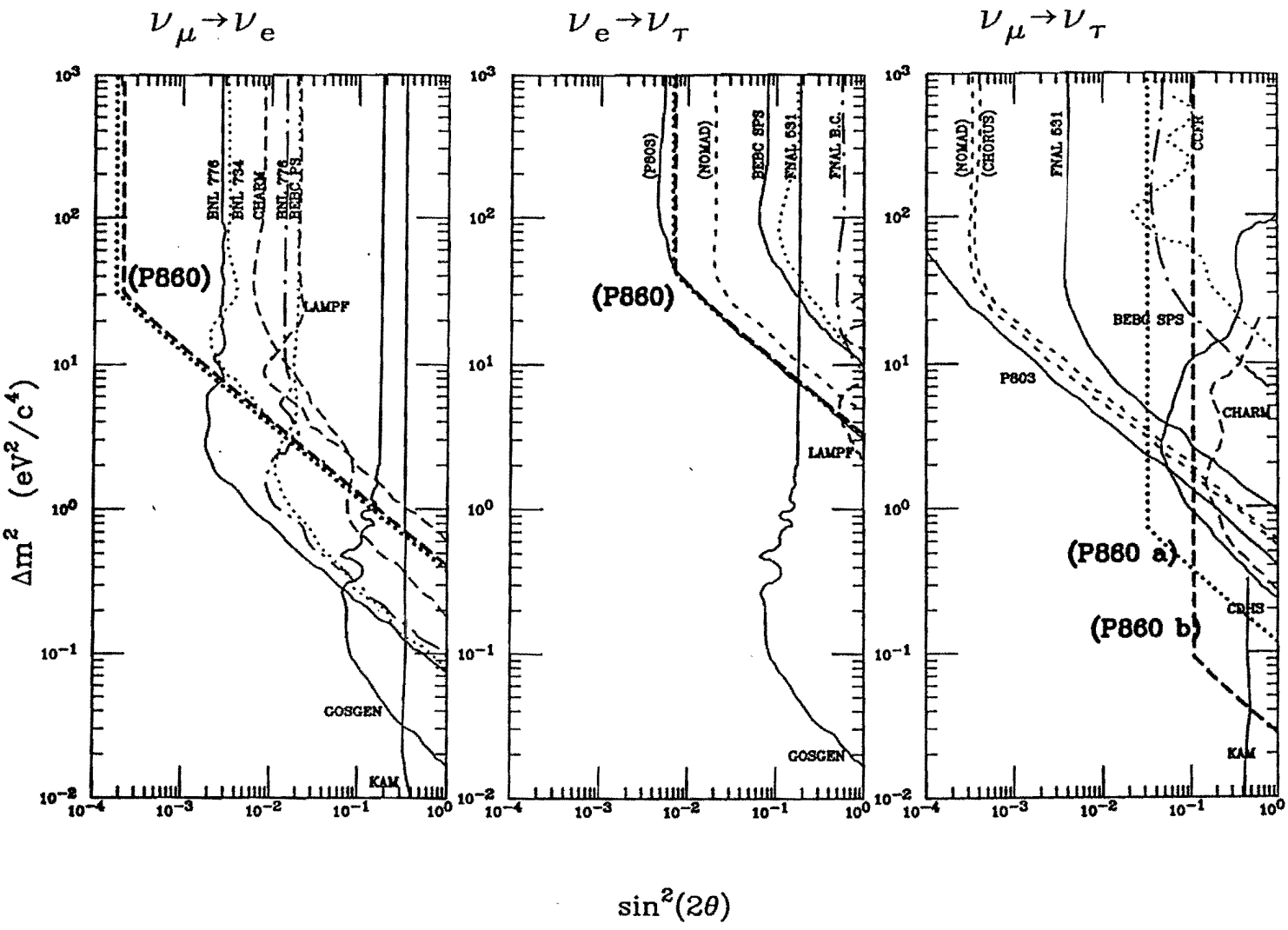

Fig. II.1 Summary of current and proposed oscillation limits for $\nu_\mu \rightarrow \nu_e$, $\nu_e \rightarrow \nu_\tau$, and $\nu_\mu \rightarrow \nu_\tau$. Other proposals are enclosed in parenthesis. P860 limits for $\nu_\mu \rightarrow \nu_e$ and $\nu_e \rightarrow \nu_\tau$ are shown for both multi-batch main ring running with positive beam and Main Injector multi-batch running with negative beam. For $\nu_\mu \rightarrow \nu_\tau$ the limits are shown for 3 GeV at 10 km (P860b), and 9 GeV at 3 km (P860a).

revised
10/12/92

P-860

A SEARCH FOR NEUTRINO OSCILLATIONS

USING THE FERMILAB DEBUNCHER

M.J. Murtagh
Brookhaven National Laboratory, Upton, NY 11973

J. Boyer, Y. Ho, W. Lee*, E. Mannel, and J. Mechalakos
Columbia University, 538 West 120th St., New York, NY 10027

A. Bross, M. Gormley, C. Kim, S. O'Day, and H. Park
Fermilab Accelerator Laboratory, P.O. Box 500, Batavia, IL 60510

K.S. Kang and D.W. Kim
Kangnung National University, Kangnung, Korea

J.S. Kang
Korea University, Seoul, Korea

J. Kim
Seoul National University, Seoul, Korea

* Spokesman

P-860

A SEARCH FOR NEUTRINO OSCILLATIONS USING THE FERMILAB DEBUNCHER

Preamble

This document is a response to the letter we received from John Peoples regarding the PAC deliberations on our proposal, P860; it also responds to conversations we have had with individual members of the PAC and laboratory management. We have combined here the salient features of our original proposal, submitted in January 1992, the Addendum to that proposal, submitted in May 1992, our responses to the recent PAC questions, and new material in the sections on the background estimates and the detector. We have recently entered into discussions with the Research Division at Fermilab to validate our cost estimates for the detector, and to define, cost, and schedule the hall and other facilities required for the experiment. The Accelerator Division has validated the numbers used in our rate calculations (Appendix B). This document, therefore, represents our present, revised proposal for a ν oscillation program using the Fermilab Debuncher.

The present Fermilab Long-Range Schedule has a Fixed Target run beginning in mid-1997, after Collider Run II. We believe that, with adequate support, our experiment would be ready for data taking at the beginning of this Fixed Target run. For this to happen, it is essential that the detector building be available earlier so we can install and test some of the detector during Collider Run II.

In order to preserve our momentum and to strengthen the collaboration, it is essential that we have a clear decision on the physics merits of this proposal from the PAC at their next meeting. We hope that their actions will clear the way for a firm decision on the detector building schedule and the required accelerator related upgrades. We expect to finalize the design of the detector during 1993 and to build and test the first (prototype) module at Nevis during 1994, dependent on approval by NSF as well as Fermilab. By the end of this period, we expect to have

placed the major orders for all the components. Upon completion of the detector building, we hope to begin installation of the first module and the assembly of all the other modules in the detector building. This should ensure a substantial test of the initial modules during Collider Run II and should allow us to have the entire detector completed by the start of the subsequent Fixed-Target run.

I. INTRODUCTION

This proposal presents a unique program of ν oscillation searches that exploit the features of a flavor-tagged ν beam emerging from the Fermilab Debuncher used as a μ storage ring. The primary focus of this experiment is on $\nu_e \rightarrow \nu_\tau$ oscillations, a channel in which this experiment has no serious competition. Our experiment is also sensitive to a wide range of parameters for $\nu_e \rightarrow \nu_\mu$ oscillations and, in a different configuration, is sensitive to $\nu_\mu \rightarrow \nu_\tau$ oscillations. Our expected limits are, in general, better than those given in published data, and they are competitive with those of proposed experiments. If there is a real signal within our projected limits, we believe that the beam systematics in this experiment are such that we will be able to identify and defend the effect with real confidence. Certainly, the beam systematics in our experimental approach are very different from those in other approved proposals.

The initial phase of the program will focus on a short baseline experiment and, therefore, on the $\nu_e \rightarrow \nu_\tau$ and $\nu_e \rightarrow \nu_\mu$ searches. The detector would be located in line with one of the straight sections of the Debuncher ring. For acceptance reasons, it is advantageous to locate it as close to the ring as possible, while still allowing for adequate shielding to reduce the stray beam flux from the Debuncher. With this detector location, the experiment will be primarily a search at small mixing angle. The detector is relatively simple, since its primary requirement is to identify and measure the sign of μ's above 1 GeV. As with most ν detectors, it consists of a primary module which is then repeated to give enough mass to get an acceptable event rate for the process of interest. The primary module consists of a toroid to provide a magnetic field and tracking chambers to measure the μ tracks.

We originally proposed a second phase to the experiment in which the subsequent addition, at some later time, of a second detector 5 to 10 km from the Debuncher would be particularly interesting for a $\nu_\mu \rightarrow \nu_\tau$ oscillation search. We understand that the PAC will not consider this aspect of the proposal now, but they will consider it together with other such proposals which might appear for the Main Injector era. Consequently, we have relegated most of our thoughts on this topic to Appendix C. It is, however, worth mentioning here a couple of advantages to our approach. First, the low ν energy from the Debuncher system implies that the far detector does not have to be very far or very large to give an equivalent E/L and an acceptable event rate when compared to beams from the Main Injector itself. Secondly, the nature of the ν beam from the π/μ flux in the Debuncher may remove many of the serious concerns about the relation between the flux shapes in the near and far detectors.

II. PHYSICS MOTIVATION

The possibility that ν's might oscillate has been the subject of much theoretical speculation and experimental effort (Ref. 1). While there have occasionally been experimental indications of positive results, none of these has been confirmed by other experiments. Indeed, the strength of most of these results has gradually diminished in light of different or improved experiments.

Accelerator-based oscillation searches have primarily focused on $\nu_\mu \rightarrow \nu_e$ oscillations (Fig. II.1). Accelerator ν beams are predominantly ν_μ beams with $\sim 1\%$ contamination from ν_e's. Since the ratio of ν_e to ν_μ in the beam is essentially determined by the ratio of π's to K's in the beam from the production target, one is looking for an increase in the rate of electrons in a relatively well understood situation. While these experiments have produced the majority of oscillation results, they are limited by the beam contamination from ν_e, electron identification problems in counter experiments, and the lack of a sign measurement on the shower.

With the notable exception of the Fermilab emulsion experiment E531, accelerator based searches for ν_μ oscillations to final states other than ν_e have, for the

most part, been disappearance experiments (Fig. II.1). Disappearance experiments are inherently limited in their mixing angle limits, as they involve the subtraction of large numbers. They are also devoid of any clear signature and rely totally on calculations of the ν flux as a function of distance from the source. In contrast to this situation, experiment E531 was an appearance experiment which looked in an emulsion target for short lived particles which could be consistent with τ's. This experiment had a relatively large mass limit, as it was a high energy experiment. There are essentially no accelerator limits for ν_e beams, since there are no high flux ν_e beams. The limits from reactor experiments have good mass range but, since they are disappearance experiments, they provide rather poor mixing angle limits.

The most intriguing hint of ν oscillations is in the realm of solar ν's. The disagreement between the solar model calculations and the measurement of solar ν fluxes can be interpreted in a very elegant way using the MSW (Ref. 2) matter oscillation conjecture. This provides ν oscillation solutions with a mass difference in the 10^{-6} eV^2 to 10^{-4} eV^2 range. If one assumes that the mixing is greatest between the nearest mass states, then this would be interpreted as mixing between ν_e and ν_μ. If one also assumes that there is a reasonable ν mass hierarchy, such as naturally occurs in many Grand Unified Theories, then one might expect to observe $\nu_\mu \rightarrow \nu_\tau$ oscillations in the energy regime of available accelerators (Ref. 3). The indications from all the present evidence and conjecture are that the most fruitful areas for ν oscillation searches at accelerators are in the channels $\nu_\mu \rightarrow \nu_\tau$ and $\nu_e \rightarrow \nu_\tau$. To date, these have been the least explored channels.

The proposed experiment is for a clean ν_e beam with no ν_μ contamination. Since most of the beam energy spectrum is above the threshold for τ production, it is ideal for $\nu_e \rightarrow \nu_\tau$ searches. The detector is close to the target, so the E/L for the experiment is ~ 40. This will restrict the mass difference squared limit to 1–10 eV^2.

II.1. Other Conventional Physics

The production of charm quarks in the deep inelastic processes and the subsequent fragmentation of charm quarks to charmed particles has been extensively studied at high energies. At these energies, it is assumed that most of the charmed particles observed in the reactions are dominated by charmed mesons. However, at lower energies, it is believed that charmed baryons may be a significant fraction of the charmed particles produced. Therefore, it is of interest to measure the production of charmed baryons in ν reactions.

The exclusive charm baryon reactions for ν production are:

$$\nu_\mu + n \rightarrow \mu^- + \Lambda_c \tag{1}$$

$$\nu_\mu + p \rightarrow \mu^- + \Sigma_c^{++} \tag{2}$$

$$\nu_\mu + n \rightarrow \mu^- + \Sigma_c^{+} \tag{3}$$

$$\nu_\mu + p \rightarrow \mu^- + \Sigma_c^{*++} \tag{4}$$

$$\nu_\mu + n \rightarrow \mu^- + \Sigma_c^{*+} \tag{5}$$

The cross sections for these processes have been calculated by R.E. Shrock and B.W. Lee. Using the now well measured masses of Λ_c and D^* , we have calculated the production cross section of reactions 1, 2, and 3. The results of these calculations are shown in Fig. II.2. During positive polarity running, a significant number of Λ_c^+ particles will be produced from the ν's from π decays. The flux as a function of energy is shown in Fig. II.3, while the product of the ν flux times the Λ_c^+ production cross section in shown in Fig. II.4. Since the ν energy is below threshold for D production the only charmed particles produced will be baryons.

It is expected that there will 20K Λ_c^+ produced in the detector during a 40 week run. Multiplying the decay branching ratio of Λ_c^+ to semileptonic decay to μ's (5%) and a geometric acceptance of 10%, it is expected that $\sim$ 100 dimuon events will be observed. With this sample it should be possible to measure the cross section times the branching ratio to about 10% for Λ_c^+ ν production.

III. OPERATIONAL ASPECTS OF THE FERMILAB DEBUNCHER USED AS A MUON STORAGE RING FOR NEUTRINO OSCILLATION STUDIES

During conventional collider operation, π^-'s, μ^-'s, and e^-'s are captured along with the $\bar{p}$'s in the Debuncher ring. Within the first few turns, the majority of the π^-'s decay to give μ^-'s and $\bar{\nu}_\mu$'s. The μ^-'s which are trapped in the ring, decay over many turns producing ν_μ's and $\bar{\nu}_e$'s. The Debuncher, therefore, naturally produces a time-separated $\bar{\nu}_e$ beam. Its energy distribution extends to 9 GeV, so much of the beam is above the threshold for producing τ leptons. Since $\bar{\nu}$'s produce ℓ^+'s when they interact, there are two beam sources which can produce a μ^+. The first comes from "early" $\bar{\nu}_\mu$'s from the π^- decays. The second is from the "late" $\bar{\nu}_e$'s, which have oscillated to either $\bar{\nu}_\mu$'s or to $\bar{\nu}_\tau$'s. In principle, then, the observation of a μ^+ in the detector during the latter part of the Debuncher beam cycle (after the first 10 turns, or 10 pion lifetimes) is a clear signal of the presence of ν oscillations. The absence of any significant beam background for a μ^+ should make the observation of an oscillation effect a relatively systematic-free measurement. The background from real or fake μ^+'s from conventional ν interactions is addressed in detail below, but it does not significantly limit the search.

During normal collider operations, the Debuncher is set to collect negative secondaries from the production target. If one severs the connection to collider running and uses the Debuncher to collect π^+'s, there is an increase in our event rate due to the difference between ν and $\bar{\nu}$ cross sections. However, in neither case is the flux really adequate for the oscillation searches being proposed. To improve the flux, we have proposed that the Main Ring be run in a multibatch mode rather than the present single-batch mode. This produces a significant overall improvement in the rate and provides an adequate flux for our experiment. Once the Main Injector is on-line, there will be another improvement in flux, but even in this case, we would argue for running in multibatch mode. The possibilities inherent in the multiple running options: running in Collider or Fixed-Target mode, with or without multibatch operation, pre or post Main Injector can lead to a great deal

of confusion when trying to discuss rates. The PAC has asked us to focus on 3 well defined running conditions. The fluxes for these running modes are discussed in detail in Section IV, and the conclusions are summarized here.

A. Collider Run II, with the experiment running purely parasitically.

The flux in this case in not adequate for the experiment. However, it is sufficient for setting up and debugging the detector. So, we would argue very strongly that we should have a building in place and be installing and testing the initial modules of the detector during this run.

B. A possible Fixed-Target run after Collider Run II, with the experiment being compatible with a fixed target program.

If the Main Ring is run in a single-batch mode, then the flux is inadequate. However, if the Main Ring is run in a multibatch mode, we believe that we will be able to make a significant oscillation search which would be compatible with any proposed Fixed-Target running. In this case we would ask that the Debuncher be set to focus positives, since this will also help to increase the event rate.

This multibatch mode of operation requires the construction of a fast extraction kicker (rise and fall time of 0.5 microseconds) for the Main Ring and the development of a new lithium lens for the $\bar{p}$ target station. It is likely that the fast kicker could be the same as the one now under development for the Main Injector. There appears to be sufficient space in the E-17 medium straight section of the Main Ring to accommodate a kicker with these characteristics; i.e., no significant changes to the Main Ring lattice are required. Building a reliable, rapid-cycling (15 Hz) lithium lens would require significant lead-time and a substantial development effort. However, much of the groundwork for such an effort has been carried out by the Novosibirsk group (Ref. 4), who have tested prototype liquid lithium lenses with significantly larger diameters than would be required. In addition, a new lithium lens will eventually be needed for Main Injector running, so a development effort in this area is needed beyond the requirements of P860. We have had discussions with the Accelerator Department about both of these issues and

their positive comments are contained in the memo from Steve Holmes which is in Appendix B.

We believe that in 40 weeks of running in this configuration we can make significant $\nu_e \rightarrow \nu_\tau$ and $\nu_e \rightarrow \nu_\mu$ measurements.

C. The Main Injector Collider Run III, with the experiment being compatible with the Simultaneous Collider and Fixed-Target operation of the Main Injector.

In the simplest mode of operation during this run, only one batch is sent to the $\bar{p}$ target. In this case, the flux is about 1/3 of the flux for the multibatch Fixed-Target running discussed above in "B". However, if the Main Injector is run in a multibatch mode with multiple batches being sent to the $\bar{p}$ target, then the flux will be comparable to that for the multibatch Fixed-Target option. Since the Collider will be set to focus negatives in this case, the actual event rate will be approximately one half of that achieved in the Fixed-Target mode discussed above.

In summary, running mode (A) is suitable for setting up and debugging the detector while both (B) and (C) are adequate for the measurements we wish to make, provided the accelerator is running in the appropriate multibatch mode.

IV. EVENT RATES

The Fermilab Debuncher ring is a strong focusing synchrotron with a circumference of 500 meters, situated between Giese and Indian Roads (Fig. IV.1). During normal collider running, it accepts negative secondaries which originate at the $\bar{p}$ production target and are transported through the AP-2 beam line. Secondaries whose phase space coordinates lie within the momentum acceptance [8.9 GeV/c $\pm$ 2%] and transverse admittance [$A(x) = A(y) = 25\pi\text{mm} \times mrad$] of the Debuncher ring are injected and captured in the Debuncher. The particle composition of the first-turn beam in the Debuncher is dominated by pions, but it contains electrons, μ's, and $\bar{p}$'s as well.

Parasitic measurements of the fluxes of pions, electrons, μ's, and $\bar{p}$'s which are injected into and circulate in the Debuncher were made during the fall of 1991.

Appendix A contains a detailed summary of the novel experimental technique used, together with the measured results for the circulating μ flux in the Debuncher. As described in this appendix, the measurements are quoted in terms of the ratio of the μ^- flux to $\bar{p}$ flux. The measured result is $\mu^-/\bar{p} = 1.0 \pm 0.2$; the μ^- and $\bar{p}$ fluxes which circulate in the Debuncher are nearly identical.

From the measured $\mu^-/\bar{p}$ ratio one can calculate the number of μ's per week that is available in the Debuncher. As outlined in the introduction, the number of μ's per week depends upon the running period (Collider Run II, Fixed-Target, or Collider Run III) and the expected machine parameters. In this section, the machine parameters and the expected μ flux per week for each period are summarized. The machine parameters used here have been reviewed with the Accelerator Division (Cf. memo from Steve Holmes reproduced in Appendix B) for the following running modes: Collider Run II with the experiment running parasitically, a Fixed Target run operating the Main Ring in multi-batch mode with the Debuncher operating in a positive polarity mode, and the Main Injector Collider Run III with the Debuncher operating in a negative polarity mode. The running parameters and μ flux available per week are summarized in Table IV.1.

In estimating ν fluxes and interaction rates, it should be noted that only 13% of the μ's decay in the straight section of the Debuncher pointing at the detector. In addition, the first few turns (~ 10) are dominated by ν_μ from π decay, and the present electronic design is only active for 400 μsecs. This amounts to cutting 20% of the captured μ flux, i.e., the effective live-time is 80%.

The ν_μ energy distribution from the decay of the primary 9 GeV/c π's in the Debuncher is shown in Fig. IV.2a; while the $\bar{\nu}_\mu$ and ν_e energy distributions from the captured 9 GeV/c secondary μ decays are shown in Fig. IV.2b and Fig. IV.2c, respectively. All these calculations are for the ν's which are emitted at less than 10 mrad from the initial meson or μ direction. This corresponds to ν's with the potential to interact in the fiducial volume of the detector.

The number of π's and μ's, as a function of turn number, is shown in Fig. IV.3. As noted earlier, after a few (~ 10) turns, the ν flux from π decays is negligible. The μ flux continues to be significant for at least two hundred turns. In the decay

TABLE IV.1

Running Parameters

	PRE-MI		POST-MI	
Run Period	Collider II	Fixed Target	Single Batch Mode	Multibatch Mode
Protons/pulse	3.0×10^{12}	2.5×10^{13}	5.0×10^{12}	2.0×10^{13}
Antiprotons/proton	2.0×10^{-5}	2.0×10^{-5}	2.0×10^{-5}	2.0×10^{-5}
Cycle time(sec)	2.133	3.467	1.467	1.827
μ's/antiproton	1.0	1.0	1.0	1.0
Effective hours/week	110	130	130	110
Weeks/run	40	40	40	40
Pions/run	2.3×10^{16}	1.4×10^{17}	6.5×10^{16}	1.7×10^{17}
μ's/run	4.5×10^{14}	2.7×10^{15}	1.3×10^{15}	3.4×10^{15}

$\mu^+ \rightarrow e^+ + \nu_e + \bar{\nu}_\mu$, the energy and angular distribution of ν_e and $\bar{\nu}_\mu$ are given by

$$\frac{d^2 N_{\bar{\nu}_\mu}}{dx\ d(\cos(\theta))} = x^2(3-2x)\left[1 - \left(\frac{1-2x}{3-2x}\right)\cos(\theta)\right]$$

and

$$\frac{d^2 N_{\nu_e}}{dx\ d(\cos(\theta))} = x^2(1-x)[1-\cos(\theta)]$$

where $x = E_\nu/(m_\mu/2)$ and θ is the angle between the ν_μ and the polarization vector in the μ rest system (Ref. 5).

Initially, the μ^+ polarization is left handed. Assuming that there is no dynamic depolarization mechanism, the number of high energy ($E_\nu > 6$ GeV) ν_e and $\bar{\nu}_\mu$ entering the detector are time separated. This can be seen in Fig. IV.4 which shows the number of ν_e and $\bar{\nu}_\mu$ into the detector as a function of turn number.

The quasi elastic cross sections for ν_e, $\bar{\nu}_e$, ν_τ, and $\bar{\nu}_\tau$ are shown in Fig. IV.5 while the inelastic cross sections are shown in Fig. IV.6. It is clear from these distributions that, for the Debuncher energy regime, the ν_τ cross section is predominantly quasi elastic and single pion while the conventional ν interactions are dominantly deep inelastic.

The integrals of the flux $\times$ cross section for the relevant ν species and partial cross sections for both positive and negative polarity running are shown in Table IV.2. The effects of Fermi motion are included in the calculation. This has little effect on the basic ν interaction rates, but it does increase the ν_τ rates by $\sim 10\%$.

In calculating the event rates, it is assumed that all ν's produced within 10 mrad of the nominal μ beam direction pass through the fiducial volume of the detector. As will be clear when the detector is discussed later, this is a very reasonable approximation. The detector will start 75 feet from the end of the Debuncher straight section. It will have 600 modules, each module containing a $2''$ Fe absorber plate and space for timing and position measuring detectors for a total dimension in the beam direction of $\sim 190'$.

The numbers of μ's per run for the various scenarios are given in Table IV.1. Assuming that the detector has the 600 modules of Fe defined above, and the 10 mrad beam is contained in the fiducial volume, the various ν event rates per 40 week run are given by

$$N_\nu = \epsilon \times N_\mu \times F_\nu \times Mz,$$

where N = number of μ per run; $\epsilon = 0.13 \times 0.80$ is the fraction of decays into the detector while the electronics are live, F_ν is given in Table IV.2; and $Mz = 6 \times 10^{23} \times 7.87 \times 5 \times 600\text{cm}^2$ is the longitudinal fiducial tonnage.

The total number of interactions expected for each of the primary ν species in the beam for a 40 week run is given in Table IV.3 for the three running modes discussed above. The ν_μ rate is considerably higher because the ν_μ's arise from the direct decay of the primary pion beam, and the π/μ ratio at the entrance to the Debuncher is 50/1. The τ rates assume 100% mixing from ν_e.

TABLE IV.2

F_ν for 9 GeV positive and negative Debuncher settings.

$F_{\nu_\mu} \equiv \int \mathrm{FLUX}(E)\sigma(E)dE \quad 10^{-40}\mathrm{cm}^2/\mathrm{pion}$ for ν_μ

Beam Polarity	Positive	Negative
QE	17.2	11.3
CCSP	15.9	10.8
CCDIS	76.4	34.3
TOTAL	109.5	56.5

$F_{\nu_e} \equiv \int \mathrm{FLUX}(E)\sigma(E)dE \quad 10^{-40}\mathrm{cm}^2/\mu$ for ν_e

Beam Polarity	Positive	Negative
QE	22.9	16.2
CCSP	21.1	15.4
CCDIS	145.2	66.2
TOTAL	189.2	97.8

$F_{\nu_\tau} \equiv \int \mathrm{FLUX}(E)\sigma(E)dE \quad 10^{-40}\mathrm{cm}^2/\mu$ for ν_τ

Beam Polarity	Positive	Negative
QE	6.5	4.2
CCSP	2.8	1.8
CCDIS	4.5	2.0
TOTAL	13.8	8.0

$F_{\bar{\nu}_\mu} \equiv \int \mathrm{FLUX}(E)\sigma(E)dE \quad 10^{-40}\mathrm{cm}^2/\mu$ for $\bar{\nu}_\mu$

Beam Polarity	Positive	Negative
QE	16.8	22.7
CCSP	16.0	21.0
CCDIS	75.6	166.2
TOTAL	108.4	210.0

TABLE IV.3

Number of Events in the Detector

	PRE-MI		POST-MI	
Run Period	Collider II	Fixed Target	Single Batch Mode	Multibatch Mode
ν_μ interactions	183×10^3	2188×10^3	524×10^3	1396×10^3
ν_e interactions	6×10^3	77×10^3	18×10^3	48×10^3
$\bar{\nu}_\mu$ interactions	14×10^3	43×10^3	40×10^3	107×10^3
ν_τ interactions	500	5400	1500	4000

V. BACKGROUNDS

The primary signature for a charged current ν interaction is a fast, relatively forward going, lepton. This feature is retained even if one considers the secondary μ's from τ decay. The acceptance for such μ's in the present experiment, if one requires the μ to be greater than 1 GeV/c and to have an angle to the beam direction with $\cos\theta < 0.8$, is $\sim$ 60%. Since the ν_τ cross section at Debuncher energies is primarily quasi elastic, genuine τ interactions will be characterized by a forward going energetic μ in a relatively low multiplicity event. A typical quasi elastic τ event is shown in Fig. V.1. The figure shows a 7 GeV ν_τ interacting to produce a 4.4 GeV τ decaying to a 3.7 GeV muon. Only hits from the charged tracks in the event are shown. The cleanliness of the event, characterized by the lack of additional connected tracks, is apparent. The event selection criteria exploit these features for rejecting charged and neutral current interactions of ν_e and $\bar{\nu}_\mu$ while retaining most of the ν_τ interactions.

We have calculated the rejection ratios for four possible background sources: (i) charged current interactions of ν_e and $\bar{\nu}_\mu$; (ii) neutral current interactions of ν_e and $\bar{\nu}_\mu$; (iii) charmed meson production from ν_μ and $\bar{\nu}_\mu$ interactions; and (iv) charmed baryon production from ν_μ and $\bar{\nu}_\mu$ interactions.

V.1. Charged and Neutral Current Interactions of ν_e and $\bar{\nu}_\mu$

Our preliminary event selection criteria consists of two stages – the first of which requires the event to contain an energetic, forward-going track of the appropriate charge within the fiducial volume. Specifically, the first stage selection criteria require:

- a track of the appropriate charge with momentum ≥ 1.0 GeV/c.
- that the track originate within the fiducial volume.
- that the production angle, θ, be small: $\cos\theta \geq 0.8$.

Extensive Monte Carlo calculations have been performed to determine the efficiency of these criteria for rejecting conventional charged and neutral current interactions of ν_e and $\bar{\nu}_\mu$ using the event generator ETEST (Ref. 6) developed for the E776 neutrino experiment at Brookhaven National Laboratory (BNL) and extensively tested in that experiment. (Work is also in progress to determine the expected background from the actual data taken by the E776 collaboration in the wide band neutrino beam at BNL. While this beam momentum peaks at 1.3 GeV/c, there is a long tail, and approximately 7% of the flux at the E776 location is above 4 GeV.)

The second-stage event selection criteria are designed to eliminate the remaining ν_e, $\bar{\nu}_\mu$ interactions while discarding only a small fraction of the ν_τ interactions. The second-stage analysis essentially selects very clean events which contain a single energetic track consistent with being a μ of the appropriate charge. The additional stage-2 selection criteria applied are as follows:

- There must be only one track in the event and it must have the appropriate charge.
- The track must have hits in at least 12 planes of the detector with no visible kinks.

- There must be no additional hits at the origin of the track that are not clearly associated with the track.

Deep Inelastic Interactions

The ETEST event generator was used to generate 50K events each of ν_e and ν_μ charged and neutral current deep inelastic events. Typical events are shown in Fig. V.2 and Fig. V.3. These event samples were then analyzed to determine the number of events with a charged pion that satisfied the first stage selection criteria. The analysis indicates that 10% of the deep inelastic events pass the stage-1 selection criteria. These results are not surprising and indicate that at these energies very few energetic pions are produced. Most of the incident ν energy is retained by the final state lepton. The probability of a ν_e or $\bar{\nu}_\mu$ interaction satisfying the stage-1 selection criteria is P1<0.1.

To study the remaining background events, 5000 deep inelastic events each of ν_e and $\bar{\nu}_\mu$ charged and neutral current interactions were simulated by coupling the ETEST event generator to a GEANT representation of the proposed detector. The simulation incorporates the decay probability of final state π's and μ's within the detector as well as secondary interactions of final state particles. Events with a single track of the appropriate charge which penetrated at least 75 cm (6 interaction lengths) of the segmented toroidal magnet were selected for hand scanning. These events were analyzed using the stage-2 selection criteria. Based on the analysis of these event samples, no events passed the second stage criteria which selects clean events containing a single track consistent with being a μ of the appropriate charge. The probability of a ν_e or $\bar{\nu}_\mu$ deep inelastic interaction satisfying the stage-2 selection criteria is P2$< 2 \times 10^{-4}$. The net probability that a ν_e or $\bar{\nu}_\mu$ charged or neutral current interaction masquerade as a ν_τ interaction is P1$\times$P2$< 2. \times 10^{-5}$. The expected number of ν_e, $\bar{\nu}_\mu$ deep inelastic interactions during the Fixed Target and Collider III runs are summarized in Table V.1. With a rejection ratio of greater than 2×10^{-5}, we expect less than 1 background event from ν_e or ν_μ charged or neutral current deep inelastic interactions.

Single Pion Interactions

Charged current and neutral current single pion production can also provide a source of π's which can mimic μ's either through the decay of the π without a

TABLE V.1

Expected Number of Deep Inelastic Events

Beam Polarity	Positive	Negative
ν_e charged current	58K	33K
ν_e neutral current	18K	13K
ν_μ charged current	30K	81K
ν_μ neutral current	12K	32K

visible kink, or if the π passes the μ selection criteria. Charged current and neutral current single pion events were generated using the ETEST event generator. Less than 2×10^{-2} of these events survived the stage-1 selection criteria described above. It is estimated that less than 3×10^{-3} of these events will produce a single track with the appropriate charge traveling more than 6 interaction lengths, 10 planes. The net probability that a single pion interaction will masquerade as a ν_τ interaction is $P \leq 2\times10^{-2}\times3\times10^{-3} = 6\times10^{-5}$. The number of charged current and single pion interactions expected during the Fixed Target and Collider III run are summarized in Table V.2. With a rejection ratio of greater than $2.\times10^{-4}$ we expect less than 1 background event from ν_e or ν_μ charged or neutral current single pion interactions.

TABLE V.2

Expected Number of Single Pion Events

Beam Polarity	Positive	Negative
ν_e charged current	8K	8K
ν_e neutral current	3K	3K
ν_μ charged current	6K	10K
ν_μ neutral current	3K	3K

TABLE V.3

Expected Number of Charm Events

Beam Polarity	Positive	Negative
D Production	60	700
Λ_c Production	0	2600

The selection criteria summarized above are quite severe and could probably be somewhat relaxed, particularly the stage-2 criteria which define "clean" events. We point out that these criteria discard all charged current deep inelastic ν_τ interactions – a significant fraction (25-30%) of the potential oscillation signal. In Section VI, where the oscillation limits are discussed, contributions from deep inelastic ν_τ interactions are not included in the potential signal.

V.2. Charmed Meson and Baryon Production from ν_μ, $\bar{\nu}_\mu$ Interactions

Charm production can produce a potential background, D production and Λ_c^+ production in charged current ν_μ interactions. For positive running, there will be no Λ_c^+ events since production of charm baryons is forbidden in $\bar{\nu}_\mu$ quasi elastic charged current interactions. The number of expected charm events expected is given in Table V.3. The probability of the charm candidate producing a background event is reduced by the following:

- $BR(D \rightarrow \mu X) = 10\%$, $BR(\Lambda_c^+ \rightarrow \mu^+ X) = 5\%$.
- Missing the μ from the charged current interaction; 10%.
- Acceptance for the μ from the charm decay; 30%.
- Interaction having a clean vertex; 10%.

The resulting number of charm events producing a single muon of the proper sign is estimated to be ≤ 1.

VI. OSCILLATION LIMITS

The probability that a neutrino of type ν_a and energy E_ν (GeV) oscillates to a neutrino of type ν_b at a distance L (Km) from the neutrino source is given by

$$P \equiv P(\nu_a \rightarrow \nu_b) = \sin^2 2\alpha \ \sin^2\left(1.27\Delta m^2 \frac{L}{E}\right),$$

where Δm^2 (eV^2) is the difference in mass of the neutrino mass eigenstates. This probability is compared to the experimental error in order to determine the region in the Δm^2- $\sin^2 2\alpha$ space to which the detector is sensitive. The region in Δm^2-$\sin^2 2\alpha$ space excluded experimentally is given by

$$P \leq \sin^2 2\alpha \ \sin^2\left(1.27\Delta m^2 \frac{L}{E}\right).$$

In the limit of small Δm^2 the excluded region simplifies to

$$\Delta m^2 \sin 2\alpha \geq 0.8 \frac{E}{L}\sqrt{P},$$

while for very large Δm^2 it reduces to

$$\sin^2 2\alpha \geq 2P.$$

As is clear from the above formula, the small Δm^2 limit is controlled by the E/L for the experiment, while the mixing angle limit is determined by the statistical and systematic errors in the measurement. For the present proposal, $E/L \sim 40$, so the emphasis in these measurements will be on the mixing angle limit.

The number of ν_a interactions in the detector, $N^{\mathrm{int}}_{\nu_a}$, is given by:

$$N^{\mathrm{int}}_{\nu_a} = M_Z \int \phi_{\nu_a} \sigma_{\nu_a} \, dE.$$

The flux of neutrinos of type ν_b, ϕ_{ν_b}, produced by the oscillations of neutrinos of

the type ν_a to type ν_b is given by

$$\phi_{\nu_b} = P \times \phi_{\nu_a}.$$

Therefore, the number of ν_b interactions in the detector is

$$\begin{aligned} N^{\text{int}}_{\nu_b} &= M_Z \int \phi_{\nu_b}\, \sigma_{\nu_b}\, dE \\ &= M_Z \int P\, \phi_{\nu_a}\, \sigma_{\nu_b}\, dE. \end{aligned}$$

Assuming that the probability of oscillation does not change rapidly as a function of E over the range considered, then

$$\begin{aligned} \frac{N^{\text{int}}_{\nu_b}}{N^{\text{int}}_{\nu_a}} &= P \times \frac{\int \phi_{\nu_a}\, \sigma_{\nu_b}\, dE}{\int \phi_{\nu_a}\, \sigma_{\nu_a}\, dE} \\ &= P \times \frac{F_{\nu_b}}{F_{\nu_a}}. \end{aligned}$$

Therefore,

$$P(\nu_a \rightarrow \nu_b) \equiv \frac{N^{\text{int}}_{\nu_b}}{N^{\text{int}}_{\nu_a}} \times \frac{F_{\nu_a}}{F_{\nu_b}},$$

where $N^{\text{int}}_{\nu_i}$ is the number of interactions of neutrino type i and F_{ν_i} is the integral of Flux $\times$ cross section for neutrino type i as listed in Table IV.2.

The limits for $\nu_e \rightarrow \nu_\mu$ oscillations, assuming that only quasi elastic and single pion events are being considered, can then be determined as follows:

$$P(\nu_e \rightarrow \nu_\mu) = \frac{N^{\text{int}}_{\nu_\mu}}{N^{\text{int}}_{\nu_e}} \times \frac{F_{\nu_e}}{F_{\nu_\mu}},$$

where $N^{\text{int}}_{\nu_i}$ is the number of quasi elastic and single pion interactions for neutrino species ν_i and F_{ν_i} is the corresponding cross section. For ν_e and ν_μ interactions the cross sections are the same. So the probability of $\nu_e \rightarrow \nu_\mu$ oscillations is

$$P(\nu_e \rightarrow \nu_\mu) = \frac{N^{\text{obs}}_{\nu_\mu} - N^{\text{back}}_{\nu_\mu}}{\text{Acceptance} \times N^{\text{int}}_{\nu_e}}.$$

If the number of observed events is the same as the expected background events then an upper limit for Δm^2 and $\sin^2 2\alpha$ can be determined for $\nu_e \rightarrow \nu_\mu$

TABLE VI.1

Limits for $\sin^2 2\alpha$ and Δm^2

	Fixed Target	Collider Run III
ν_e Interactions	17.3×10^3	15.6×10^3
	$\nu_e \rightarrow \nu_\mu$	
$\sin^2 2\alpha$	2.6×10^{-4}	2.9×10^{-4}
Δm^2	0.36 eV^2	0.39 eV^2
	$\nu_e \rightarrow \nu_\tau$	
$\sin^2 2\alpha$	1.2×10^{-2}	1.5×10^{-2}
Δm^2	2.5 eV^2	2.8 eV^2

and $\nu_\tau \rightarrow \nu_\mu$ oscillations based on the experimental error. The upper limit for $\nu_e \rightarrow \nu_\mu$ oscillations is

$$P(\nu_e \rightarrow \nu_\mu) \leq \frac{\delta}{N_{\nu_e}^{\rm int}},$$

where δ is the experimental error in the background. A similar calculation leads to the upper limit on the mixing probability for $\nu_e \rightarrow \nu_\tau$ oscillations;

$$P \leq \frac{\delta}{\text{Acceptance} \times BR(\tau \rightarrow \mu\nu\nu) \times N_{\nu_e}^{\rm int}} \times \frac{F_{\nu_e}}{F_{\nu_\tau}},$$

where $BR(\tau \rightarrow \mu\nu\nu) = 0.17$, the muon acceptance is 62%, and F_{ν_i} is given in Table IV.2.

For the upper limits presented here, it is assumed that only quasi elastic and single pion events are considered. As discussed in Section V on backgrounds, no background candidate events are expected to be observed. In this case the experimental error is given by the Poisson mean for which 0 events are observed at the 90% confidence level, 2.30. The number of quasi elastic and single pion events, and limits for $\sin^2\theta$ at large Δm^2, and Δm^2 at maximal mixing for both running periods being considered are given in Table VI.1. The limits for the Fixed Target run are shown in Fig. II.1.

VII. OTHER EXPERIMENTAL METHODOLOGIES FOR NEUTRINO OSCILLATION EXPERIMENTS

There are a number of other approved neutrino oscillation experiments. Of relevance to the present proposal are the CHORUS (WA 95) and NOMAD (WA96) proposals at CERN and the LSND (LA-11842-P) proposal at LAMPF. In comparisons between these proposals and ours, we have restricted our critique to the actual data presented in the proposals and to the $\nu_e \rightarrow \nu_\mu$ and $\nu_e \rightarrow \nu_\tau$ oscillation modes. The CHORUS proposal is for an appearance search for $\nu_\mu \rightarrow \nu_\tau$, with primary emphasis on small mixing angle. It does not address the $\nu_e \rightarrow \nu_\mu$ and $\nu_e \rightarrow \nu_\tau$ oscillation modes. The NOMAD proposal is primarily addressing the $\nu_\mu \rightarrow \nu_\tau$ mode, but since the detector has very good electron detection capabilities and, since there is a small ($\sim 1\%$) ν_e contamination in the neutrino beam, they will be able to put a limit on a $\nu_e \rightarrow \nu_\tau$ oscillation in the absence of any positive signal. The limit given in the original NOMAD proposal ($\sin^2 2\alpha < 3.6 \times 10^{-2}$) is shown, along with the limit in the present proposal and limits from published data, in Fig. II.1. However, the Δm^2 limit at maximal mixing shown for the NOMAD experiment in this figure (figure 12 in CERN-SPSLC/91-21) is not consistent with the $\sin^2 2\alpha$ limit stated above and the E/L ratio of 40 for NAOMAD. In addition, the text of the NOMAD proposal also states that the expected background for the electron channel is 5.6 events. With their stated number of electron candidates (7700) and their overall "efficiency to the ν_τ " of 2.24×10^{-2}, their stated limit in this channel is $\sin^2 2\alpha < 6.7 \times 10^{-2}$. At maximal mixing with E/L of 40, their Δm^2 limit is then approximately 6 eV^2. NOMAD submitted an addendum to their proposal (CERN-SPSLC/91-48) in August of 1991. In this document the total number of ν_e charge current events is 13,200. They do not show a new exclusion plot, but do state a new limit for $\sin^2 2\alpha$ in the $\nu_e \rightarrow \nu_\tau$ oscillation mode of 1.5×10^{-2} It is not clear to us whether this limit applies to a "global" analysis of τ candidates and whether or not it is for 2 years of running. This limit does not appear to be consistent with the shown number of background events, the overall efficiency to the ν_τ for the various modes and the total number of ν_e charge current events. In a general context, the experimental systematics of our experiment and NOMAD are

very different. In our experiment there is a pure ν_e beam with trivial backgrounds while the NOMAD ν_e beam is a small contamination in the dominant ν_μ beam. Finally, the NOMAD detector employs a number of state-of-the-art technologies and their analysis relies on sophisticated kinematic cuts that will require large statistics in order to establish a signal.

The LSND proposal is a search for a $\nu_e \rightarrow \nu_\mu$ oscillations using a large Cherenkov detector. The E/L for this experiment is more favorable than that of our experiment so, in principle, it should yield a better low mass limit. It is difficult, however, to directly compare our experiment with LSND. The mixing angle limit quoted by LSND represents almost 2 orders of magnitude improvement over the earlier LAMPF experiment, E645, which fell far short of its own projected goal. Again, the strength of P-860 is the cleanliness of the beam and the simplicity of the potential backgrounds. In the LSND case, the experiment relies on a beam which is a small component of the dominant beam. The ν's for LSND are produced by protons impacting a beam-dump. The dominant ν flux is from stopped π's, and these ν's are not energetic enough to produce μ's when they interact. The actual ν's for this experiment are the few ν's produced by π's decaying in flight before they stop. It would appear to be difficult to absolutely normalize the flux in this case. In addition, while this type of detector has been used successfully underground, this is its maiden flight as a surface detector. Furthermore, there are the usual problems of cosmic rays, due to the poor LAMPF duty cycle, and beam related neutron background to contend with. Overall, there are many potential difficult systematic problems in the LAMPF proposal which can play havoc with the expected small mixing angle limit and, to some extent, with the small Δm^2 limit.

VIII. DETECTOR DESIGN

In order to achieve the experimental goals the detector system must have the following attributes:

- Angular acceptance out to 10 mrad for ν's generated at the center of the Debuncher straight section.
- Sufficient mass to be able to detect the number of events needed to satisfy the physics objectives.
- Momentum and charge determination for μ energies above 1.0 GeV.

A preliminary design of a detector to accomplish these goals has been made. The detector is a conventional modular iron toroid design using Iarocci tubes to measure the position of charge tracks and scintillator counters to provide a cosmic ray trigger for calibrating the detector. Each toroid module contains 40 planes of iron absorber, 40 planes of Iarocci tubes, and 4 planes of scintillator. A four turn coil is used to provide the toroidal field. A schematic drawing of a single toroid module is shown in Fig. VIII.1a,b. Five different radius modules are used to optimize the detector to the 10 mrad acceptance requirement. The total detector consists of 15 modules which are octagonally shaped with an overall length of 190 feet, with a total mass estimated to be 0.72×10^3 tons.

The optimization of the detector dimensions was performed by using a simple ν beam Monte Carlo to optimize the acceptance for τ producing ν's. The Monte Carlo produced 9.0 GeV/c μ's which were allowed to decay over a 60 m decay volume. The ν_e's from the decays were traced into the detector located 20 m from the end of the decay volume. An interaction point was chosen randomly over the 50 m detector length. The ν was then weighted by the quasi elastic cross section for τ production. The detector was assumed to consist of 15 modules as described below with 5 different radii. The radii were then chosen such that $\sim$ 90% of the weighted interaction vertices were located $\geq$ 25 cm from the outer edge of the modules. The diameter for the central opening was chosen such that $\leq$ 2% of the

interactions occurred in the central region. The radial distribution as a function of z for generated and accepted events are shown in Fig. VIII.2.

VIII.1. Toroid Modules:

Each module consists of 40 planes of octagonal shaped, 2 in. thick iron absorber. Following each plane of iron is a plane of Iarocci tubes used for measuring the track position. In addition, following every tenth plane of Iarocci tubes is a plane of 1 in. thick scintillator The gap spacing between the planes of iron absorber is 2.5 in. for gaps containing both Iarocci tubes and scintillator and 1.25 in. for gaps containing only Iarocci tubes. The total length for a complete module excluding supporting frame is 140 in. A central opening passes through each of the modules to accommodate the water cooled copper conductor for the toroid coil. The coil is four turns looping around each side of the module to provide a toroidal field in the iron. The total power consumption for the full detector is estimated to be 700 Kw. Each turn of the coil is divided into 2 sections for cooling. A water flow rate of .25 ft^3/min through each section of the turn will be sufficient to cool the coil. The parameters for each of the different radius modules are given in Table VIII.1.

TABLE VIII.1

Module Parameters

Module Type	I	II	III	IV	V
Radius (cm)	75.	85.	95.	1.05	115.
Central Hole Dia.(in.)	4.0	4.0	6.0	6.0	6.0
Conductor o.d.(in.)	$.75 \times .75$	$.75 \times .75$	1.25×1.25	1.25×1.25	1.25×1.25
i.d.(in.)	$1/8 \times 1/8$	$1/8 \times 1/8$	$3/16 \times 3/16$	$3/16 \times 3/16$	$3/16 \times 1/16$
Current (amps)	5000	5559	6390	6948	7506
Power (kW)	51.25	64.59	31.06	37.25	44.10
Iarocci Modules	800	880	1000	1080	1200
Mass (kg)	28.5×10^3	38.0×10^3	47.6×10^3	57.1×10^3	69.8×10^3

VIII.2. SCINTILLATOR:

In order to provide a calibration trigger, each module contains 4 planes of scintillator. The scintillator planes are octagon shaped to match the iron absorber and 1 in. thick with the same transverse measurements as the iron absorber plates. A schematic drawing of a scintillator plane is shown in Fig. VIII.3. The scintillation light is collected by two $1.0 \times 1/2$ in.^{2} waveshifter bars imbedded in the scintillator. The waveshifter is read out by a photomultiplier tube located on the top end of each bar.

VIII.3. IAROCCI TUBES:

Tracking information is provided by the Iarocci tubes. Iarocci tubes have been successfully used in a number of experiments and have been proven to be rugged devices that can be mass produced at a relatively low cost (Ref. 7).

The Iarocci planes will be constructed from 8-tube modules. The structure of an 8-tube module is shown schematically in Fig. VIII.4. The module is constructed from an open PVC profile with eight 0.9×0.9 cm^2 cells separated by 0.1 cm thick walls. The profile is coated on the interior with a high resistivity graphite paint to form the cathode surface. A 100 μ m diameter Cu/Be wire is strung down the center of each cell, supported approximately every 50 cm by PVC spacers. The profile is inserted into a PVC sleeve and sealed at each end by an endcap to form the gas volume. The endcap assembly provides connections for high voltage and gas. The overall width of the module is approximately 8.4 cm.

The Iarocci modules are inserted into an outer PVC sleeve to form a complete Iarocci module. This double sleeve arrangement allows for easy replacement of the 8 tube modules, should that become necessary. The outer sleeve is bonded horizontally to a 1/6 in. thick glass-steel laminate with copper cladding on each side. The laminate will be routed on the inner side to form wide copper strips to provide the readout for the Iarocci tubes. The strip will run vertically on one side and horizontally on the other side to form simultaneous x-y readout. To accommodate the coil for the toroid, the central region will consist of 4 shorter modules separated in the center providing a central opening.

Iarocci tubes are conventionally operated using a gas mixture of 25% Argon and 75% isobutane. This gas mixture however has the disadvantage of being extremely flammable. The SLD collaboration has investigated nonflammable gas mixtures for use in the SLD Warm Iron Calorimeter (Ref. 8). These studies indicate that a mixture of 2.5% Argon, 9.5% isobutane, and 88% CO_2 possesses the same operating characteristics as the Argon-isobutane mixture, but is considered nonflammable by the U.S. Bureau of Mines. This nonflammable gas mixture will be used and the Iarocci tubes operated at a voltage of approximately 4.9Kv. The resulting signals should be large enough to avoid signal-to-noise problems and will allow the use of low-cost front end electronics. Gas will be provided to each plane of Iarocci tubes via a gas manifold system located on the side of each toroid module.

VIII.4. Assembly:

The toroid modules will be constructed as single units by stacking planes of iron, Iarocci tubes, and scintillator on a support structure in sequence. Once all the planes have been installed, the copper coils of the toroid will be installed and, finally, gas, cooling water, and electrical connections will be made to form a completed module. It is assumed that the experimental hall is of sufficient size to allow the construction *in situ*.

VIII.5. Trigger and Data Acquisition Electronics:

A conceptual design for the detector electronics has been completed. The physics goals of the experiment place the following requirements on the electronics:

- Momentum and charge determination for μ energies above 1.0 GeV with a spatial resolution of ~ 0.3 cm
- Reject background events by looking at activity near the vertex which is not associated with the μ.
- A time resolution of order 100 nsec in order to associate individual hits with events.

To satisfy the physics requirements and to cope with the basic features of the strip readout of Iarocci tubes, it is necessary not only to measure the time of the signal but also the pulse area in both the x and y strips and the correlation between the two directions.

Studies have recently been made at Nevis to determine the strip width required to achieve the required spatial resolution of 0.3 cm for measuring the curvature and vertex activity. These studies used 1 cm pitch readout strips read into a digital scope to record the pulse shape. The pulse shape was recorded for the triggering strip and several neighboring strips. When a signal is present in the triggering strip, a signal is also present in several of the neighboring strips. The strength of the signal on the strip is a function of both the width of the strips and the distance from the anode wire. With a strip width of 1 cm, 3 strips have a significant signal above threshold for a single hit of the wire.

Based on these studies, a scheme using 1 cm strips in two orthogonal directions has been chosen. The signals from three adjacent strips will be combined with an analog add to form a single readout and digitization channel. Interpolating the pulse area from neighboring strips will yield an error of less than 1 strip, 1 cm. Correlations between x and y pulse areas should be adequate to differentiate a single hit verses multiple hits.

Signal and Data Flow:

A diagram of the signal flow is shown in Fig. VIII.5. Approximately one-quarter of the signal charge on the anode wire is induced onto the readout strip nearest to the gas discharge. The signal is 5-20 millivolts and with an intrinsic width of 50 nsec. The shaper conditions the signal to meet the requirements of the sampling system. The shaper output is sampled by the FADC and stored in the memory during the beam "on" period. At the end of the beam "on" period digital encoder modules perform zero suppression and further compress the data by formatting and packing the data. The data is then transferred to the DAQ computer for writing to tape. In addition, the DAQ computer performs diagnostic analysis on a prescaled number of events to insure the integrity of the data.

The Shaper:

The function of the shaper is to condition the signal for the sampling system to get the total pulse area and time information. The signal is broadened so at least three samples are available and the signal is amplified so that it is large compared to the noises introduced by the sampling pipeline.

The total signal charge is about 3 pC. Since an interpolation factor of only 10 is required, it is quite conservative to assume that the front end amplifier and shaper need to have a noise level of less than 100 fC. In fact, even with three 1 cm strips ganged together, the total readout strip capacitance will be less than 300 pf for a 2 m length. This translates into a detector induced noise of less than 1 fC, so there is indeed a large factor of safety.

The shaping is accomplished by a series of integration and derivatives. Because the chamber pulses fall more slowly than they rise, a single integration is required to further slow the rise, and an RC derivative is needed to restore the second integration. A second RC derivative is also needed to eventually restore the baseline.

The FADC:

The flash recorder consists of four sections: A receiver amplifier, a fast sampling ADC, memory and the data control. When the WRITE clock is on, a 6-8 bit FADC samples the amplifier output voltage from the pulse once every 100 nsec for the duration of 100 ps. This sampling rate will require the FADC to run at about 10 MHz, thus offering a wide selection of low cost devices to chose from. The digitized signals are then written to an 6-8×4096 random access memory where they are stored until readout is initiated at the end of the beam "on" period (Ref. 9).

Trigger and System Control:

The electronics will operate in a continuous sampling mode. Since the arrival time of the ν beam with respect to the machine clock is well known, it is straightforward to latch the 400 μsec of data. The use of the continuous sampling mode

eliminates the need to set up a trigger based on preconceived ideas of the information in the detector. The writing process is stopped by a system trigger and the last 400 μsec of data is then read out.

Trigger type information is distributed via the Control Links. Trigger timing is implicit in the fast clocks which are sent as bursts during the trigger interval with the required number of cycles. The clock is generated centrally and then is fanned out with equal times to all front end data acquisition elements. Memory address counters are reset from the leading clock.

Data are written directly to the computer memory via the Data Link. The Data Link provides two functions: 1) To identify those recorder modules that contain nonzero data and 2) to perform data suppression, data formatting, and readout. A detailed description of the system can be found in Ref. 9.

Higher level triggers are carried out in software. The data are ordered by readout according to event number, data type, increasing signal number, and time. Interrupts are used to indicate the completion of data streams, starting addresses, and word counts. A multiple event buffer space is set up in computer memory so that the event processing time can be averaged over many events for efficient utilization of the processing bandwidth. The computer regulates the data acquisition by inhibiting triggers whenever the processing gets too far behind. Error flags and diagnostic data inserted into the data stream, together with the test pulse system, provide for system maintenance.

VIII.6. Detector Summary

The physical characteristics of the detector are summarized in Table VIII.2.

TABLE VIII.2

DETECTOR SUMMARY

Dimensions Front:	$5.0 \times 5.0 \times ft^2$
Back:	$8.0 \times 8.0 \times ft^2$
Length	190 ft
Tonnage	0.72K tones
Number of planes of Iarocci tubes	600
Total number of wires	120,000
Total number of electronics channels	79,000
Number of planes of scintillator	60
Number of photomultiplier tubes	120

APPENDIX A

We have measured the flux of circulating muons in the Debuncher by employing a slight modification of a technique used by G. Dugan in 1987 to measure the number of pions and electrons which get injected into the Debuncher. This technique relies upon the use of a non-destructive, ref pickup to measure the bunch structure of the beam on a turn-by-turn basis.

The beam arrives in the Debuncher, at the location of the pickup, in 84 narrow bunches ($\sigma_t \approx 1$ nsec) with a spacing of about 18 nsec. The fast particles (pions, muons and electrons) are separated from the slow particles (antiprotons) by about 8 nsec. Hence, fast and slow particles can be identified by looking at the time structure of the output from the ref pickup. As the beam circulates in the Debuncher, the pions decay in a few turns ($\gamma c\tau_\pi \approx 1$ turn), while the electrons spiral into the low energy edge of the machine, due to the emission of synchrotron radiation, and are lost after 14 turns. After more than 14 turns the only particles left are muons and antiprotons.

The results of turn-by-turn measurements made in 1987 are summarized in Fig. A1. In these data there was no indication of a signal representing circulating

muons - which are expected to be the only fast particles remaining beyond turn number 14. The absence of a "bunched" muon signal for turn 15, however, is not necessarily an indication that there are no muons in the debuncher. This can be understood by calculating the muon debunching time:

$$T_D = \frac{(\Delta T)_{ref}}{\frac{\eta \delta P}{P}}$$

For muons, $\eta = .017$ and $T_D = 27.6\mu$sec (17 turns), i.e., the muons are completely debunched after 17 turns and, consequently, induce no signal on the ref pickup. We have checked the rate at which muons debunch by performing a simulation which uses the longitudinal difference equations to study the bunch shape as a function of turn number in the Debuncher. The results, shown in Fig. A2 for a bunch injected ($N = 1$) with $\Delta t = \pm 0.5$ nsec and $\delta P/P = \pm 2.0\%$, illustrate the rate at which the injected muons debunch and indicate complete debunching in 15–17 turns. The ref pickup technique is thus not sensitive to circulating muons in turns beyond turn 14.

An examination of Fig. A1 suggests that it is straightforward to measure the bunched muon signal by killing the electrons in the beam prior to injection into the Debuncher and then measuring the number of fast particles on turns 5–11 using the ref pickup.

The most appealing method for killing the electrons is to insert a lead radiator at the end of the AP-2 transport line. Between the last two quadrupoles in this line (IQ32 and IQ33), the betatron amplitudes are reasonably small (4–8m.) and the emittance blowup of the muon bunches due to multiple scattering should be small.

We have studied the effectiveness of radiator thicknesses of 0.25, 0.50, and 1.0 radiation lengths on removing electrons from the beam at the end of the AP-2 transport line. The program EGS was used to determine the energy of the leading (maximum energy) electron exiting the radiator for electrons of energy 9.0 GeV incident on the radiator. (The simulation was also checked analytically using a formula from Tsai [Ref. A.1].) The results are shown in Figure A3. If we impose

an 8.7 GeV cut on the electron energy for it to be captured in the Debuncher, then for radiator thicknesses of 0.25, 0.50, and 1.0 radiation length, 40%, 11%, and 0.15%, respectively, of the incident electrons will survive the cut. We have chosen to use a radiator thickness of 1 radiation length in order to guarantee that electrons do not contribute to our muon signal.

Our measurements were performed, parasitic to the running of E-760, during the last several months. A one radiation length lead absorber was inserted into the AP-2 transport line, completely eliminating electrons from the beam. We used a Tektronix DSA 602 digital sampling analyzer to measure the time structure of the signal from the pickup. The DSA 602 has an analog bandwidth of 1 GHz, samples at 2 Giga-samples/second, and has a memory depth of 32,000 samples. We could, therefore, capture data for nine turns during a measurement. The data were taken in the following manner. Each measurement was an average over 64 pulses (each pulse containing 84 bunches). We first captured data for turns 1 through 9 and then set the DSA trigger delay to capture turns 9 through 17. The two data sets were normalized such that the $\bar{p}$ flux for turn 9 was equal. Fig. A4 shows the raw data for approximately 10 bunches for turns 3,4, and 5. In turns 3 and 5, we see the 8 nsec separation between the $\beta = 1$ particles and the $\bar{p}$'s. On the even turns, the $\bar{p}$ bunches are approximately in time with the $\beta = 1$ particles and thus the ref bunch structure shows only one peak. Therefore, in order to determine the individual particles fluxes, only data from the odd turns were usable. For each of the odd turns between turns 3 and 11, we averaged 60 of the 84 bunches to produce a "bunch averaged" time structure for each of the turns. The data for turns 5,7,9, and 11 are shown in Fig. A5. These data were fit to two Gaussians plus a constant. (The fit curves are also shown in Fig. A5.) From the fit parameters (amplitude and σ) we could then determine, for each turn, the area under the two Gaussians. These numbers are directly proportional to the flux of $\beta = 1$ particles and $\bar{p}$'s. In order to determine the flux of muons, we then only had to make a correction for the number of pions remaining at each turn. In order to do this, we used the measured $\beta = 1$ particle flux from turn 1, assumed that this entire flux was due to pions, calculated the number of pions remaining after each turn, and then subtracted that number from the measured $\beta = 1$ flux for that turn to determine the number of

Table A.1
Particle Flux Measurements

Turn	Flux($\beta = 1$)	Flux($\bar{p}$)	$\frac{(\beta=1)}{\bar{p}}$	$\frac{\mu}{\bar{p}}$
1	33572	—	—	—
3	6251	2126	2.94	0.80
5	2232	1287	1.73	1.12
7	1597	1171	1.36	1.27
9	1306	1132	1.15	1.14
11	934	1122	0.83	0.83

muons. Our results are shown in Table A.1 for turns 3–11.

We have also modeled the AP-2 line and the Debuncher ring in a DECAY_TURTLE simulation in order to compare our muon flux measurements with expectations. The simulation uses measured magnetic field strengths and gradients for the beam line and ring magnets and measured apertures for all elements. Particles are ray-traced from the target station, through the AP-2 beam line, through the Debuncher injection channel and through the first three revolutions in the Debuncher. We compare the results of the simulation to the muon flux measurements by calculating the ratio of the expected number of muons after three turns in the ring to the number of pions at the end of the beam line. An ion chamber measurement of the pion flux at the end of the beam line allows us to normalize the calculation.

This model calculation of the circulating muon flux accounts for the contribution from pion decay in the beam line as well as the ring. Consequently, it should be directly comparable to the muon flux measurement. The calculated flux agrees with the experimental data to within 10% and reinforces our belief that we have a reasonably good representation of the aperture limitations in both the transport line and the Debuncher ring.

APPENDIX B

The following is the letter from Steve Holmes reviewing the machine parameters for Collider Run II, Fixed-target running, and Collider Run III.

Fermilab

Fermi National Accelerator Laboratory
P.O. Box 500, Batavia, Illinois 60510
Phone: 708-840-4468 FAX: 708-840-4552

Accelerator Division Headquarters

September 1, 1992

Professor Wonyong Lee
Columbia University
Nevis Laboratories
P.O. Box 137
Irvington, N.Y. 10533

Dear Wonyong,

At the request of both you and the Fermilab Physics Advisory Committee I have reviewed with your collaborators the assumptions for accelerator performance upon which the proponents of P-860 are basing rate calculations. It appears that the critical parameters are protons/pulse, antiproton production efficiency, Main Ring cycle time, and running efficiency. I am proposing here a set of numbers which I would regard as "realistic" for the time frames given. "Realistic" means that I would have some confidence that all four of the levels listed could be obtained simultaneously with reasonable regularity. I am also offering some comment with regard to the feasibility of the proposed multibatch operational modes.

Let me make a few comments on each of these parameters and how they might evolve.

Protons/pulse: We are currently operating at about 1.3×10^{12} protons per pulse in Main Ring. Once we are tuned up we should achieve 1.8×10^{12}. This number is expected to rise to 3×10^{12} following the linac upgrade, scheduled for implementation in the spring-summer of 1993. After that the number will not rise until completion of the Main Injector when 5×10^{12} is expected. Note that these numbers are based on single Booster batch operation. I have encouraged your collaborators to pursue thoughts on multibatch schemes.

Antiproton Production Efficiency: Efficiency, measured as the ratio of antiprotons stacked to protons on target, is currently about 1.1×10^{-5}. It is believed that the number of antiprotons circulating in the Debuncher ring is approximately 50% higher than this. We are counting on this number reaching, and being maintained at, 1.4×10^{-5} for the remainder of the decade. I would suggest that a realistic number for antiproton production efficiency measured in the Debuncher is 2×10^{-5}.

Cycle Time: We are currently running the Main Ring with a 2.4 second cycle. It is believed by members of the Main Accelerator Department that this can be reduced to 2.1 seconds. Since the repetition frequency has to be a multiple of 15 Hz I suggest using 2.133 seconds.

Running Efficiency: This is the hardest to estimate and depends upon how it is defined. Mike Gormley points out that when defined as stacking hours achieved/stacking hours scheduled 66% was achieved in the previous collider run. This number ignores the effects of: 1)shot setup time, including time to reestablish stacking following a shot; 2)time for machine studies; and 3)accesses for CDF and/or D0 (irrelevant with the Main Injector). The point is that I anticipate that during collider running CDF and D0 are going to be calling the shots and so we won't be putting beam on the production target 100% of the time that we are capable of doing so.

Fermilab

Fermi National Accelerator Laboratory
P.O. Box 500, Batavia, Illinois 60510
Phone: 708-840-4468 FAX: 708-840-4552

Accelerator Division Headquarters

Since I'm not really sure what the running efficiency means I would suggest using 110 hours per scheduled week during collider run II and 130 hours per week with the Main Injector. During a fixed target run I would guess 130 hours could also be achieved.

Multibatch Operation: P-860 has proposed a significant increase in the proton targetting rate based on multibatch operations in Main Ring (Main Injector). Two implementations are possible--one in which ten (four) Booster batches are loaded into Main Ring (Main Injector) followed by batch-by-batch extraction at 15 Hz; a second in which a batch coalescing operation is undertaken prior to targetting. Both techniques are feasible in principle. However, both will require R&D effort. The 15 Hz batch-by-batch extraction will require development of a 15 Hz kicker and lithium lens. The 15 Hz kicker is probably not such a big deal, the lithium lens is probably harder. However, we are going to have to develop a more rapid cycling lens for use in the Main Injector era anyway. The multibatch coalescing scheme would require a new rf system and a new target system. In addition significant simulation work needs to be completed to assure ourselves that the Main Ring has sufficient momentum aperture to accomodate the required manipulations.

The Accelerator Division would undertake the required R&D, with reasonable assurance of success, if this experiment goes ahead. We would like to see the P-860 collaboration provide the intellectual leadership on these efforts. Since I regard the batch-by-batch extraction scheme as the more solid at the moment I have listed it in the table.

Summary: I propose using the following for the sake of calculation:

	Collider Run II	Fixed Target	Collider Run III	
MR Protons/pulse	3×10^{12}	2.5×10^{13} *(1)*	5×10^{12}	2×10^{13} *(2)*
Antiprotons/proton	2×10^{-5}	2×10^{-5}	2×10^{-5}	2×10^{-5}
MR (MI) Cycle time (sec)	2.133	3.467	1.467	1.867
Hours/week	110	130	130	110

(1) Total intensity in Main Ring derated by 16.7% due to 8 GeV lifetime.

(2) The two columns listed under Collider Run III correspond to a dedicated $\bar{p}$ production mode (left) and simultaneous $\bar{p}$ production/multibatch operation (right).

Sincerely yours,

Stephen D. Holmes

cc
C. Ankenbrandt
R. Dixon
M. Gormley
J. Peoples
T. Yamanouchi

APPENDIX C

The second phase of the experiment is a search for ν_μ oscillations via ν_μ disappearance. This phase would be a long baseline, 2 detector experiment with a second detector located a few kilometers from the Debuncher providing good Δm^2 sensitivity. This would be orthogonal to the $\nu_\mu \rightarrow \nu_\tau$ appearance experiments presently under construction at CERN and the proposed emulsion experiment P803 at Fermilab. These are all sensitive to small mixing angles but are not sensitive to small Δm^2. The inference from the solar neutrino data is to search for ν_μ oscillations at small Δm^2 (Fig. II.1). In addition, the recent results from Kamiokande and IMB of a depletion of atmospheric ν_μ's relative to ν_e's can be interpreted as as an oscillation effect at small Δm^2 with reasonably large mixing.

For this phase of the experiment there are two possible options for the second detector. The first is to construct a second identical detector, leaving the first detector near the debuncher to monitor the ν_μ flux and continue with the $\nu_e \rightarrow \nu_\tau$ search should the physics justify it. The second option would involve moving a portion, $\sim$ 90%, of the near detector to the far detector location. The remaining 10% of the detector would remain located near the Debuncher straight section to monitor the ν_μ flux. For both options, the far detector would be located in line with the the AP-2 transfer line to the Debuncher. The neutrino flux arising from pion decays in the AP-2 transfer line has the advantage of higher flux, $\sim$ 20, than the neutrino flux in the Debuncher. This increase arises from the fact that the pion decay distance in AP-2 is 150 m while only 13% of the pion decays beyond 280 m provide the Debuncher flux, and the momentum bite of the AP-2 transfer line is $\pm$8% compared to $\pm$2% for the Debuncher.For the purposes of calculating the event rates, locations for the long baseline detector of 3 km and 10 km from the end of the AP-2 transfer line are considered. In addition, two energy settings, 3 GeV and 9 GeV, for the AP-2 transfer line and Debuncher will be used. Clearly, the 9 GeV operation is compatible with Collider running but the 3 GeV setting is not. In order to calculate the number of pions at 3 GeV compared to 9 GeV, the Monte Carlo EVENTQ developed for BNL E776 using the secondary particle production model NUCRIN for projectile momentum was used. The number of

pions at 3 GeV relative to 9 GeV was determined to be 0.7 and 0.9 for positive and negative beams respectively.

Understanding and accounting for the difference in the neutrino energy and flux at the two detectors is crucial for the ν_μ disappearance search. Given an angle θ between the pion and neutrino in the lab frame, $\gamma^2\theta^2 << 1$ for the far detector. For the near detector, events with $\gamma^2\theta^2 << 1$ are also chosen. In this case, determination of both the neutrino flux and energy in the near and far detectors is straightforward. Note that the average angular divergence of the pion beam in both the AP-2 transfer line and the Debuncher is ~ 1 mrad.

Charged current ν_μ events will be identified as all events with a clearly identified muon. Since the detectors will have good energy resolution, the sensitivity of this phase of the experiment will be dominated by the statistics in the far detector. The numbers of charged current ν_μ events expected to be observed in the far detector for a 40 week run operating the Main Injector in a multi-batch mode with negative beam are summarized in Table C.1.

TABLE C.1

Number of events in long baseline detector.

	3 GeV	9 GeV
3 km. positive	3.5K	44K
3 km. negative	1.7K	23K
10 km. positive	0.3K	3.8K
10 km. negative	0.1K	2.1K

If the number of events observed in the second detector is the same as the expected number based on the rate in the first detector and the experimental error is dominated by the event rate in the second detector, then the upper limit of the

mixing probability is

$$P \leq \frac{1.3 \times \delta}{\epsilon \times N_{\nu_\mu}},$$

where δ is the experimental error, $\sqrt{N_{\nu_\mu}^{\rm int}}$, 1.3 corresponds to 90% of the area under one side of the Gaussian, and ϵ is the detector acceptance and detection efficiency, $\sim 60\%$. For maximal mixing, the small Δm^2 limit is

$$\Delta m^2 \leq 0.8 \times \frac{E}{L} \times \sqrt{P}.$$

The limits for Δm^2 for the two different energy settings and detector locations are summarized in Table C.2.

TABLE C.2

Δm^2 imits for the long baseline detector $\nu_e \rightarrow \nu_\mu$ search.

	3 GeV	9 GeV
3 km. positive	$0.15 ev^2$	$0.24 ev^2$
3 km. negative	$0.18 ev^2$	$0.28 ev^2$
10 km. positive	$0.08 ev^2$	$0.13 ev^2$
10 km. negative	$0.11 ev^2$	$0.16 ev^2$

REFERENCES

Ref 1: BNL Neutrino Workshop, M. Murtagh Ed., 1987.

References for limits in Fig. II.1:

$\nu_e \rightarrow \nu_\mu$

BNL 776: L. Borodovsky et al., Phys. Rev. Lett. 68, 274(1992).
BNL 734 : L. Ahrens et al., Phys. Rev. D31, 2732 (1985).
CHARM: R. Eichler, Nucl. Phys. B (Proc. Suppl.) 3, 389 (1988).
BEBC PS: C. Angelini et al., Phys. Lett. 179B, 307(1986).
LAMPF: T. Dombeck et al., Phys. Lett. 194B, 591 (1987).
GOSGEN: G. Zacek et al., Phys. Rev. D34, 2621 (1986).

$\nu_e \rightarrow \nu_\tau$

BEBC SPS: O. Erriquez et al., Phys. Lett. 102B, 73 (1981).
FNAL 531: N. Ushida et al., Phys. Rev. Lett. 57, 2897 (1986).
FNAL B.C. (Bubble Chamber): N.J. Baker et al., Phys. Rev. Lett. 47, 1576 (1981).
LAMPF : P. Nemethy et al., Phys. Rev. D23, 262 (1981).

$\nu_\mu \rightarrow \nu_\tau$

CCFR: I. E. Stockdale et al., Phys. Rev. Lett. 52, 1384 (1984).
CDHS: F. Dydak et al., Phys. Lett. 134B, 281 (1984).
CHARM: F. Bergsma et al., Phys. Lett. 142, 103 (1984).

Ref 2: S.P. Mikheyev and A.Yu. Smirnov, Nuovo Cimento 9*C*,17 (1986);
L. Wolfenstein, Phys. Rev. *D17*, 2369 (1978).

Ref 3: W.J. Marciano, "Neutrino Physics – A Theoretical Perspective"
BNL Neutrino Workshop, M. Murtagh Ed., 1987.

Ref 4: B.F. Bayanov, T.A. Vseolozhskaya, Yu.N. Petrov, and G.I. Silvestrov
"The Investigation and Design Development of Lithium Lenses With Large Operating Lithium Volume."
(Novosibirsk, IYF), Proceedings, High Energy Accelerators,

587-590 (1988).

Ref 5: E.D. Cummins and P.H. Bucksbaum, "Weak Interactions of Leptons and Quarks", Cambridge University Press.

Ref 6: N. Kondakis, Ph.D. Thesis, Columbia University (1989).

Ref 7: W. Busza, "Experience with Iarocci Tubes Produced on a Large Scale", Published in SLAC Colliding Beam, 210 (1987).

Ref 8: A.C. Benvenuti et al., Nucl. Instr. and Meth. *A284*, 339 (1989).

Ref 9: M. Atiya et al., Nucl. Instr. and Meth. *A300*, 542 (1991).

Ref A.1: Y. Tsai, Rev. of Mod .Phys. Vol. 46, No. 4, 815 (1974).

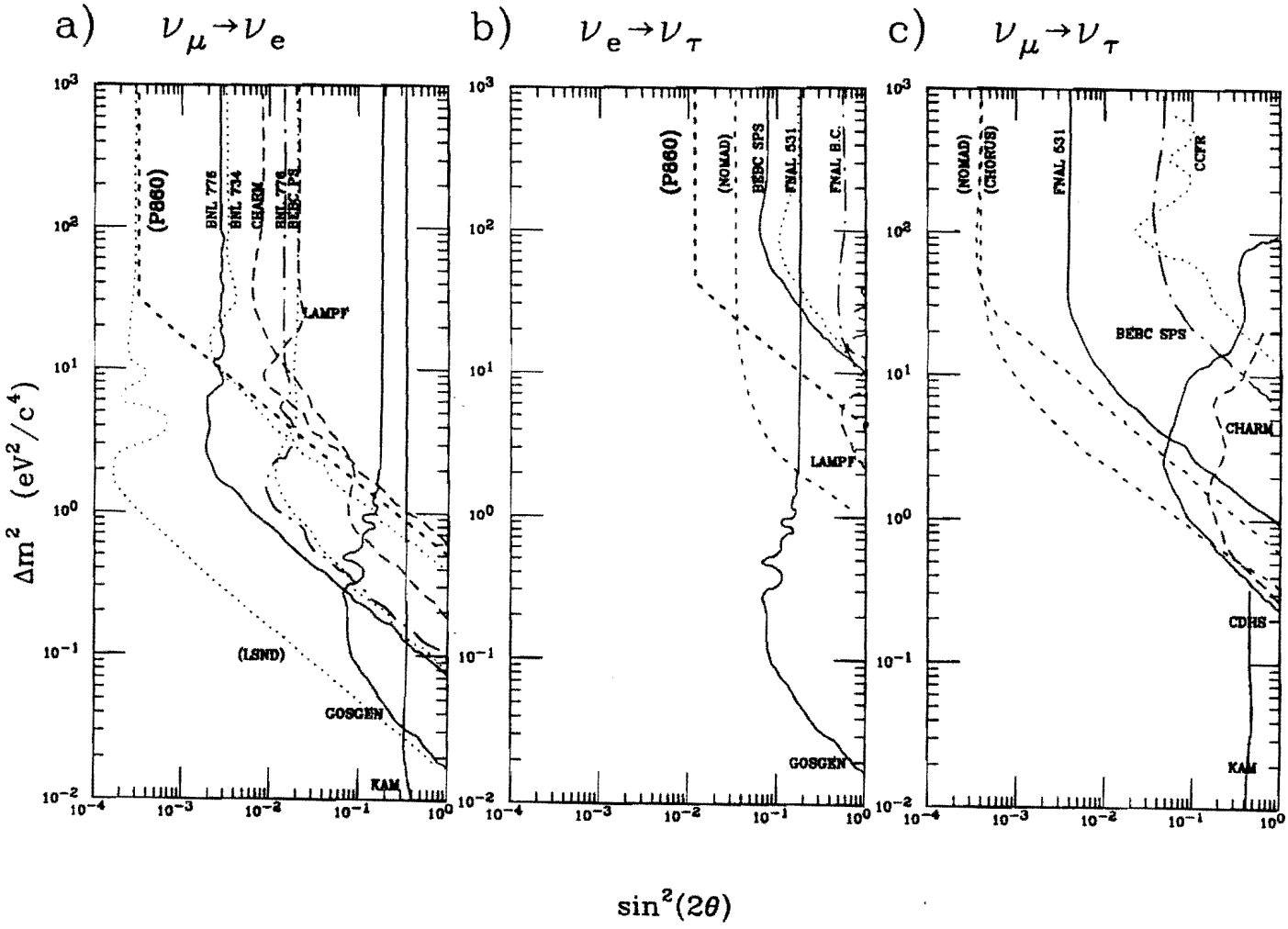

Fig. II.1: Current published and proposed neutrino oscillation limits for a) $\nu_e \rightarrow \nu_\mu$, b) $\nu_e \rightarrow \nu_\tau$, and c) $\nu_\mu \rightarrow \nu_\tau$. P860 Limits are for Fixed Target running.

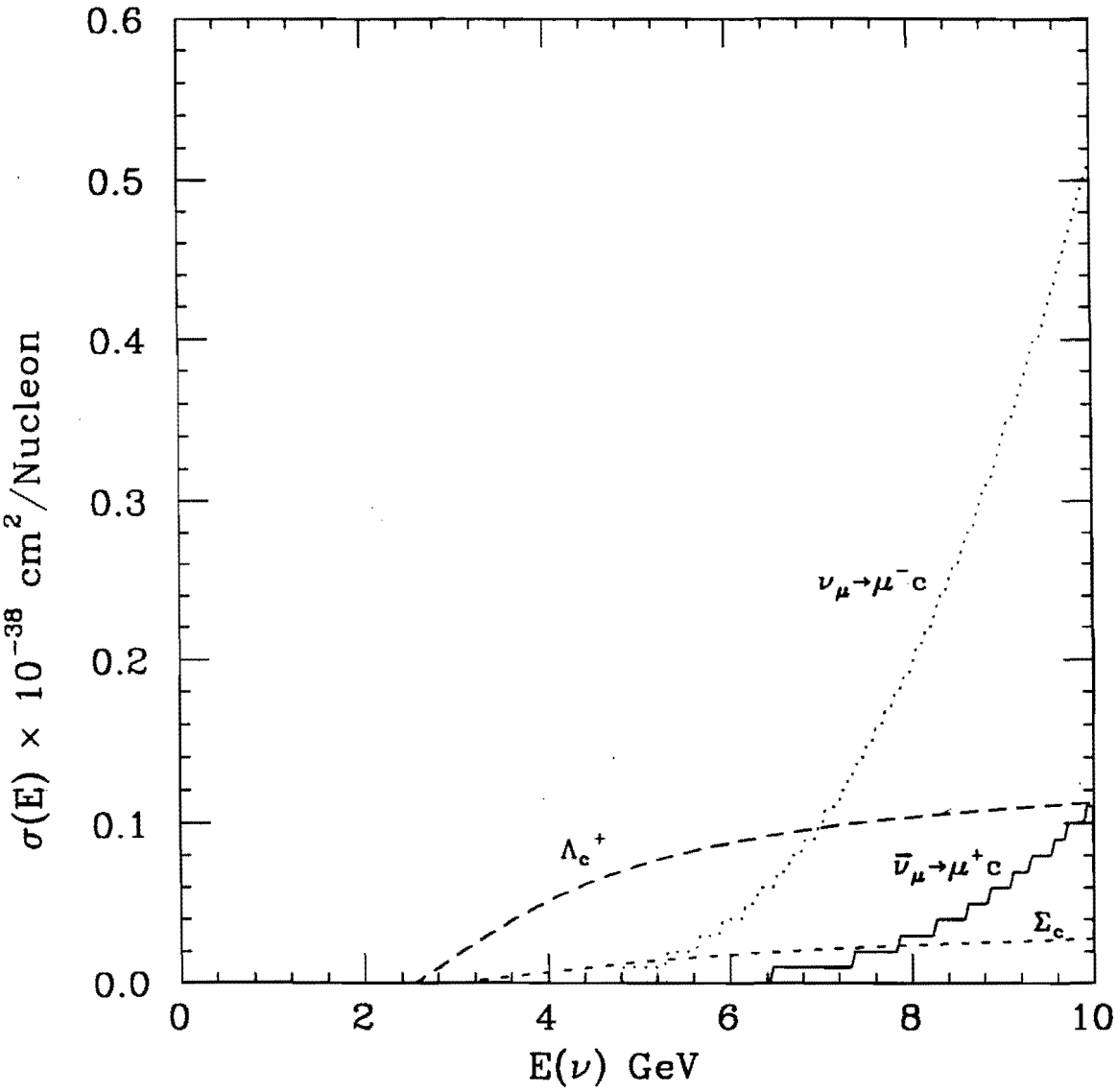

Fig. II.2: Charm cross sections for Λ_c^+, Σ_c, and inclusive D production.

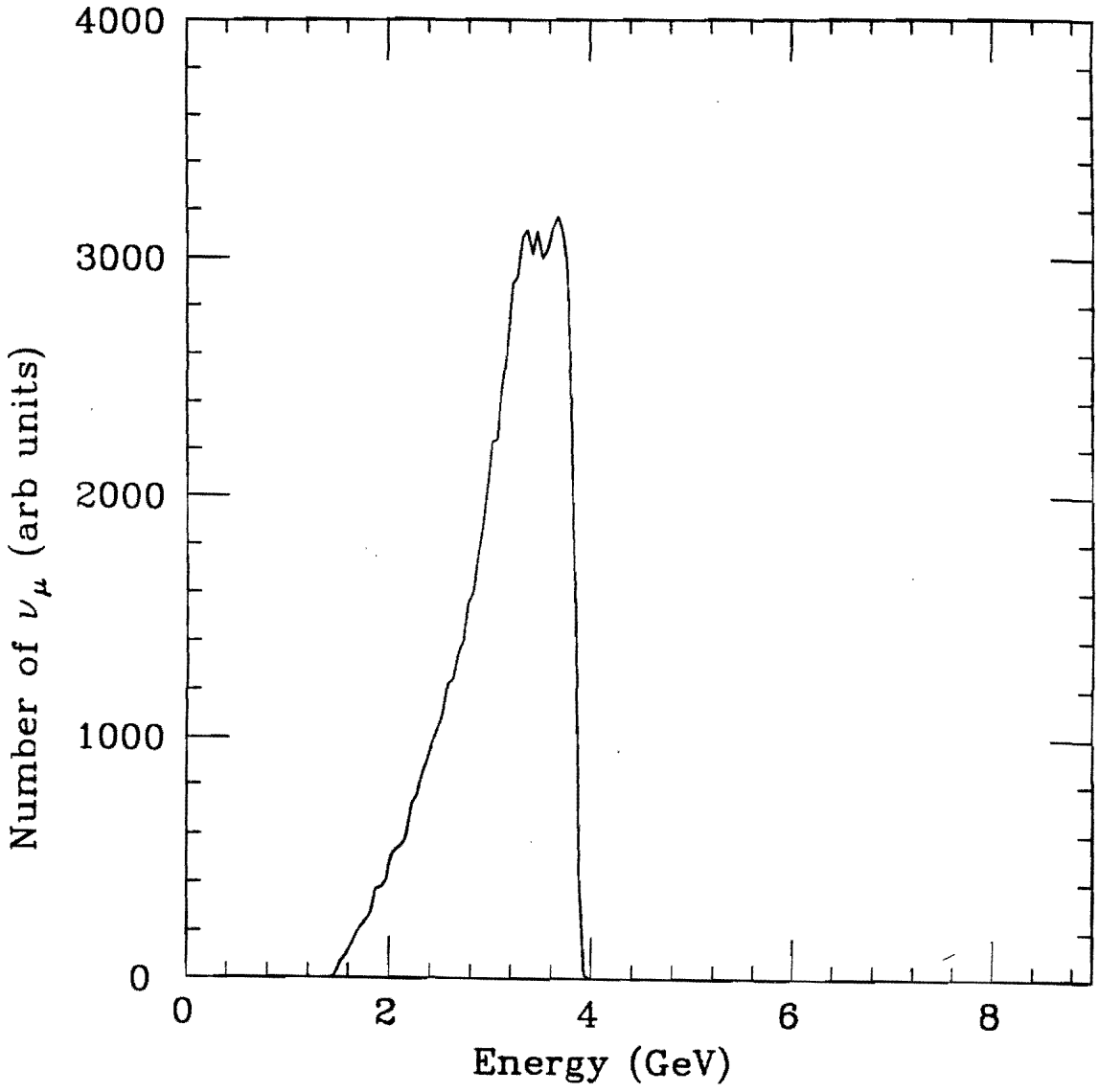

Fig. II.3: Energy spectrum for ν_μ from π decays.

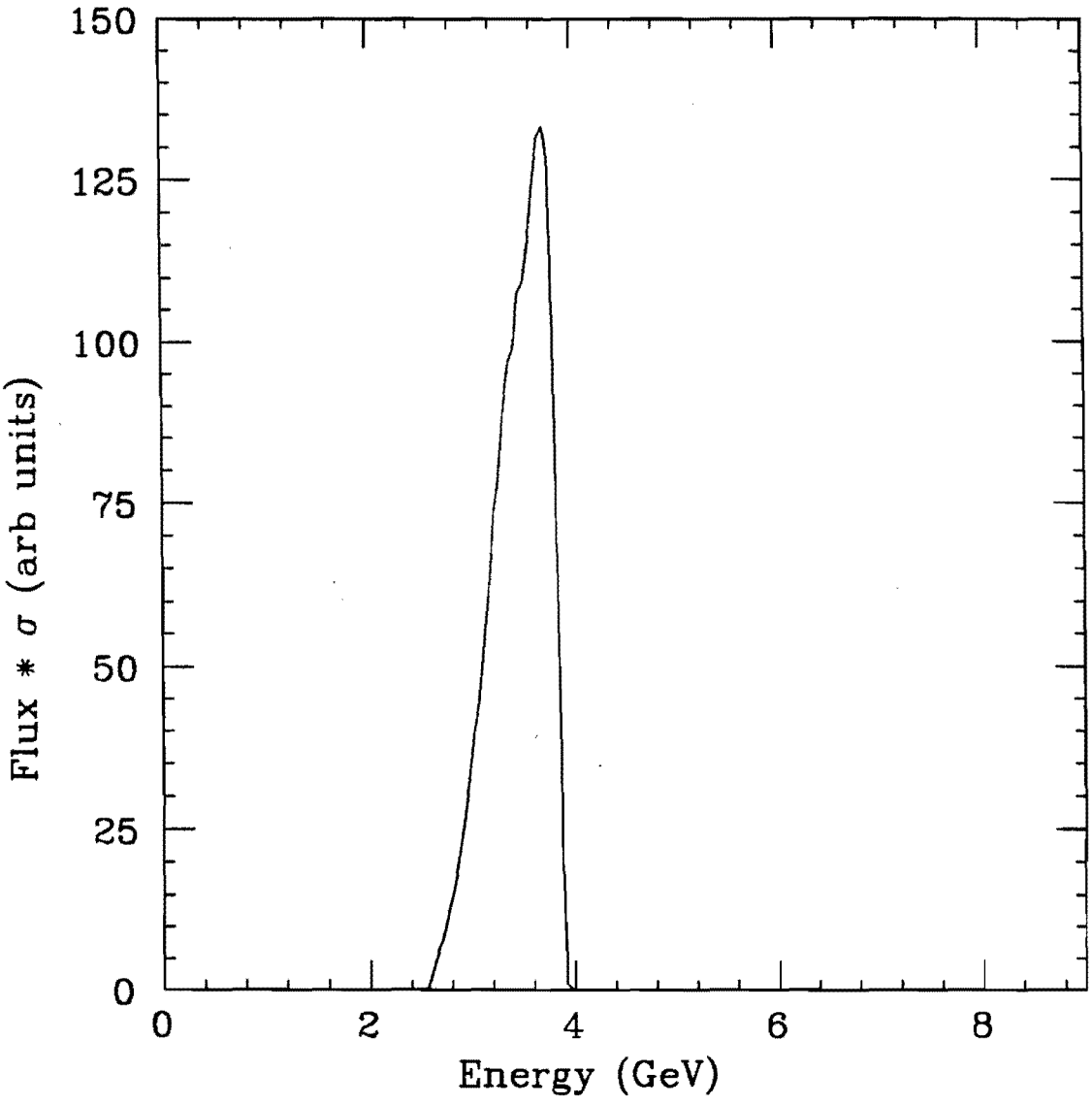

Fig. II.4: Flux × cross section for Λ_c^+ production.

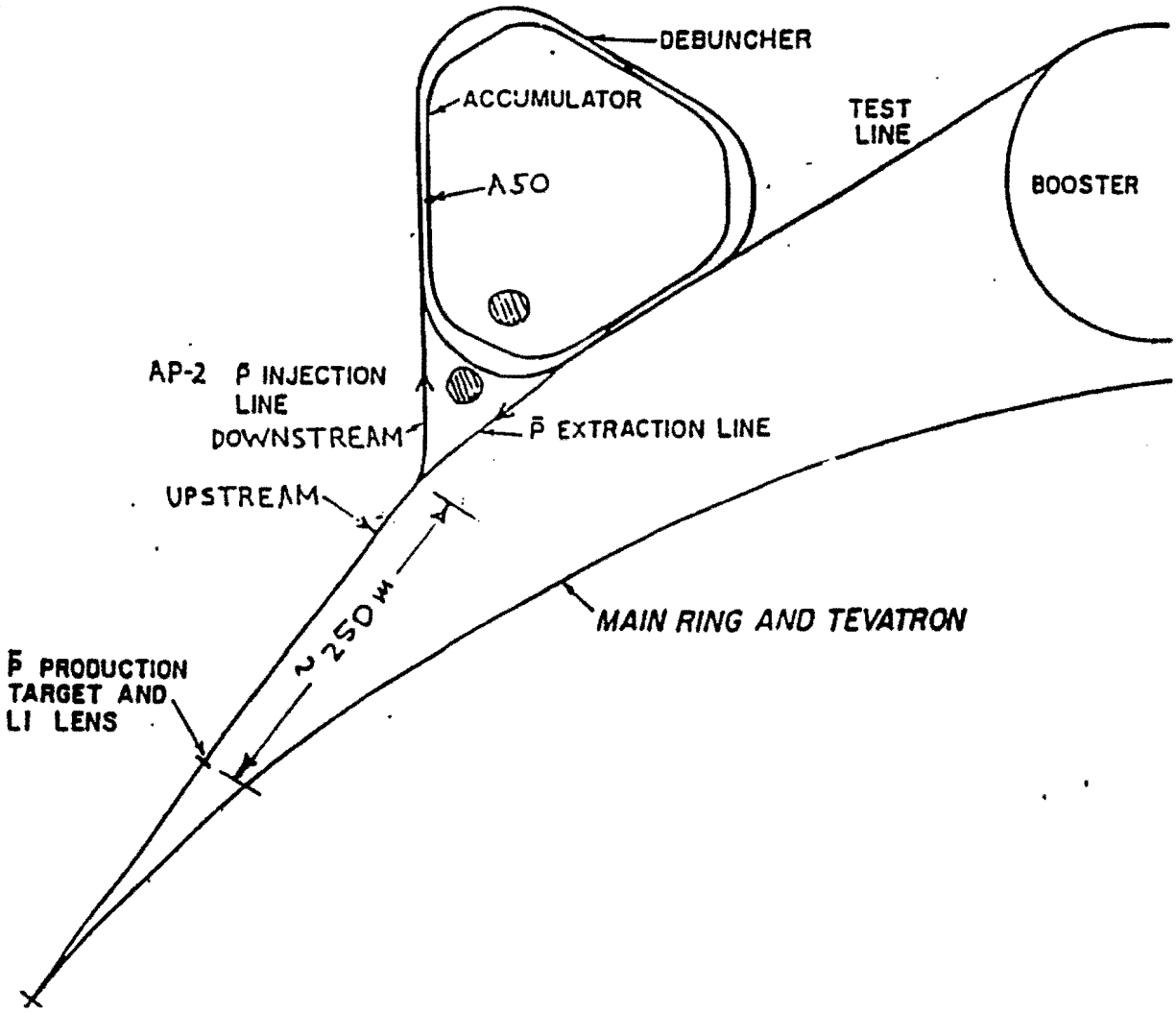

Fig. IV.1: Fermilab Debuncher storage ring.

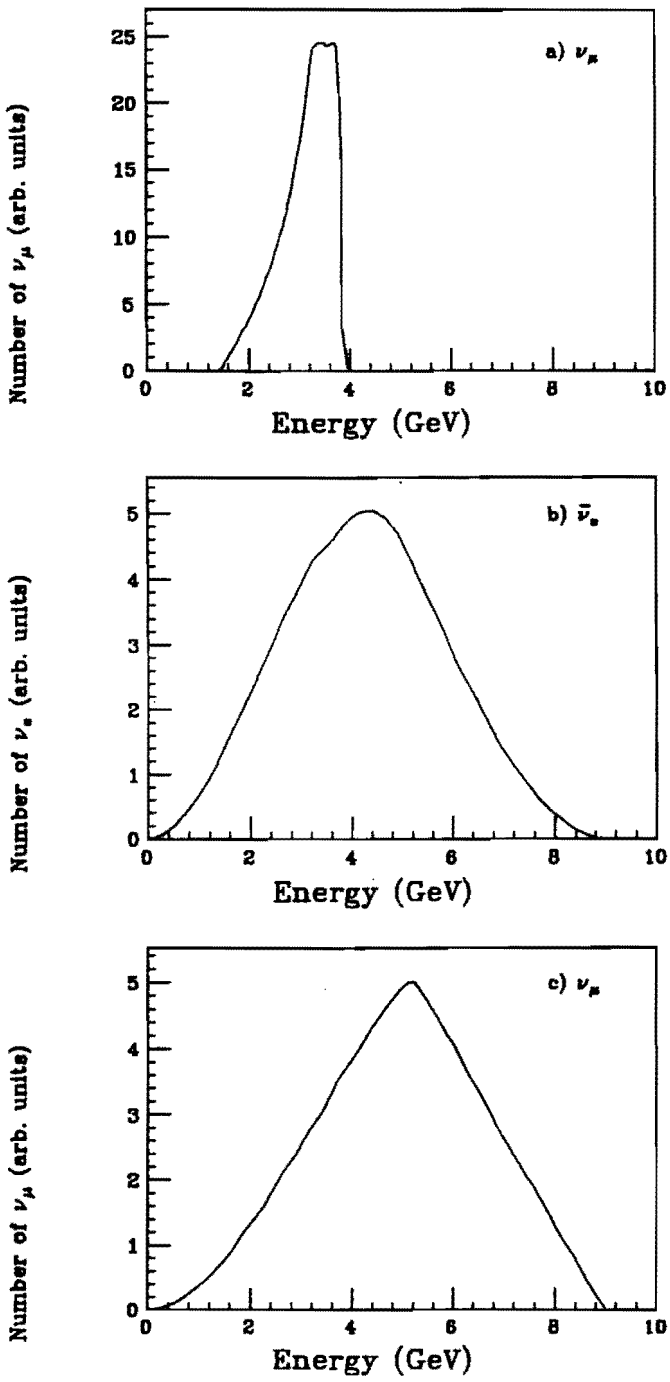

Fig. IV.2: The neutrino energy spectra from the Debuncher with a 10 mrad cut. The Debuncher energy is 9 GeV.

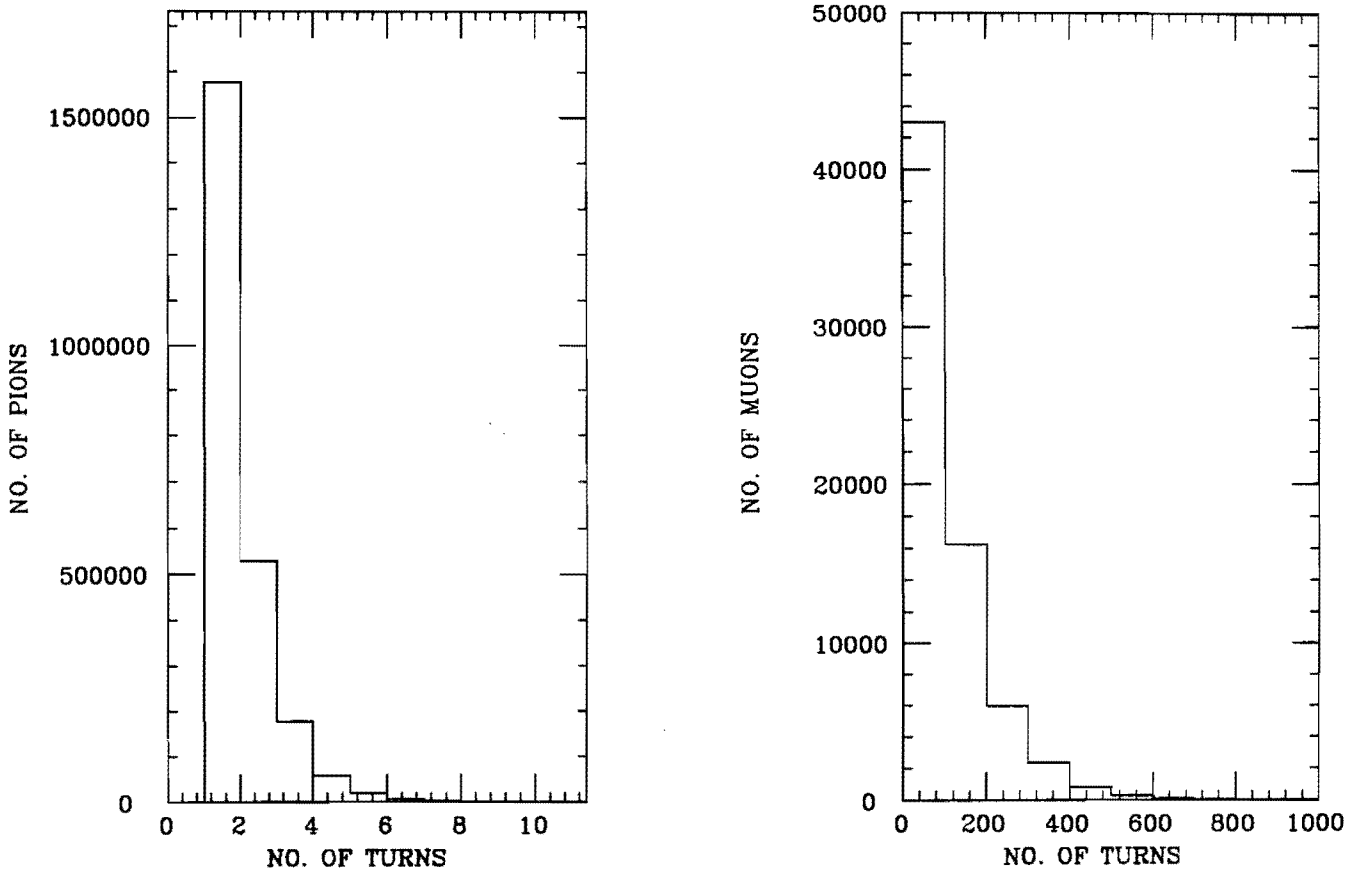

Fig. IV.3: The number of pions and muons in the debuncher as a function of number of revolutions.

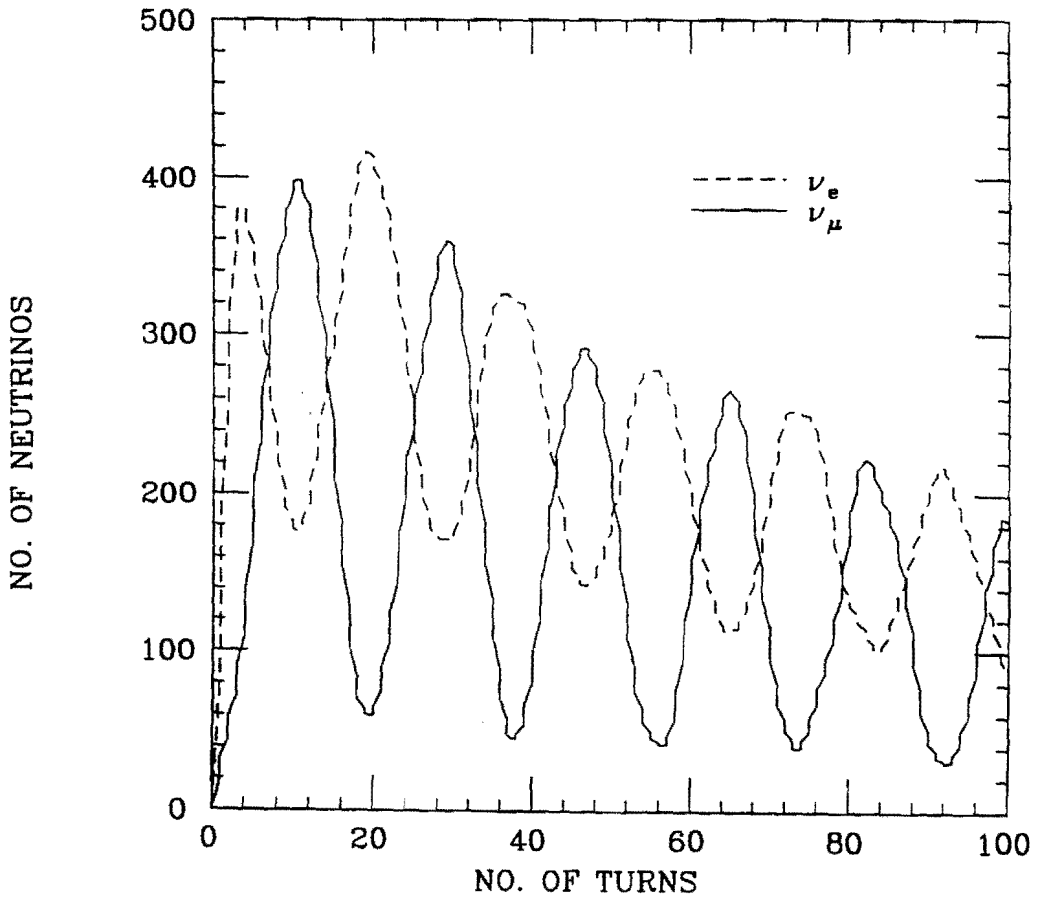

Fig. IV.4: The number of high energy ν_e and $\bar{\nu}_\mu$ accepted by the detector as a function of number of turns. A 10 mrad, 6 GeV energy cut is applied.

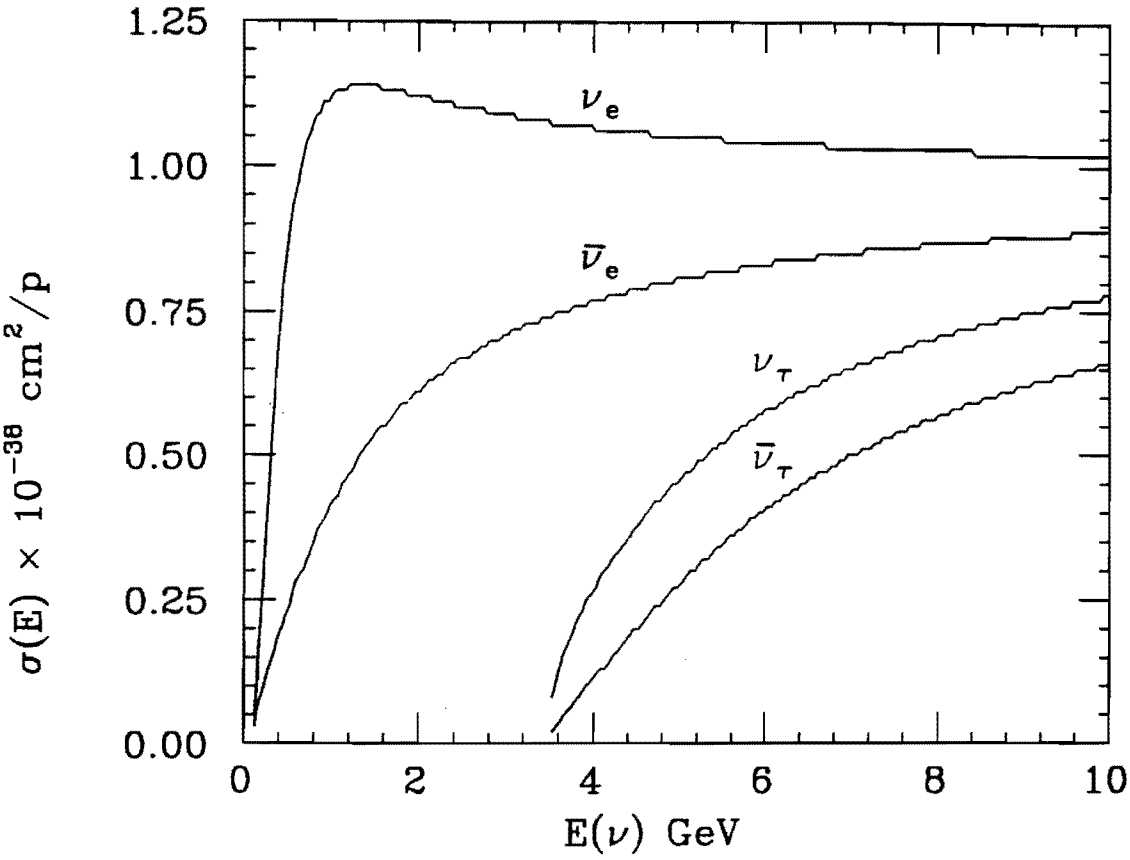

Fig. IV.5: Quasi elastic cross section for ν_e, $\bar{\nu}_e$, ν_τ, and $\bar{\nu}_\tau$.

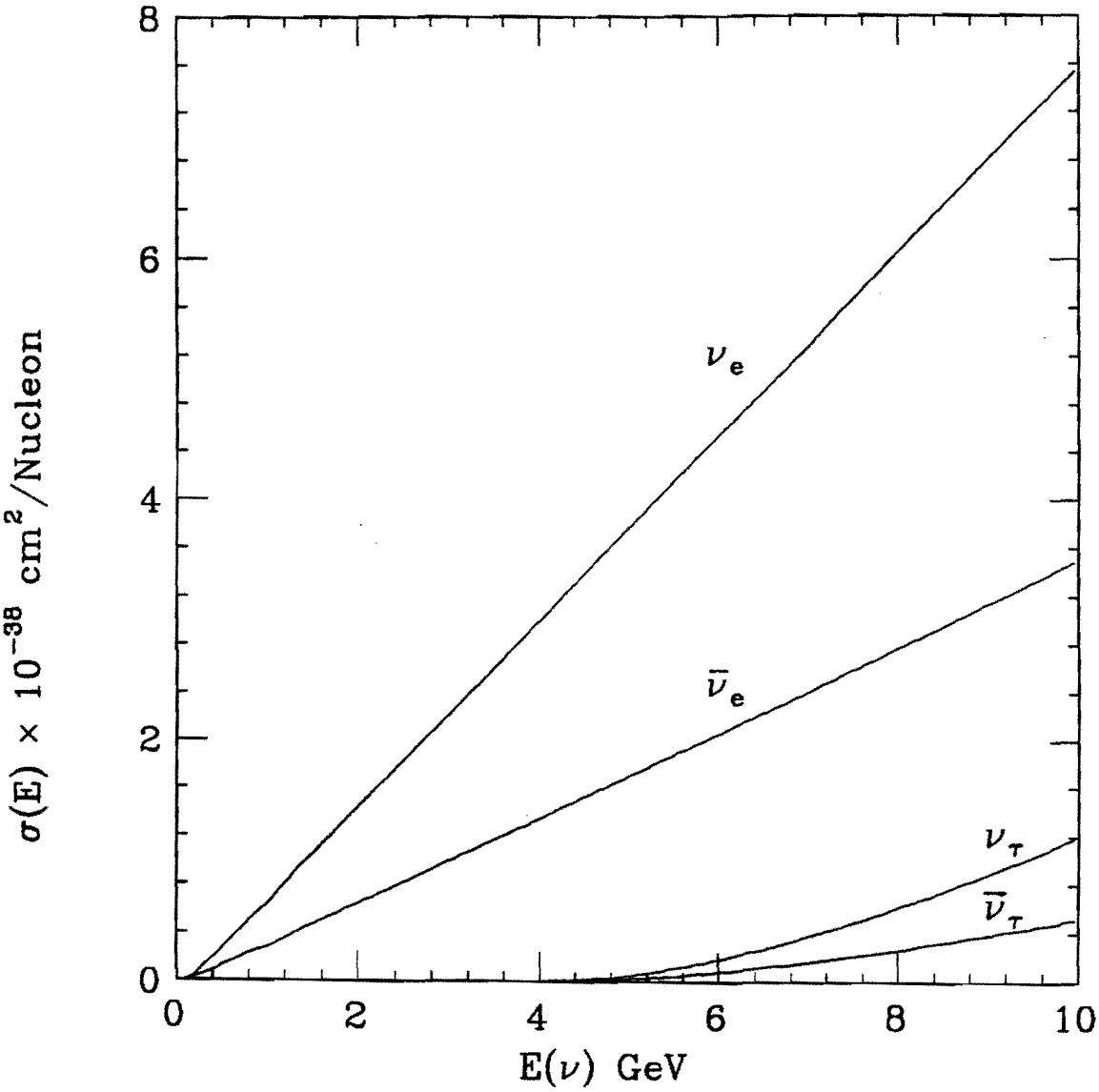

Fig. IV.6: Inelastic cross section for ν_e, $\bar{\nu}_e$, ν_τ, and $\bar{\nu}_\tau$.

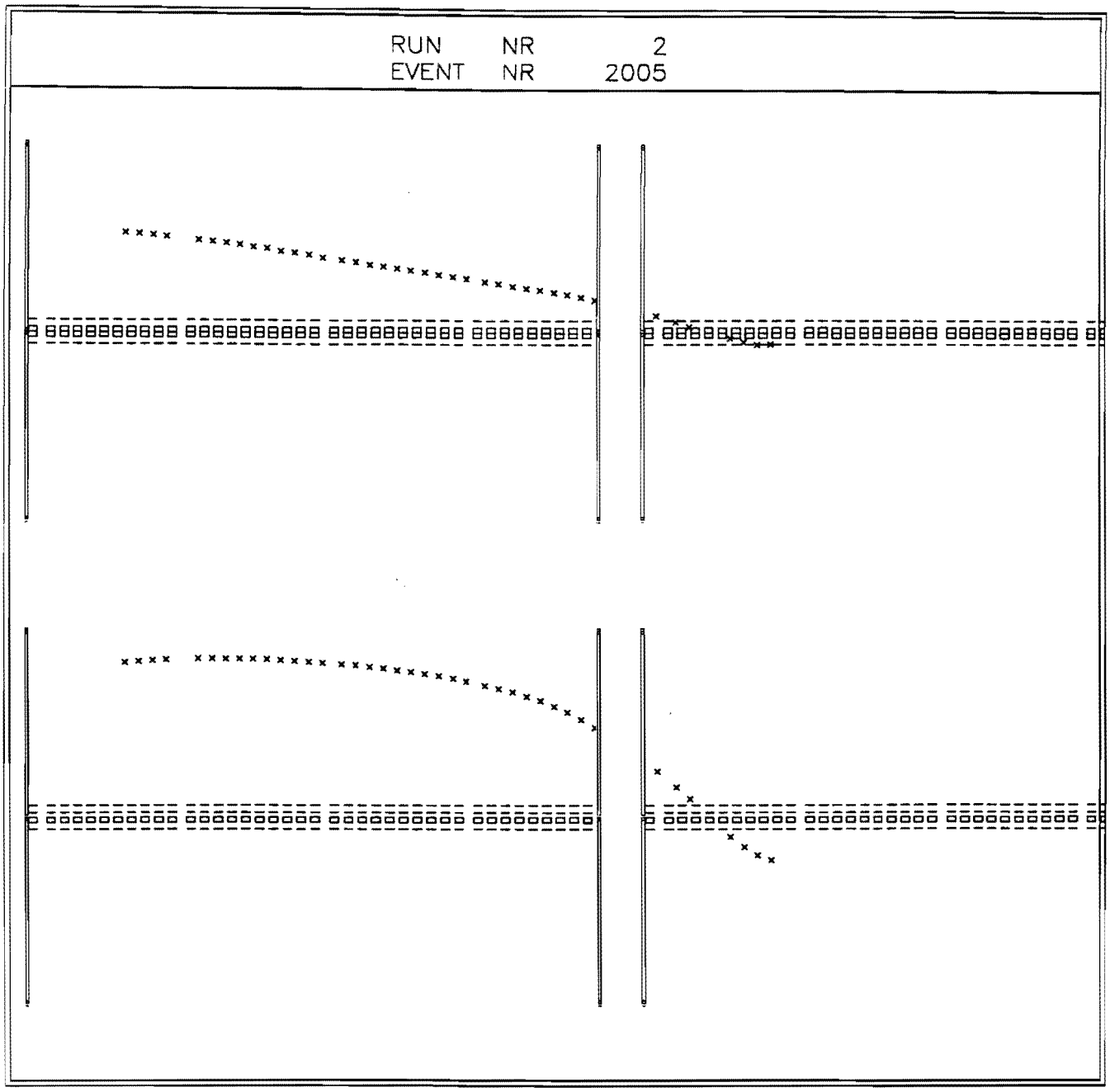

Fig. V.1: A typical quasi elastic τ event using a GEANT simulation of the proposed detector. The figure depicts a 7 GeV ν_τ interacting to produce a 4.4 GeV τ^+ decaying to a 3.7 GeV μ^+.

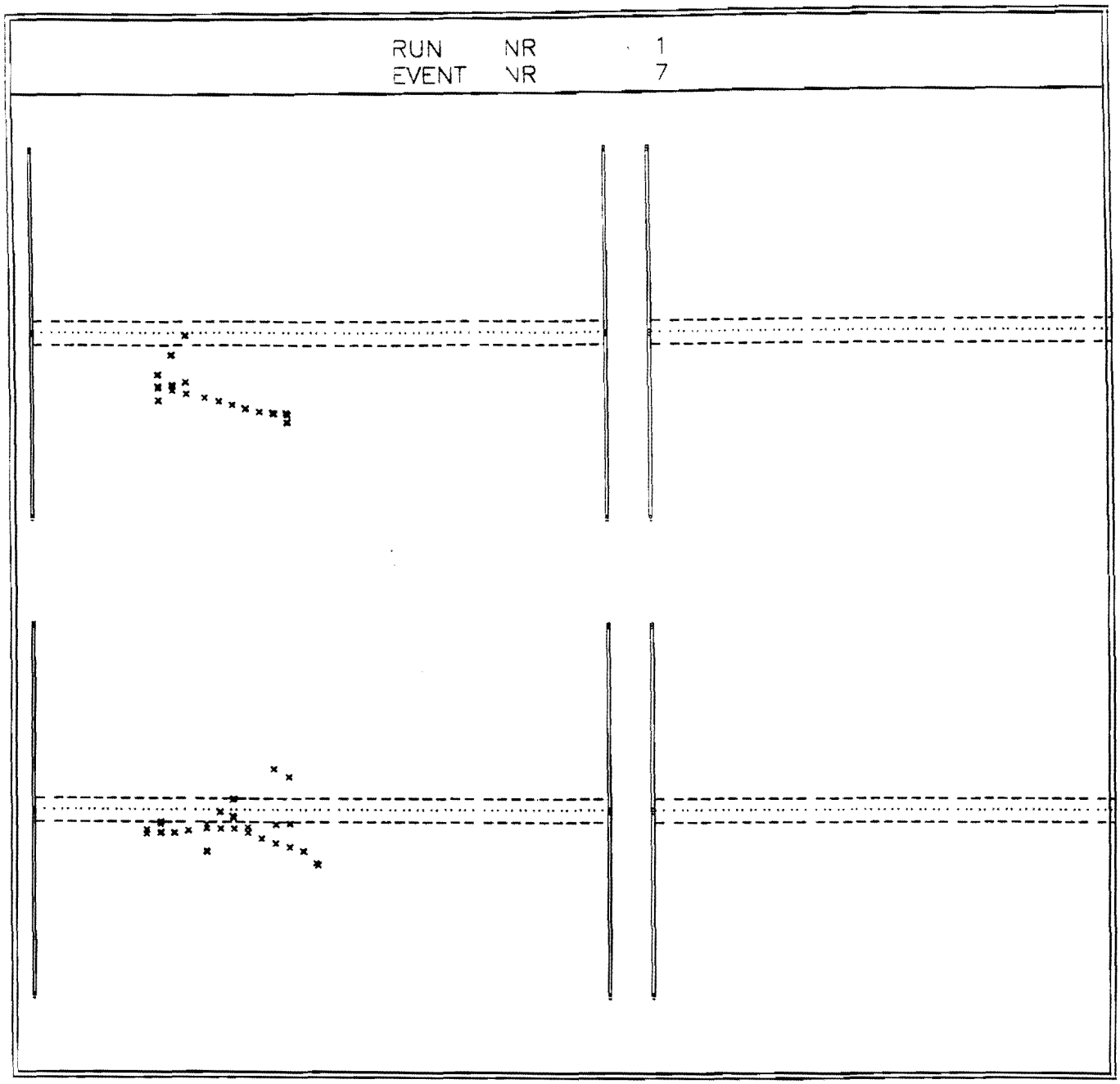

Fig. V.2: Typical ν_e interactions: a) Charged current interaction, b) Neutral current interaction.

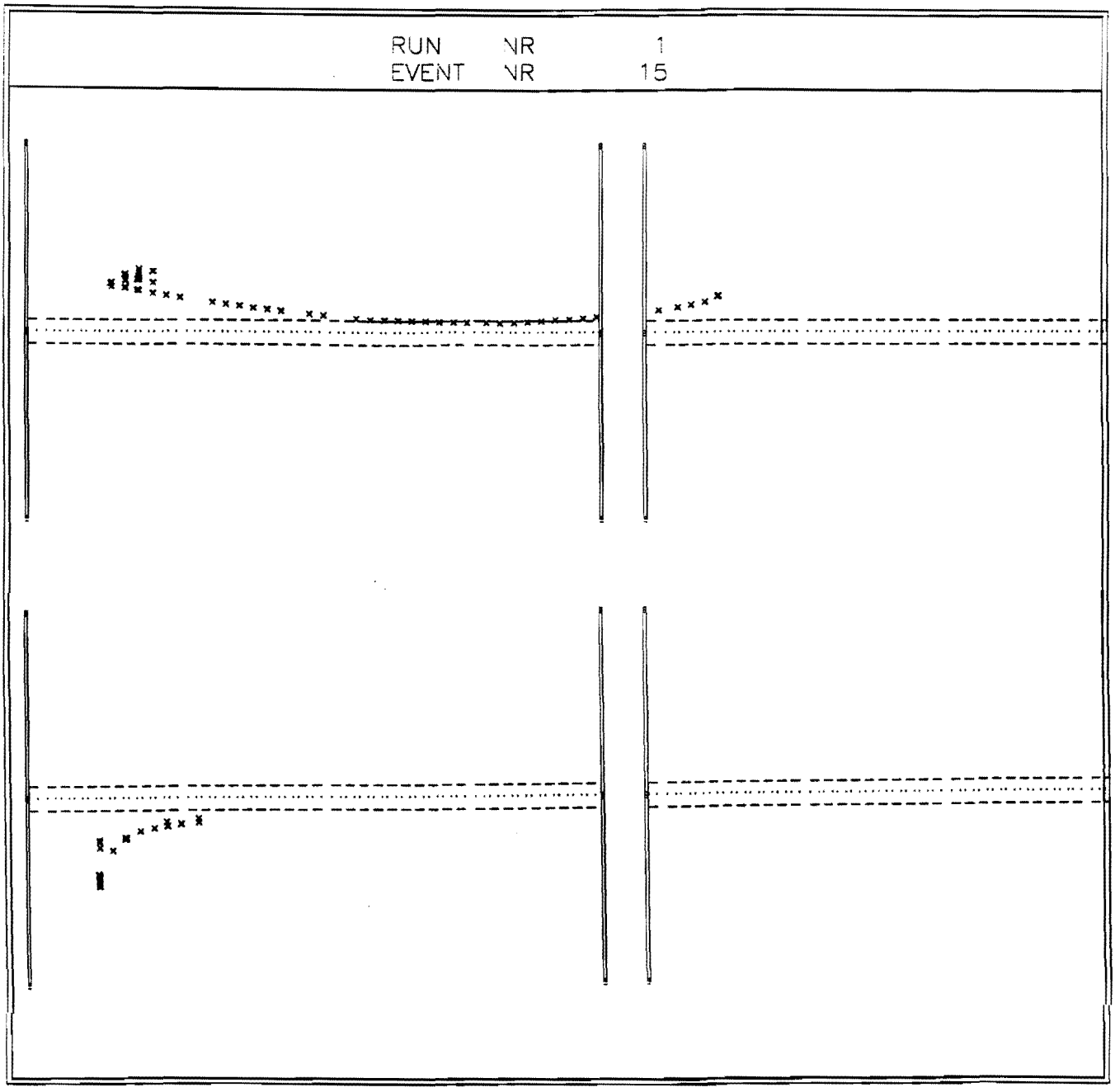

Fig. V.3: Typical ν_μ interactions: a) Charged current interaction, b) Neutral current interaction.

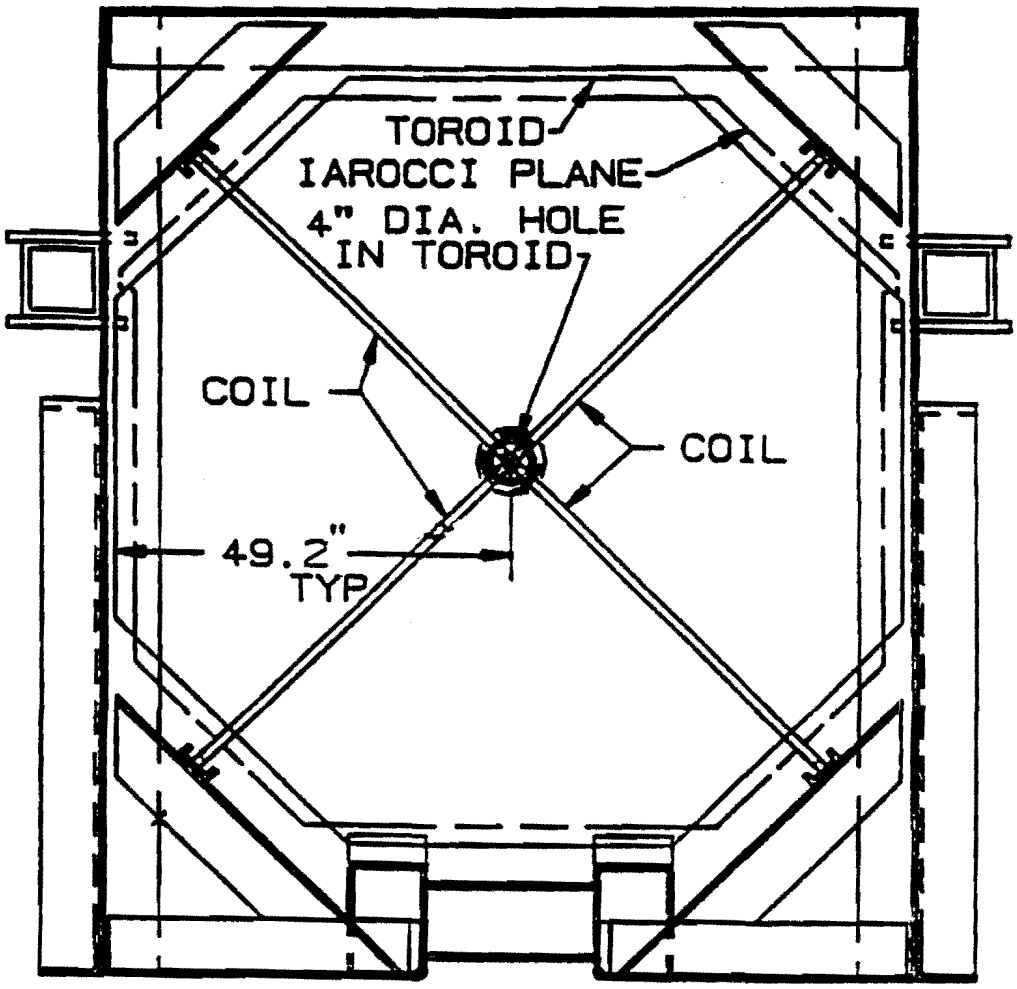

Fig. VIII.1a: Schematic drawing of the proposed detector (front view).

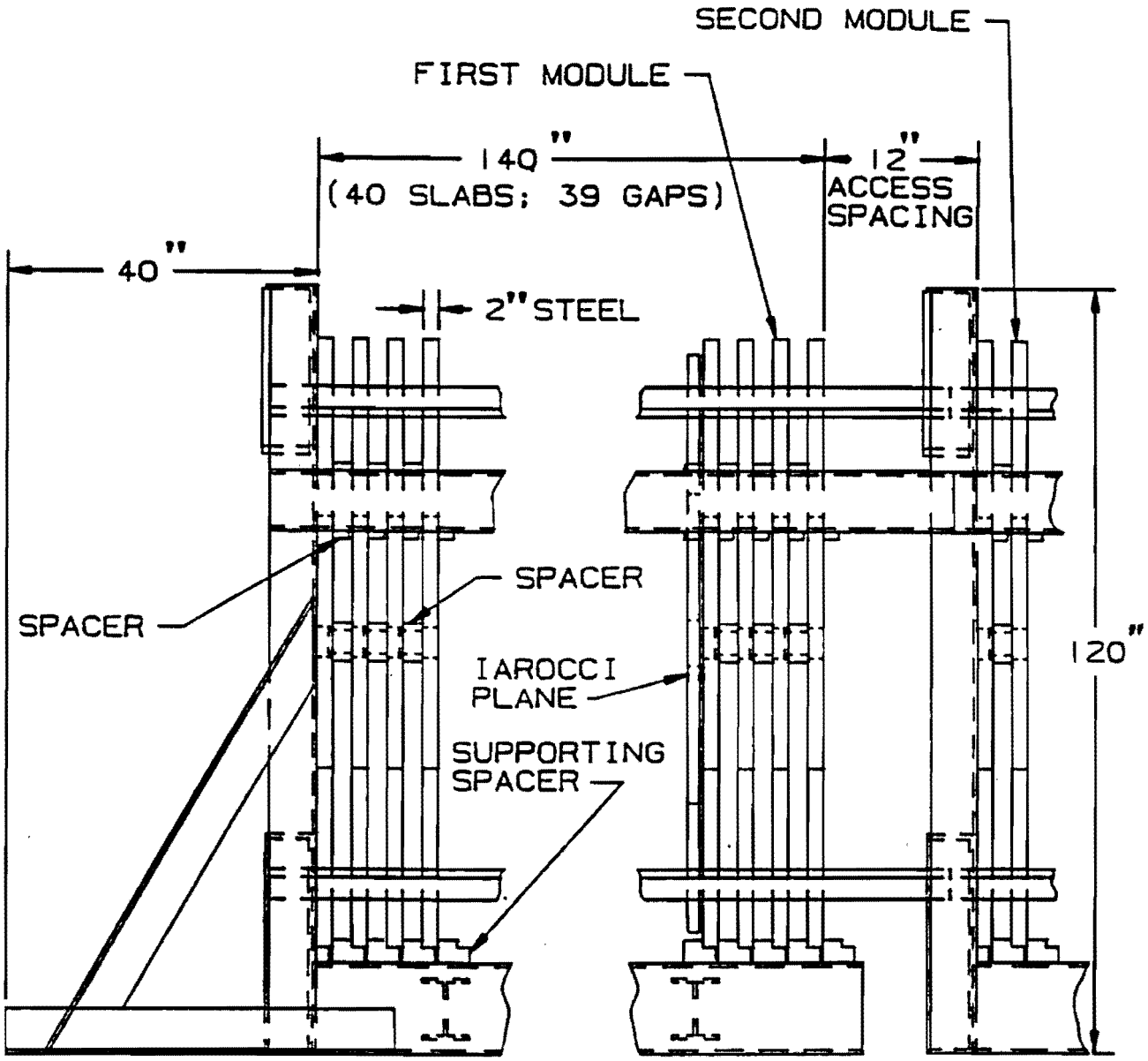

Fig. VIII.1b: Schematic drawing of the proposed detector (side view).

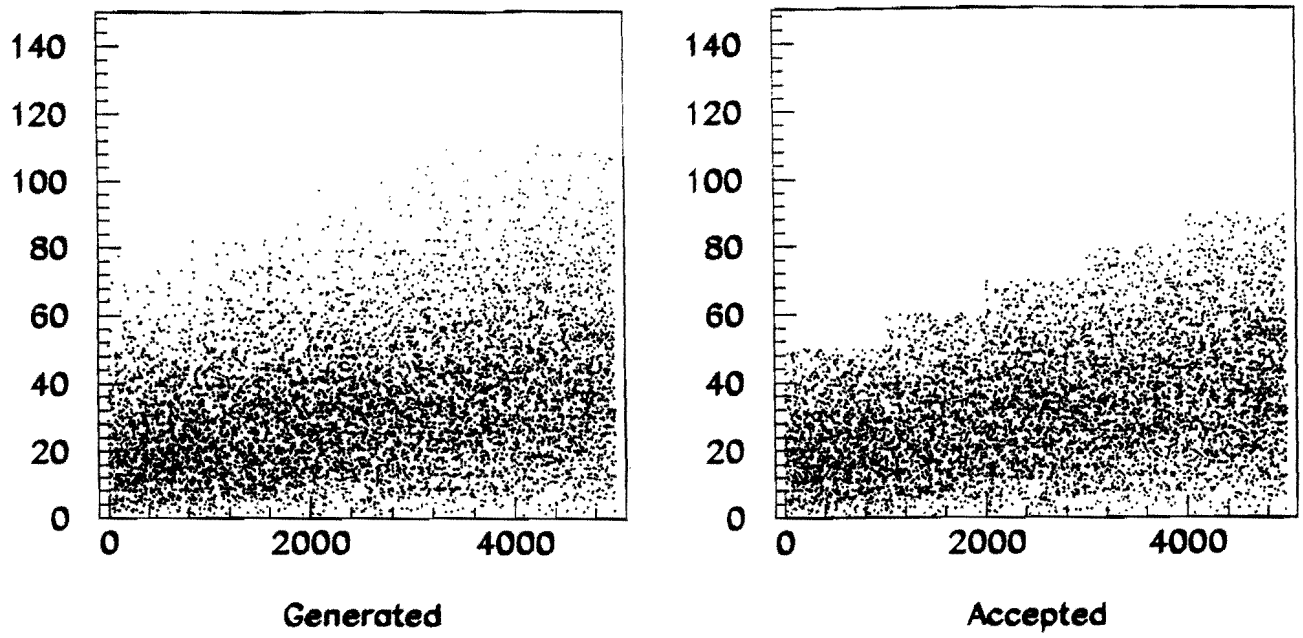

Fig. VIII.2: Radial distribution of interactions as a function of z. The interactions are weighted by the tau quasi elastice cross section. a) Generated interactions. b) Interaction accepted in the detector.

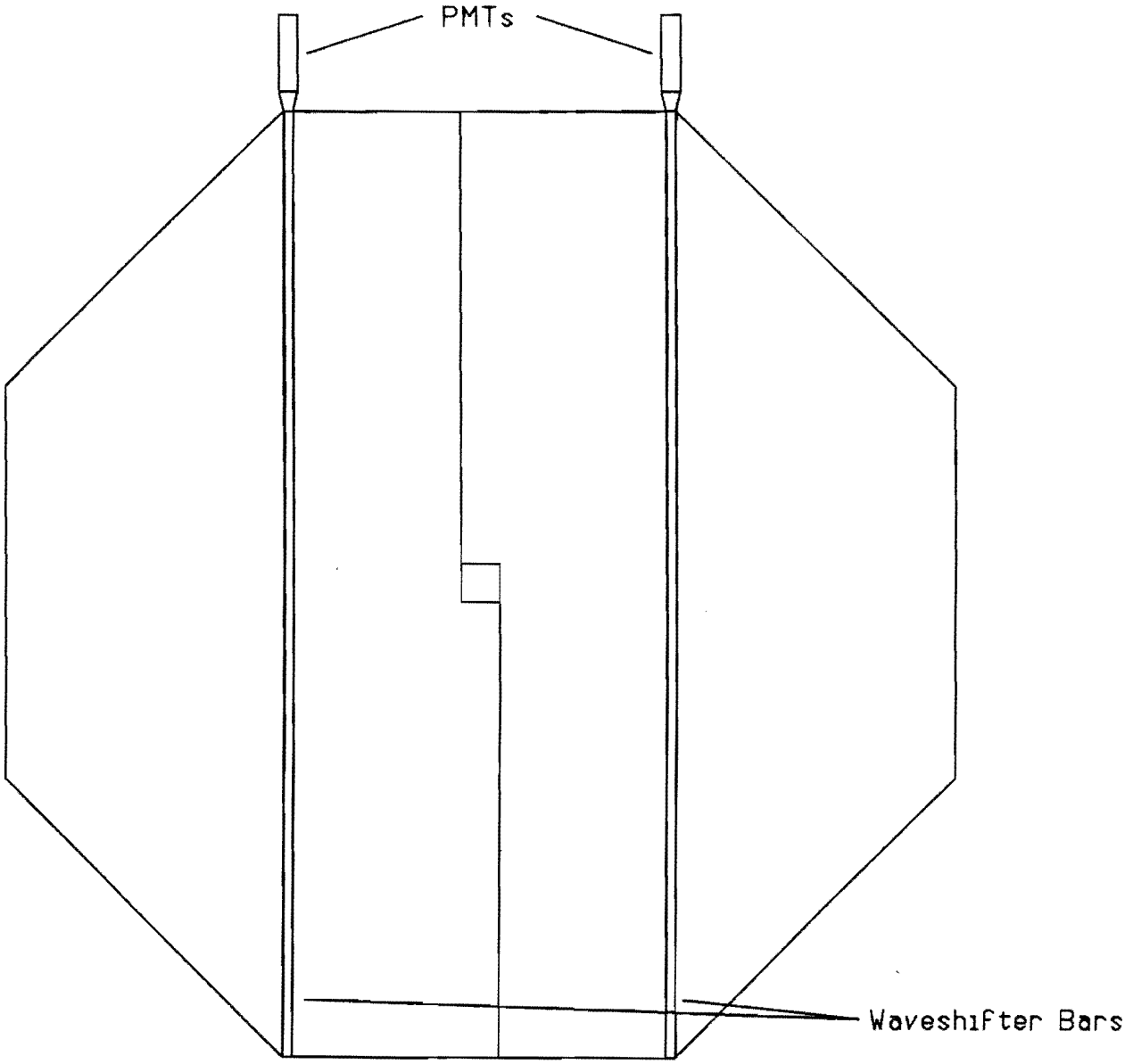

Fig. VIII.3: Schematic drawing of a scintillator plane.

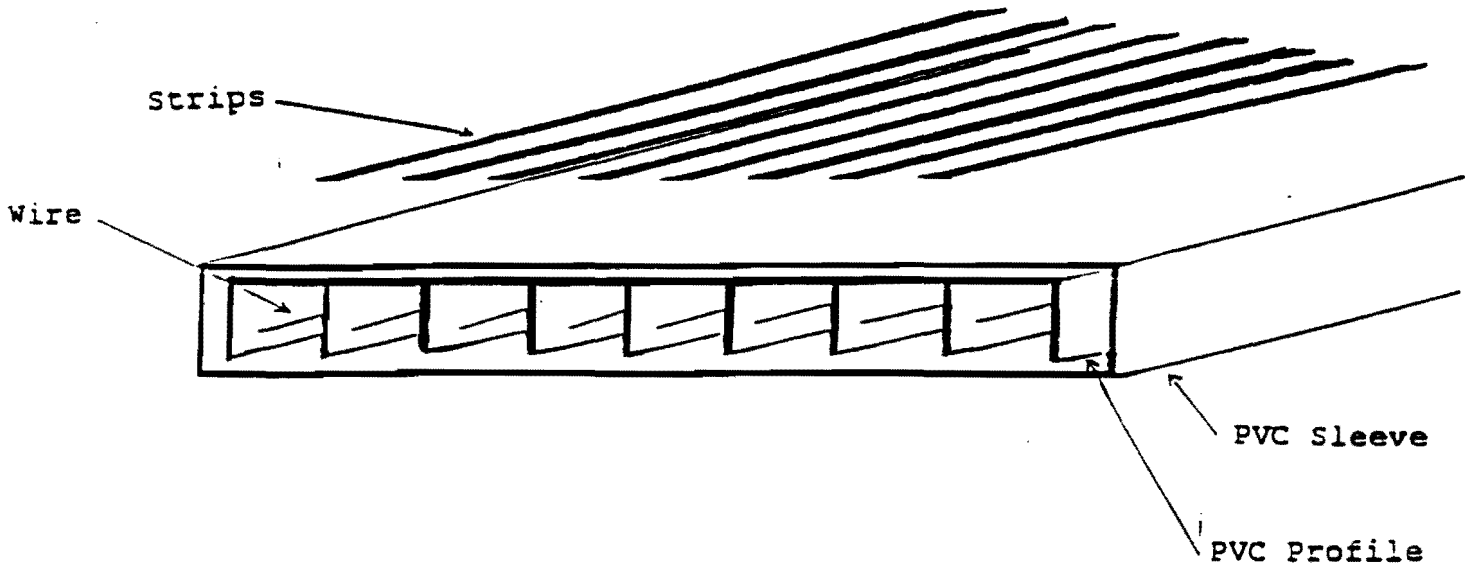

Fig. VIII.4: Schematic drawing of an Iarocci tube module.

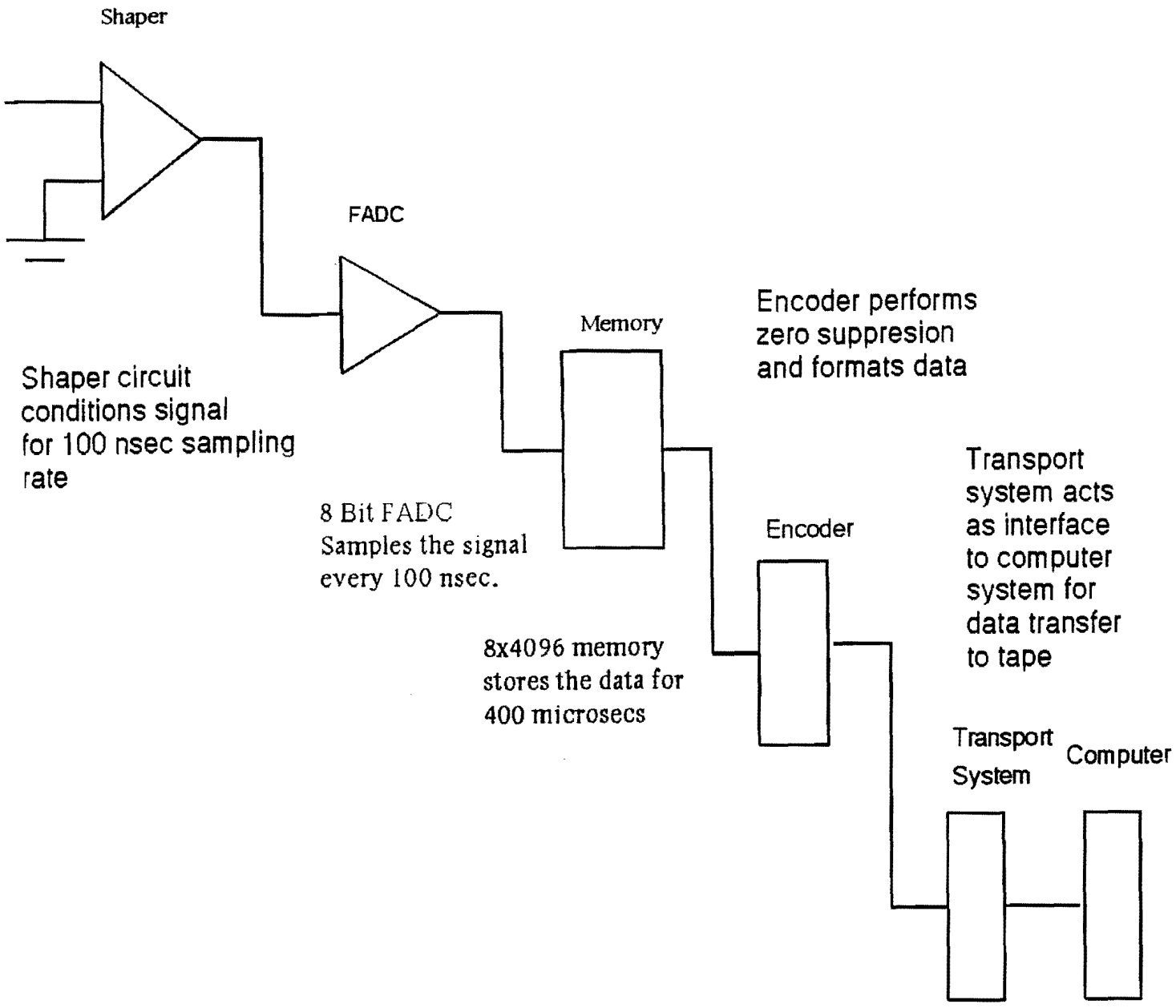

Fig. VIII.5: Data flow diagram.

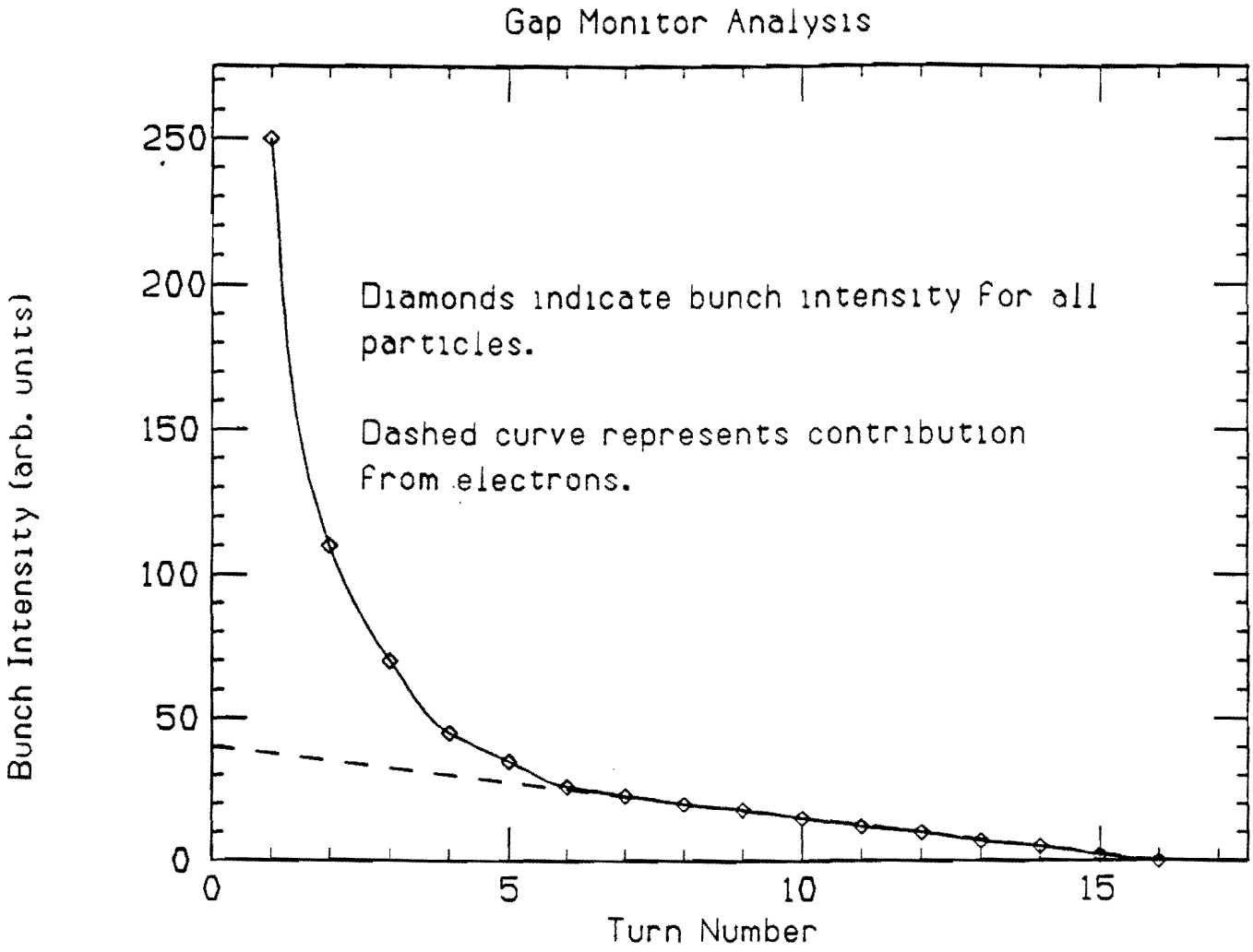

Fig. A1: 1987 μ flux measurement results

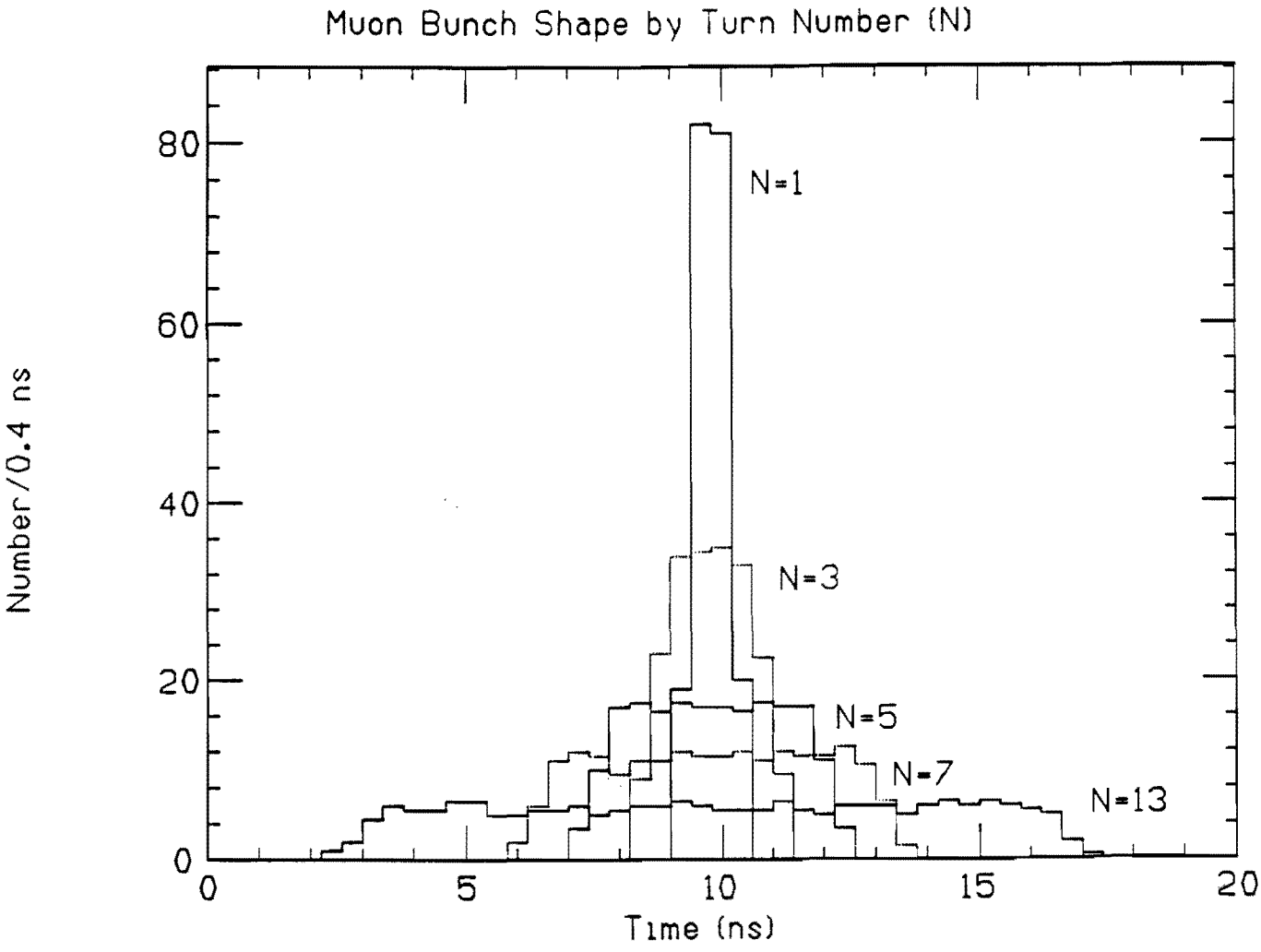

Fig. A2: μ **bunch shape as a function of turn number.**

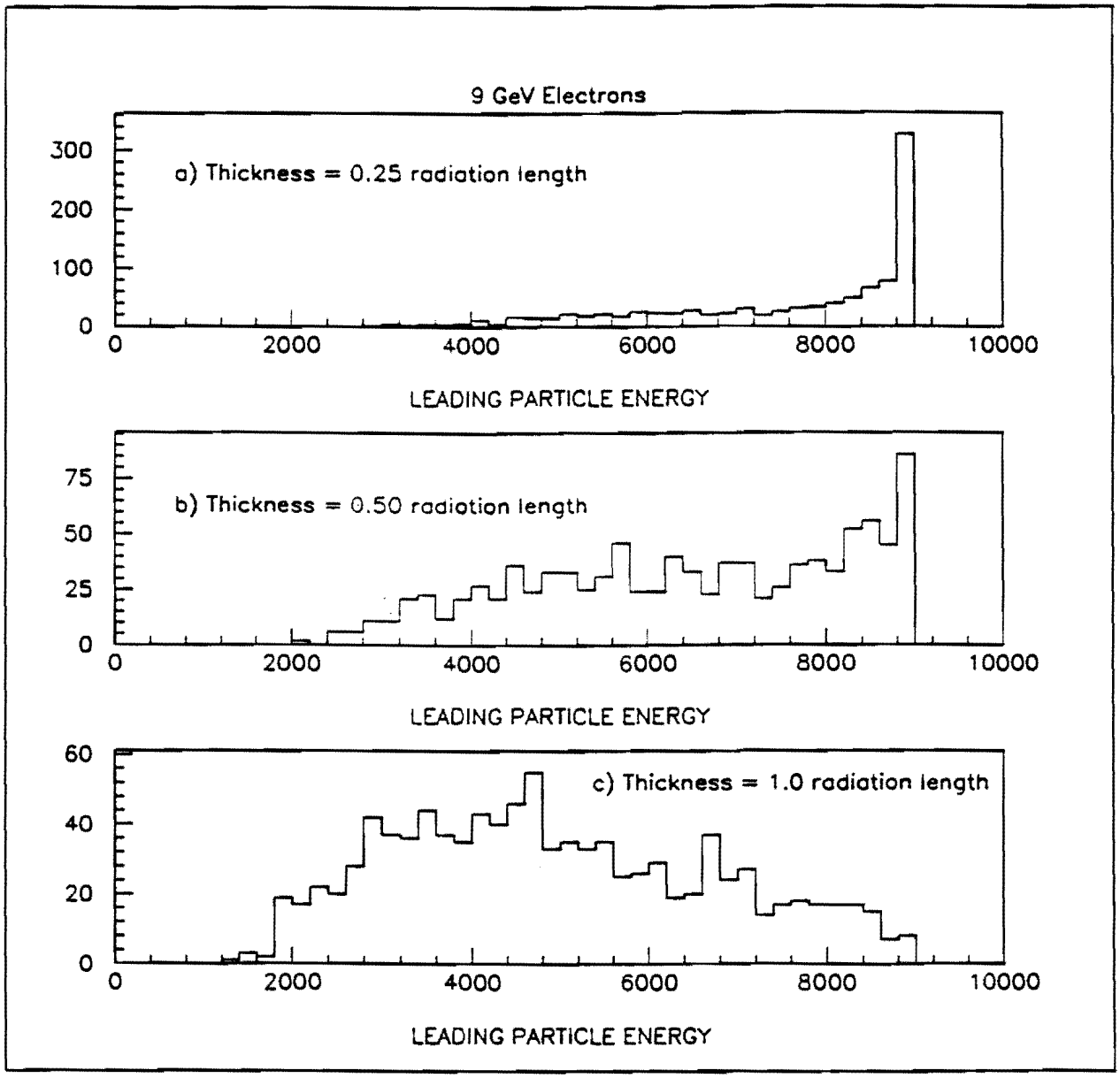

Fig. A3: Leading e^- energy for a) 0.25 rad length lead, b) 0.50 rad. length lead, and c) 1.00 rad length lead.

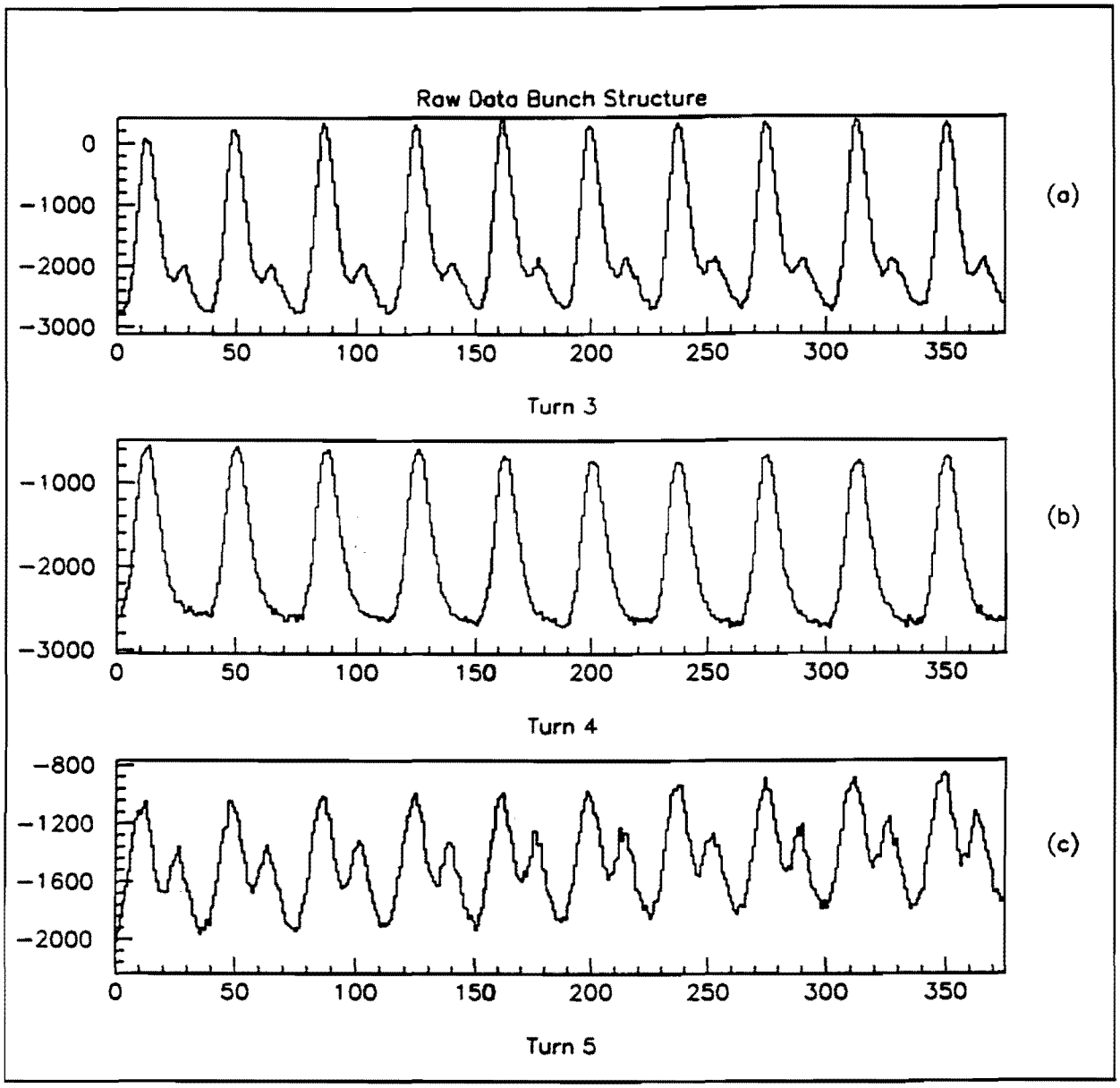

Fig. A4: Debuncher bunch structure for a) turn 3, b) turn 4, and c) turn 5.

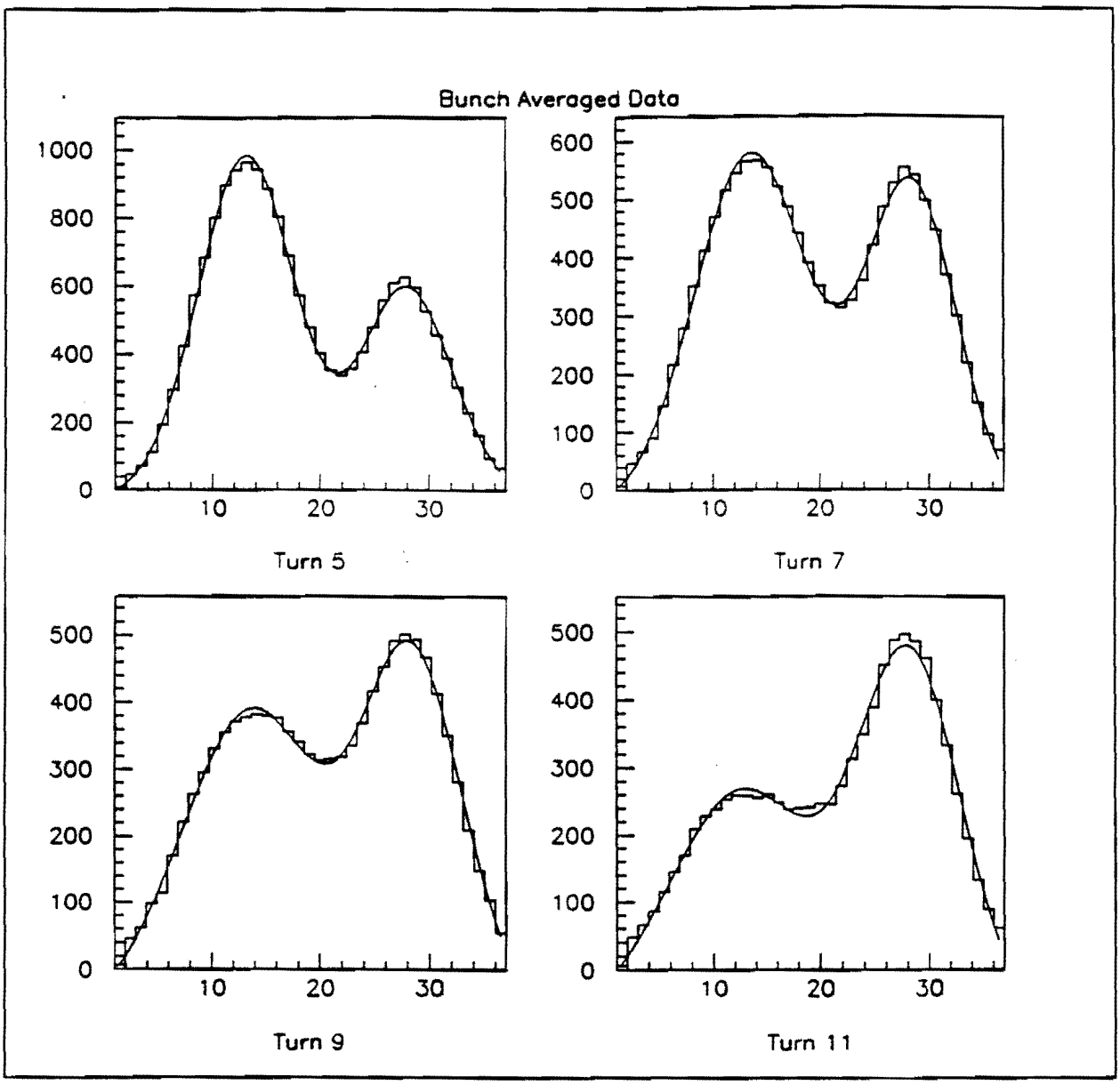

Fig. A5: Time averaged bunch structure for turns 5, 7, 9, and 11. The fit results of double Gaussian plus constant function is superimposed on the data.